Technical University of Munich
TUM School of Natural Sciences

Particle attenuation within dark matter spikes

Gonzalo Herrera Moreno

Complete reprint of the dissertation approved by the TUM School of Natural Sciences of the Technical University of Munich for the award of the

Doktor der Naturwissenschaften (Dr. rer. nat.)

Chair: Prof. Dr. Elisa Resconi

Examiners:

1. Prof. Dr. Alejandro Ibarra
2. Priv.-Doz. Dr. Mathias Garny

The dissertation was submitted to the Technical University of Munich on 05.09.2023 and accepted by the TUM School of Natural Sciences on 13.09.2023.

"If you look for a meaning, you'll miss everything that happens"

Andrei Tarkovsky

"In general I think that in art you only have the responsability to tell the truth"

Ken Loach

"There are more things in heaven and earth, Horatio, than are dreamt of in your philosophy"

William Shakespeare

"I've often lost myself, in order to find the burn that keeps everything awake"

Federico García Lorca

A mi abuelo Ramón, que solía decir: "Ahora toca apretar los dientes, y tirar pa'lante"

Thesis advisor: Prof. Dr. Alejandro Ibarra *Gonzalo Herrera Moreno*

Particle attenuation within dark matter spikes

ABSTRACT

Dark matter indirect detection searches have historically focused on additional contributions to the expected astrophysical fluxes due to annihilations and/or decays of dark matter particles. However, the dark matter particle may predominantly interact with the standard model sector via *scatterings*, attenuating the emitted astrophysical fluxes from some sources, and potentially changing its spectral shape. It is known that adiabatically-growing black holes at the center of galaxies are expected to enhance the density of dark matter particles at sub-parsec distances, forming *dark matter spikes*. Interestingly, multi-messenger observations of *Active Galactic Nuclei (AGN)* suggest that cosmic rays are accelerated in the vicinity of the black hole, producing high-energy neutrinos and gamma-rays that can be observable at Earth. Therefore, AGN constitute a good particle dark matter laboratory, due to their large fluxes of standard model particles with high energies, the large density of dark matter particles that they host, and the availability of multi-messenger channels to interpret the underlying physical processes taking place at the source. Uncertainties are still large, but in this thesis we demonstrate that our current knowledge on AGN allows to place robust and strong constraints on dark matter scatterings with standard model particles, and perhaps hint a detection.

Thesis advisor: Prof. Dr. Alejandro Ibarra *Gonzalo Herrera Moreno*

Partikelabschwächung innerhalb von Dunkle Materie-Spitzen

Zusammenfassung

Die Suche nach indirekten Hinweisen auf Dunkle Materie hat historisch gesehen hauptsächlich auf zusätzliche Beiträge zu den erwarteten astrophysikalischen Flüssen durch Annihilationen und/oder Zerfälle von Dunkle Materie-Teilchen fokussiert. Es ist jedoch möglich, dass das Dunkle Materie-Teilchen hauptsächlich durch Streuung mit dem Standardmodell-Sektor wechselwirkt, wodurch die ausgesendeten astrophysikalischen Flüsse einiger Quellen abgeschwächt werden und sich möglicherweise ihre spektrale Form ändert. Es ist bekannt, dass adiabatisch wachsende Schwarze Löcher im Zentrum von Galaxien erwartungsgemäß die Dichte der Dunkle Materie-Teilchen in subparsec-Entfernungen erhöhen und sogenannte *Dunkle Materie-Spitzen* (Dark Matter Spikes) bilden. Interessanterweise deuten multi-messenger Beobachtungen von Aktiven Galaktischen Kernen (AGN) darauf hin, dass kosmische Strahlen in der Nähe des Schwarzen Lochs beschleunigt werden und hochenergetische Neutrinos und Gammastrahlen erzeugen, die auf der Erde beobachtbar sind. Daher stellen AGNs ein gutes Labor für Dunkle Materie-Teilchen dar, aufgrund ihrer hohen Flüsse von Standardmodell-Teilchen mit hoher Energie, der großen Dichte an Dunkler Materie-Teilchen, die sie beherbergen, und der Verfügbarkeit von multi-messenger Kanälen, um die zugrunde liegenden physikalischen Prozesse in der Quelle zu interpretieren. Die Unsicherheiten sind noch groß, aber in dieser Arbeit zeigen wir, dass unser derzeitiges Wissen über AGNs es ermöglicht, robuste und starke Einschränkungen für die Streuung von Dunkler Materie mit Teilchen des Standardmodells festzulegen und vielleicht sogar eine Entdeckung andeuten.

Publications in the context of this thesis

- *Probing Light Dark Matter through Cosmic-Ray Cooling in Active Galactic Nuclei*, Gonzalo Herrera and Kohta Murase, 2307.09460
- *New constraints on the dark matter-neutrino and dark matter-photon scattering cross sections from TXS 0506+056*, Francesc Ferrer, Gonzalo Herrera and Alejandro Ibarra, JCAP 05 (2023) 057, 2209.06339
- *Direct detection of non-galactic light dark matter*, Gonzalo Herrera and Alejandro Ibarra, Phys.Lett.B 820 (2021) 136551, 2104.04445
- *Enhanced prospects for direct detection of inelastic non-galactic dark matter*, Gonzalo Herrera, Alejandro Ibarra and Satoshi Shirai, JCAP 04 (2023) 026, 2301.00870
- *Implications of non-galactic dark matter for sub-GeV direct detection searches*, Gonzalo Herrera and Alejandro Ibarra, J.Phys.Conf.Ser. 2156 (2021) 012040, PoS EPS-HEP2021 (2022) 161

Acknowledgements

I am grateful to my supervisor Alejandro Ibarra for giving me the opportunity to complete a PhD in his group, for all the exciting discussions and projects, as well as for the support to attend many conferences and schools to enhance my skills. Most importantly, from him I learned the importance of simplicity and analyticity in physics. This lesson will probably accompany me during my whole career.

I want to thank all my collaborators for teaching me a lot about physics and for all the interesting discussions that we had during the completion of the projects of this thesis. Especially I want to thank Kohta Murase, Francesc Ferrer, Stefano Scopel, Satoshi Shirai, Gaurav Tomar, Mar Císcar-Monsalvatje, Anja Brenner and Merlin Reichard. I also want to thank other colleagues that assisted me and offered helped when I needed it, like Raimund Strauss, Federica Petricca, Elisa Resconi, Mathias Garny, Klaus Dolag, Francesca Capel, Diego Restrepo, Óscar Zapata, Carlos Yaguna, Riccardo Catena, Felix Kahlhöefer, Gianfranco Bertone, Tongyan Lin, Anton Baushev, Walter Winter and Chengchao Yuan, among others that I am probably forgetting (apologies!).

More generally, I want to thank all the people in Academia that I have met over these years, and that have helped me to begin to build a community and understand certain things about this field. I especially want to thank Miguel Escudero for being my unpaid mentor (all the beers I payed him are negligible compared to his delicious dinners during the pandemic). My friendship and esteem for Miguel grows with time, like wine. He is a truly close and generous person, and a good professional when the conversations came down to physics. I also want to thank Gaurav Tomar for being a very close and professional collaborator when I started my PhD thesis. I learned a lot from him, not only about dark matter, but also about Hinduism and the benefits of meditation. Now both became part of my daily routine. My acknowledgement also to Xabier Marcano, for nice hikes in the alps and conversations about life over beer, and also for giving me very useful insights about academia. Infinite thanks to Andreas Rappelt, for being my mentor during the Master Thesis, and keeping to help and give support during my PhD, when he was already out of academia. I also want to thank Motoko Fujiwara for our intense and exciting discussions about physics that made the time in the faculty more human. My acknowledgment also goes to Jérôme Vandecastelee, for nice discussions over lunch and for giving me many useful tips about academia. I acknowledge all the other t30d group members, Anja, Merlin, Boris, Lukas, Di for interesting discussions over coffee, about physics and beyond physics.

I also want to thank my students! To Yu Chen, with whom I learned a lot about

boosted dark matter during her master thesis. We had a lot of fun with python. And to Pablo Figueroa, who committed the terrible mistake to ask me, freshly started PhD student, to supervise his bachelor thesis. We had a lot of fun learning together about light dark matter physics.

I don't forget all the incredible young physicists that I met in schools and conferences, and with many of whom I have discussed about physics and kept in contact. Especially to my friend Guillermo Abellán, for all the fun we had together, but also to many others like Dominik Fuchs, Julien Laux, Raquel Galaza, Adriana Menkara, Silvia Gasparotto, Toni Bertólez and Jorge Terol (again I am forgetting many people).

I am very grateful to my close friends Carlos Luis (aka "Carlu") and Santi (aka "Conche") for the enormous support over the years and in particular during the thesis. In the most difficult moments they were always there for me. It warms my heart to see that we maintain the same critical view on the world and enthusiasm about philosophy and arts that we had when we met each other with 18 years old. I want to thank Santi, Fran and Carlos for their support and friendship during all these years, first in Madrid, and now here in Munich (I can't get rid of them!). Javi, for hours and hours of laughing, eating lots of fast food and spending time on the streets of Munich and Madrid. I am also very grateful to my group of friends from my hometown for keeping me close to the ground, and especially to Enrique for his closeness when a deep conversation was needed. I also want to thank my friend Pablo for very interesting discussions and for literally teaching me python and linux from scratch when I started my master thesis. To Sofía, Rosa and Alberto for their friendhsip all these years. I can't forget David, Elia and Nina for the warm conversations and dinners. I am also grateful to my friends Valeria, Lupe and Nerea, although they probably hate me for not replying whatssapps sometimes.

I am immensely grateful to Mar. Her company and support have been the only way to get rid of thoughts and worries on academia. She has taught me to love carefully, and to be present when the moment requires it. When my anxiety suddenly arised and I most needed her, she held me and patiently helped me recover. I am very lucky to have her by my side, not only for all these things, but also for the constant illuminating discussions and projects that we face in common. We have too much fun together, and in peace.

I also want to dedicate this thesis to my family. They always supported me and believed in me. To my grandparents for teaching me the values of effort and curiosity, and in particular to my grandfather Juan for making me fall in love with poetry. To my father, who passed me his enthusiasm with paintings, sculptures, architecture, literature and history since I was a child. To my brother, for being there every time the situation was needed, and for being one my first call and support in secret, when problems appeared in my life. He was also a reference model of effort and sacrifice for me. And I dedicate this thesis to my mother, of course. I still remember when she called me 10 minutes before the deadline to apply for a bachelor's degree in Spain and I was 17 years old. She was almost crying and asking me to change physics for some engineering career, because she

was concerned about my future. I could convince her then that this is what I wanted, and she supported me since unconditionally. I made it through so far! More or less...

Contents

Chapter 1

Introduction

Finding the nature of dark matter remains one the most pressing open questions in physics after roughly half a century of worldwide efforts. Astrophysical and cosmological evidence for dark matter started early in the XX century. However, I took a bit longer for a large part of the particle physics community to shift their focus from unification of forces, the hierarchy problem, the nature of neutrino masses, or the baryon asymmetry of the Universe towards studying particle physics models able to account for the dark matter of the niverse. Arguably the first dark matter candidate arised from supersymmetric theories, since the lightest supersymmetric particle was stable on cosmological timescales and neutral. Parallelly, cosmological simulations and local observations established predictions for the amount of dark matter present in the Milky Way and its phase space distribution. The quest for the neutralino had begun, provoking a fruitful collaboration between astrophysicists, cosmologists and particle physicists sustained until today.

Soon, different detection approaches were proposed, ranging from the direct scatterings of dark matter particles from the Milky Way halo at Earth-based detectors, to indirect searches focusing on the products of annihilation or decays of dark matter particles, and to potential production of these particles in collider experiments. The paradigm was established: Weakly Interacting Dark Matter Particles (WIMPs) in the GeV-TeV scale were theoretically motivated by supersymmetry, and we had several fronts to hunt for these particles. While numerous hints and potential signals popped-up over the years, most of them went away after more careful analyses, and the LHC continued to lack a signal of supersymmetric particles. Part of the community started to deviate from the main road, and began to study the phenomenological implications of other dark matter candidates, such as sterile neutrinos, axion-like particles or light particles in the MeV scale. To be fair, those particle physics models are almost contemporary in origin to the WIMP, and none of them has provided an undoubtful signal either.

All these frameworks originally had favoured and theoretically motivated certain regions of the parameter space, some of which still today remains unexplored experimentally. But most importantly, the flexibility of those theories has largely increased in the last $\sim$ 10 years, providing new large regions of parameter space yet to be explored and that may account for the dark matter of the Universe. This probes that model-building tasks have been crucial to change mindsets and question the established paradigms, and indicate that we are entering an era where novel phenomenological approaches and dedicated experiments are needed to probe new regions of the parameter space which weren't

thought to be theoretically motivated in the past.

We have seen tremendous improvements, creativity and efforts in the last years to explore novel phenomenological aspects of dark matter sectors, whether using different astrophysical environments, cosmological probes, or different signatures at indirect, direct or collider experiments. The community took into account all possible aspects at play such as different portals of the dark sector to the standard model, different experimental set-ups, and distribution or components of dark matter particles in the Universe.

In this context, this thesis aims to provide a new phenomenological probe of dark matter particles, consisting in their interactions with standard model particles in Active Galactic Nuclei (AGN), which potentially attenuate the emitted fluxes observed in neutrinos and photons at Earth. Given the high-energies carried by standard model particles at these sources, their large fluxes, and the expected large densities of dark matter particles, we will demonstrate that AGN provide a powerful probe of dark matter scatterings with protons, electrons, photons and neutrinos.

In particular, we will explore the implications of dark matter scatterings with standard model particles in the inner regions of active galaxies, which are strongly influenced by the presence of a supermassive black hole (SMBH) at its center. There is accumulating evidence that active galactic nuclei (AGN) are able to accelerate protons and electrons to high energies (TeV-PeV), producing high energy gamma rays via leptonic and hadronic processes, and neutrinos via hadronic processes. There is evidence indicating that the acceleration of protons and electrons, and subsequent emission of neutrinos and photons can happen at sub-parsec distances from the central black hole. Coincidentally, adiabatically-growing black holes are expected to form a dark matter spike, with large density, extending over its region of gravitational influence, which is also expected to lie at sub-parsec scales. The scatterings of dark matter particles with standard model particles in the vicinity of the black hole could then suppress the total emitted fluxes of photon and neutrinos, as well as change its spectrum at different energies. In this thesis, we discuss this possibility, by exploring the interactions of dark matter particles with photons, neutrinos, protons and electrons from several multimessenger sources.

The thesis is organized as follows. In section 2 we discuss our current astrophysical and cosmological evidence for dark matter. In section 3, we discuss some historically motivated particle dark matter candidates, focusing on those models to which we have devoted our attention during this thesis. In section 4, we will summarize the different experimental techniques that have been explored over the years to search for particle dark matter, discussing current constraints and prospects for the dark matter candidates proposed in section 3. Then we take a little detour in section 5 to introduce our current knowledge of AGN sources, discussing multimessenger observations, the astrophysical modelling of the neutrino and gamma ray production, as well as cosmic ray acceleration and cooling in the vicinity of the central black hole. In section 6, we discuss the dark matter distribution in galaxies, focusing on the formation of dark matter spikes by adiabatically-growing black holes. In section 7, we discuss the attenuation of standard model particle fluxes from AGN due to scatterings with dark matter particles in the vicinity of black holes, deriving constraints on the scattering cross section of dark matter particles with neutrinos, photons, protons and electrons, and suggesting values that

might help to interpret observations from NGC 1068. Finally, in section 8, we present our conclusions. Further, we provide an additional section of *Varietés* 9, where we present short stories explored during my PhD studies, but which are, in principle, disconnected from the main body of work presented in the thesis. We also present an Appendix A with additional details and information relevant for both the main body of work and the *Varietés*.

Chapter 2

Evidence for dark matter

Although the discussion about the existence of invisible matter in the form of dark stars, dark planets, dark nebulae or dark clouds was already active in the XIX century, [1], it was not until the beginning of the XX century that the first theoretical estimates of the amount of dark matter in the Milky Way were performed. Kelvin, only by using Newtonian mechanics and the kinetic theory of gases, proposed a method to relate the size of the galaxy and the velocity dispersion of stars, concluding from observations that many of them could be extinct and dark, [2]. E.Öpik, J.H. Kapteyn, J.C. Jeans, and J.H. Oort tried to measure the local matter density in the solar neighborhood but did not find compatible results, [3]. It was in two papers of 1933 and 1937, [4, 5], when the first compelling observational evidence of dark matter was found by Zwicky. He applied the virial theorem to the Coma Cluster and estimated a mass-to-light ratio of ~ 500, which could only be explained due to the existence of an additional source of non-luminous matter. After some years in which caveats to Zwicky's publication were discussed, [6] and alternative explanations to the high mass-to-light ratio were provided, [7], the measurement of rotation curves of stars in galaxies of Vera Rubin and collaborators, [8], consolidated the dark matter paradigm.

In this section, we discuss evidence for the presence of dark matter in the Universe. In subsection 2.1, we present compelling astrophysical evidence for the presence of dark matter in galaxies, clusters of galaxies and even larger structures. This evidence requires little to no assumption on the cosmological model of the Universe. In subsection 2.2, we introduce the ΛCDM model in some detail, presenting observational evidence for the presence of dark matter in the Universe and theoretical consistency probes of this model.

2.1 Astrophysical evidence for dark matter

As we discussed previously, the first indication of dark matter in the Universe was derived by Zwicky for clusters of galaxies [4]. A modern estimate for the Coma cluster goes as follows: the amount of gas and galaxies in the Coma cluster is $M \simeq 1.6 \times 10^{14} M_{\odot}$. Using the virial theorem, the average kinetic energy and potential energy in a system are related via

$$2\langle T \rangle + \langle U_{\rm tot} \rangle = 0 \tag{2.1}$$

where the potential energy is

$$|U| = \frac{GM^2}{R} \tag{2.2}$$

and the kinetic energy is

$$T = \frac{1}{2} M \left\langle v^2 \right\rangle = \frac{3}{2} M \left\langle v_{\parallel}^2 \right\rangle \tag{2.3}$$

where $v_{\parallel}$ is the tangential velocity of galaxies. For the measured values of the velocities of galaxies in the Coma cluster, Zwicky found

$$M \simeq 1.9 \times 10^{15} M_{\odot} \tag{2.4}$$

which is ~ 10 larger than visible matter. The estimate done by Zwicky on the mass to light ratio applied to galaxy clusters. A smaller scale probe of the presence of dark matter is given by rotation curves of galaxies. These represent the circular velocity $v_{rot}(r)$ of stars as a function of their distance to the galactic center. For illustration purpose, we can naively assume a spherically symmetric density distribution $\rho(\vec{r}) = \rho(r)$ for the galaxy. From Newtonian mechanics, the shape of the rotation curve can be derived equating the gravitational force produced by the mass enclosed in the sphere of radius r and the centripetal force of an object at this position

$$\frac{GM(r)m}{r^2} = \frac{mv_{rot}^2}{r} \tag{2.5}$$

and

$$v_{rot} = \sqrt{\frac{GM(r)}{r}}, \tag{2.6}$$

where

$$M(r) = \int_0^r 4\pi\rho(r')r'^2 dr'. \tag{2.7}$$

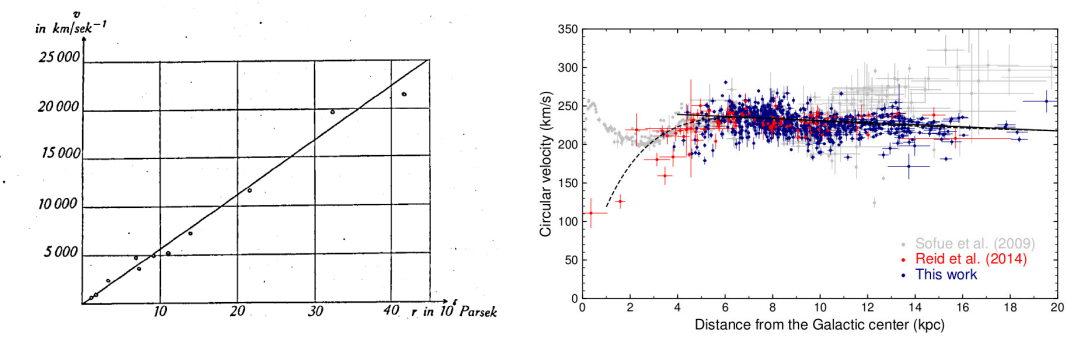

Figure 2.1: *Left panel*: we show an original plot from Zwicky's paper, showing the velocities of extragalactic clusters of galaxies as a function of distance [4]. *Right panel*: recent measurements of the Milky Way rotation curve from classical cepheids, taken from [9].

At the center of the galaxy the density is roughly constant and $v_{rot} \propto r$. This can only approximate the observed rotation curve at the very core of the galaxy, see Figure 2.1.

For stars orbiting the outer part of the galaxy, $M(r)$ is equal to the total mass of the galaxy, thus constant, and $v_{rot} \propto r^{-1/2}$. In the case of spiral galaxies, this approximation is well justified, since they typically present a bulge at the core which contains most of the luminous matter. The prediction for v_{rot} in the outer region of galaxies is incompatible with observations, that show an approximately flat profile in the outskirts of, see Figure 2.1. This discrepancy can be explained by considering an additional, non luminous, source of gravitational potentials present on the galaxy beyond the baryonic disk.

Another astrophysical probe of dark matter arises from the strong gravitational lensing observed from some cluster of galaxies, and the weak gravitational lensing observed from surveys of galaxies.

In general relativity, a point mass deflects light ray with impact parameter b by an angle approximately equal to

$$\hat{\alpha} = \frac{4GM}{c^2 b} \tag{2.8}$$

where G is the gravitational constant, M the mass of the deflecting object and c the speed of light. This is an idealized scenario, but in reality the deflecting objects are not point masses. In the linear approximation of general relativity, and assuming that the deflection is small enough, the born approximation allows to express the deflection from an extended mass as [10]

$$\overrightarrow{\hat{\alpha}}(\vec{\xi}) = \frac{4G}{c^2} \int d^2\xi' \int dz \rho\left(\vec{\xi}', z\right) \frac{\vec{b}}{|\vec{b}|^2}, \vec{b} \equiv \vec{\xi} - \overrightarrow{\xi'} \tag{2.9}$$

where z is the line-of-sight coordinate, and $\vec{b}$ is the vector impact parameter of the actual ray path from the infinitesimal mass $d^2\xi' dz \rho\left(\vec{\xi}', z\right)$ located at the coordinates $\left(\vec{\xi}', z\right)$.

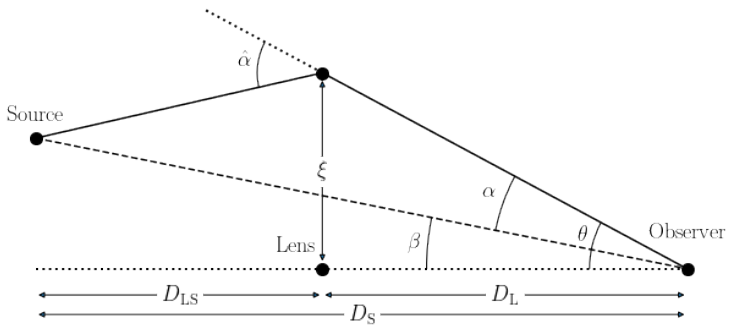

Figure 2.2: Diagram showing the angles and distances involved between source, lens, observer and image

For most astronomical lenses, the distances between the observer, the lens and the

source are much larger than the site of the less, and the deflection angle becomes

$$\overrightarrow{\hat{\alpha}}\left(\vec{\xi}\right) = \frac{4G}{c^2}\int \frac{\left(\vec{\xi}-\vec{\xi}'\right)\Sigma\left(\vec{\xi}'\right)}{\left|\vec{\xi}-\vec{\xi}'\right|^2} d^2\xi' \tag{2.10}$$

where $\Sigma\left(\vec{\xi}'\right) = \int \rho\left(\vec{\xi}', z\right) dz$. This is called the thin lens approximation. The difference between the unlensed angular position $\vec{\beta}$ and the observed position $\vec{\theta}$ is the deflection angle, reduced by a ratio of distances, given by the lens equation (See Figure 2.2 for an schematical view of the angles involved):

$$\vec{\beta} = \vec{\theta} - \vec{\alpha}(\vec{\theta}) = \vec{\theta} - \frac{D_{LS}}{D_S}\overrightarrow{\hat{\alpha}}\left(\overrightarrow{D_L\theta}\right) \tag{2.11}$$

where D_{LS} is the distance from the lens to the source, D_S is the distance from the observer to the source, and D_L is the distance from the observer to the lens. The Jacobian between the unlensed and lensed coordinate systems is

$$\frac{\partial\beta_i}{\partial\theta_j} = \delta_{ij} - \frac{\partial\alpha_i}{\partial\theta_j} = \delta_{ij} - \frac{\partial^2\psi}{\partial\theta_i\partial\theta_j} \tag{2.12}$$

where $\psi(\vec{\theta})$ is the deflection potential of the lens

$$\psi(\vec{\theta}) = \frac{2D_{LS}}{D_L D_S c^2}\int \Phi\left(D_L\vec{\theta}, z\right) dz \tag{2.13}$$

depending on a scaled projection of the gravitational potential Φ of the lens. This formalism is valid for strong gravitational lensing.

Strong gravitational lensing from clusters can produce arcs, multiple images (thus multiple solutions of equation 2.11) or Einstein rings, and the mass distribution of the cluster can be inferred from it. Confrontations of these measurements with the masses inferred from electromagnetic observations allows to estimate the dark matter mass of the cluster.

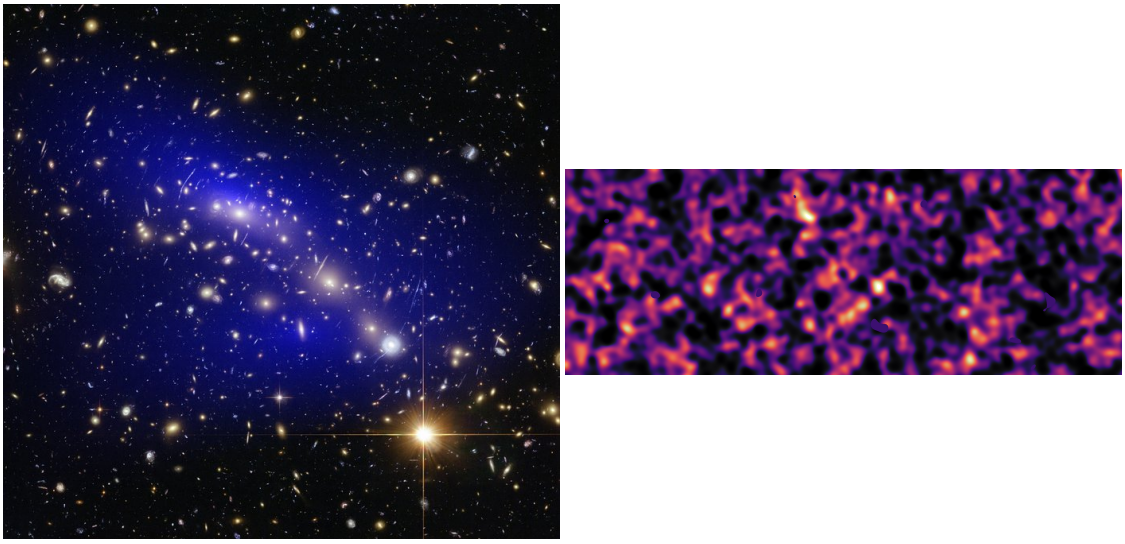

Figure 2.3: *Left panel*: Lensing image of the galaxy cluster MACS J0416.1-2403, where the inferred dark matter distribution is shown in blue color [11]. *Right panel*: Dark matter map for a patch of sky based on cosmic shear analysis of a Kilo-Degree survey, where the dark matter is shown as coloured regions over the baryonic (dark) regions [12].

However, in most situations, the deflection angle induced from a single background source is too small to be detected. In this case, by means of a systematic alignment of background sources around the lensing mass, the foreground mass can still be inferred. This technique is called weak gravitational lensing. A variant of weak gravitational lensing that has provided maps of the dark matter distribution in large patches of the sky is known as cosmic shear. The gravitational lensing by large-scale structure induces an intrinsic alignment in background galaxies, but his effect is subtle compared to lensing by clusters of galaxies or galaxy lensing, with a distortion of only $\sim 0.1\% - 1\%$. The thin lens approximation does not always work in this regime, because structures can be elongated along the line of sight. Instead, the distortion can be derived by assuming that the deflection angle is always small. In this case, the deflection can be derived from assuming that the gravitational potential is slowly varying everywhere. As in the thin lens case, the effect can be written as a mapping from the unlensed angular position $\vec{\beta}$ to the lensed position $\vec{\theta}$, but in this case the Jacobian of the transform can be written as an integral over the gravitational potential Φ along the line of sight

$$\frac{\partial \beta_i}{\partial \theta_j} = \delta_{ij} + \int_0^{r\infty} \mathrm{drg}(r) \frac{\partial^2 \Phi(\vec{x}(r))}{\partial x^i \partial x^j} \tag{2.14}$$

where r is the comoving distance, x^i are the transverse distances, and

$$g(r) = 2r \int_r^{r\infty} \left(1 - \frac{r'}{r}\right) W\left(r'\right) \tag{2.15}$$

is the lensing kernel, defining the efficiency of lensing for a distribution of sources $W(r)$. In the left panel of figure 2.3, we show an image obtained with strong gravitational lensing from the cluster of galaxies MACS J0416.1-2403, with a map of the inferred dark matter distribution shown in blue color. In the right panel of the figure we show an image of a patch of the sky obtained by cosmic shear with the Kilo-Degree survey (KiDS), that support the presence of dark matter (coloured in the plot) in large scale structures, and that suggests that dark matter may be more smoothly distributed throughout space than in standard cosmological scenarios.

Since the observation in 2006 of the galaxy cluster 1E0657-558, the Bullet Cluster, [13], collisions of galaxy clusters have also been argued as a proof of the existence of dark matter. These works typically construct a map of the gravitational potential using weak gravitational lensing, which measures the distortions of images of background galaxies caused by the gravitational deflection of light by the cluster's mass. While this shows that most of the matter remains in the individual clusters after the collision, the thermal X-ray emission map shows that most of the baryonic matter is concentrated in the collision region. This can be appreaciated in the left panel of Figure 2.4

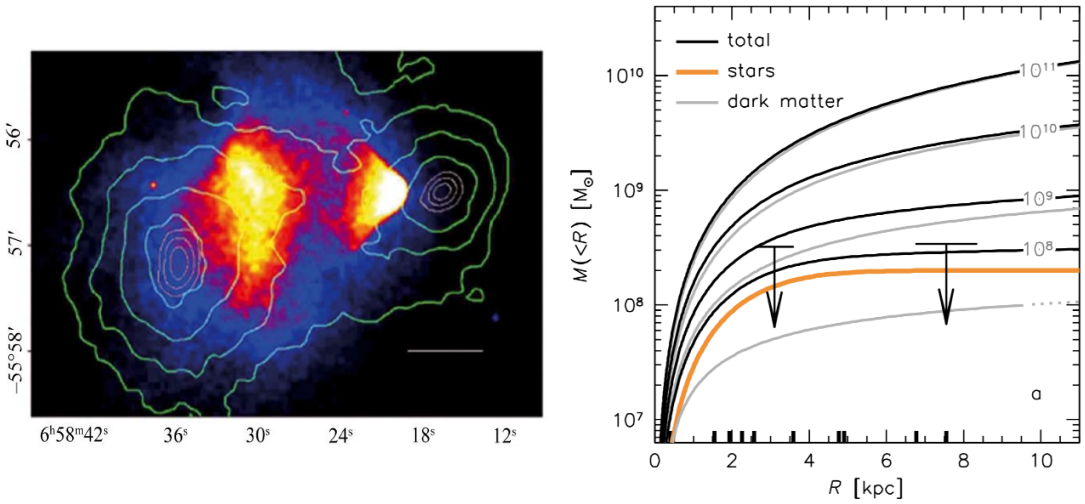

Figure 2.4: *Left panel*: Gravitational lensing and electromagnetic maps of the Bullet Cluster, [13]. The green contours show the weak-lensing reconstructions, and the color gradient is the thermal X-ray emmission map. The center of the gravitational potential are shifted with respect to the strongest X-ray emission regions of the plasma. *Right panel*: Enclosed mass profiles for NFW halos of different masses as a function of radii in NGC1052–DF2, confronted with the stellar mass profiles and the upper limits on the total mass obtained in [14]. The dynamical mass of NGC1052–DF2 is consistent with the stellar mass, and the dark matter halo is significantly lighter than expected.

This effect has been observed not only in the Bullet Cluster but on several further colliding galaxies. Since there is ~ 5 times more mass in the form of gas than stars, the

discrepancy between the weak lensing map and the thermal X-ray emission can only be explained by the presence of dark matter. In this interpretation stars and dark matter move nearly collisionless away from the center of the collision, while baryonic matter from both cluster interacts electromagnetically and remains in the center. The observation of collisions of galaxy clusters challenge the so-called MOND (Modified Newton Dynamics) theories, which propose that the gravitational evidence for dark matter is due to a modification of the law of gravity at large scales, [15].

Some observations of dark matter-free galaxies also provide evidence for the dark matter paradigm [14, 16]. Studies of the radial velocities of objects within the ratio of mass of the dark matter halo and the mass of baryonic matter is of order unity, and consistent with zero. This can be appreciated in the right panel of Figure 2.4. Violent astrophysical processes during galaxy formation, such as mergers, are expected to disrupt the dark matter content of a galaxy in certain cases. However, in modified gravity theories, a dark matter-like signature should always be detected, since it is an unavoidable consequence of the presence of ordinary matter. Indeed, For a typical MOND acceleration scale of $a_0 = 3.7 \times 10^3$ km^2 s^2 kpc^1 the expected velocity dispersion of NGC1052–DF2 is $\sigma \sim (0.05 G M_* a_0)^{1/4} \sim 20$ km s^{-1}, two times larger than the upper limit on the observed velocity dispersion.

2.2 Cosmological evidence for dark matter

It was Hubble in a paper in 1929 who provided a firm observational evidence for a linear relation between distance d and recession velocity v of galaxies, the Hubble's law [17]. [1]

$$v = Hd. \tag{2.16}$$

In his paper, Hubble plots the velocities and distances of 24 nebulae, with speeds up to about 1000 km/s (i.e. a redshift around 0.03), see Figure 2.5. To obtain them he used the brightest star and Cepheid methods.

[1] Theoretical and observational grounds for the expansion of the Universe were already present during the 1910's and 1920's. Other authors deserve relevance for Hubble's turning point paper, particularly Slipher, who was the first to measure the redshift of an extragalactic nebula [18].

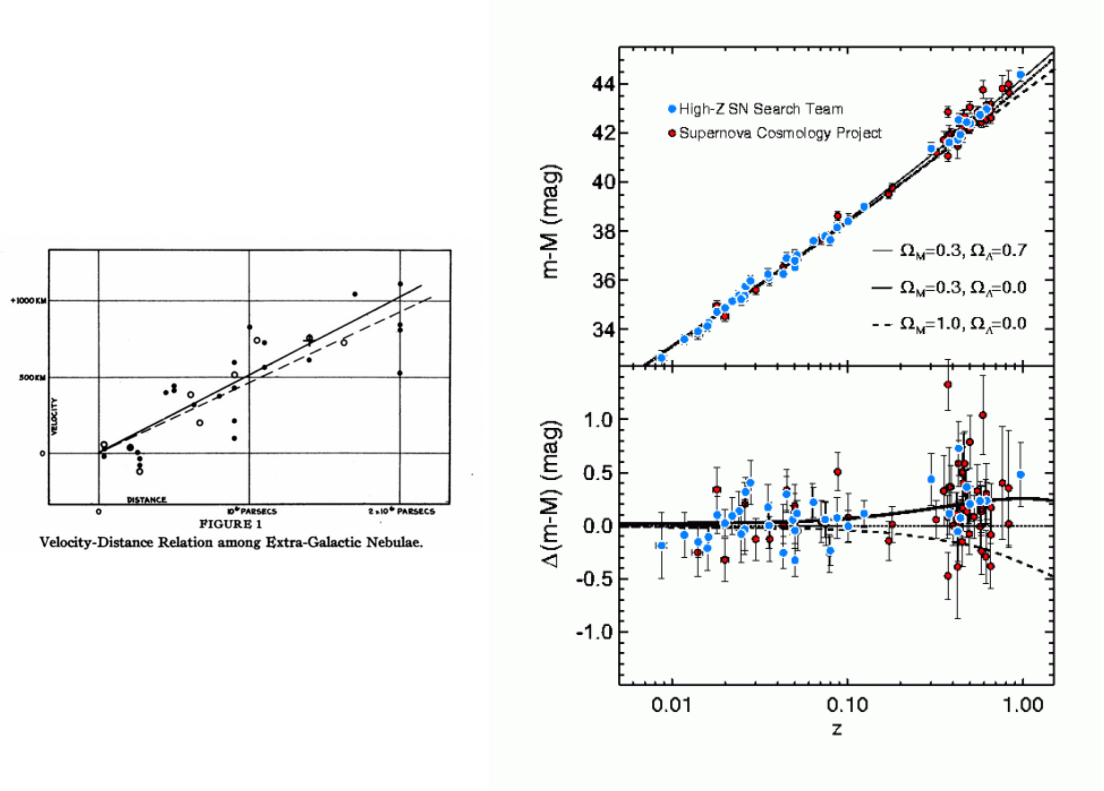

Figure 2.5: *Left panel*: Original plot from Hubble's paper in 1929. Radial velocities, corrected for solar motion, are plotted against distances estimated from involved stars and mean luminosities of nebulae in a cluster [17]. *Right panel*: Distance vs redshift for Type Ia Supernovae, as done by two independent groups, the High-z Supernova Search Team [19] and the Supernova Cosmology Project [20]. The lines represent the expectations for different cosmological models. They represent an Einstein-de Sitter model in which the universe is completely dominated by matter ($\Omega_M = 1$, $\Omega_\Lambda = 0$), a universe with less matter ($\Omega_M = 0.3$, $\Omega_\Lambda = 0$), and a model consistent with all supernova data corresponding to $\Omega_M = 0.3$, $\Omega_\Lambda = 0.7$). The lower panel show the same diagram normalised to the model of an empty universe. It can be appreciated that the distant supernovae lie above the line for an empty universe and require some contribution by the cosmological constant.

Since Hubble's discovery, additional evidence for the expansion of the Universe has been obtained, and two independent groups showed via the study of type I supernovae that the Universe is not only expanding, but it does so in an accelerated way [19, 20], see the right panel of Figure 2.5.

The expansion of the Universe stems from the cosmological principle, which assumes that at first approximation, the universe is homogeneous and isotropic. The accelerated expansion of the Universe helped further to establish the ΛCDM model of cosmology,

where the expansion of the Universe is driven by dark energy, a prediction of Einstein equations given by the cosmological constant, and the Universe also contains dark matter in addition to baryonic matter.

An expanding universe can be described by the Friedmann-Lemaitre-Robertson-Walker (FLRW) metric [21].

$$ds^2 \equiv g_{\mu\nu}dx^\mu dx^\nu = -dt^2 + a(t)^2\left(\frac{dr^2}{1-kr^2} + r^2 d\Omega^2\right) \tag{2.17}$$

where $a(t)$ is the scale factor of the Universe, and k is the curvature parameter. The homogeneity of the FLRW background implies $\partial_i P^\mu = 0$, and after some manipulations one can show that

$$\frac{\dot{p}}{p} = -\frac{\dot{a}}{a} \rightarrow p \propto \frac{1}{a} \tag{2.18}$$

Thus, the physical three-momentum of any particle (both massive and massless) decreases with the expansion of the universe. This allows to establish a connection of the scale factor with the physical redshift, since the wavelength of a photon is $\lambda = h/p$, one finds

$$z \equiv \frac{\lambda_0 - \lambda_1}{\lambda_1} \rightarrow 1 + z = \frac{1}{a\left(t_1\right)} \tag{2.19}$$

where $a(t_0) \equiv 1$ has been defined. Now it is possible to recover Hubble's law, motivated by observations of distant nebulae in 1929, just from the starting assumption of a FLRW metric. The scale factor at time t_1 may be expanded in series

$$a\left(t_1\right) = a\left(t_0\right)\left[1 + \left(t_1 - t_0\right)H_0 + \cdots\right] \tag{2.20}$$

where H_0 is the Hubble constant [2]

$$H_0 \equiv \frac{\dot{a}\left(t_0\right)}{a\left(t_0\right)}. \tag{2.21}$$

and then $z = H_0\left(t_0 - t_1\right) + \cdots$. For close objects, $t_0 - t_1$ is the physical distance d (in units with $c = 1$). Thus, the redshift increases linearly with distance

$$z \simeq H_0 d. \tag{2.22}$$

And the slope in a redshift-distance diagram measures the current expansion rate of the universe, H_0. To deal with uncertainties in those measurements, it became conventional to define

$$H_0 \equiv 100h\mathrm{kms}^{-1}\mathrm{Mpc}^{-1}, \tag{2.23}$$

[2] The physical velocity of an object is $v^i_{\mathrm{phys}} \equiv \frac{dx^i_{\mathrm{phys}}}{dt} = a(t)\frac{dx^i}{dt} + \frac{da}{dt}x^i \equiv v^i_{\mathrm{pec}} + Hx^i_{\mathrm{phys}}$ which has two contributions, the so-called peculiar velocity (velocity measured by a comoving observer), $v^i_{\mathrm{pec}} \equiv a(t)\dot{x}^i$, and the Hubble flow, Hx^i_{phys}, where the Hubble parameter is defined as $H \equiv \frac{\dot{a}}{a}$

where the parameter h is used to keep track of how uncertainties in H_0 propagate into other cosmological parameters. Today, our measurements of H_0 are more precise, see Table 2.2.

The evolution of the universe is determined by the Einstein equation

$$G_{\mu\nu} = 8\pi G T_{\mu\nu} \tag{2.24}$$

which relates the Einstein tensor $G_{\mu\nu}$ to the stress-energy tensor $T_{\mu\nu}$, relating curvature and matter content of the Universe. The stress-energy tensor of a perfect fluid reads

$$T^{\mu}_{\nu} = (\rho + p)U^{\mu}U_{\nu} - p\delta^{\mu}_{\nu} \tag{2.25}$$

where $U^{\mu} \equiv dx^{\mu}/ds$ is the relative four-velocity between the fluid and the observer, and ρ and p are the energy density and pressure in the rest-frame of the fluid. Conservation of energy and momentum in minkowski space translate into the following conservation equation for the stress energy tensor

$$\partial_{\mu}T^{\mu}_{\nu} = 0 \rightarrow \dot{\rho} + 3\frac{\dot{a}}{a}(\rho + P) = 0 \tag{2.26}$$

leading to the continuity equation. The time-independent equation of state for pressure and density $\omega = p/\rho$ thus determined the evolution of the energy density of the different components of the universe with the scale factor. In ΛCDM, The universe is composed of cold dark matter ($w = 0$), radiation ($w = 1/3$) and vacuum energy ($w = -1$), therefore

$$\rho \propto a^{-3(1+w)} \tag{2.27}$$

and

$$\rho \propto \begin{cases} a^{-3} & \text{matter} \\ a^{-4} & \text{radiation} \\ a^{0} & \text{vacuum} \end{cases} \tag{2.28}$$

Solving Einstein equations for the FLRW metric and the energy-momentum tensor of a perfect fluid yields the Friedmann equations

$$\frac{\dot{a}^2}{a^2} = \frac{8\pi G}{3}\rho - \frac{k}{a^2} \tag{2.29}$$

and

$$\frac{\ddot{a}}{a} = -\frac{4\pi G}{3}(\rho + 3p) \tag{2.30}$$

we note that the first friedmann equation indicates that the Hubble rate $H \equiv \dot{a}/a$ represents the expansion rate of the Universe. For a flat universe with $k = 0$ we can thus determine the critical density of the Universe today:

$$\rho_{\text{crit}} = \frac{3H_0^2}{8\pi G} = 2.8 \times 10^{11} h^2 M_{\odot}\text{Mpc}^{-3} \tag{2.31}$$

and the ratio of the energy density of a given species and the critical density of the Universe is typically used

$$\Omega \equiv \frac{\rho}{\rho_c}. \tag{2.32}$$

The friedmann equation can be written as

$$\frac{H^2}{H_0^2} = \Omega_r a^{-4} + \Omega_m a^{-3} + \Omega_k a^{-2} + \Omega_\Lambda. \tag{2.33}$$

where $\Omega_k \equiv -k/\left(H_0\right)^2$, and all the fractional energy densities are defined at $a(t) = a_0$. The observed values of the cosmological parameters can be extracted from the cosmic microwave background (CMB) anisotropies and are given in Table 2.2 [22]. From the friedmann equations and the continuity equation, one can track the evolution of the scale factor and the different epochs of the history of the Universe, where different forms of matter dominated the energy budget of the universe. For a flat Universe, one finds

$$a(t) \propto \begin{cases} t^{1/2} & \text{radiation domination} \\ t^{2/3} & \text{matter domination} \\ e^{Ht} & \text{dark energy domination} \end{cases} \tag{2.34}$$

The matter and radiation fractional energy densities become equal at $z_{eq} \sim 3300$, shortly before the cosmic microwave background (CMB) was released.

Cosmological Parameters (Planck 2018)	
Hubble constant	$H_0 = 67.4 \pm 0.5$ km/s^{-1}Mpc^{-1}
Baryonic matter	$\Omega_b h^2 = 0.0224 \pm 0.0001$
Dark Matter	$\Omega_{\mathrm{DM}} h^2 = 0.120 \pm 0.001$
Dark Energy	$\Omega_\Lambda = 0.6889 \pm 0.0056$

The Cosmic Microwave Background (CMB) radiation is one of the most compelling arguments in favour of dark matter. In the early stages of the universe, at the time of recombination (redshift $z \approx 1100$), radiation decoupled from matter and since then, photons travelled freely. The almost perfect black-body CMB spectrum shows the temperature (2.728 K), or the inverse wavelength, of the microwaves that we receive on Earth from these early times, see Figure 2.6. When looking closely at this spectrum, one finds fluctuations in the μK scale, [22].

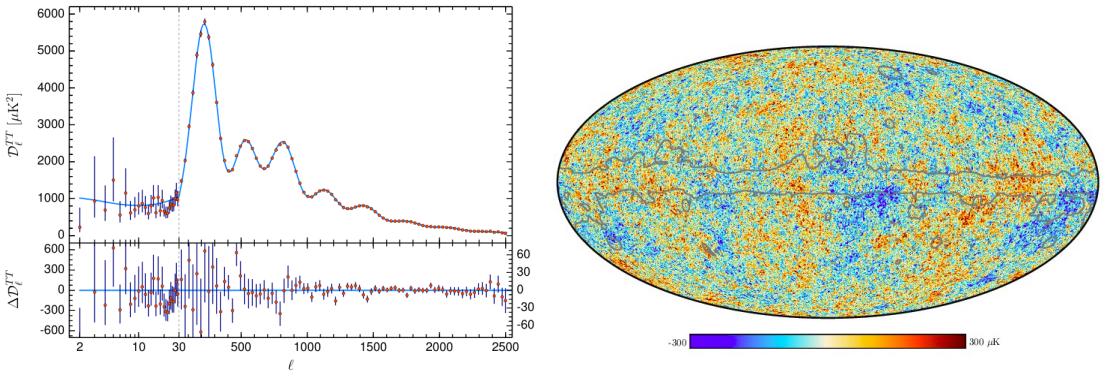

Figure 2.6: *Left panel*: Planck satellite measurement of the CMB angular power spectrum in terms of the multipole moment l, [22]. The first peak is correlated with the amount of baryonic matter. The measured position and height of the second and third peaks are consistent with a dark matter abundance of roughly 5 times higher than baryonic matter. *Right panel*: Planck satellite sky map of the CMB temperature anisotropies

The temperature anisotropies of the CMB are explained as baryon acoustic oscillations, [23]. Previous to the recombination era, when the free electrons still strongly scattered the photons of the cosmic plasma, this rang with sound waves excited by the initial perturbations of the inflaton field [24]. The photon radiation pressure keeps the ionized gas from clustering, and this pressure leads to relativistic sound waves that propagate until the plasma becomes neutral at recombination. The mechanism then freezes and CMB photons carry information about the baryonic density profile in their temperature profile. Photons coming from dense baryonic regions loose energy by escaping the gravitational potential and are redshifted. On the other hand, photons coming from diluted regions are blueshifted with respect to the average CMB photon temperature. This is called the Sachs-Wolfe effect [25]. Since the coupling of dark matter and baryons to photons is different, the power spectra of temperature and polarization fluctuations depend crucially on the ratio between both components.

Another comological probe of dark matter corresponds to redshift $z \approx 4 \times 10^8$, when Big Bang nucleosynthesis takes place and light elements are formed [26]. It starts with the production of deuterium and ends up with the production of helium

$$p + n \rightarrow {}^2\mathrm{H} + \gamma \tag{2.35}$$

$$ {}^3\mathrm{H} + {}^2\mathrm{H} \rightarrow {}^4\mathrm{He} + n, \tag{2.36}$$

though low probability reactions up to ^{7}Li also occured. While the fraction of baryons that make up the helium abundance is mainly sensitive to the n/p ratio at the time of nucleosynthesis [26], which from Boltzmann statistics is $\sim 1/7$ and leads to $\sim 25\%$ of the mass of baryons forming helium ^{4}He, the deuterium, helium ^{3}He and ^{7}Li abundances depend on the baryon density at the time of nucleosynthesis, see Figure 2.7.

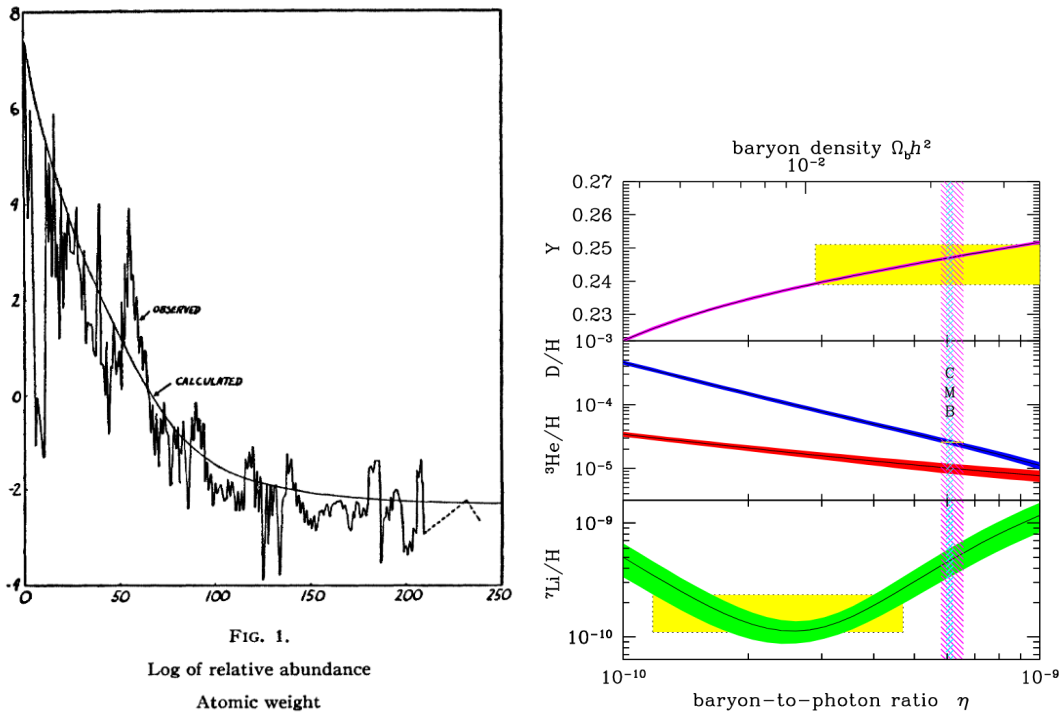

Figure 2.7: *Left panel:* Original figure from the seminal paper on Big Bang Nucleosynthesis [26]. It shows the relative abundances of various nuclear species, which decrease rapidly for the lighter elements and remain approximately constant for the elements heavier than silver. *Right panel:* Primordial abundances of light elements as a function of the baryon density relative to photons and the CMB observations. The bands show the 95%CL range. Boxes indicate the observed light element abundances. The narrow vertical band indicates the CMB measure of the cosmic baryon density, while the wider band indicates the BBN $D + {}^4\mathrm{He}$ concordance range (both at 95% CL), [27]

Deuterium, due to its stability (binding energy of 2.2 MeV), is a good thermometer of the baryon density at nucleosynthesis, since it is only destroyed hereafter, like in the evolution of starts, but never enduringly produced. Therefore, the amount of deuterium, but also of other light elements in the universe can be used to set an upper limit in the baryon density. Therefore BBN, which provides a measure of the baryon density, indicates the existence of dark matter when combined with the measure of the matter density coming from the CMB.

Another cosmological probe steams from baryon acoustic oscillations (BAO) imprints on sky surveys, aside from its impact on the angular power spectrum of the CMB. In the early universe, dark matter and baryons gradually clustered together after the epoch of recombination. On small scales, BAO will be damped due to non-linear structure formation. On larger scales, there is currently no theoretical reason to expect systematic distortions greater than $\sim 1\%$ in the BAO positions between the galaxies and the linear

matter distribution, and this small effect was indeed confirmed in 2005 through comprehensive galaxy redshift surveys, notably the Sloan Digital Sky Survey and the 2dF Galaxy Redshift Survey. Further, Galaxy redshift surveys also allow to map the galaxy distribution in the Universe. These maps are distorted due to the method employed to estimate distances from observed redshifts. The redshift of a galaxy is influenced not only by the dominant Hubble expansion term but also by the galaxy's peculiar velocity. Thus, the average expansion rate of superclusters should be slower than cosmic mean due to their gravity, and voids should expand faster on average. Remarkably, this feature was observed in the 2dF Galaxy Redshift Survey, showing agreement with ΛCDM.

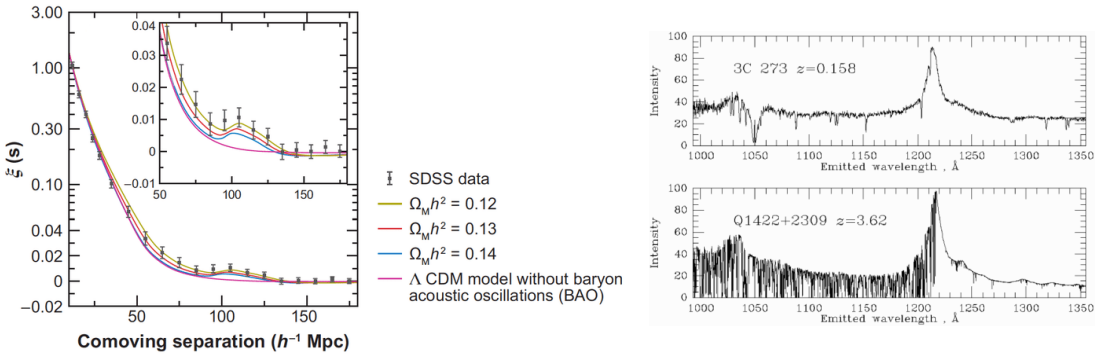

Figure 2.8: *Left panel*: Two-point galaxy correlation function in redshift space from SDSS data. The detection of the baryon acoustic peak in the clustering of luminous red galaxies in the Sloan Digital Sky Survey can be clearly appreciated [28]. *Right panel*: Spectrum of the nearby quasar 3C273 (above) vs another quasar at high redshift. The clouds that produce the absorption lines are much more numerous at high redshifts, as can be appreaciated in the dense array of absorption lines results. Thus, the Lyman-alpha forest.

Finally, the pattern of absorption lines from the Lyman-α transition of neutral hydrogen in the spectrum of distant galaxies and quasars also provides insights on the distribution of galaxies in the Universe and its large-scale structure, and probes to be consistent with ΛCDM. Further, the formation of structures such stars, galaxies and clusters of galaxies from the initial density perturbations require the presence of dark matter. Ordinary matter interacts with radiation, and the universe is radiation dominated at early times. Consequently, the perturbations would be washed out by radiation before structures can be formed. Dark matter solves this problem since it is not affected so strongly by radiation, and density perturbations can grow. This is perhaps not a probe of dark matter but another theoretical consistency check of ΛCDM.

Chapter 3

Particle dark matter candidates

Since the advent of the ΛCDM cosmological model, a variety of particles arising in beyond the standard model (BSM) scenarios have been proben to be able to account for the dark matter of the Universe. Here, we introduce some particle dark matter candidates proposed over the years, discussing model-building, early universe production and some detection aspects. There are plenty of viable dark matter candidates not shown in this list. We will be focusing on those scenarios that have been studied phenomenologically at some point in this thesis, paying particular attention to light dark matter candidates.

3.1 Neutrinos

The only electrically neutral and long-lived particles in the Standard Model are neutrinos, and since they are massive [29], they become natural dark matter candidates.

Bounds on neutrino masses from their impact in cosmology were already derived in the 60's and 70's [30, 31]. These works set the stage for a work from Szalay and Marx not only deriving bounds on neutrino masses, but also suggesting the possibility that neutrinos with $m_\nu \sim 10$ eV may account for the dark matter of the Universe. Later on, Hut, Lee and Weinberg simultaneously pointed out that neutrinos with masses $m_\nu \gtrsim 2$ GeV can be produced in the Big Bang with a relic abundance that does not overclose the Universe [32, 33].

A few years later, a variety of papers appeared discussing the possibility that neutrinos may actually constitute the dark matter of the Universe, based on a preliminary measurement of the neutrino mass with tritium beta decay of 30 eV, which was later probed wrong [34, 35]. In fact, the current upper limit on the electron antineutrino mass from KATRIN, $m_\nu \lesssim 0.9$ eV is incompatible with neutrinos being the dark matter of the Universe [36].

Here we summarize this argument. Neutrinos remain in thermal equilibrium up to temperatures of a few MeV due to weak interactions with other standard model particles, then they freeze-out. The relic density of neutrinos can be calculated as [37]

$$n_\alpha = \frac{6}{4}\frac{\zeta(3)}{\pi^2} T_\nu^3 \tag{3.1}$$

where $T_\nu \simeq (4/11)^{1/3} T_\gamma \simeq 1.96$ K $\simeq 10^{-4}$eV^2. The matter density of neutrinos at the time when they are non relativistic is given by the sum of neutrino masses

$$\rho_\nu \simeq n_\alpha \sum m_i \tag{3.2}$$

So, in order for neutrinos to constitute the total relic abundance, this sum should be about 11.5 eV [38].

Another probe of neutrinos not being the majority of the dark matter of the Universe arised from early cosmological simulations of structure formation [39]. Neutrinos constitute hot-dark matter and would form large structures first, then fragmented into smaller halos, while cold dark matter particles would form larger structures hierarchically. As we already mentioned in section 2.2 The data from galaxy surveys agrees with the cold dark matter paradigm [40]. Further, the phase space density of fermionic dark matter dominated objects should not be larger than the density of degenerate Fermi gas. This allows to derive an independent lower bound of a few eV on the mass of fermionic dark matter particles, from the observations of dwarf galaxies, the so-called Tremainne-Gunn bound[41, 42].

3.2 Sterile neutrinos

One of the simplest beyond the standard model theories consists in including a singlet fermion to its matter content, ν_R. The gauge and Lorentz symmetries then allow for a Majorana mass term and Yukawa couplings to the standard model lepton doublet L

$$\mathcal{L}_{\nu_R} = \frac{1}{2}\overline{\nu_R^c} i \not{\partial} \nu_R - \frac{1}{2} m_{\nu_R} \overline{\nu_R^c} \nu_R - y \bar{L} \nu_R \widetilde{H} + \text{ h.c. } , \tag{3.3}$$

where $\widetilde{H} = i\tau_2 H^*$, with H the Standard Model Higgs doublet. These singlet fermions are denoted sterile neutrinos or right handed neutrinos due to their Yukawa coupling y to the active neutrinos ν in the lepton doublet $L = (\nu, e_L)$, and may explain the smallness of the active neutrino masses via the see-saw mechanism [43–47]. In the original formulations of the see-saw mechanism, the smallness of the active neutrino masses stems from $\sim v/m_{\nu_R}$, where $v = 174$ GeV is the Higgs field expectation value. Therefore, the predicted mass of the sterile neutrinos is much larger than the electroweak scale. However, in order for sterile neutrinos to constitute the dark matter of the Universe, they need to be stable in cosmological timescales. The decay into three active neutrinos $\nu_R \to \nu\nu\nu$ sets an upper limit on the sterile neutrino mass and mixing to active neutrinos [48, 49]

$$\theta^2 < 3.3 \times 10^{-4} \left(\frac{10\text{keV}}{m_{\nu_R}} \right)^5 \tag{3.4}$$

where $\theta^2 \equiv \sum_{\alpha=e,\mu,\tau} |\theta_\alpha|^2$. This bound implies that the contribution of sterile neutrino dark matter to the neutrino masses is smaller than the solar neutrino mass difference. Thus, at least two more sterile neutrinos are typically invoked to explain the neutrino masses, allowing for the third state to be a dark matter candidate.

Thermal sterile neutrinos would overclose the Universe when freezing-out via annihilations (see next section for a specific discussion in the context of the WIMP). Non-thermal production of sterile neutrinos in the early Universe avoid this complication, and were originally proposed by Dodelson and Widrow [50]. In their set-up, if sterile neutrinos constitute the dark matter, perturbations on scales smaller than

the Jeans length $\lambda_J \equiv \left(\pi v_s^2 m_{\rm Pl}^2/\rho\right)^{1/2}$ (where v_s is the speed of sound) oscillate like pressure waves. Further, perturbations on scales smaller than the freestreaming scale $\lambda_{\rm FS} \equiv a\int_0^t dt' \left\langle (p/E)^2 \right\rangle^{1/2}/a\left(t'\right)$ are exponentially damped, see Figure 3.2

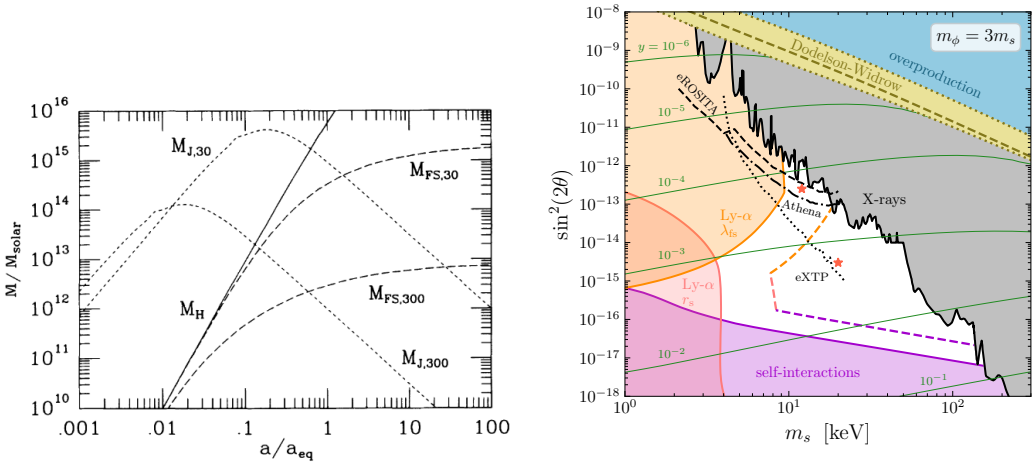

Figure 3.1: *Left panel:* Figure from the original paper from Dodelson and Widrow proposing light sterile neutrinos as a dark matter candidate [50]. It shows the mass scales in hot dark matter and warm dark matter as a function of scale factor. M_H gives the mass within the horizon, M_{FS}, M_J gives the freestreaming/Jeans mass for a 30 eV and 300 eV sterile neutrino. Similarly the Jeans mass of these neutrinos is shown. For light neutrinos, the damping and horizon scales are similar at matter-radiation equality, while for sterile neutrino dark matter there is a large disparity between the scales. *Right panel:* Available parameter space in the sterile neutrino mixing vs mass, assuming neutrino self interactions with a scalar mediator with mass $m_\phi = 3m_{\nu_R}$. Green lines show values of the Yukawa coupling that can reproduce the dark matter relic abundance. The Dodelson-Widrow mechanism is ruled out by X-ray observations, and sterile neutrinos lighter than ~ 4 keV are ruled out by Lyman-alpha considerations, but there is still a region of the parameter space awating to be tested [51].

Aside from the dominant decay channel into three channels, the sterile neutrino also decays radiatively into an active neutrino and a photon $\nu_R \to \nu + \gamma$[1]. The decay width of this process is [55]

[1]This decay proceeds via a magnetic moment, which is suppressed in the SM and hardly detectable $\mu_\nu = \frac{eG_F m_\nu}{8\sqrt{2}\pi^2} = 3\times 10^{-20}\mu_B\left(\frac{m_\nu}{0.1\text{eV}}\right)$. However, in extensions of the SM, the neutrino magnetic moment might be enhanced by orders of magnitude, eg [52–54], allowing its testability with current and future solar and reactor neutrino experiments. Most of these proposals invoke new physics at the TeV scale.

$$\Gamma_{\nu_R \to \gamma\nu} = \frac{9\alpha G_F^2}{256\pi^4}\theta^2 m_{\nu_R}^5 = 5.5 \times 10^{-22}\theta^2 \left[\frac{m_{\nu_R}}{1\text{keV}}\right]^5 \text{sec}^{-1}. \tag{3.5}$$

Which is suppressed by ~ 2 orders of magnitude w.r.t the main decay channel. However, it produces a monochromatic photon with energy $E = \frac{1}{2}m_{\nu_R}$, which could be distinguisable from other continuum astrophysical backgrounds of photons reaching the Earth, specially from regions with large dark matter column densities. A few years ago, an unidentified X-ray line at $E \sim 3.5$keV was detected from Galaxy clusters, Andromeda and the Milky way, which could be explained by sterile neutrino dark matter with a mass of $m_{\nu_R} \sim 7$ keV and a mixing angle of $\theta \sim 10^{-10}$, varying by less than an order of magnitude depending on the choice of the dark matter profile of these clusters and galaxies [56–58]. However, the non-instrumental or astrophysical origin of the signal is disputed, and the parameter space favoured for sterile neutrino dark matter explaining the observation is contrived by X-ray observations [59–61]. More complicated but also motivated scenarios can allow for a region of the keV sterile neutrino parameter space to be able to account for the dark matter of the Universe [62–67], and be in the reach of future X-ray experiments, see e.g the right panel of Figure 3.2.

3.3 Axions

The strong-CP problem refers to the fact that QCD lagrangian contains the CP-violating term

$$\mathcal{L}_{\text{QCD}} \supset \bar{\Theta}\frac{g^2}{32\pi^2}G^{a\mu\nu}\tilde{G}_{a\mu\nu}, \tag{3.6}$$

where $G^{a\mu\nu}$ is the gluon field strength tensor and $\bar{\Theta}$ is related to the phase of the QCD vacuum. Non-perturbative effects give rise to an electric dipole moment of the neutron, which is however constrained. This sets an upper limit on the CP-violating phase of $\bar{\theta} \lesssim 10^{-10}$, which is believed to be unnaturally small.

One possibility to solve this problem was proposed by Peccei and Quinn in 1977 [68], introducing a new global $U(1)$ symmetry along with a complex scalar field that spontenously breaks the symmetry, and $\bar{\theta}$ is driven to zero. Soon after, Wilczek and Weinberg independently pointed out that the breaking of the Peccei-Quinn symmetry below the electroweak scale gives rise to a pseudo-Nambu-Goldstone boson, named the axion [69, 70]. The axion becomes massive due to the Peccei-Quinn symmetry being broken by the chiral anomaly, yielding an axion mass of $m_a \sim f_\pi m_\pi / f_a$, where f_π is the m_π are the pion decay constant and mass, and f_a is the axion decay constant, related to the scale where the Peccei-Quinn symmetry is broken.

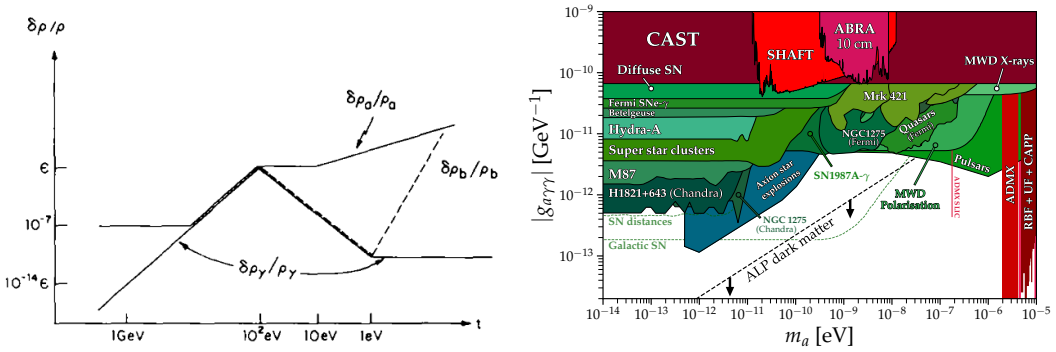

Figure 3.2: Original figure from one of the pioneering papers on axion dark matter, from Axenides, Brandenberger and Turner [71]. It shows the time evolution of of galactic scale ($10^{12} M_\odot$) fluctuations for baryons, photons and axions. In the radiation dominated era ($T \sim 100 - 10$eV), the axion overdensity spectrum $\delta\rho_{\rm a}/\rho_{\rm a}$ does not grow, while the primordial photon and baryon fluctuations start to decrease due to the Silk damping. In the matter dominated era but before recombination ($T \sim 10 - 1$eV), axion fluctuations grow as $t^{2/3}$, while the photon and the baryon fluctuations continue to decrease. After recombination, the Silk damping has ended and the baryon fluctuations quickly follow the axion fluctuations. Because the photon is decoupled, the primordial photon perturbations stay the same. *Right panel:* Parameter space of axion-photon coupling vs axion photon mass [72]. Values below the dotted black line allow for axion to compose the dark matter of the Universe [73–75]. Bounds from a variety of observables approach this region [76–78], which is however yet poorly tested.

Soon after the axion was proposed, different groups noticed that the energy density stored in the oscillations of the classical axion field does not dissipate rapidly, which sets un upper limit on the decay constant of $f_a \lesssim 10^{12}$ GeV, otherwise the axion density would overclose the universe [79–81]. These works probed that axions may comprise the dark matter of the Universe. Depending on whether the Peccei-Quinn phase transition occurs before or after inflation, the axion dark matter density is determined by a a harmonic motion, or via the Kibble mechanism forming topological deffects in the Peccei-Quinn field [82]. Besides the so-called QCD axion, Axion Like Particles (ALPs) unable to solve the QCD problem but sharing similar features with the axion have been proposed as a potential dark matter candidate. The axion and ALP parameter space able to comprise the dark matter of the Universe still remains largely unconstrained for axion masses $m_a \lesssim 1$ eV, see the right panel of Figure 3.3 showing a compilation of constraints on the axion-photon coupling vs axion mass from a variety of astrophysical, cosmological and laboratory probes.[2].

[2] Axion also couple to gluons and electrons, and the parameter space of those couplings look differently. For electrons, the yukawa coupling leads to compton-like inelastic processes $e\gamma \to ea$. In section 7.3 we will consider a variant of this scenario, where the ALP couples to a dark matter fermion.

3.4 WIMPS

Supersymmetric particles were soon identified as a potential Weakly Interacting Massive particle (WIMP) candidate. Early discussions on the role of supersymmetry in cosmology hinted the possibility of gravitinos (the supersymmetric partner of the graviton) accounting for the dark matter of the Universe [32, 83]. However, it was with the advent of the Minimal Supersymmetric Standard Model (MSSM) that several other supersymmetric candidates began to be considered [84]. The stringent constraint on the proton lifetime required the introduction of and additional symmetry, named R-parity:

$$R = (-1)^{2s+3B+L} \tag{3.7}$$

where s is the spin of the particle, and B and L correspond to the baryon and lepton numbers of the particle. All supersymmetric particles have opposite parity than standard model ones. There is an additional consequence of this symmetry, since it implies that the lightest supersymmetric particle is stable, and thus, a potential dark matter candidate. A few following works were important in establishing the lightest supersymmetric particle as a dark matter candidate, and in particular the case of the photino [85–88]. Collider, direct and indirect detection possibilities were addressed soon after [88–90][3].

An additional supporting argument in favour of supersymmetric particles arised from the apparent coincidence between the relic density of dark matter of the Universe, and an interaction cross section of the electroweak scale, as predicted in the freeze-out mechanism. When the WIMP annihilation rate became comparable to the expansion rate of the Universe, the WIMPs freeze-out from equilibrium with the thermal plasma, i.e

$$\Gamma_{\mathrm{DM}} H \sim \frac{T_f}{M_{pl}} \tag{3.8}$$

where T_f is the freeze-out temperature and M_{pl} is the planck mass.

For a given annihilation rate $\Gamma_{\mathrm{ann}} = n_\chi \langle \sigma_{\mathrm{ann}} v \rangle$, the dark matter relic abundance at T_f can be can be expressed in terms of the thermally averaged dark matter annihilation cross section, σ_{ann} , and the Møller velocity, $v_{\mathrm{Møl}} = \sqrt{(\vec{v}_1 - \vec{v}_2)^2 - (\vec{v}_1 \times \vec{v}_2)^2}$ [92–94].

$$\Omega_{\mathrm{DM}} h^2 \simeq \frac{m_{\mathrm{DM}} n_{\mathrm{DM}}\,(T_0)}{\rho_c} h^2 = \frac{T_0^3}{\rho_c} \frac{x_f}{M_{pl}} \frac{1}{\langle \sigma_{\mathrm{ann}} v_{\mathrm{Møl}} \rangle_f} h^2, \tag{3.9}$$

where $T_0 \approx 2.35 \times 10^{-13}\mathrm{GeV}$ is the temperature of the Universe today, $\rho_c \approx 8 \times 10^{-47} h^2 \mathrm{GeV}^4$ is the critical energy density, $x_f = m_{\mathrm{DM}}/T_f$ and $\vec{v}_{1,2}$ are the velocities of both annihilating DM particles. Note that Møller velocity is equal to the relative velocity of two DM particles $|\vec{v}_1 - \vec{v}_2|$ in the center-of-mass frame.

The freeze-out value of x_f is estimated by assuming that the number density of WIMPs is equal to the the non-relativistic equilibrium number density $n_{\mathrm{DM}} \approx n_{\mathrm{DM,\,eq}} \simeq g_{\mathrm{DM}} \left(m_{\mathrm{DM}} T / 2\pi\right)^{3/2} \exp\left(-m_{\mathrm{DM}}/T\right)$, where g_{DM} is the number of degrees of freedom for

[3] The first explicit mention on the possibility of supersymmetric particles comprising the dark matter of the Universe was done by Pagels and Primack [83, 91].

the dark matter particles. Taking the value measured by Planck, $\Omega_{\rm DM}h^2 \approx 0.12$ one finds $x_f \approx 25$ for $m_{\rm DM} \approx 100{\rm GeV} - 10{\rm TeV}$. Using these values in equation 3.9, one finds that the correct relic abundance is found for

$$\langle \sigma_{\rm ann} v \rangle_f \approx 3 \times 10^{-26}\ {\rm cm}^3/{\rm s}, \tag{3.10}$$

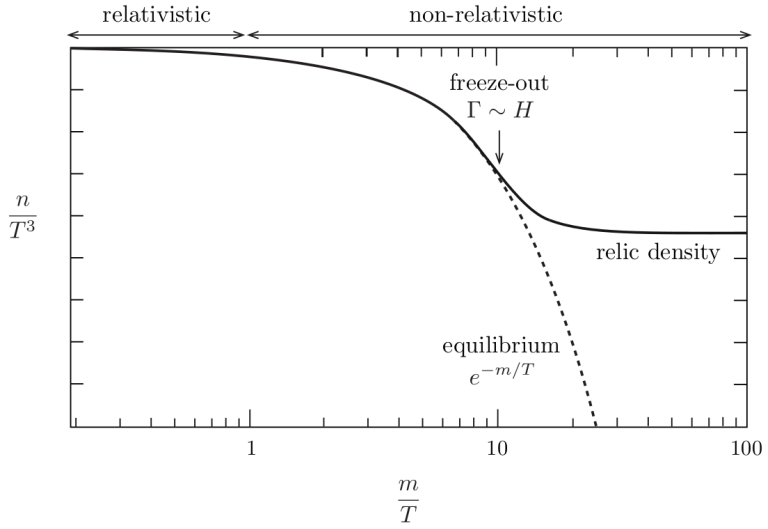

Figure 3.3: Scheme of the freeze-out mechanism [21]. At high temperatures, $T \gg m$, the dark matter abundance follows its equilibrium distribution. When the Hubble rate and the interaction rate become comparable, the particles freeze out and maintain a density that is much larger than the Boltzmann-suppressed equilibrium abundance. For larger values of the thermally averaged self-annihilation cross section, the dark matter particle decouples later, and the relic density today becomes smaller.

For typical velocities $v \sim 0.1$c one obtains a cross section typical of the electroweak scale, say $\sigma \sim G_F^2 T_f^2$, with G_F the Fermi constant, and $T_f \sim m_\chi/25$. This apparent coincidence has been dubbed as the WIMP "miracle".

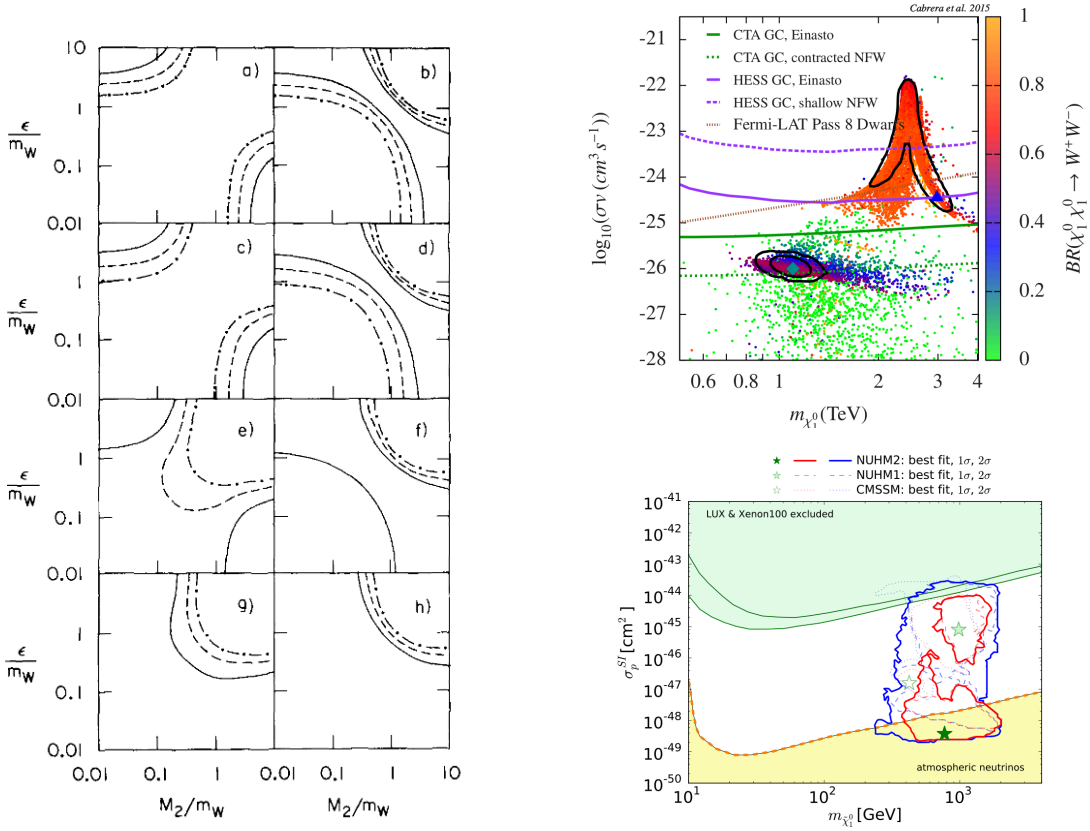

Figure 3.4: *Left panel:* Original plot from the pioneering work on supersymmetric relics from Ellis, Hagelin, Nanopoulos, Olive and Sredinicki [88]. It shows mass contours for neutralinos (solid = 20GeV, dashed = 30GeV, dot-dashed = 40GeV) as functions of the Higgsino gauge coupling $|\varepsilon|$ and the Wino mass M_2. Each plot represents a different choice of the vacuum expectation values of the Higgs doublet superfields (v_1/v_2) and the sign of the gauge coupling (ε) : (a) $v_1 = v_2, \varepsilon > 0$; (b) $v_1 = v_2, \varepsilon < 0$; (c) $v_1 = 2v_2, \varepsilon > 0$; (d) $v_1 = 2v_2, \varepsilon < 0$; (e) $v_1 = 4v_2$, $\varepsilon > 0$; (f) $v_1 = 4v_2, \varepsilon < 0$; (g) $v_1 = 8v_2, \varepsilon > 0$; (h) $v_1 = 8v_2, \varepsilon < 0$. *Right panel:* The upper plot shows model predictions on the parameter space of neutralino self-annihilation cross section into W bosons vs the neutralino mass, in the phenomenological minimal supersymmetric standard model (pMSSM), confronted with constraints from dark matter indirect detection searches and future projections [95]. The lower plot shows model predictions in the parameter space of neutralino-nucleon spin-independent scaterring cross section vs neutralino mass, in the constrained MSSM (CMSSM) and Non-Universal Higgs model (NUHM) [93, 96, 97]. In all three realizations of supersymmetry there are neutralino compositions that evade current constraints.

The reasoning of the final years of the last century was at play: The naturalness

and the hierarchy problem suggested new physics at the electroweak scale, and the relic density of dark matter particles in the universe is consistent with those scales within the freeze-out paradigm, so the WIMP was clearly theoretically well motivated. A posteriori, one can argue that the freeze-out is indeed a simple and elegant explanation of the dark matter relic abundance, but its prediction is not unique of the electroweak scale. Indeed, the cross section will typically be determined by ratios of couplings and the dark matter and mediator mass, yielding consistent values of the relic abundances in a wider range, $m_{\rm DM} \sim 10$ MeV-10 TeV [98, 99]. While the freeze-out is simple, the supersymmetric candidates at the electroweak scale are far from that adjective, since these theories involve plenty of additional parameters unrelated to the dark matter mass and interaction strength. However, despite some efforts and unjustified claims based on the stringent bounds from dark matter direct and indirect detection searches (See sections 4.2 and 4.3 for a detailed treatment), it is worth stressing that the WIMP is far from being ruled out. Only the simplest scenarios, where the dark matter is produced thermally, and its portal to the SM proceeds via a Z-boson or a Higgs begun to be seriously constrained in recent years [100–104][4]. Other WIMP proposals beyond the lightest supersymmetric particle still remain viable, such as singlet scalars, the scotogenic model, t-channel mediators, or multi-component dark matter, among other models [107–110]. In the next section we discuss inelastic dark matter in some detail, a scenario which is not subject to the stringent constraints from direct detection experiments.

3.5 Inelastic dark matter

The stringent limits on the elastic scattering cross-section of WIMPs discussed in previous section do not necessarily hold in scenarios where the dark matter particle cannot scatter elastically with a nucleus or an electron. This seemingly strong assumption naturally arises in some models. For instance, the elastic scattering mediated by vector current is forbidden for Majorana dark matter χ, due to the Majorana nature of fermion: $\bar{\chi}\gamma^\mu\chi = 0$ [111]. However, Majorana dark matter particles may leave an imprint in direct search experiments if they could scatter inelastically producing a heavier Majorana fermion χ' in the final state, since there is an off-diagonal fermion current $\bar{\chi}'\gamma^\mu\chi \neq 0$. This scenario is approximately realized in the Minimal Supersymmetric Standard Model, when the lightest supersymmetric particle is almost a pure Higgsino state, and the other supersymmetric particles are very heavy. In this case, the elastic scattering of the Higgsino dark matter is suppressed by the large sfermion and gaugino masses, while it has a large inelastic scattering cross section by the electroweak gauge interactions [112, 113]. Scenarios of inelastic dark matter have also been motivated phenomenologically, *e.g.* in

[4] In [105] we provided a method to combine the results of several experiments in probing the non-relativistic effective theory (NREFT) of dark-matter nucleon interactions, accounting for interferences among operators. While some operators of the effective theory are strongly constrained from the combination of experiments, others remain untested in certain directions of parameter space, particularly those coherent operators expected to dominate the scattering with nucleons in most UV complete models. Further, astrophysical uncertainties can affect upper limits by 1 to 2 orders of magnitude at most, as we studied in [106]

[112, 114–126].

In the following, we will discuss two simplified scenarios where the elastic scattering channel of dark matter particles with nucleons is suppressed with respect to the inelastic one[5]. First, if the dark matter particle is a real scalar, its vector coupling to nuclei is forbidden by Bose symmetry. Consider a complex scalar $\phi = \frac{1}{\sqrt{2}}(a + ib)$ coupled to an Abelian gauge field A_μ. Its vector interaction comes from

$$|D_\mu \phi|^2 \supset -g A_\mu \left(a\partial^\mu b - b\partial^\mu a\right) \tag{3.11}$$

The real scalars a and b are degenerate if the only mass term is $-m^2|\phi|^2$, but introducing a small additional mass term $-\delta^2\phi^2 +$ h.c., splits this degeneracy. The additional mass term breaks gauge invariance, but in can arise once the gauge symmetry is broken. This example is realized in the minimal supersymmetric standard model where sneutrinos constitute the dark matter, and the scale of the mass splitting is naturally predicted as $\delta \sim 100$keV.

Inelastic dark matter can also be realized for fermionic particles. A dark matter Dirac fermion $\psi = (\eta\bar{\xi})$ has vector and axial-vector couplings to quarks:

$$\bar{\psi}\gamma_\mu \left(g'_V + g'_A\gamma_5\right) \psi \bar{q}\gamma^\mu \left(g_V + g_A\gamma_5\right) q \tag{3.12}$$

If the couplings are all of comparable order, the largest contribution to the low-energy scattering of ψ off nuclei will come from the vector-vector term, which will yield an amplitude that scales roughly as the number of nucleons. The axial-axial piece yields a smaller spin-dependent contribution, and the vector-axial pieces is suppressed in the non-relativistic limit.

If, in addittion to a dominant Dirac mass term for ψ, the Lagrangian also contains a small Majorana mass term

$$\frac{\delta}{2}(\eta\eta + \bar{\eta}\bar{\eta}) \tag{3.13}$$

the Majorana fermion mass eigenstates are

$$\chi_1 \simeq \frac{i}{\sqrt{2}}(\eta - \xi)m_1 = m - \delta \tag{3.14}$$

$$\chi_2 \simeq \frac{1}{\sqrt{2}}(\eta + \xi)m_2 = m + \delta. \tag{3.15}$$

The vector current couples χ_1 to χ_2, with a small additional contribution $\sim \delta/m$ coupling each mass eigenstate to itself:

$$\bar{\psi}\gamma_\mu\psi \simeq i\left(\bar{\chi}_1\bar{\sigma}_\mu\chi_2 - \bar{\chi}_2\bar{\sigma}_\mu\chi_1\right) + \frac{\delta}{2m}\left(\bar{\chi}_2\bar{\sigma}_\mu\chi_2 - \bar{\chi}_1\bar{\sigma}_\mu\chi_1\right) \tag{3.16}$$

And one can see that the elastic scattering channel is supressed by δ/m χ_1. There is still a spin-dependent elastic scattering channel available, but the inelastic process

[5] Similar realizations have been discussed in the literature for leptophilic inelastic dark matter scattering with electrons, see e.g [127–132]

will dominate given that the coherent enhancement a factor $\sim A^2$ overcomes than the suppression due to the inelasticity. Therefore, heavy targets are ideal to probe inelastic dark matter models.

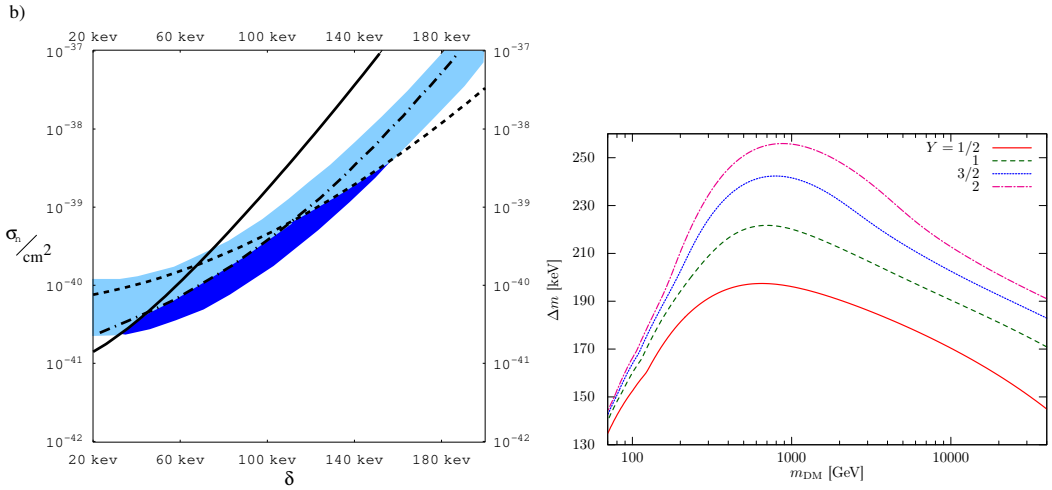

Figure 3.5: *Left panel:* Region satisfying both DAMA and CDMS constraints in the inelastic dark matter mass splitting and cross section plane $\delta - \sigma_n$ plane (in dark blue), for (a) $m_\chi = 50$GeV, (b) $m_\chi = 100$GeV, (c) $m_\chi = 300$GeV [133].*Right panel:*Lower bound on the mass splitting as functions of the DM mass, for different values of the dark matter hypercharge Y [112]

Inelastic dark matter models initially received attention in the early 2000's as a possible explanation to the DAMA dark matter signal compatible with constraints from the CDMS experiment, see the left plot of the Figure 3.5, where a region of parameter space compatible with the signal and other constraints is shown in blue [133]. Today, the constraints on the mass splitting between the two dark matter states are much stronger, but mass splittings of the order keV, motivated by Supersymmetry, still remain viable for electroweakly-interacting dark matter with hypercharge Y, see the right plot of Figure 3.5[6].

3.6 Light dark matter

The stringent limits derived on the dark matter coupling to nucleons with direct detection experiment are relaxed at sub-GeV dark matter masses due to the limitation of experiments to measure low-energy recoils in the detector. The parameter space of sub-GeV dark matter is therefore not so strongly constrained, and several proposals have

[6]The maximum mass splitting probed by experiments is limited by their recoil energy range of interest, and by the velocity of the dark matter particle. In the *Varieté* 9.1.3, we derive enhanced constraints and prospects for the detection of inelastic dark matter from the flux of non-galactic dark matter particles at Earth, whose velocities are larger than the escape velocity of the Milky Way.

been put in recent years to probe this region of the parameter space with a variety of observables, as well as trying to construct models that can induce the observed relic abundance of dark matter.

Historically, light fermions were disfavoured by the so-called Lee-Weinberg bound [33] [7]. The result from Lee and Weinberg implied that the lightest supersymmetric particle, stable via R-parity, cannot be significantly lighter than a few GeV in order to reproduce the dark matter relic abundance. This bound, however, does not apply if the dark matter particle is a scalar or pseudoscalar particle, as initially pointed out by Boehm, Ensslin, Silk and Fayet [137, 138].

If the dark matter particles self-annihilate, and neglecting co-annihilations, the annihilation cross section required for a thermal relic is approximately [139].

$$\sigma v \simeq 6 \times 10^{-27} \times \frac{x_f}{\sqrt{g_\star}} \left(\frac{\Omega_{\rm DM} h^2}{0.12} \right)^{-1} \ {\rm cm}^3 {\rm s}^{-1} \tag{3.17}$$

where

$$x_f = m_{\rm DM}/T_f \simeq 17.2 + \ln\left(g/g_\star\right) + \ln\left(m_{\rm DM}/{\rm GeV}\right) + \ln\sqrt{x_f} \tag{3.18}$$

which is mildly dependent on the dark matter mass. For particles in the MeV-GeV range, $x_f \sim 12 - 19$ and g, $g_\star$ are the number of internal and relativistic degrees of freedom, respectively. It was shown in [138] that these values can be achieved for MeV scalar dark matter candidates with non-chiral couplings to standard model fermions, while respecting astrophysical and cosmological constraints in some regions of the parameter space (for a detailed review, see [140]).

An interesting alternative to evade the Lee-Weinberg bound while having thermal light dark matter fermions consists in introducing an asymmetry in the number density of dark matter particles vs antiparticles, in analogy to baryons [141]. In this case, there is a connection between the dark matter and baryon densities that can explain the close ratio of abundances

$$\frac{\rho_{\rm DM}}{\rho_B} \sim 5 \tag{3.19}$$

suggesting $m_{\rm DM} \sim 5$ GeV, although lower values of the dark matter mass are possible, depending on the model. In this scenario, the dark matter relic abundance is not determined by the self-annihilating cross section, but it is mostly dependent on its mass $m_{\rm DM}$. [8]. Defining the present day dark matter-anti dark matter ratio as $\eta_{\rm DM} = \frac{\Omega_{\bar{\rm DM}}}{\Omega_{\rm DM}}$, the required light dark matter annihilation cross section at freeze-out to achieve a particular

[7] Piet Hut submitted a paper a few weeks before Lee and Weinberg, noticing already that neutral relics from the Big Bang with masses above 3 GeV wouldn't overclose the Universe [32]. Lee and Weinberg's merit was perhaps that they acknowledged explicitely that heavy neutral leptons could close the Universe. It is worth mentioning that other works appeared in the following weeks arriving to similar conclusions [134–136]

[8] The underlying idea of asymmetric dark matter had been explored already in the 80's and 90's, where several authors attempted to connect the dark matter and baryon asymmetries via electroweak sphalerons [142–145].

residual symmetric component $\eta_{\rm DM}$ is [146, 147]

$$\langle\sigma v\rangle_f \simeq \frac{s_0 x_f}{0.264\Omega_{\rm DM}\rho_c\sqrt{g_{*,f}}M_{\rm pl}}\ln\left(\frac{1}{\eta_{\rm DM}}\right) \simeq c_f \times 5\times 10^{-26}\ {\rm cm}^3/{\rm s}\times\ln\left(\frac{1}{\eta_{\rm DM}}\right), \quad (3.20)$$

where c_f is an $\mathcal{O}(1)$ factor. $s_0 \approx 2969.5\ {\rm cm}^{-3}$ and $\rho_c \approx 1.0540h^2\times 10^4{\rm eV/cm}^3$ are the entropy density and critical density today. The CMB sets a bound on the annihilation cross section when $\eta_{\rm DM} \ll 1$ (see [148, 149])

$$\langle\sigma v\rangle_{\rm CMB} < \frac{2.42\times 10^{-27}\ {\rm cm}^3/{\rm s}}{2f}\left(\frac{m_{\rm DM}}{1{\rm GeV}}\right)\left(\frac{1}{\eta_{\rm DM}}\right) \quad (3.21)$$

where f gives the efficiency of energy deposition at redshift z and thus depends on the spectrum photons, neutrinos and $e^{\pm}$ resulting from light dark matter annihilation. The dependence of $f(z)$ on z is generically mild. For dark matter annihilation channels to charged leptons or pions, $f \sim 0.2-1$, while it is $f \sim 1$ for annihilation only to $e^{\pm}$. Then, for s-wave annihilation, one can combine equations 3.20 and 3.21 to place a lower bound on the thermal asymmetric dark matter annihilation cross section in order to reproduce the relic abundance and evade CMB constraints [147]

$$\frac{\langle\sigma v\rangle_f}{c_f\times 5\times 10^{-26}\ {\rm cm}^3/{\rm s}} \gtrsim \begin{cases} \ln\left(40c_f f\times\frac{1{\rm GeV}}{m_{\rm DM}}\right)+\ln\ln\left(40c_f f\times\frac{1{\rm GeV}}{m_{\rm DM}}\right), & m_{\rm DM}\lesssim f\times 10{\rm GeV} \\ 2 & ,m_{\rm DM}\gtrsim f\times 10{\rm GeV} \end{cases} \quad (3.22)$$

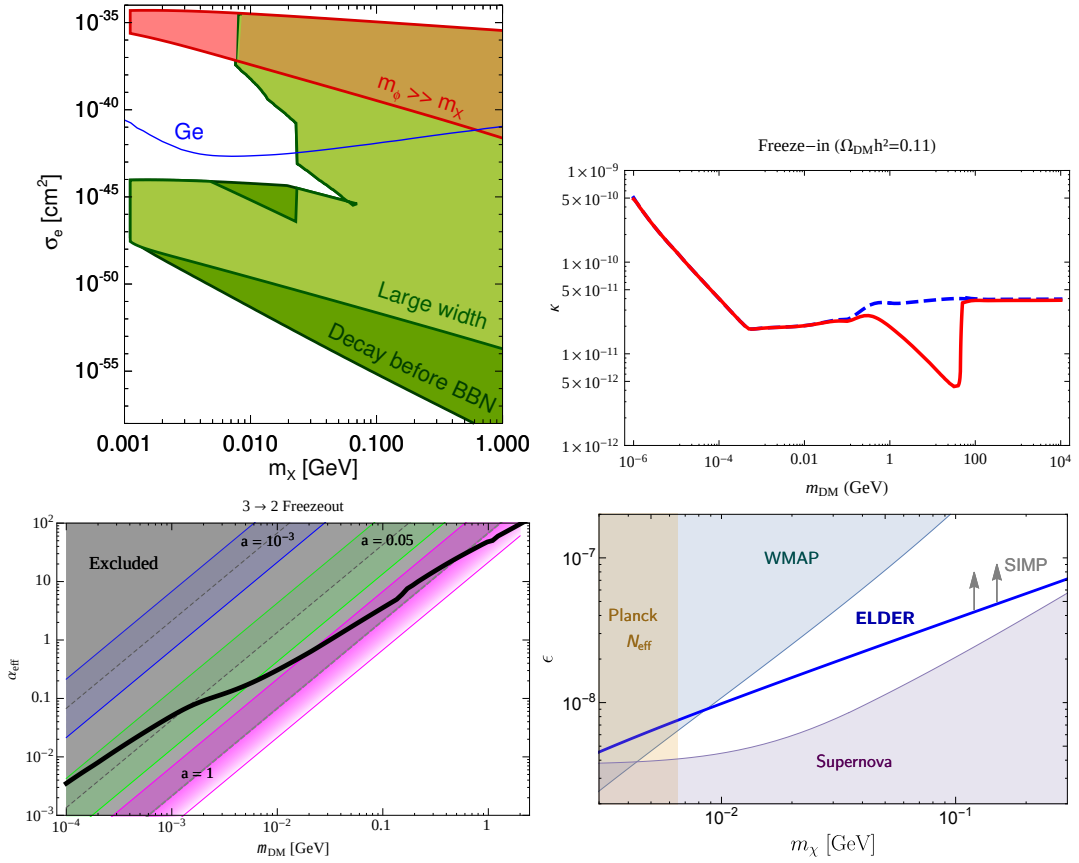

Figure 3.6: *Upper left panel:* Parameter space of light dark matter-electron scattering cross section vs mass, for a vector mediator m_ϕ. The green region may account for the DM relic abundance for $m_\phi m_{\rm DM}$, and the red region for $m_\phi \gg m_{\rm DM}$ [147]. *Upper right panel:* Combination of values of dark matter coupling strength to the standard model (parametrized as $\kappa \equiv \epsilon \cos\theta_W \sqrt{\alpha'/\alpha(1-\epsilon^2)}$) vs dark matter mass that reproduce the relic abundance via freeze-in in the vector mediator model [150]. The red line shows the contribution of both the γ and Z channels, and the dashed blue line is only for the γ. *Lower left panel:* Effective coupling between the dark and standard model sectors $\alpha_{\rm eff}$ as a function of the DM mass (black solid line) in the $3 \to 2$ freeze-out scenario. Coloured regions show values motivated by small scale structure anomalies [151]. *Lower right panel:* Combinations of parameters favoured in the Elastically Decoupling dark matter model (ELDER) confronted with constraints from different observables [152].

Another interesting alternative to evade the Lee-Weinberg bound arises when considering strongly interacting dark matter particles. It was shown in [151, 153] that thermal dark matter may freeze-out via $3 \to 2$ processes, where three dark matter particles inter-

act producing two dark matter particles. Then, a small kinetic mixing between the dark and the visible sectors is needed in order for the two sectors to thermalize. A generalized geometric mean can give an idea of the typical thermal relic mass in this scenario, in analogy to the WIMP miracle

$$m_{\rm DM} \sim \alpha_{\rm eff} \left(T_{\rm eq}^2 M_{\rm Pl}\right)^{1/3} \sim 100{\rm MeV} \tag{3.23}$$

where $\alpha_{\rm eff}$ is the effective coupling constant of the self-interacting dark matter, and $T_{\rm eq}$ is the matter-radiation equality temperature. In this setup, the dark sector must be in thermal equilibrium with the standard model sector while the $2 \to 2$ annihilation into standard model particles is suppressed. These authors found that this can be realized for values of the coupling strength in the range $10^{-9} \lesssim \epsilon \lesssim 3 \times 10^{-6}$.

In previously discussed scenarios, the dark matter relic density is determined via processes that change dark matter quantum number. In [152], a mechanism for thermal light dark matter was proposed, where the freeze-out happens via elastic scatterings of dark matter particles off standard model particles. This mechanism is similar to the SIMP, but here the elastic scattering process decouples first while the self-annihilation process remains active. This is different from the SIMP case, where the self-annihilation process is the first to decouple. The range of coupling values that allows to reproduce the relic abundance are however similar to the SIMP case, hence this mechanisms are difficult to distinguish in practice.

Another possibility that has received attention in recent years consists in light dark matter not being produced thermally. Hall, Jedamzik, March-Russell and West proposed that dark matter may not be in thermal equilibrium with the standard model plasma after inflation, due to is extremely weak interactions with the bath particles [154]. Despite its feeble interactions, the dark matter could be produced when the temperature of the Universe drops below its mass, assuming the dark matter is heavier than the standard model particles to which is coupled. The abundance of dark matter then "freezes-in" with a yield that increases as the interaction strength between the dark matter and the standard model becomes larger.

Whereas for the conventional freeze-out just the dark matter particle is of interest for the determination of the dark matter abundance, in the freeze-in mechanism both the feebly interacting massive particle (FIMP) and the lightest particle in the thermal bath that carries the symmetry (LOSP) are important. The freeze-in mechanism requires particles of very long lifetime

$$\Gamma_{\rm freeze-in} \sim \lambda^2 m \sim \frac{v^3}{M_{\rm PL}^2} \tag{3.24}$$

where m is the mass of the FIMP or the LOSP, $m \sim v$ and $\lambda \sim v/M_{\rm PL}$. The heavier of the LOSP and FIMP will generically decay to the lighter one with a short lifetime.

The freeze-in mechanism is dominated by decays or inverse decay, and the relic density is obtained for couplings

$$\lambda \simeq 1 \times 10^{-12} \left(\frac{m_\phi}{m_{\rm DM}}\right)^{1/2} \left(\frac{g_* \left(m_\phi\right)}{10^2}\right)^{3/4}. \tag{3.25}$$

where ϕ is the LOSP, and the LOSP decay rate is $\Gamma_\phi = \lambda^2 m_\phi / 8\pi$ [154][9].

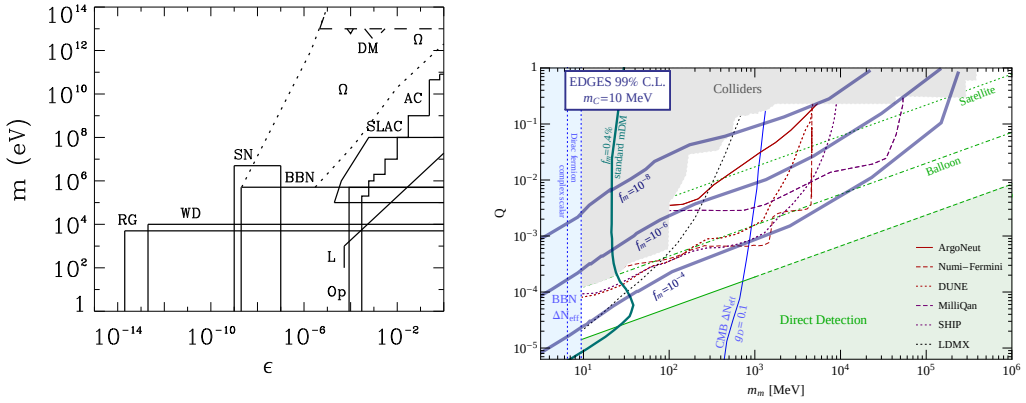

Figure 3.7: *Left plot*: Early compilation of constraints on the millicharged dark matter mass vs kinetic mixing from astrophysics, cosmology and laboratory probes, from Davidson, Hannestad and Raffelt [157]. *Right plot*: Current constraints on the parameter space of millicharged dark matter [158]. The green region is constrained by direct detection experiments, the grey region is constrained by collider searches, and the region on the left of the thin blue line is constrained by measurements of $N_{\rm eff}$ [159]. Projections from several experiments are shown in dotted lines, and the thick dark blue line show regions of the parameters pace that can explain the 21-cm signal from EDGES, for different values of the fractional density of millicharged DM w.r.t to the total DM density of the Universe.

So far, we have argued the possibility of achieving the dark matter relic abundance when the dark matter particle is light, but no concrete particle physics model has been discussed. Let us conclude the section by discussing a simple $U(1)$ extension of the standard model under which the dark matter particle is charged, since this is the benchmark model used for light dark matter phenomenological studies. Let us start with the most general lagrangian corresponding to two gauge groups $U(1)$ and $U(1)'$ [160–162]

$$\mathcal{L}_0 = -\frac{1}{4}(F_{\mu\nu}F^{\mu\nu} + F'_{\mu\nu}F'^{\mu\nu}) - \frac{\epsilon}{2}F'_{\mu\nu}F'^{\mu\nu} + eJ_\mu A^\mu + J'_\mu A'^\mu \tag{3.26}$$

where the gauge boson A^μ couples to the SM current, and the "paraphoton" or "dark photon" A'^μ couples to the dark matter, with e and e' coupling constants, and ϵ is the kinetic mixing between the field strenght tensors. For now, we focus on the case in which the dark photon is massless. The kinetic terms can be diagonalized by rotating the gauge fields with the following transformation

[9] Some variations of the original formulation of the freeze-in mechanism leading to viable light dark matter particles are [155, 156]

$$\begin{bmatrix} \frac{1}{\sqrt{1-\epsilon^2}} & 0 \\ \frac{-\epsilon}{\sqrt{1-\epsilon^2}} & 1 \end{bmatrix} \begin{bmatrix} \cos\theta & -\sin\theta \\ \sin\theta & \cos\theta \end{bmatrix} \tag{3.27}$$

where θ is an arbitrary angle as long as the paraphoton is massless. The lagrangian becomes

$$\mathcal{L} = \left[\frac{e'\cos\theta}{\sqrt{1-\varepsilon^2}}J'_\mu + e\left(\sin\theta - \frac{\varepsilon\cos\theta}{\sqrt{1-\varepsilon^2}}\right)J_\mu\right]A'^\mu + \left[-\frac{e'\sin\theta}{\sqrt{1-\varepsilon^2}}J'_\mu + e\left(\cos\theta + \frac{\varepsilon\sin\theta}{\sqrt{1-\varepsilon^2}}\right)J_\mu\right]A^\mu \tag{3.28}$$

For the choice of the arbitrary angle $\theta = \arctan\left[\epsilon/\sqrt{1-\epsilon^2}\right]$ one gets

$$\mathcal{L}' = e'J'_\mu A'^\mu + \left[-\frac{e'\varepsilon}{\sqrt{1-\varepsilon^2}}J'_\mu + \frac{e}{\sqrt{1-\varepsilon^2}}J_\mu\right]A^\mu \tag{3.29}$$

and we can see that the paraphoton is coupled only to the dark current J'_μ while the SM photon is coupled to both currents, with strength $\varepsilon e/\sqrt{1-\varepsilon^2}$ to the dark one. Thus, if the paraphoton is massless the dark matter is millicharged. This is a very economical set up with only three free parameters, the kinetic mixing ϵ, the gauge coupling e', and the dark matter mass[10].

The paraphoton may however be massive. The Stückelberg mechanism may generate a mass term, fixing the angle θ. It can be shown that in this case the SM photon couples only to the SM current, while the paraphoton couples to both. However, in the presence of Stuckelberg mass mixing, the dark matter may be millicharged. In Figure 3.7, we show constraints in the parameter space of millicharged dark matter particles[11]. For masses above $m \gtrsim 1$GeV, this model is poorly constrained, while at lower masses strong constraints from astrophysics and cosmological observables apply.

[10] The kinetic mixing parameter can be present at tree level or be generated at 1-loop. The latter contribution relates the values of the gauge coupling and the kinetic mixing in concrete BSM models. The loop supression of the kinetic mixing might be compensated by logarithmic contributions depending on the masses of the particles i, j involved in the loop, as $\epsilon \propto \frac{ee'}{48\pi^2}\log\frac{m_i^2}{m_j^2}$. The logarithmic enhancement depends on the model under consideration [163–165]

[11] Millicharged DM has been studied phenomenologically widely in this thesis. In section 7.3, we consider millicharged DM interactions with photons as a pontential explanation of the deficit of gamma-ray observations NGC 1068. In the *Varietés* 9.1.2 and 9.1.3, this model is considered in the context of elastic and inelastic dark matter-electron scatterings in direct detection experiments.

Chapter 4

Dark matter searches

In this section, we will discuss different detection methods proposed to search for the dark matter candidates presented in the previous section. In subsection 4.1 we will briefly introduce dark matter searches at accelerators. In subsection 4.2 we will direct dark matter searches, and in subsection 4.3, we will discuss indirect dark matter searches. We will be focusing on searches for WIMPS, inelastic dark matter and light dark mater.

4.1 Accelerator dark matter searches

Previous to the advent of supersymmetric theories [166], and the discovery of the Z-boson at colliders in 1983, the possibility to search for neutrinos in e^+e^- collisions and Kaon decays had already been put into the table [167][1].

Like neutrinos, dark matter produced at accelerators would in most cases pass through the detector invisibly. Modern attempts to find GeV-TeV dark matter at the LHC have been performed in the framework of effective field theories (EFT), simplified models, and more complete theories such as supersymmetry, e.g [168–176]. EFT's present some advantages w.r.t simplified models, for example, they have a limited number degrees of freedom (interaction scale, dark matter mass) and allow for a model independent comparison with direct detection searches, while simplified models require at least four model parameters: the mediator mass, dark matter mass and coupling strengths of the mediator to the dark sector and the standard model ($m_\phi, m_\chi, g_\chi, g_q$), and don't allow for a model independent comparison with direct detection experiments. Nonetheless, EFT's are only valid at current colliders for quite heavy mediators $m_\phi^2 \gg q^2 \gg \sqrt{s} = 13$ TeV. In the framework of simplified models, there are two differentiated dark matter searches : mono-X searches and mediator searches. The first consists on looking for single jet, photon, higgs, or Z events, while mediator searches look for resonances like a Z' mediator in dijet or dilepton events.

Collider dark matter searches depend on the choice of the couplings g_χ, g_l, g_q to dark matter, standard model leptons and quarks, respectively. Fixing these values allow for comparison with the dark matter relic density and with direct and indirect detection results on the mass-cross section plane, see Figure 4.1. Collider bounds are more stringent than direct detection limits at low dark matter masses $m_\chi \leq 6$ GeV for the standard spin-independent interaction. However, collider bounds on dark matter are more cor-

[1]Special thanks to Felix Kahlhöfer for drawing our attention to this paper.

rectly presented in the mass-mass plane of the mediator and dark matter particle. The translation of LHC results to direct-indirect detection results is difficult to interpret, since LHC results only hold for the mediator under consideration and the specific choice of the couplings taken. Constraints on some thermal dark matter models from colliders probe crucial and complementary to other dark matter searches in certain regions of parameter space. In fact, for Dirac dark matter fermions with masses below 100 GeV, it becomes difficult to find regions of parameter space that satisfy all constraints while maintaining the EFT validity at LHC energies [177].

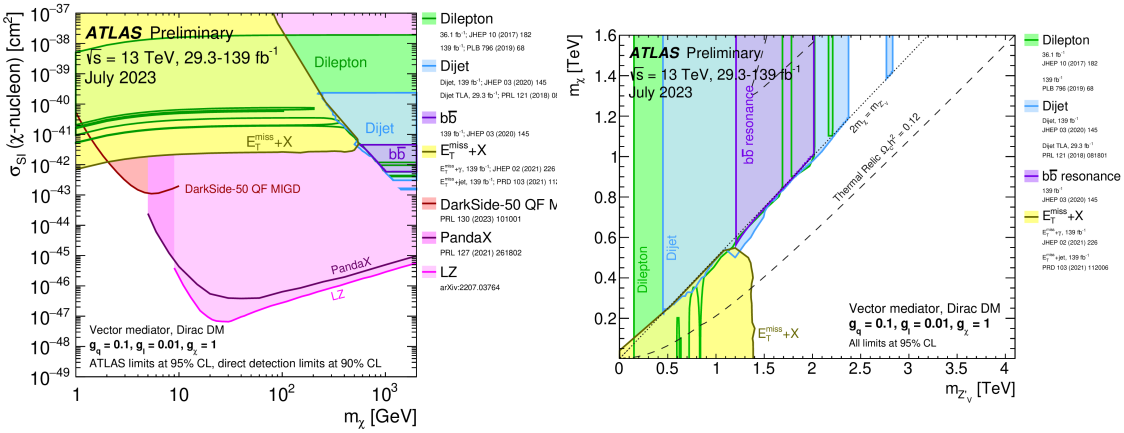

Figure 4.1: *Left panel*: Upper limits on the spin independent dark matter–nucleon scattering cross-section for a Z' mediator with leptophilic vector couplings, confronted with results from direct detection experiments. *Right panel*: Upper limits on the dark matter mass mediator plane from colliders, confronted with values that satisfy the relic abundance of dark matter in a simplified model, for specific choices of the couplings [178].

Light dark matter particles might also be produced at accelerators. For example, dark photons (A') (see section 3.6 for an introduction to this model) might be produced at accelerators via bremsstrahlung ($eZ \to eZA'$), annihilation ($e^+e^- \to A'\gamma$), Drell-Yann ($q\bar{q} \to A'$), meson decays ($\pi^0 \to A'\gamma$) or vector meson-dark photon conversion ($\rho \to A'$), among other possibilities [179–184]. Once the dark photon is produced, it might decay into visible or invisible states. If the decay into dark sector states is kinematically supressed, the dark photon will decay into visible states promptly for $\varepsilon \gtrsim \mathcal{O}(10^{-3}) \times (10\text{MeV}/m_{A'})$, otherwise its decay point will be displaced from the production point. If the dark photon mass satisfies $m_{A'} > 2m_\chi$, with χ the lightest dark matter state, the invisible decay into $\chi\bar{\chi}$ will dominate. This scenario can be searched by looking at missing energy in the detector, or by looking at interactions of the χ particle in a detector downstream of the A' production point.

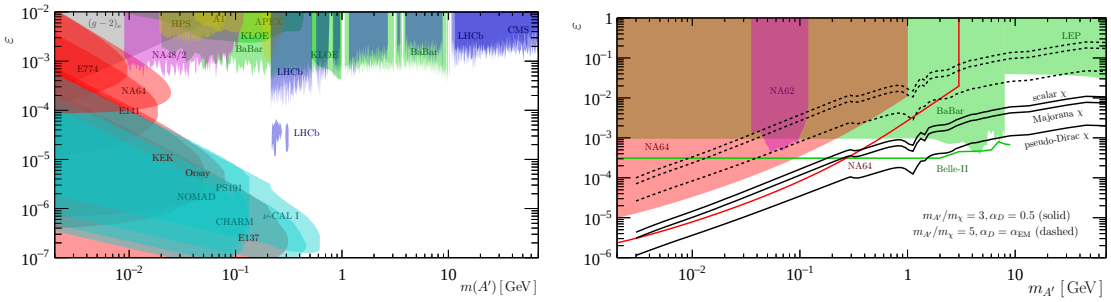

Figure 4.2: *Left panel*: Constraints on visible dark photon decays from electron beam dumps (red), proton beam dumps (cyan), electron-positron colliders (green), pp collisions (blue), meson decays (purple) and electron fixed target experiments (yellow). The constraint from the anomalous magnetic moment of the electron is shown in grey [185]. *Right panel*: Current constraints (shaded regions) and projected constraints (solid coloured lines) on invisible dark photon decays. The solid and dashed black lines correspond to thermal dark matter targets[2]

A compilation of constraints from accelerators on the dark photon mass vs kinetic mixing to the standard model from both visible and invisible decays can be found in Figure 4.2. The constraints are confronted with values of the kinetic mixing vs mass that can account for the relic density of dark matter in some simplified models, by relating the thermally averaged annihilation cross section in the early universe with the dark sector parameters relevant for the decay width in the accelerator via

$$\langle \sigma v \rangle \propto \frac{\varepsilon^2 \alpha_D m_\chi^2}{m_{A'}^4} \tag{4.1}$$

and, as apparent from the plots, models with $m_{A'}/m_\chi < 3$ are ruled out in most regions of parameter space, while lighter dark matter particles can evade accelerator constraints. It has been shown that current and future neutrino experiments play an important role in constraining regions of the parameter space beyond the reach of conventional collider accelerator searches, e.g [186–192]

4.2 Direct dark matter searches

After a paper from Drukier and Stodolsky at the Max Planck Institute in Munich proposing detectors to search for neutrino-nucleus scattering [193], Goodman and Witten proposed to use those detectors to search for dark matter particles in the halo of our galaxy [89]. Goodman and Witten (and shortly after Ira Wassermann [194]) proposed several candidates, among which there were dark matter particles scattering coherently with the nuclei via spin-independent couplings, and dark matter particles scattering via spin-dependent couplings. Soon after, two low-background germanium ionization experiments placed the first direct constraints on the spin-independent and spin-dependent

dark matter-nucleon couplings [195, 196], from a non subtantial excess of recoil events w.r.t to the background expectation[3], see the left panel of Figure 4.3. These first searches were merely counting event experiments, and an interesting variant introducing a temporal dependence of the dark matter signal rate was proposed soon after [199]. The combination of the Earth's motion around the Sun and the Sun's motion through the dark matter halo would induce an annual modulation in the scattering rate, which may help to distinguish the dark matter signal from other backgrounds. Since then, several experiments have explored the parameter space of dark matter-nucleon scatterings with different detector technologies, based on total scattering rate or modulation signals. Among these, there are light scintillators, based for example in NaI crystals, like DAMA/LIBRA, [200], cryogenic ionization detectors, based for example in Germanium, like EDELWEISS or CDMS [201, 202], liquid noble experiments, usually based in Xenon, like XENON1T and PandaX, [203, 204], or bubble chambers, filled with C_3F_8 in the case of PICO, [205]. The sensitivity of these experiments has increased tremendously over the years, getting close to observe the coherent elastic scattering of solar neutrinos, which would constitute an irreducible background for WIMP searches [206, 207].

Of particular importance was the observation of a modulation-like signal at the DAMA experiment, based on Sodium Iodine detectors (NaI), at the Gran Sasso national laboratory [208]. The DAMA collaboration has consistently confirmed the presence of this signal over the years [200], which however seems incompatible with the lack of signals at different direct detection experiments, some of them dedicated to look for the same annual modulation signature [209–215].

[3]These experiments were originally designed to search for neutrinoless beta decay. This has been a constant pattern on the BSM physics community over the years. Several experiments originally designed to search for a concrete BSM scenario have been repurposed to search for different scenarios. Examples are numerous, but we can mention some examples such as direct dark matter experiments as new solar neutrino detectors (as XENON1T [197]), or proton decay and neutrino experiments as dark matter laboratories (as Super-Kamiokande [198]).

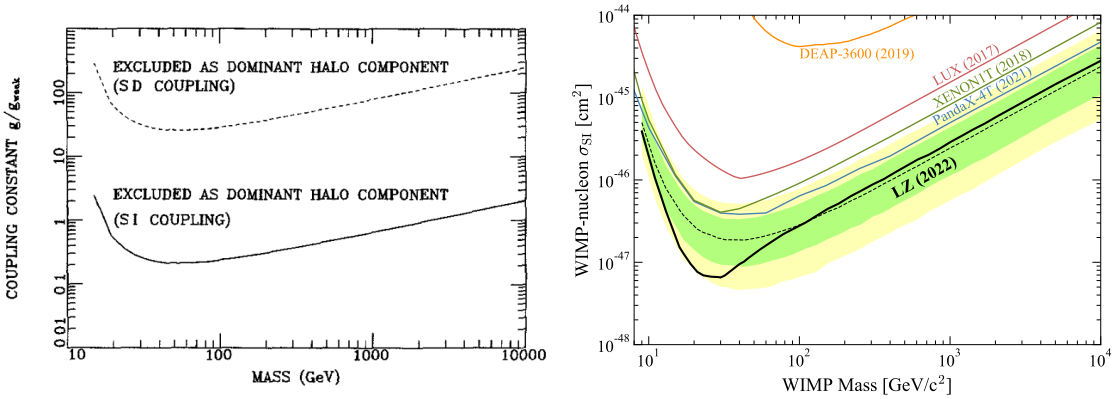

Figure 4.3: *Left panel*: First upper limit on the WIMP-nucleon scattering cross section vs dark matter mass with a direct detection experiment, from Ahlen, Avignone, Brodzinski, Drukier, Gelmini and Spergel [195]. The interaction strength is parameterized as $g/g_{\rm weak} = (\sigma/\sigma_{\rm weak})^{1/2}$ where $\sigma_{\rm weak}$ is the weak scattering cross section of heavy neutrinos with Germanium (spin-independent for Dirac neutrinos, and spin-dependent for Majorana neutrinos). A local density of dark matter particles in the halo of $\rho_{\rm DM} = 0.38$ GeV/cm^3 was assumed, and a Maxwellian velocity distribution with escape velocity of 550 km/s. The lowest value of the cross section constrained is $\sigma^{\rm SI} \sim 10^{-35}$ cm^2. *Right panel*: Currently strongest upper limit on the WIMP-nucleon scattering cross section from the LUX-ZEPLIN experiment [216]. Values of the spin-independent scattering cross section as low as 10^{-47}cm^2 are ruled out, which represents an improvement of ~ 12 orders of magnitude w.r.t to the first upper limit derived in 1987.

In the following, we describe the direct detection formalism necessary to compute the expected WIMP-nucleus recoil rate on a certain experiment.

The dark matter-induced scattering off the nucleus N_i in the detector can be expressed as

$$\frac{dR}{dE_R} = \sum_i \frac{\xi_i}{m_{A_i}} \int_{v \geq v^i_{\rm min}(E_R)} {\rm d}^3 v \mathscr{F}(\vec{v} + \vec{v}_\odot) \frac{{\rm d}\sigma_i}{{\rm d}E_R}(v, E_R)\,. \tag{4.2}$$

Here, $m_{N,i}$ is the target nuclei i mass and ξ_i is the mass fraction of the nuclei isotope under consideration. $\mathscr{F}(\vec{v} + \vec{v}_\odot)$ is the dark matter flux at Earth (expressed in the galactic frame)

$$\mathscr{F}_{\rm SHM}(\vec{v}) = \frac{\rho^{\rm loc}_{\rm SHM}}{m_{\rm DM}} v f_{\rm SHM}(\vec{v}). \tag{4.3}$$

with $m_{\rm DM}$ the dark matter mass. $\rho_{\rm DM}$ is the dark matter local density, and $f_{\rm SHM}(\vec{v})$ is the velocity distribution of dark matter particles in the galactic rest frame. The local density of dark matter particles can be inferred from the motion of tracers, or from global

measurements of the mass distribution in the galaxy from the rotation curve, yielding values in the range $\rho_{\rm DM} \sim 0.2 - 0.85$ GeV/cm^2 [217]. The velocity distribution of the dark matter particles is assumed to be a Maxwell-Boltzmann truncated at the escape velocity of the Milky Way (expressed in the Solar frame):

$$f_{\rm SHM}(\vec{v}) = \frac{1}{(2\pi\sigma_v^2)^{3/2} N_{\rm esc}} \exp\left[-\frac{|\vec{v}|^2}{2\sigma_v^2}\right] \quad \text{for } v \leq v_{\rm esc}\,. \tag{4.4}$$

Here, $v = |\vec{v}|$, $\sigma_v = 156$ km/s is the velocity dispersion [218, 219], $v_\odot \approx 232$ km/s is the local velocity of the Sun with respect to the galactic frame [4], and $v_{\rm esc} = 544$ km/s is the escape velocity from our Galaxy [221, 222]. Further, $N_{\rm esc}$ is a normalization constant, given by:

$$N_{\rm esc} = \text{erf}\left(\frac{v_{\rm esc}}{\sqrt{2}\sigma_v}\right) - \sqrt{\frac{2}{\pi}}\frac{v_{\rm esc}}{\sigma_v}\exp\left(-\frac{v_{\rm esc}^2}{2\sigma_v^2}\right)\,. \tag{4.5}$$

For our chosen parameters, $N_{\rm esc} \simeq 0.993$. The contribution to the local dark matter flux from the Milky Way halo then reads:

This assumptions refer to the Standard Halo Model (SHM), which is the benchmark parametrization used by theorists and experimentalist to infer the dark matter particle properties with direct detection experiments. This model presents uncertainties and caveats[5]. $v_{min,i}(E_R)$ is the minimum velocity necessary to induce a given recoil energy

$$v_{min}(E_R) = \frac{1}{\sqrt{2 m_N E_R}}\left(\frac{E_R\,(m_\chi + m_N)}{m_\chi} + \delta\right) \tag{4.6}$$

, with δ the mass splitting between the initial and final dark matter states, if the scattering is inelastic.

The total spin-independent WIMP-nucleus i scattering cross section arising from scalar and vector couplings between WIMPS and quarks reads

$$\sigma_0^{\rm SI} = \frac{\mu_{A_i}^2}{\pi}\left[(Z f^p + (A-Z) f^n)^2 k + \frac{B_N^2}{64}\delta(k-1)\right]. \tag{4.7}$$

where $k = 1$ for Majorana particles (vector contribution vanishes) or $k = 0$ for Dirac particles. Assuming equal coupling to protons and neutrons $f^p = f^n$ as well as Majorana dark matter, the expression reduces to

$$\sigma_0^{\rm SI} = \frac{\mu_{A_i}^2}{\pi} A_i^2 (f^p)^2. \tag{4.8}$$

[4] The velocity of the Sun with respect to the galactic rest frame is given by $\vec{v}_\odot = \vec{v}_{\rm LSR} + \vec{v}_{\odot,pec}$, where $\vec{v}_{\rm LSR} = (0, v_c, 0)$ is the motion of the local standard of rest (LSR), $v_c \approx 220$ km/s, and $\vec{v}_{\odot,pec} = (11.1, 12.24, 7.25)$ km/s is the Sun's peculiar motion [220].

[5] In the *Varieté* 9.1, we propose a refinement of the SHM including non-galactic dark matter particles bound to the Local Group and the Virgo Supercluster, but not the Milky Way, and thus with larger velocities than the particles in the halo. Further, we study its impact in direct detection experiments. Additionally. in [106], we proposed a method to parametrize uncertainties in the dark matter velocity distribution with information divergences, and assess the results from several experiments for different deviations from the common Maxwell-Boltzmann parametrization.

Direct detection experiments use different target nuclei so it is convenient to write the differential scattering rates in terms of the WIMP-proton cross section. In the case of $f^p = f^n$, the WIMP-proton and the WIMP-nucleus at zero momentum transfer cross sections are related as

$$\sigma_0^{\mathrm{SI}} = \frac{\mu_{A_i}^2}{\mu_{\mathscr{N}}^2} A_i^2 \sigma_{\mathscr{N}}^{SI}, \tag{4.9}$$

where $\mathscr{N} = n, p$ and μ_{A_i} are the dark matter-nucleon respectively the dark matter-nucleus reduced mass. strength to protons and neutrons. $F_i^2(E_R)$ is the nuclear form-factor, for which the Helm prescription is typically assumed [6], and $\sigma_{\mathscr{N}}^{\mathrm{SI}}$ is the spin-independent scattering cross section off the nucleus at zero momentum transfer. The differential dark matter-nucleus scattering cross section reads

$$\frac{d\sigma_i^{\mathrm{SI}}}{dE_R} = \frac{m_{A_i} \sigma_0^{\mathrm{SI}} F_i^2(E_R)}{2\mu_{A_i}^2 v^2}, \tag{4.10}$$

where σ_0^{SI} is the total, point-like WIMP-nucleon cross section at zero momentum transfer. Taking this into account, the differential scattering cross section in terms of the interactions with nucleons is given by

$$\frac{d\sigma_i^{\mathrm{SI}}}{dE_R} = \frac{m_{A_i}}{2\mu_{\mathscr{N}}^2 v^2} A^2 \sigma_{\mathscr{N}}^{\mathrm{SI}} F_i^2(E_R) \tag{4.11}$$

where all the information on the WIMP model is encoded in $\sigma_{\mathscr{N}}^{SI}$.

Spin-dependent interactions arise from the axial-vector coupling between dark matter and quarks. The resulting differential cross section for a fermionic (spin 1/2) WIMP off a nucleus i is given by

$$\frac{d\sigma_i^{\mathrm{SD}}}{dE_R}(v, E_R) = \frac{2\pi m_{A_i}}{3\,\mu_{\mathscr{N}}\, v^2\,(2J+1)} \sigma_{\mathscr{N}}^{\mathrm{SD}} S_{A_i}(E_R)\ , \tag{4.12}$$

with J the total spin of the nucleus, $S_{A_i}(E_R)$ the nuclear structure function, and $\sigma_{\mathscr{N}}^{\mathrm{SD}}$ is the spin-dependent scattering cross section off the nucleon $\mathscr{N} = n, p$ at zero momentum transfer.

The total scattering rate is then given by

$$R = \mathcal{E} \cdot \int_0^\infty \sum_i \epsilon_i(E_R) \frac{dR_i}{dE_R} dE_R, \tag{4.13}$$

where $\mathcal{E} = M \cdot T$ is the exposure of the detector, with M its mass and T running time of the experiment. $\epsilon_i(E_R)$ are the recoil efficiencies of the nucleus N_i, determined experimentally.

The main difference from the spin-independent dark matter-nucleus interactions is that the spin-dependent differential scattering cross section does not increase with the

[6] The Helm form factor implies that the WIMP-nucleus scatterings are distributed as electron-nucleus scatterings.

number of nucleons, but rather depends on the nucleus spin J. Indeed, spin-dependent interactions can be tested only on isotopes with $J \neq 0$. Furthermore, the differential cross section is proportional to the expectation values of the spin content in the proton group respectively the neutron group in the nucleus $\langle S_{A_i} \rangle$, which differ for different isotopes and do not favour heavy ones, [223]. Thus, the ideal targets to test spin-dependent interactions are constituted elements with $J \neq 0$, $\langle S_{A_i} \rangle = 1/2$ and low masses. Some examples include Fluorine at PICO, or ^{17}O at CRESST, [224]. For spin-independent interactions, the differential cross section scales with the squared number of nucleons A^2 for $f^p = f^n$, so that heavy nuclei is favoured w.r.t light nuclei. For this reason heavy target elements such as ^{184}W at CRESST or ^{131}Xe at XENON1T are preferred.

Direct detection experiments lose sensitivity at sub-GeV masses due to their minimum energy threshold and velocity of dark matter particles reaching the detector (typically assumed to be the escape velocity of the Milky Way)[7]. Some experiments are aiming to achieve low energy thresholds in order to probe sub-GeV dark matter scatterings with nucleons, but the improvements in recent years have been modest [228]. However, other alternatives to extend the sensitivity reach without improving current technologies significantly have been proposed.

For example, the ionization signal stemming from the Migdal effect after the nucleus recoils allows to extend the sensitivity of some experiments, see Figure 4.4[8]. Unlike it happens for elastic scatterings, if the dark matter scatters inelastically with the detector, the limitation in sensitivity is a limitation in probing larger mass splittings between the two dark matter particles. From the experimental side, the sensitivity is limited by the maximum energy recoil considered in experiments.[9]. In the right panel of Figure 4.4, we show current constraints (calculated by ourselves) from different experiments on the parameter space of dark matter-nucleon scattering cross section vs mass splitting, for a dark matter mass of $m_{\rm DM} = 1$TeV, and confronted with different values of the dark matter hypercharge in electroweakly interacting dark matter models, where the inelastic scattering cross section can be dominant, and is given by [112]

$$\sigma^{\rm inel} = \frac{G_F^2 Y^2}{2\pi} \left[N - \left(1 - 4\sin^2\theta_W\right) Z \right]^2 \mu_{A_i}^2 . \tag{4.14}$$

with G_F is the Fermi constant, θ_W is the weak mixing angle, and μ_{A_i} is the reduced mass in the DM-target nucleus systems.

[7] Several low-threshold direct detection experiments observe sharply rising event rates below a few hundred eV, and larger than expected from common backgrounds. The characteristics of these excesses are different for every experiment and seem unlikely to be caused by dark matter, see e.g [225–227]

[8] In the *Varieté* **??** we discuss the Migdal effect in some detail, further calculating the irreducible ionization background from coherent elastic neutrino nucleus scattering, and its potential distinguisability from a Migdal dark matter signal.

[9] In the Varieté 9.1.3, we discuss the sensitivity reach and kinematics of direct detection experiments to inelastic dark matter in more detail, and derive the strongest constraints to date in sensitivity to scattering cross section from the LUX-ZEPLIN experiment, and in sensitivity to mass splittings from a radiopurity $CaWO_4$ measurement [229, 230], and the consideration of non-galactic dark matter particles

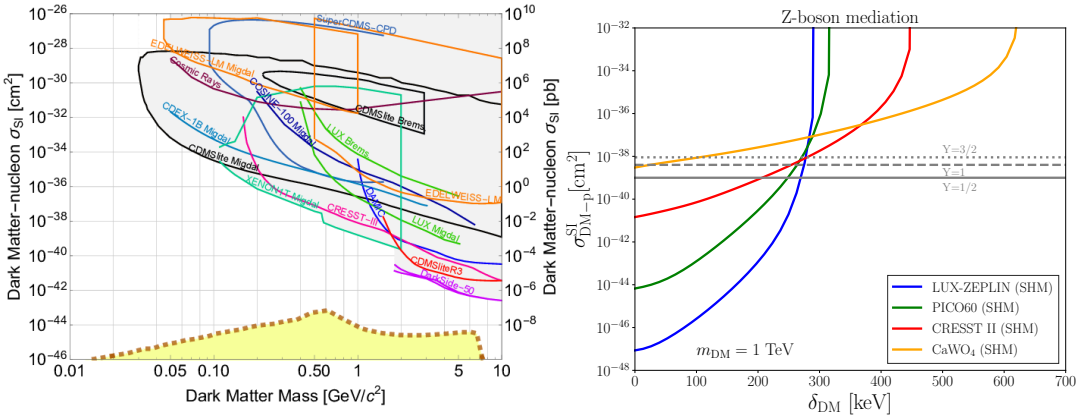

Figure 4.4: *Left panel*: Direct detection constraints on the sub-GeV dark matter-nucleon scattering cross section vs dark matter mass, from elastic scatterings and from the ionization signal induced by the Migdal effect. The yellow region corresponds to the neutrino floor [231]. *Right panel*: Direct detection constraints on the inelastic dark matter-nucleon scattering cross section vs dark matter mass splitting from a variety of experiments, confronted with model prediction for electroweakly interacting dark matter with different hypercharges.

The dark matter particle may also scatter with the electrons in the detector. In fact, if the dark matter is light enough, it may be able to ionize electrons without inducing detectable nuclear recoils. The differential ionization rate induced by dark matter-electron inelastic scattering in liquid xenon, with mass splitting between the two dark matter states given by $\delta_{\rm DM}$, reads [232]:

$$\frac{dR_{\rm ion}}{d\ln E_{er}} = N_T \sum_{n,l} \int_{v \geq v^{nl}_{\rm min}(E_{er})} {\rm d}^3 v \mathscr{F}(\vec{v} + \vec{v}_\odot) \frac{{\rm d}\sigma^{nl}_{\rm ion}}{d\ln E_{er}}(v, E_{er}) \,, \tag{4.15}$$

where N_T is the number of target nuclei and

$$v^{nl}_{\rm min}(E_{er}) = \sqrt{\frac{2}{m_{\rm DM}}(E_{er} + |E^{nl}| + \delta_{\rm DM})} \tag{4.16}$$

is the minimum dark matter velocity necessary to ionize a bound electron in the (n,l) shell of a xenon atom (with energy E^{nl}), giving a free electron with energy E_{er}. Further, $d\sigma^{nl}_{\rm ion}/d\ln E_{er}$ is the differential ionization cross section, given by:

$$\frac{d\sigma^{nl}_{\rm ion}}{d\ln E_{er}}(v, E_{er}) = \frac{\bar{\sigma}_{\rm DM-e}}{8\mu^2_{\rm DM,e} v^2} \int_{q^{nl}_{\rm min}}^{q^{nl}_{\rm max}} dq q \left| f^{nl}_{\rm ion}(k', q) \right|^2 |F_{\rm DM}(q)|^2 \,. \tag{4.17}$$

Here, $\mu_{\rm DM,e}$ is the reduced mass of the dark matter-electron system, $\bar{\sigma}_{\rm DM-e}$ is the dark matter-free electron scattering cross section at fixed momentum transfer $q = \alpha m_e$,

$\left|f_{ion}^{nl}(k',q)\right|^2$ is the ionization form factor of an electron in the (n,l) shell with final momentum $k' = \sqrt{2m_e E_{er}}$ and momentum transfer q, and $F_{\rm DM}(q)$ is a form factor that encodes the q-dependence of the squared matrix element for dark matter-electron scattering and depends on the mediator under consideration. It is from the following factorization

$$\bar{\sigma}_e \equiv \frac{\mu_{\chi e}^2}{16\pi m_\chi^2 m_e^2} \overline{|\mathcal{M}_{\chi e}(q)|^2}\Big|_{q^2=\alpha^2 m_e^2} \tag{4.18}$$

and

$$\overline{|\mathcal{M}_{\chi e}(q)|^2} = \overline{|\mathcal{M}_{\chi e}(q)|^2}\Big|_{q^2=\alpha^2 m_e^2} \times |F_{\rm DM}(q)|^2 . \tag{4.19}$$

$\bar{\sigma}_e$ is equal to the non-relativistic dark-matter-electron elastic scattering cross section, but with the 3-momentum transfer q fixed to the reference value αm_e (appropriate for atomic processes). $\overline{|\mathcal{M}_{\chi e}(q)|^2}$ is the squared matrix element for dark-matter-electron scattering, averaged over initial and summed over final spin states. For fermionic dark matter charged under a dark $U(1)$ symmetry group with gauge coupling g' and kinetic mixing ϵ, the cross section at fixed momentum transfer and dark matter form factor reads

$$\bar{\sigma}_e = \frac{16\pi\mu_{\chi e}^2 \alpha\alpha'\varepsilon^2}{\left(m_{A'}^2 + \alpha^2 m_e^2\right)^2} \simeq \begin{cases} \frac{16\pi\mu_{\chi e}^2\alpha\alpha'\xi^2}{m_{A'}^4}, & m_{A'} \gg \alpha m_e \\ \frac{16\pi\mu_{\chi e}^2\alpha\alpha'\varepsilon^2}{(\alpha m_e)^4}, & m_{A'} \ll \alpha m_e \end{cases} \tag{4.20}$$

and

$$F_{\rm DM}(q) = \frac{m_{A'}^2 + \alpha^2 m_e^2}{m_{A'}^2 + q^2} \simeq \begin{cases} 1, & m_{A'} \gg \alpha m_e \\ \frac{\alpha^2 m_e^2}{q^2}, & m_{A'} \ll \alpha m_e \end{cases} \tag{4.21}$$

and we find compact expressions for ultralight and heavy mediators.

The maximum and minimum values of the momentum transfer needed to ionize a bound electron in the (n,l) shell recoil with energy E_{er} from the interaction of a dark matter particle with speed v are:

$$q_{\rm min}^{\rm max}(E_{er}) = m_{\rm DM} v \left[1 \pm \sqrt{1 - \left(\frac{v_{\rm min}^{nl}(E_{er})}{v}\right)^2}\right], \tag{4.22}$$

with $v_{\rm min}^{nl}(E_{er})$ defined in Eq. (9.46). Finally, the total number of expected ionization events reads $\mathcal{N} = R_{ion} \cdot \mathcal{E}$, with R_{ion} the total ionization rate, calculated from integrating Eq.(9.45) over the experimentally measured recoil energies, and $\mathcal{E}$ the exposure (*i.e.* mass multiplied by live-time) of the experiment.

In semiconductor detectors, the electron excitation rate induced by dark matter-electron inelastic scatterings, with a mass splitting $\delta_{\rm DM}$, reads [233, 234]

$$R = \frac{1}{\rho_T} \frac{\bar{\sigma}_{\rm DM-e}}{\mu_{\rm DM,e}^2} \frac{\pi}{\alpha} \int d^3v \frac{\mathscr{F}(\vec{v}+\vec{v}_\odot)}{v} \int \frac{d^3q}{(2\pi)^3} q^2 |F_{\rm DM}(q)|^2 \int \frac{d\omega}{2\pi} \frac{1}{1-e^{-\beta\omega}} \, {\rm Im}\left[\frac{-1}{\epsilon(\omega,\vec{q})}\right] \delta\left(\omega + \delta_{\rm DM} + \frac{q^2}{2m_\chi} - \vec{q}\cdot\vec{v}\right) ,$$

where w is the energy deposited in the material, $\vec{q}$ is the momentum transfer of the process, and ρ_T is the target density. The rate involves an integration of the Electronic Loss Function (ELF) of the target material, which has been calculated for several materials [234]. For the dielectric function $\epsilon(\omega, \mathbf{q})$, one typically uses the Lindhard method, which treats the target as a non-interacting Fermi liquid. Finally, the total number of events reads $\mathcal{N} = R \cdot \mathcal{E}$, with $\mathcal{E}$ the exposure (*i.e.* mass multiplied by live-time) of the experiment.

The non-observation of a significant excess of electron recoils in a given experiment allows to set upper limits on the dark matter-electron scattering cross section, for a given dark matter mass and a given mass splitting between the dark matter particle and the heavier neutral state. We show in Figure 4.5 a compilation of constraints for elastic dark matter electron scatterings in the ultralight $F_{\rm DM} = \alpha^2 m_e^2/q^2$ mediator, heavy mediator $F_{\rm DM} = 1$, electric dipole interaction $F_{\rm DM} = \alpha^2 m_e^2/q$, and magnetic dipole interaction, whose form factor is non-trivial. Values of the cross section favoured by some thermal production models (discussed in section 3.6) are shown for comparison. [10].

[10] In the Varietés 9.1.2 and 9.1.3 we derive constraints on dark matter-electron elastic and inelastic scatterings in these scenarios, including the non-galactic components.

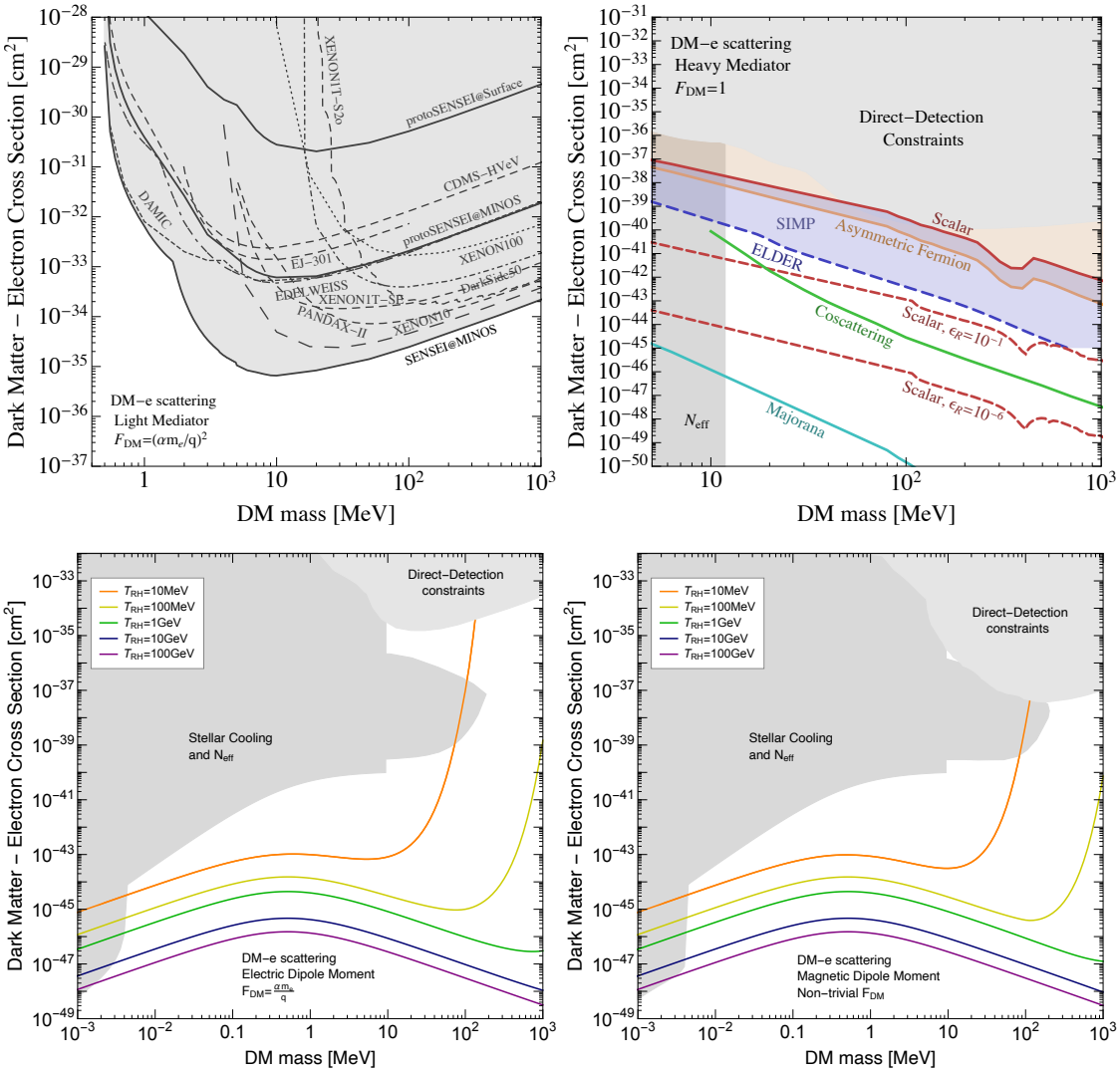

Figure 4.5: Direct detection constraints on the dark matter electron scattering cross section vs dark matter mass from a variety of experiments (dominant ones today are SENSEI, DAMIC and XENON1T [235–237]) [238], for light dark matter models, an ultralight mediator (upper left), a heavy mediator (upper right), an electric dipole moment (lower left) and a magnetic dipole moment (lower right). Complementary constraints from stellar cooling and $N_{\rm eff}$ measurements are shown for comparison. Further, the plots contain favored values in some thermal [147, 151, 152, 239], and non-thermal production mechanisms (freeze in, for different values of the reheating temperature $T_{\rm RH}$ [240])

We have seen that the parameter space of dark matter-nucleon interactions is strongly constrained at the GeV scale, but experiments continue to probe smaller values of the

scattering cross section, aim to target blind spots in the NREFT, or increase their reach in mass splitting[11]. The parameter space of sub-GeV dark matter-nucleon and dark matter-electron interactions is even less constrained, and current and future experiments aim to reach the thermal and non-thermal production targets in the future. Also, from the theoretical side several ideas are emerging in recent years allowing to probe light dark matter directly, of outmost importance boosted components to the flux at Earth are being considered [129, 241–264]).

4.3 Indirect dark matter searches

Two articles published in 1978 opened the field of searching for dark matter particles via the products of its annihilations and decays that reach the Earth [34, 265]. The first following works focused on the gamma-ray signal coming from regions of high dark matter density in the Universe, which could induce gradients distinguisable from the astrophysical background for thermal values of the WIMP annihilation cross section. A few years later other ideas appeared. Most notably, it was pointed out that the measured antiproton and positron fluxes could also be used to set strong constraints on self-annihilating dark matter [266], and that dark matter particles might be captured gravitationally from the Sun and annihilate at the core into neutrinos detectable at Earth [267]. It was shown that the capture and annihilation processes may attain equilibrium under certain circumstances. Another important milestone happened during the last decade, when it has been extensively discussed that dwarf spheroidal galaxies provide the strongest indirect detection constraints on dark matter, due to its high dark matter density and low baryonic density [268, 269].

If the energy of the products of dark matter annihilation or decays do not change between production and reception[12], the spectrum at Earth of the particle i is given by [270]

$$\frac{dN_i}{dEdtd\Omega} = \frac{A}{4\pi}\frac{dN_i}{dE} \times \begin{cases} \frac{\langle\sigma v\rangle}{2m_{\rm DM}} \int_0^\infty \rho(\vec{r})^2 dr & \text{annihilation} \\ \frac{1}{m_{\rm DM}\tau} \int_0^\infty dr\rho(\vec{r}) & \text{decay} \end{cases} \tag{4.23}$$

where $\frac{dN_i}{dE}$ is the differential final particle energy spectrum. From this expression it can be already noticed that the presence of small-scale substructure could potentially increase the annihilation rate. Dark matter halos are thought to form hierarchically, and annihilation can be enhanced in these substructures, since $\langle\rho^2\rangle \neq \langle\rho\rangle^2$, and the former is the relevant quantity for annihilation. For decaying dark matter, however, substructure is less relevant, since the signal is controlled by $\frac{1}{R^2}\int\rho(\vec{r})dV \sim M/R^2$, where M is the total mass of the source. This approximation is valid as long as the source is distant

[11] The predicted mass splittings in split supersymmetry or the inert doublet model is of order keV for TeV scale dark matter, although it can be higher, depending on the gaugino masses or the details of the symmetry breaking, respectively

[12] In reality, particles undergo latter processes, such as decays, upscattering, absorption or redshifting. The propagation needs to be taken into account, except for dark matter direct annihilation or decays into neutrinos. This is done via the diffusion equation $\frac{\partial\psi}{\partial t} = D(E)\nabla^2\psi + \frac{\partial}{\partial E}(b(E)\psi) + Q(\vec{x}, E, t)$

enough $r \approx R$. Thus, the best constraints on decaying dark matter steam from galaxy cluster surveys.

A crucial paper that would change the field of dark matter matter indirect detection was published by Gondolo and Silk in 1999, showing that adiabatically growing black holes would form a cusp of dark matter particles in its vicinity, which could enhance the annihilation rate of dark matter particles ($\propto \int \rho^2_{\rm DM}(r)dr$) in the galactic centre w.r.t to the pre-existing profile by up to ~ 10 orders of magnitude, depending on the inner halo slope and density [271].[13].

Several excesses that could be explained with annihilations or decays of dark matter particles were discussed over the years, some of which still remain present, while others have been ruled out. Of particular importance was a paper by Goodenough and Hooper analysing Fermi telescope data and finding an excess of events in the direction of the galactic center, that was at the moment hardly explicable with astrophysical backgrounds, and that was well fitted by annihilating dark matter particles, see the right plot of the Figure 4.6. Today we know that the morphology of the signal is better fitted by a population of milisecond pulsars, but the discussion remains active, *e.g* [272–281].

[13] In section 6.2, we discuss in some detail the physics of adiabatically growing black holes and formation of dark matter spikes. Later, in section 7, the impact of such dark matter overdensities in the attenuation of cosmic rays around black holes is studied.

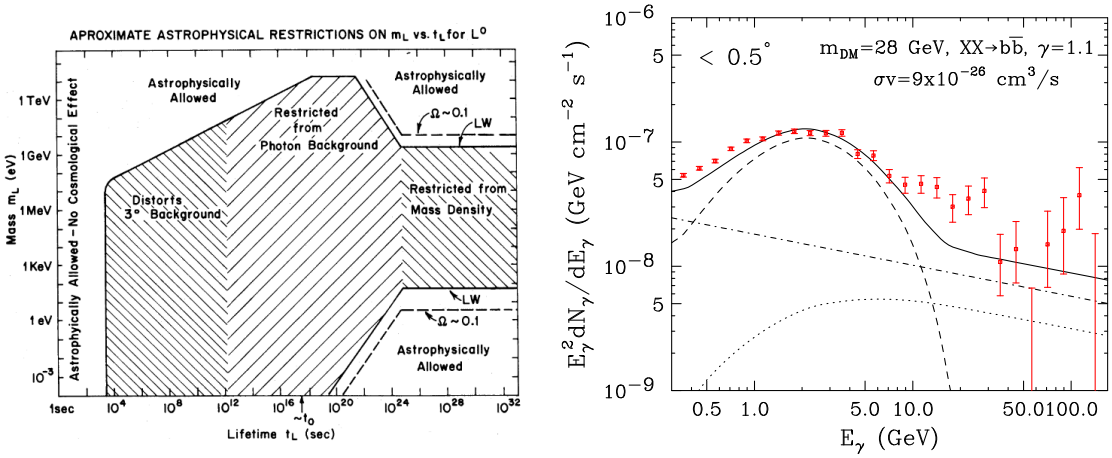

Figure 4.6: *Left panel*: Figure from one of the pioneering works on the indirect detection of dark matter, from Gunn, Lee, Lerche, Schramm and Steigman [34]. It shows constraints on the parameter space of dark matter (in reality, heavy neutral leptons) mass vs lifetime, assuming the decay mode produces at least one photon. Long lifetimes are ruled out otherwise the dark matter would overclose the Universe. For intermediate lifetimes (note $t_0 \approx$ age of the universe) the bounds come from limits on the astrophysical γ-ray background. Shorter timescales, but still greater than the time of big bang nucleosynthesis, are constrained by distortions in the present microwave background. *Right panel*: Galactic center gamma ray excess and its potential explanation via annihilations of WIMPs in the dark matter halo, from the seminal paper by Goodenough and Hooper [282]. The gamma-ray spectrum measured by the Fermi Gamma Ray Telescope within 0.5° of the Milky Way center is shown in red. The astrophysical contributions from a TeV point source located at the Milky Way's dynamical center and the diffuse background are shown in dotted and dot-dashed lines, respectively. Finally, the dashed line denotes the predicted spectrum from a 28GeV dark matter particle annihilating to $b\bar{b}$ with a cross section of $\sigma v = 9 \times 10^{-26}$ cm^3/s, and NFW-like halo with $\gamma = 1.1$. The solid line denotes the sum of all contributions.

Current constraints on the dark matter annihilation cross section rule out thermal GeV scale dark matter up to $\sim$ 100 GeV by white dwarf measurements, depending on the annihilation channel under consideration, see Figure 4.7. Direct annihilation or decays into neutrinos is however not strongly constrained [283–290], and sub-GeV dark matter is also poorly constrained in most channels due to the lack of telescopes sensitive in the MeV range. However, if sub-GeV dark matter annihilates (or decays) into leptons, these could upscatter low-energy photons in the galaxy and generate detectable X-ray emission [149, 291], see the right plot of figure 4.7. Comparable constraints can be derived from CMB distortions [292–294].

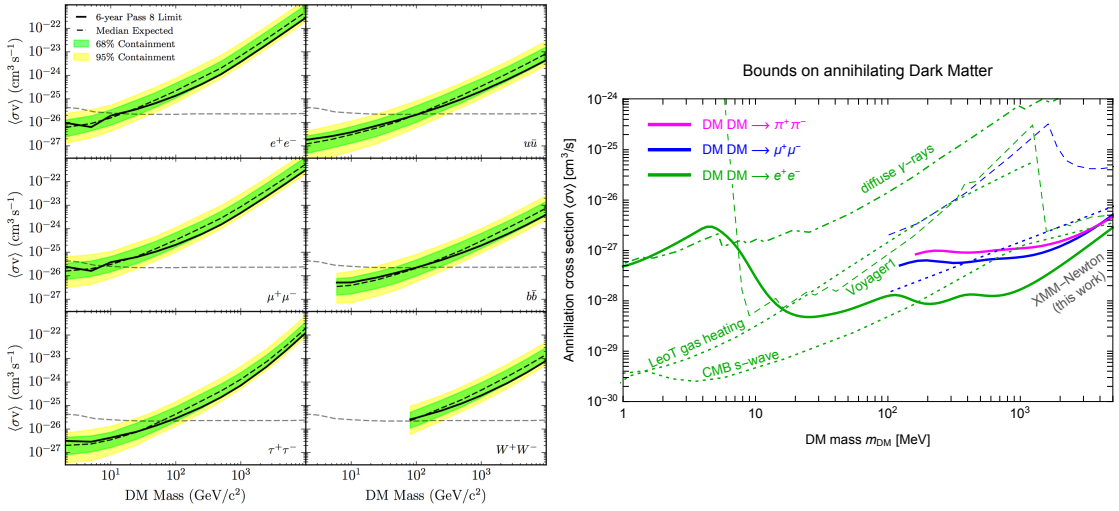

Figure 4.7: *Left panel*: Upper limits on the WIMP thermally averaged self-annihilation cross section as a function of the WIMP mass, from Fermi-LAT observations of dwarf spheroidal galaxies. The thermal relic values are shown in grey. *Right panel*: Upper limits on the sub-GeV dark matter self-annihilating cross section, for different leptonic final states. The strongest constraints on final electron positron states comes from a combination of XMM-Newton data and CMB observations.

The seminal paper from [267] offfered an interesting direction in the field, since it provides a way to correlate the dark matter scattering cross section with standard model particles and its thermally averaged annihilation cross section. This allows to compare indirect detection searches results with direct detection experiments. Here we review the standard formalism[14].

Dark matter particles can be gravitationally captured in the sun, scattering with the sun nuclei, sinking to the core, where they can annihilate into standard model particles, see Figure 4.9. This could enhance the solar neutrino flux detectable on earth. A WIMP with a velocity v_∞ at large distances from the sun has a velocity $w(r) = \sqrt{v_\infty^2 + v_{sun,esc}^2(r)}$ at a distance r from the center of the sun, being $v_{sun,esc}(r)$ the escape velocity of the sun at a radius r.

[14] In [105], we discussed this formalism in the context of the non-relativistic effective theory of dark matter-nucleon interactions, and derived constraints accounting from operator interferences and combine them with direct detection results.

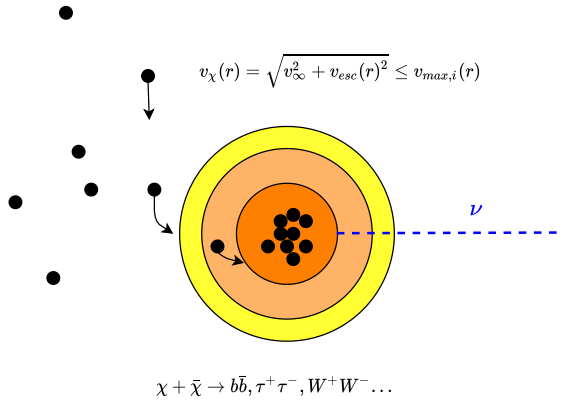

Figure 4.8: Schematic representation of the dark matter capture mechanism. The dark matter particle velocity at radii r must be smaller than a certain maximum velocity which depends on the recoiling element, see equation **??**, in order to be captured. Once accumulated in the core, dark matter particles can annihilate into standard model particles. Some annihilation channels studied by experimental neutrino collaborations are shown.

Dark matter particles get gravitationally captured when they transfer enough energy to the nucleus to have velocities lower than $v_{esc,sun}(r)$. This sets a minimum value of the energy that a dark matter particle χ needs to loose by scattering in order to be captured, which is $E_R^{min} = \frac{m_\chi}{2} v_\infty^2$. The capture rate per unit time is defined as

$$\Omega(w) = \nu_N(r) w \int_{E_R^{min}}^{E_R^{max}} dE_R \frac{d\sigma}{dE_R}(w, E_R), \tag{4.24}$$

where $\nu_N(r)$ is the number density profile of the nucleus N, $\frac{d\sigma}{dE_R}$ is the differential scattering cross section (which will be discussed in next section) and the maximal recoil energy $E_R^{max} = 2\mu_{\chi,N}^2 w^2 / m_N$. he capture rate per unit volume is

$$\frac{dC}{dV} = \frac{\rho\chi}{m_\chi} \int_0^{v_{max(r)}} dv^3 \frac{f(\vec{v})}{v} w\Omega(w), \tag{4.25}$$

The total capture rate is obtained integrating equation 4.25 over the total solar volume

$$C = \sum_i \int_0^{R\odot} dr 4\pi \cdot r^2 \nu_{N_i} \frac{\rho_{loc}}{m_\chi} \int_0^{v_{max}(r)} dv^3 \frac{f(\vec{v})}{v} \left(v^2 + v_{sun,esc}(r)^2\right) \int_{m_\chi v^2/2}^{2\mu_{\chi,N_i}^2 \left(v^2 + v_{sun,esc}(r)^2\right)/m_{N_i}} dE_R \frac{d\sigma_{\chi,i}}{dE_R}(w, E_R). \tag{4.26}$$

Thermal WIMPs can self-annihilate in the core of the sun once their number density n is large enough. The annihilation rate is proportional to n^2 and reads

$$\Gamma_A = \frac{1}{2} C_A n^2, \tag{4.27}$$

where C_A is the annihilation constant for the sun. Scattering of dark matter particles with nuclei inside the sun can also increase their velocity above the escape velocity of the sun. This process is called thermal evaporation, and must be included in the evolution of the number density of dark matter particles, which can be written as

$$\frac{dn}{dt} = C - C_A n^2 - C_E n, \tag{4.28}$$

where C_E is the evaporation rate of dark matter particles in the sun. By specifying the initial condition $n(t = 0) = 0$, we can solve equation 4.28 obtaining

$$n(t) = \sqrt{\frac{C}{C_A}} tanh\left(\frac{t}{\tau}\right), \tag{4.29}$$

where $\tau = 1/\sqrt{C \cdot C_A}$ is the equilibration time. After sufficient time $t \gg \tau$, the number of dark matter particles does not vary anymore. C_A can be estimated

$$C_A = 1.2 \cdot 10^{-52} \cdot \left(\frac{\langle \sigma v \rangle}{2.2 \cdot 10^{-26} cm^3 s^{-1}}\right) \cdot \left(\frac{m_\chi}{TeV}\right)^{\frac{3}{2}} \frac{1}{s}. \tag{4.30}$$

If we take a typical WIMP thermally averaged cross section $\langle \sigma v \rangle \geq 10^{-28} \frac{cm^3}{s}$, with mass $m_\chi = 100$ GeV and the age of the sun to be $t_\odot = 4.5 \cdot 10^9$, we obtain

$$\left(\frac{t_\odot}{\tau}\right) = tanh(t_\odot \cdot \sqrt{C \cdot C_A}) \approx 1 \tag{4.31}$$

when using capture rates currently probed by IceCube or Super-Kamiokande. We can assume $n(t) = \sqrt{\frac{C}{C_A}}$ which leads to the following annihilation rate

$$\Gamma_A = \frac{C}{2} \tag{4.32}$$

so that, for every two captured dark matter particles there is one annihilation event, i.e all captured dark matter particles end up annihilating in the core of the sun. In this framework, the number of high energetic solar neutrinos coming from the sun is completely determined by the capture rate of dark matter particles. This statement only holds for certain dark matter-nucleus scattering cross section and velocity distributions. Furthermore, this approximation is sensitive to the WIMP mass and thermally averaged cross section and could no longer be valid in certain regions of the parameter space.

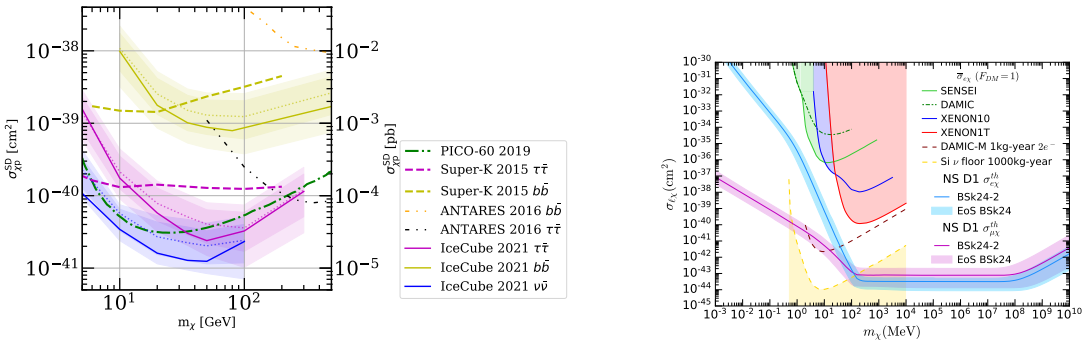

Figure 4.9: *Left panel*:Upper limits on the spin-dependent dark matter-proton scattering cross section from Super kamiokande and IceCube deepcore experiments, from a non substantial excess of high-energy neutrinos in the direction of the Sun, compared to the limits from the PICO 60 experiment [295]. *Right panel*: Sensitivity (threshold cross section) to the spin-independent dark matter-electron scattering cross section from potential future observations of nearby neutron stars [296]. The equation of state used is BSk24.

Variants of these initial idea have been proposed over the years, with interesting results. Potential observations of nearby neutron star emission could reveil heating signatures via scattering and annihilations of dark matter particles in its interior, *e.g* [117, 119, 297–305]. Similar signatures can be searches in observations of white dwarfs, brown dwarfs, exoplanets, and other compact objects [306–313]. The minimum dark matter mass that can be probed with these objects due to evaporation effects is however disputed [314].

Recently, we have proposed active galactic galactic nuclei as a source able to set strong constraints on dark matter interactions with photons and neutrinos [315], and protons and electrons [316], via an attenuation of the emitted particle fluxes from these sources. This is a new indirect detection technique, and we will discuss it in detail in section 7.

Chapter 5

Cosmic rays in the vicinity of black holes: Theory and observations

Emission lines from the nuclei of distant galaxies (such as NGC 1068) were already observed at the beginning of the twentieth century[1] [319, 320], but its systematic study began with the work of Seyfert in 1943 [321], who analysed the nuclear emission lines from 6 galaxies.

A milestone in the field occured a few years later, with the discovery of quasars (first by Schmidt in 1963 [322]), extragalactic sources emitting ~ 100 times more powerfully than other radio galaxies previously identified. Their large luminosities and unusual spectra indicated that the powering source might not be ordinary stars. It took a few extra years to understand that accretion of gas onto supermassive black holes ($M_{\rm BH} \gtrsim 10^6 M_\odot$) was the source of these quasars, as initially suggested by Salpeter and Zeldovich in 1964 [319]. Today we denote Active Galactic Nuclei (AGN) to the compact region in the center of some galaxies that has a luminosity exceeding the luminosity expected to be produced by normal stars, as well as characteristics of the spectrum that can be differentiated from stellar emission [2].

In this section, we will discuss some aspects of the physics of Active Galactic Nuclei, which will be important in order to study the impact of dark matter particles on the emission from this objects in the latter section 7. First, we will describe some mechanisms of cosmic ray acceleration, further discussing some aspects on the possibility to accelerate cosmic rays around black holes. Later, we will introduce the leptonic and hadronic processes believed to trigger photon and neutrino emission from Active Galactic Nuclei. Finally, we will discuss some observations from different classes of AGN: blazars, non-jetted galaxies and Tidal Disruption Events.

5.1 Cosmic ray acceleration

The original idea of cosmic-ray acceleration was proposed by Fermi in 1949, where clouds of ionized gas in the interstellar medium are moving w.r.t to the galactic frame, and can reflect charged particles passing through them [323]. In this framework, particles

[1] Obervations by Fath in 1909 at the Lick observatory noticed that the spectrum of NGC 1068 showed bright and dark absorption lines [317], later confirmed by Slipher [318]

[2] The term Active Galactic Nuclei was coined by the Soviet armenian astrophysicist Viktor Ambartsumian in the 1950's [319]

will be accelerated by each encounter with a magnetic cloud coming toward them and decelerated by the encounters with magnetic clouds going away from them. The energy gain (or loss) for each encounter can be calculated by a double change of reference frame (from Galactic to cloud frame and viceversa).

In reality, the encounters of the particle with the cloud do not follow an idealized reflexion, but rather the magnetic field is turbulent and charged particles are isotropized inside the cloud [324]. Head-on collisions lead to energy gain but the energy can be lost if the cloud is moving away from the particle. The argument of Fermi acceleration is that head-on collisions are more frequent, so that particles gain energy in average with this mechanism.

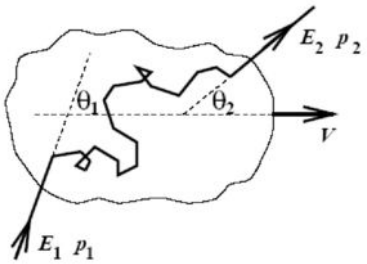

Figure 5.1: Schematic view of the encounter of a charged particle with a magnetic cloud. The particle enters the cloud and is isotropized by the magnetic turbulence. The relevant physical quantities $E_1, p_1, E_2, p_2, \theta_1, \theta_2$ needed to derive the fractional energy gain in the text are shown here.

We will derive the energy gain due to Fermi acceleration in the following. Assuming that the particles are relativistic, and assuming a double change of reference frame

$$\begin{cases} E_1' = \gamma E_1 \left(1 - \beta \cos\theta_1\right) \\ E_2 = \gamma E_2' \left(1 + \beta \cos\theta_2'\right) \end{cases} \tag{5.1}$$

where the subscripts *1* and *2* refer to the incident and outgoing angles and energies of the particle, see Figure 5.1. Using $E_1' = E_2'$ one finds

$$E_2 = \gamma^2 E_1 \left(1 - \beta \cos\theta_1\right)\left(1 + \beta \cos\theta_2'\right)$$
$$\Leftrightarrow \frac{\Delta E}{E} = \frac{E_2 - E_1}{E_1} = \frac{\beta^2 - \beta\cos\theta_1 + \beta\cos\theta_2' - \beta^2\cos\theta_1\cos\theta_2'}{1 - \beta^2}$$

to get the average energy gain, we need to average the above expression. By hypothesis, the particles are isotropized in the cloud, hence $\langle\cos\theta_2'\rangle = 0$. We now need to calculate $\langle\cos\theta_1\rangle$, the probability to have an encounter with an incidence angle θ_1 should be proportional to the relative velocity between the particles and the cloud in the case of uniformly distributed clouds. It gives $P\left(\theta_1\right) \propto v - V\cos\theta_1 (v \simeq c$ and V still being respectively the velocity of the particle and the cloud). Then

$$\langle \cos\theta_1 \rangle = \frac{\int_{-1}^{1} \cos\theta_1 \,(v - V\cos\theta_1)\, d\cos\theta_1}{\int_{-1}^{1} (v - V\cos\theta_1)\, d\cos\theta_1} = \frac{-2V/3}{2v} \simeq \frac{-2V/3}{2c} \simeq -\frac{\beta}{3} \tag{5.2}$$

which leads to

$$\left\langle \frac{\Delta E}{E} \right\rangle = \frac{\beta^2 + \beta^2/3}{1-\beta^2} \simeq \frac{4\beta^2}{3} \tag{5.3}$$

Thus, the average energy gain which is positive, and scales as β^2, so this mechanism is called second order Fermi acceleration.

The energy gain by the particles is proportional to β^2, while a mechanism of head-on collisions between particles and clouds should provide an energy gain proportional to β (first order Fermi acceleration). If there is a mechanism scaling the fractional energy like this, it would be dominant. It turns out that astrophysical shocks can provide this mechanism in the diffusive shock acceleration. Astrophysical shock waves originate from outflows propagating with velocites larger than the speed of sound. The shock is formed due to the interaction of particles with the magnetic field.

When the shock propagates through a medium, there are two distinct regions, the downstream (the region that has already been shocked) and the upstream (the region ahead the shock). The downstream and upstream physical quantities are related by three conservation laws (matter, momentun and energy conservation). Similarly to second order Fermi acceleration, we can calculate the energy gain after a charged particle has undergone a cycle upstream $\rightarrow$ downstream $\rightarrow$ upstream.

Let us denote the unprimed quantities for the upstream frame and primed quantities for the downstream frame. Let $\theta_{\rm in}$ be the the angle between the particle velocity and the shock normal at the initial shock crossing in the upstream frame and $\theta'_{\rm out}$ the angle of the particle with the shock normal in the downstream frame, when crossing the shock back to the upstream medium. On a cycle upstream $\rightarrow$ downstream $\rightarrow$ upstream, we have

$$\begin{cases} E'_{\rm in} = \gamma E_{\rm in}\ (1 - \beta\cos\theta_{\rm in}\ ) \\ E_{\rm out} = \gamma E'_{\rm out}\ (1 + \beta\cos\theta'_{\rm out}\ ) \end{cases} \tag{5.4}$$

where γ and β correspond to the velocity of the downstream medium in the upstream fluid frame, and then we have $\beta = \Delta v/c$ and $\gamma = \frac{1}{\sqrt{1-\frac{\Delta v^2}{c^2}}}$. Using $E'_{\rm in} = E'_{\rm out}$, one finds an analogous expression to the one in the second order fermi acceleration

$$\frac{\Delta E}{E} = \frac{\beta^2 - \beta\cos\theta_{\rm in}\ + \beta\cos\theta'_{\rm out}\ - \beta^2\cos\theta_{\rm in}\ \cos\theta'_{\rm out}}{1-\beta^2} \tag{5.5}$$

The crucial difference between diffusive shock acceleration and second order Fermi acceleration arises from the assumption that the shock velocity is much smaller than the charged particle velocities $v \simeq c \gg v_{\rm sh}$. In this case, the number of charged particles crossing the shock with an angle between θ and $\theta + d\theta$ through a surface dS during a time dt is

$$dN = \frac{n_0}{4\pi} v\cos\theta d\Omega dS dt = \frac{n_0}{2} v\cos\theta\sin\theta d\theta dS dt \tag{5.6}$$

where n_0 is the particle density. The probability of crossing the shock with an angle between θ and $\theta + d\theta$ is then proportional to $\cos\theta \sin\theta d\theta$, and

$$\langle \cos\theta \rangle = \frac{\int_{\theta_{\min}}^{\theta_{\max}} \cos^2\theta \sin\theta d\theta}{\int_{\theta_{\max}}^{\theta_{\max}} \cos\theta \sin\theta d\theta} = \frac{\left[\frac{1}{3}\cos^3\theta\right]_{\theta_{\min}}^{\theta_{\max}}}{\left[\frac{1}{2}\cos^2\theta\right]_{\theta_{\min}}^{\theta_{\max}}} \tag{5.7}$$

leading to $\langle \cos\theta'_{\text{out}} \rangle = \frac{2}{3}$ and $\langle \cos\theta_{in} \rangle = -\frac{2}{3}$, so one finally gets

$$\left\langle \frac{\Delta E}{E} \right\rangle = \frac{4}{3}\beta \tag{5.8}$$

so, the diffusive shock mechanism can accelerate particles, since the fractional average energy gain is positive, and it is first order since it goes linearly with β.

After the particle escapes from the region where it is being accelerated, it won't to gain further energy. This consideration imposes a limit on its maximum energy

$$\varepsilon_{\max} = qB\mathcal{R}, \tag{5.9}$$

where q is the electric charge of the accelerated particle, B is the magnetic field, and $\mathcal{R}$ is the size of the acceleration region. The formula is obtained by demanding that the Larmor radius of the particle, $R_L = \varepsilon/(qB)$, does not exceed the size of the acceleration region. This is a general geometrical argument proposed by Hillas [325], and it is useful in selecting and characterizing acceleration sites, see Figure 5.2

For diffusive shock acceleration, the maximum energy considering that particles lose energy predominantly via synchroton radiation is [326]

$$\varepsilon_{\max} \simeq \frac{3}{2}\frac{m^4}{q^4} B^{-2}\mathcal{R}^{-1} \tag{5.10}$$

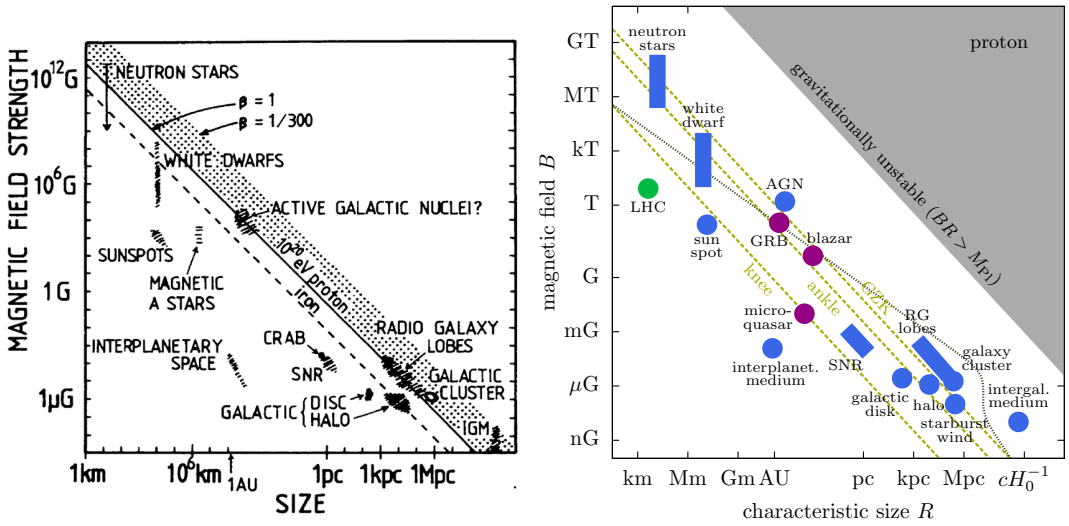

Figure 5.2: *Left panel*: Original plot from Hillas [325]. It displays upper limits on the reachable cosmic-ray energy dependent on the size of the acceleration region and magnetic field strength from different known sources at the time. *Right panel*: Modern adaptation of the Hillas plot [327]. The dotted golden lines indicate the upper limits due to the loss of confinement in the acceleration region for CRs at the knee, ankle, and the Greisen-Zatsepin-Kuzmin (GZK). The dotted gray line corresponds to a second upper limit that arises from synchrotron losses in the sources and interactions in the cosmic photon background. There are no sources expected to go beyond the gray region in this plot.

We have shown that fermi acceleration is able to produce fractional energy gains, and from the Hillas criterion we have also shown that this can lead to high proton energies. However, this is a necessary but not a sufficient condition for this mechanism to produce the cosmic rays that we observe. The particles also need to be accelerated in enough fast timescales. The particle acceleration timescale can be defined as $t_{\rm acc}$

$$t_{\rm acc}(E) = \left(\frac{1}{E}\frac{dE}{dt}\right)^{-1} \tag{5.11}$$

In the following we briefly discuss possible acceleration mechanisms in Active Galactic Nuclei responsible for the neutrino and gamma ray emission.

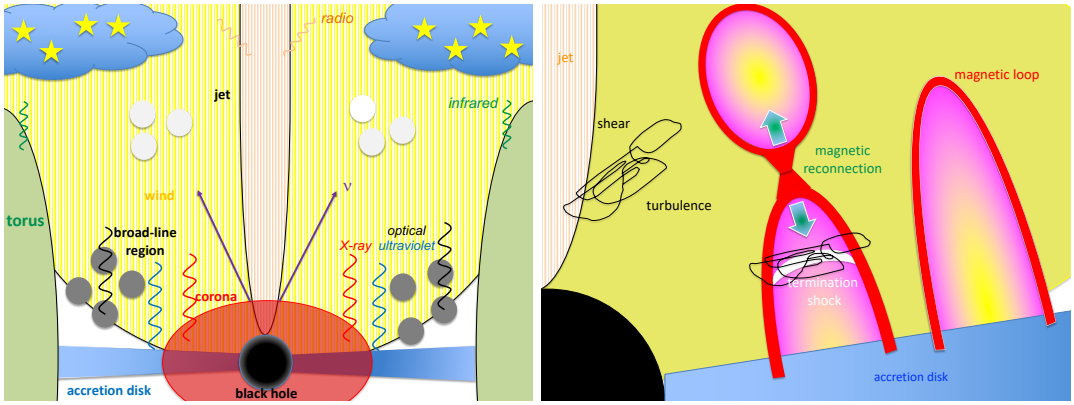

Figure 5.3: *Left panel*: Scheme of an AGN that produces high-energy neutrinos and photons. Gas accreting onto an SMBH forms an accretion disk and hot corona, from which optical, ultra-violet, and X-rays are emitted. Winds and jets may also be present. The dusty torus and starbust region emit infrared radiation. Electromagnetic emission from the disk, corona, and broad-line regions is highly obscured by the ambient photons and gas [328]. *Right panel*: Schematic picture of possible acceleration sites in the coronae [328]

Current observations of high-energy neutrinos from NGC 1068 suggest that acceleration can happen in the coronae [328, 329], see Figure 5.3. CRs may be accelerated via magnetic dissipation [330], magnetohydrodinamic turbulence and shear [331]. The stochastic acceleration timescale depends on the proton energy and reads [332, 333]

$$t_{\rm acc} = \eta_{\rm tur} \left(\frac{c}{V_A}\right)^2 \frac{H}{c} \left(\frac{\varepsilon_p}{eBH}\right)^{2-q} \tag{5.12}$$

where $\eta_{\rm tur}^{-1}$ is the energy fraction of turbulence, q is the energy dependence of the momentum diffusion coefficient, and $V_A \simeq 0.1 c \beta^{-1/2} \mathcal{R}_{1.5}^{-1/2}$ is the Alfvén velocity.

Another possibility that has been discussed for acceleration in the coronae is a magnetic reconnection leading to an upflow and a downflow. This could form a shock at which CRs are accelerated [334]. The acceleration time scale for the diffusive shock acceleration mechanism is

$$t_{\rm acc} = \eta_{\rm sho} \left(\frac{c}{V_A}\right)^2 \frac{\varepsilon_p}{eBc} \tag{5.13}$$

where the velocity of the shock is of the order of the Afvén velocity $V_s \sim V_A$, and $\eta_{\rm sho} = 20/3$ for a parallel shock.

If a jet is present, CRs could also be accelerated by shear acceleration [335]. In this case the timescale is given by

$$t_{\rm acc} = \eta_{\rm she} \beta_\Delta^{-2} \left(l_{\rm tur}/c\right) \left[\varepsilon_p / \left(eBl_{\rm tur}\right)\right]^{2-q} \tag{5.14}$$

where $\eta_{\rm she}$ is an order-of-unity factor for shear acceleration, $\beta_\Delta \propto \varepsilon_p^{2-q}$ is the the velocity difference experienced by particles and $l_{\rm tur}$ is the characteristic turbulence scale that would be a sizable fraction of the system. The shear acceleration timescale can be similar to the stochastic acceleration timescale. Particles might also be accelerated by accretion shocks [336], and in particular from winds [337], in this case the acceleration timescale goes as $t_{\rm acc} \propto \mathcal{R} v_r^{-2}$. Here the acceleration region might be at the Broad Line region or beyond ($\sim 10^4 R_S$) [338], further from the black hole than the corona ($\sim 10 - 100 R_S$).

5.2 Leptohadronic models: Photon and neutrino emission

The spectrum in photons and neutrinos from AGN is believed to be caused by a combination of leptonic processes (producing photons) and hadronic processes (producing photons and neutrinos) [339, 340], see Figure 5.4. High-energy electrons in the AGN jet can interact with low-energy photons in the surrounding environment and boost the photon's energy to higher values via inverse compton scattering. Further, the magnetic field of the AGN will cause the electrons to emit synchroton radiation in the form of radio waves, optical and X-ray photons. Another leptonic process that is present and is responsible for the attenuation of high-energy photons in the AGN is electron-positron pair production ($\gamma\gamma \to e^+e^-$), which occurs for ambient photons with threshold energy $\epsilon_{\rm min} = \frac{m_e^2 c^4}{E_\gamma}$. Electron positron annihilation occurs as well but it is believed to be less important than the rest of leptonic processes.

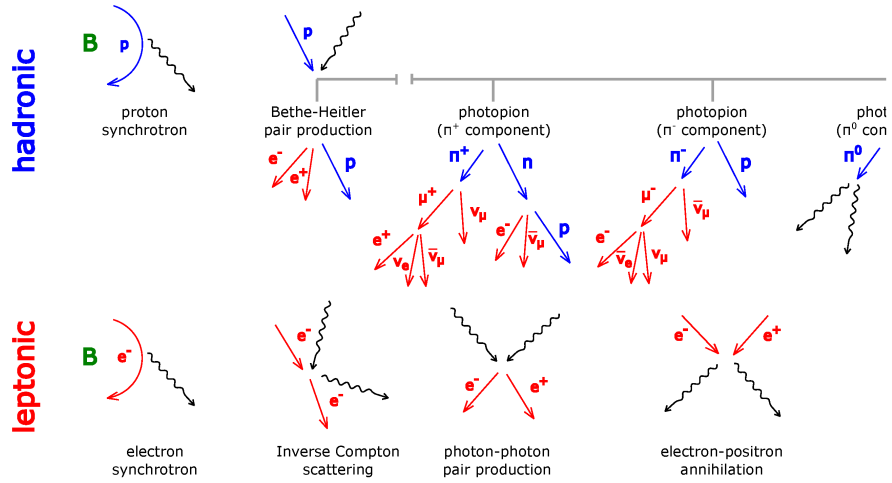

Figure 5.4: Scheme of the different leptonic and hadronic processes responsible for photon and neutrino emission in AGNs.

The main hadronic processes occuring in the AGN are proton-proton collision and proton collisions with the ambient low energy photons in the AGN. Proton-proton collisions are relevant in sources with large gas density, while proton-photon is more relevant

in sources with large photon density. In both processes, charged pions are produced, which can produce photons and neutrinos. Focusing on $p\gamma$ interactions, we have

$$p + \gamma \longrightarrow n + \pi^+ \tag{5.15}$$

where the charged pion decays into neutrinos via

$$\pi^+ \rightarrow \mu^+ + \nu_\mu \rightarrow e^+ + \overline{\nu_e} + \overline{\nu_\mu} + \nu_\mu \tag{5.16}$$

and

$$p + \gamma \longrightarrow p + \pi^0 \tag{5.17}$$

where the neutral pion decays via

$$\pi^0 \rightarrow 2\gamma \tag{5.18}$$

and these processes occur with equal probability. The energy of the resulting neutrinos is a factor of ~ 2 smaller than the photon energies $E_\nu = E_p/20 = \frac{E_\gamma}{2}$, where E_p is the energy of the incoming proton. The luminosities in neutrinos and photons are nonetheless comparable $L_\nu \sim L_\gamma$. However, as we discussed previously, the particles need to escape the source, and ambient photons may attenuate the high energy gamma rays via electron-positron pair production, while the neutrinos are impeded. The threshold energy for the $p\gamma$ process is

$$E_{\rm th} = \frac{2m_p m_\pi + m_\pi^2}{4\epsilon} \simeq 7 \times 10^{16} \left(\frac{\epsilon}{\rm eV}\right)^{-1} {\rm eV} \tag{5.19}$$

Now, astronomers can measure the energies of the ambient photons ϵ directly, so from the observations of neutrinos by IceCube, the initial proton energies can be inferred. The neutrino-gamma ray connection is partially lost due to the opacity of the $\gamma\gamma \rightarrow e^+e^-$ process, however, measurements of the ambient photon energies and densities can allow to reconstruct such connection. For example, for a population of ambient UV/optical photons $\epsilon \sim 10$ eV, and typical neutrino energies at IceCube of $E_\nu = 100$TeV, the inferred proton energy is quite high $E_p \sim 10^6$ TeV. However, for those ambient photon energies, the threshold for electron-positron pair production is quite low, only photons below $E_\gamma 20$ GeV remain unattenuated. Other hadronic processes than can contribute to photon emission are Bethe-Heitler pair production and proton synchroton emission, but these are believed to be less relevant than pp and $p\gamma$.

In the next sections, we discuss in some details observations in neutrinos and photons from different sources, identifying the potential proton and electron acceleration regions and neutrino and gamma-ray emitting regions.

5.3 Blazars

Blazars were first proposed as a common denomination for two types of AGNs, BL Lac objects and flat spectrum radio quasars (FSRQs) [341]. In these objects, a relativistic jet pointing close to our line of sight is present. The photon emission is beamed a Doppler boosted, making them very bright objects in several wavelengths.

The spectrum in photons from blazars generally present two peaks, where the low energy one can appear from infrared to X-ray energies, and it is attributed in purely leptonic models to synchroton radiation, and the higher energy peak can appear in gamma-rays or high-energy gamma-rays, and it is attributed in leptonic models to inverse compton scattering processes in the jet. The target photons for the inverse compton scattering can be provided directly by the synchroton emission at lowe energies, or can originate from a dense radiation field surrounding the supermassive black hole, and with its origin in the accretion disk reprocessed emission. In particular, the optical spectra from some blazars shows broad emission lines, indicating the existence of fast moving clouds at 0.1 to 1pc from the central black hole, while others show no weak or no emission lines in the spectra. The former case points to synchroton self compton emission models, and the latter favours external compton emission from the radiation field.

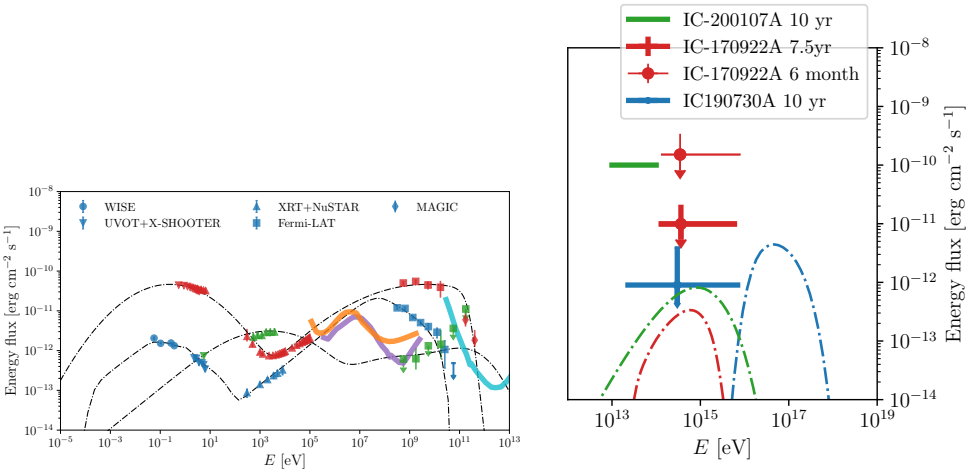

Figure 5.5: *Left panel*: Spectral energy distribution from the blazars TXS 0506+056 (red), PKS 1502+106 (blue), and 3HSP J095507.9+355101 (green) at the time of arrival of the IceCube neutrino events IC-170922A, IC-190730A, and IC-200107A respectively. The dotted lined correspond to model expectations from [342–344]. *Right panel*: Expected energy flux for TXS 0506+056 (red dot-dashed), PKS 1502+106 (blue dot-dashed), and 3HSP J095507.9+355101 (green dot-dashed) at the time of arrival of the neutrino events. The red, blue, and green arrows indicate the 90% CL upper limit on the neutrino flux for different exposures. TXS 0506+056 had the largest gamma-ray flux at the time of the neutrino arrival, thus it has the highest statistical significance.

On 22 September 2017, the IceCube neutrino observatory detected a neutrino event with an energy of 290 TeV, consistent with the direction of the gamma-ray blazar TXS 0506+056, located at a distance of 1421 Mpc [345, 346], see Figure 5.5. The neutrino alert from IceCube triggered an observation campaign ranging from radio to gamma-ray

telescopes [347]. In particular, Fermi-LAT observed an excess of gamma rays from the direction of TXS 0506+056 following the IceCube alert, with more than 5σ significance and reaching energies up to 300 GeV. On the other hand, the initial observations of TXS 0506+056 by ground based gamma-ray telescopes after the IceCube alert only lead to an upper bound on the gamma-ray flux. Nevertheless, a few days later MAGIC detected high-energy gamma-rays up to 400 GeV with a significance that reached 5σ after a few hours of observation, and these observations are compatible with the upper limits from HESS and VERITAS. Further analysis of IceCube archival data increased the number of events to 13 ± 5. If the neutrino association with the blazar TXS 0506+056 is correct, hadronic processes need to be invoked from this source aside from the leptonic channels.

The emitting region of TXS 0506+056 is expected to lie at the Broad Line Region (BLR) or beyond [320]. If the emission were closer to the central black hole, a strongest internal absorption of the 100 GeV γ-rays by the BLR would have been expected.

Furthermore, though with less statistical significance than TXS 0506+056, the IceCube collaboration has identified neutrinos from other blazars [348]. In particular, an event arrived from a direction where 90% of neutrinos have energy ~ 0.33PeV, assuming an E^{-2} neutrino spectrum, and coinciding with the direction of the blazar 3HSP J095507.9+355101. High variability emission in X-rays from thia source shortly after the neutrino arrival. Another neutrino event with ~ 300 TeV was identified from the blazar PKS 1502+106, however, the source was quiet in gamma-rays at the time of the neutrino detection.

In blazars, magnetic fields are believed to launch and collimate the jets, they have a significant role in particle acceleration and thus the flaring of blazars. Understanding the magnetic field on the scales relevant to particle acceleration is crucial. Magnetic fields can be studied by polarization observations because the angle of polarization is related to the direction of the magnetic field, and some observations are shedding light in this aspect [349].

5.4 Non-jetted galaxies

Recently, the IceCube Collaboration identified an excess of 79 events associated with the non-jetted galaxy M77 or NGC 1068, with 4.2σ significance [350] [3]. The surroundings of the supermassive black hole (SMBH) are obscure by a thick gas and dust, while X-ray studies have suggested that NGC 1068 is among the brightest AGNs in intrinsic X-rays.

The neutrino flux is $\sim$ X orders of magnitude larger than the upper limits on the gamma-ray flux placed by MAGIC at sub-TeV energies [351], and the gamma-ray flux measured by Fermi-LAT in the $0.1 - 100$ GeV energy range [352]. In leptohadronic single-zone models, high-energy neutrinos and gamma-rays are mainly produced in the same region of the Active Galactic Nucleus (AGN), mainly via meson decays in $p\gamma$ and pp interactions [353, 354]. This mechanism yields comparable fluxes in neutrinos and gamma-rays. Additionally, gamma-rays can further be produced by leptonic processes,

[3] Previously, the galaxy had been identified as a neutrino source at 2.9σ. Other galaxies are currently being observed at this significance, and a larger increase in the future is therefore likely.

which poses the question of whether standard leptohadronic models are able to accommodate the deficit of gamma rays from NGC 1068, given the neutrino flux observed by IceCube.

A potential solution to the discrepancy between traditional leptohadronic single-zone models and the telescope data relies on high-energy gamma rays and neutrinos being produced near the central supermassive black hole of NGC 1068, at the coronal region $\sim 10R_S - 1000R_S$ [328, 337, 355]. In these scenarions, NGC 1068 is obscure to gamma-rays due to attenuation with the baryonic matter present in the inner regions. Even then, these models are unable to reproduce the spectrum measured by Fermi-LAT for pp or $p\gamma$ production, overproducing gamma-rays at low energy bins, and underproducing them at the larger ones, see Figure 5.6

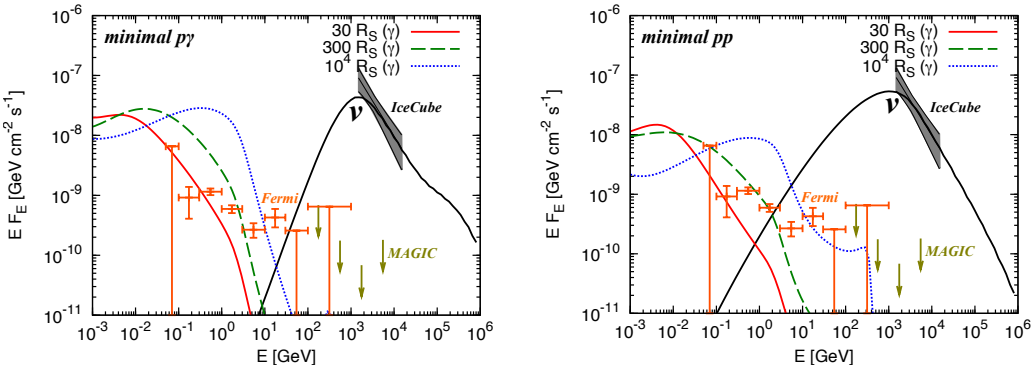

Figure 5.6: *Left panel*: Neutrino and cascaded gamma-ray spectra via pp processes in the coronae, where the inverse compton cascade contribution is significant [328]. *Right panel*: Emission in the $p\gamma$ scenario, where the Bethe-Heitler pair production enhances the cascade flux. In both cases the expected neutrino flux is compatible with observations and close to its maximum peak, and the high-energy gamma ray flux emission is below the upper limits obtained by MAGIC and Fermi-LAT. However, expected low energy gamma-ray overcome the Fermi observations.

Two-zone emission models with enhanced starbust activity with high supernova rates has been proposed as a potential source of the most energetic gamma rays [356]. In this case, the spectral energy distribution can be explained at different wavelengths while yielding a necessary ampount of neutrinos, but these models become increasingly complex and need to invoke a large number of parameters, see figure 5.7

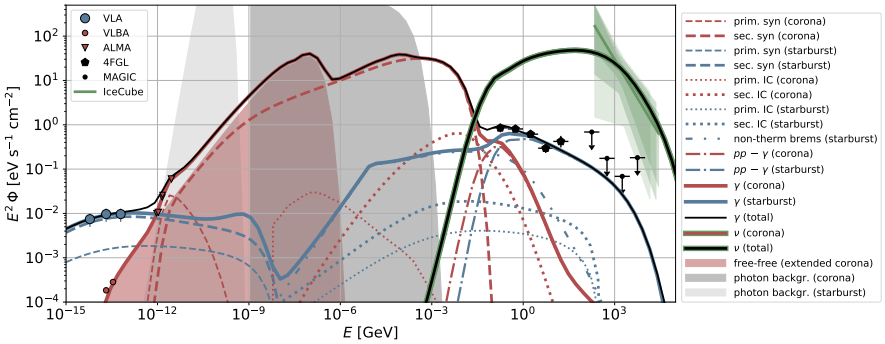

Figure 5.7: Expected spectral energy distribution in photons and neutrinos from NGC 1068 in the two-zone model, w.r.t to observations at different wavelengths. The light red area shows the emission from the corona. The dark grey area indicates the internal flux of the target radiation fields of the central AGN and the light grey area indicates the thermal emission by the starburst region. The spectral energy distribution is well fitted at all energies.

5.5 Tidal Disruption Events

Tidal Disruption Events (TDEs) occur when a star passes within a critical distance from a black hole, and its disrupted by the strong tidal force. The accretion of the released stellar matter in the vicinity of the black hole produces flares of photons in several wavelengths lasting for several days [357–359]. It has been discussed that TDEs may be sources of ultra high energy cosmic rays, which would inevitably lead to the production of high-energy neutrinos [360–363]. In recent years, independent groups have pointed out the potential detection of three TDEs (AT2019dsg, AT2019fdr and AT2019aalc) in IceCube data , with a 3.7 σ combined significance [364–367]. Further, these neutrinos show a delay of order 100 days w.r.t to the maximum of the optical-ultraviolet luminosity.

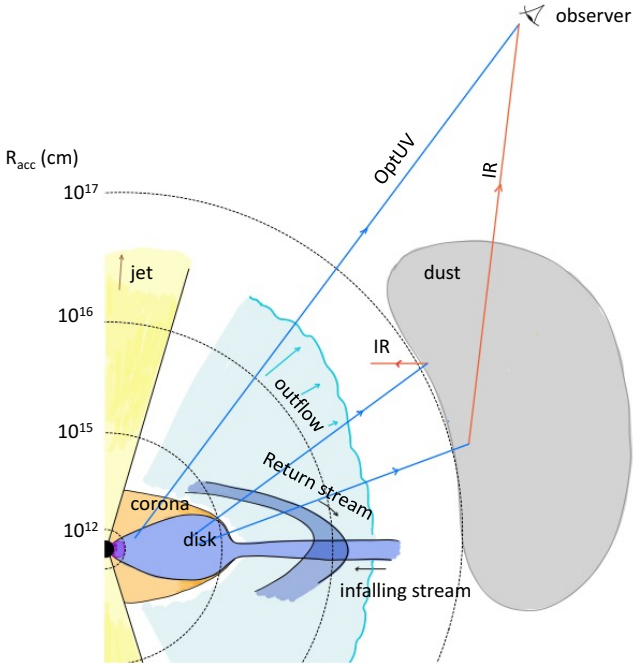

Figure 5.8: Schematic picture of a Tidal disruption event [367]. Some of the main elements are shown, such as a corona, outflows and streams. Three photon histories are sketched, representing the optical-ultraviolet flare, a delayed infrared echo emission, and backwards-emitted infrared photons. The dotted circles indicate different possibilites for the acceleration radius.

The photon and neutrino flares from TDEs are crucial to understand the matter distribution in the innermost regions of the galaxy and the physical processes happening in the vicinity of supermassive black holes (SMBH). Further, TDEs are especially important since they are typically associated with SMBH that are quiet and therefore more difficult to study than Active Galactic Nuclei, since they show no steady emission.

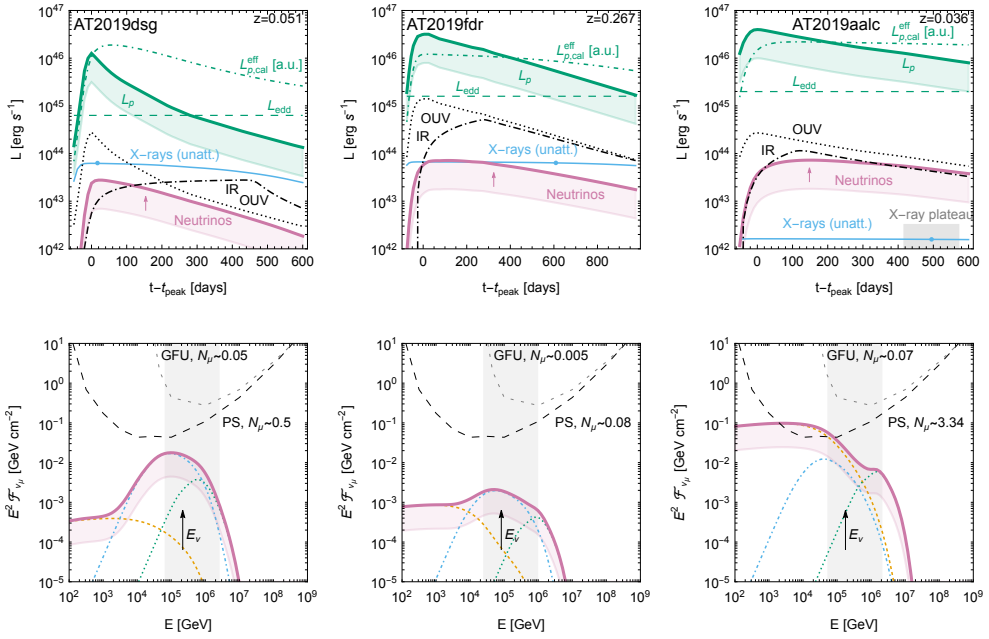

Figure 5.9: Time-dependent evolution of the luminosities (upper plots) and neutrino fluences (lower plots) in a model with moderate-energy photons interacting with X-rays. The upper plots show optical ultraviolet and infrared luminosities. The neutrino observation times are marked by arrows. In the lower plots, the total neutrino fluence is shown, as well as its origin from different targets (outflow *pp*: dashed orange, X-rays: blue dashed-dotted, OUV: green dotted). See [367] for further details.

Some studies have discussed the physical processes leading to neutrino emission from TDEs, postulating that the observed neutrino time delays with respect to the black-body peak come from the physical size of the post-disruption system, such as confinement of protons in magnetic fields over a large enough region, or propagation time delays. The neutrino emission may arise predominantly from proton-photon interactions in the corona, in the vicinity of the black hole, if high enough proton energies can be reached [367].

Chapter 6

Dark matter distribution in the vicinity of black holes

In the previous section, we have seen that Active Galactic Nuclei are able to accelerate cosmic rays to high energies, producing neutrinos and gamma-rays in the vicinity of the central black hole. In this section we discuss our knowledge on the dark matter distribution in galaxies, and in particular the potential formation of an overdensity in the vicinity of the central supermassive black hole of some galaxies.

6.1 Galactic dark matter halos: Simulations and observations

In ΛCDM, the structures of the universe are formed from small early density fluctuations, where the nature of dark matter plays a crucial role. The CMB temperature map anisotropies indicate evidence for fluctuations $\delta(x,t)$ in the primordial matter density

$$\rho(x,t) = \bar{\rho}(t)[1+\delta(x,t)], \tag{6.1}$$

where $\bar{\rho}$ is the average matter density over all space. These small density perturbations form, via gravity, the large scale structures observed in the late universe. The growth of structure are determined by the background pressure and gravity. The overall fluctuating density field can be considered as a superposition of waves with different wavelengths, phases, and amplitudes. Then, it is possible to take a Fourier transform $\delta_k \sim \sum e^{-ikr}$ and measure the power spectrum on different scales, expressed either as wavelengths l, frequencies or wave numbers $k = 1/l$, [368], see Figure 6.1.

At early times, in the radiation dominated era, density perturbations are small $\delta \ll 1$ and general relativity linear perturbation theory can be applied. Indeed, the fields are still weak, and it is possible to obtain the evolution of the density perturbations by using special relativity fluid mechanics and Newtonian gravity (Poisson equation) with a relativistic source term, [368],

$$\nabla^2\Phi = 4\pi G(\rho + 3p/c^2), \tag{6.2}$$

which leads to the following evolution of the density field

$$\ddot{\delta} + 2\frac{\dot{a}}{a}\dot{\delta} = 32\frac{\pi}{3}\rho_0\delta. \tag{6.3}$$

From equation 6.3, one sees that during radiation domination the growth is slow $\delta \sim ln(a)$, being $a(t)$ the scale factor in the FLRW metric. After matter-radiation decoupling, matter dominates the background density and the radiation pressure drops to zero, leading to a linear growth in density perturbations $\delta \sim a$. This discussion is only valid for perturbations outside the horizon, [368]. Nevertheless, in a combined picture of collisionless matter in a radiation background there is a mode of perturbations inside the horizon where the collisionless (non-relativistic) matter component of density ρ_m is perturbed relative to the relativistic radiation component of density ρ_r. This leads to a perturbations growth mode of $\delta \sim 2/3 + a/a_{eq}$, where a_{eq} is the scale factor at matter-radiation equality. For $a < a_{eq}$ the (cold) matter perturbation is "frozen", $\delta \sim constant$, while for $a > a_{eq}$ the matter perturbation grows linearly with $\delta \sim a/a_{eq}$. The overall behaviour (Mészáros effect) is therefore similar to the effects of pressure on a coupled fluid: for scales greater than the horizon, perturbations in matter and radiation can grow together, but this growth ceases once the perturbations enter the horizon, [369].

The perturbations enter the horizon in both the radiation-dominated and the matter-dominated epochs. The difference in the growth rate in these epochs set two important scales in the power spectrum of density perturbations. These are the size of the horizon at matter radiation equality, below which the power spectrum of density fluctuations flattens, and the size of the horizon when dark matter freezes out, see Figure 6.1. Small scales become non-linear first, $\delta \geq 1$ and form gravitationally bound objects that decouple from the overall expansion. This leads to a picture of hierarchical structure formation with small scale structures (like stars and galaxies) forming first and then merging into larger structures (clusters and superclusters of galaxies).

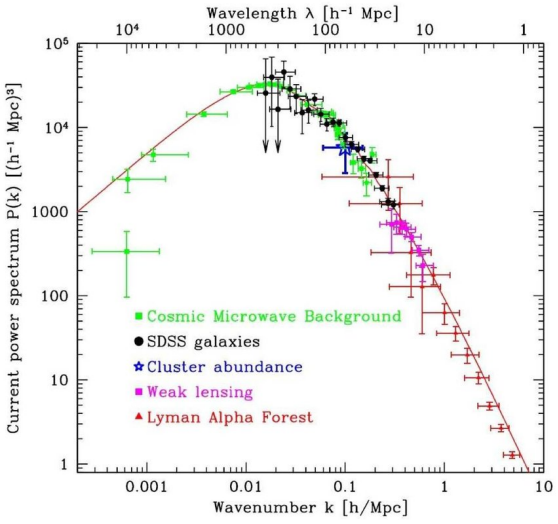

Figure 6.1: Matter power spectrum $P(k)$ versus wave number extrapolated to $z = 0$, from various measurements of cosmological structure. The solid line shows the ΛCDM best fit, [370]

Press and Schechter developed a formalism that allows to predict the number of dark matter halos of a certain mass within a given volume of the Universe from the initial overdensity field $\delta(x,t)$ peaks [369]. Halos are spherical and virialized objects formed from regions with overdensities larger than a critical overdensity $\delta(x,t) > \delta_c$. Then, further assuming that the perturbations follow a gaussian distribution with scale-dependent variance σ given by the power spectrum, and growing linearly, Press and Schechter find the halo mass function

$$\frac{dn}{dM} = \sqrt{\frac{2}{\pi}} \frac{\bar{\rho}}{M} \frac{\delta_c}{\sigma^2} \frac{d\sigma}{dM} \exp\left[-\frac{\delta_c^2}{2\sigma^2}\right] \tag{6.4}$$

which gives the number of halos with mass between M and M+dM. [1].

Using N-body simulations of structure formation in the non-linear regime, Navarro, Frenk and White showed that the density profiles of the simulated dark matter halos are shallower than r^{-2} at small radii and steeper at large radii [373, 374], with profile

$$\rho(r) = \rho_{\rm crit} \frac{\delta_{\rm char}}{(r/r_{\rm s})\,(1 + r/r_{\rm s})^2} \tag{6.5}$$

where $r_{\rm s}$ is a scale radius, and $\delta_{\rm char}$ is a characteristic overdensity. The NFW profile changes gradually from having a -1 slope near the center to -3 at large radii. The NFW profile is a good representation of the equilibrium density profiles of dark matter halos of all masses and in all CDM cosmologies. Thus, halos formed by dissipationless hierarchical clustering seem to have a universal density profile with enclosed mass

$$M(r) = 4\pi\bar{\rho}\delta_{\rm char} r_{\rm s}^3 \left[\ln(1 + cx) - \frac{cx}{1 + cx}\right] \tag{6.6}$$

where $x \equiv r/r_{\rm h}$, and

$$c \equiv \frac{r_{\rm h}}{r_{\rm s}} \tag{6.7}$$

is the halo concentration parameter, and r_h is the bounding radius of a halo. The characteristic overdensity can be related to the concentration parameter, therefore, the NFW profile is completely determined by its mass and concentration parameter, or equivalently by its scale radius and charactheristic overdensity.

Follow-up simulations found profiles showing small deviations from the NFW profile, so a general parametrization of the dark matter profile is typically used [91]

$$\rho(r) = \frac{\rho_0}{(r/r_0)^\gamma \left[1 + (r/r_0)^\alpha\right]^{(\beta-\gamma)/\alpha}} \tag{6.8}$$

where typical values of its constants are given in the following table for some models (the value of r_0 changes for different galaxies and clusters of galaxies)

[1] The Press-Schecter halo mass function is consistent with the oberved matter power spectrum observed at small wavenumbers, but recent photometric observations of high redshift galaxies by the James Webb Space telescope question its consistency at larger wavenumbers, and that of ΛCDM more generally [371, 372]

	α	β	γ	r_0(kpc)
Kra	2.0	3.0	0.4	10.0
NFW	1.0	3.0	1.0	20.0
Moore	1.5	3.0	1.5	28.0
Iso	2.0	2.0	0	3.5

where the NFW parametrization is the most usual. Generalized-NFW profiles can be constructed for $\alpha = 1$ and $\beta = 3$, and varying the value of γ in the range $0 - 2$. More recent simulations found that an old profile proposed for spherical stellar systems in the 60's, the Einasto profile, seemed to be a better fit, yielding a more flattened profile in the inner regions than the NFW profile [375, 376] The prediction from Navarro, Frenk and White of inner density profiles $\rho \propto r^{-\gamma}$, with $\gamma = 1$, seemed to be in contradiction with the rotation curves of some galaxies, that could be better fitted with cored or isothermal density profiles. This apparent discrepancy between simulations and observations has been dubbed the core-cusp problem, and remains a subject of discussion [377–379]. More accurate observations of the orbital speeds of stars and gas in the inner regions of galaxies are needed in order to reduce uncertainties.

6.2 Dark matter spikes

The evidence for the presence of black holes at the center of galaxies is well established by observations of the distribution and kinematics of stars in the inner regions of galaxies [380–382]. The origin and formation of these black holes is plausibly linked to the formation of Active Galactic Nuclei (AGN), and to the properties of galaxies hosting them.

Early works on models of galaxies with central black holes disregarded the origin of the black hole, and focused on deriving stable configurations from placing a black hole at the center of a stellar system [383, 384]. Later on, the adiabatic growth of central black holes from the accretion of baryons on long enough timescales was studied in detail. Adiabatic growth means that a substantial increase in the mass of the black hole takes place after its formation, and that the accrettion proceeds slowly [385]. Mathematically, this means that the integrals of motions of the stellar distribution do not change in time. Peebles applied this hypothesis to the isothermal sphere model, finding that a density cusp of $\rho(r) \sim r^{-1.5}$ would be formed in the inner regions of the galaxy. Further advances and refinements on this result were performed by other authors [386, 387]. Motivated by surface brightness observations that seemed incompatible with the isothermal sphere, Quinlan, Hernquist and Sigurdsson examined this problem for distributions of baryons growing at smaller radii [388]. They found that the black hole mass only affects the radius at which the cusp is formed, and that the slope of the cusp $\gamma_{\rm sp}$ is not only determined by the slope of the pre-existing profile γ, but also by the behavior of the initial phase-space density $f(E)$ as the energy approaches the potential at the center of the system $\phi(0)$ [2].

[2]The formation of baryonic cusps around black holes had already been studied in the 70's for globular clusters. In this context, the dynamical relaxation time of the stars is short compared with the age

In particular, Hernquist, Quinlan and Sigurdsson considered a model with an initial isotropic core. Here, the potential evolves as $\phi_i(r) \sim r^{2-\gamma}$ at small radii, and the initial distribution diverges as a power-law $f_i(E_i) \sim (E - \phi(0))^{-n}$. The distribution function $f(E)$ is then related to the differential energy distribution $N(E)dE$ (the number of stars with energies in the range E to $E + dE$) as

$$N(E) = g(E)f(E) \tag{6.9}$$

where the density of states $g(E)$ reads

$$g_i\left(E_i\right) \sim \int_0^{\phi_i^{-1}(E_i)} dr r^2 \sqrt{\phi_i(r) - E_i} \sim E_i^{(8-\gamma)/2(2-\gamma)} \tag{6.10}$$

Approximating the final potential by a keplerian potential around the black hole, the energy varies with radius as $E_f \sim 1/r$, allowing to relate the density $\rho_f(r)$ to $N_f\left(E_f\right)$ and $N_i\left(E_i\right)$ by

$$\rho_f(r) \sim r^{-2} N_f\left(E_f\right)\left(\frac{dE_f}{dr}\right) \sim r^{-4} N_i\left(E_i\right)\left(\frac{dE_i}{dE_f}\right). \tag{6.11}$$

The adiabatic growth assumption requires invariance of the action (angular momentum for circular orbits, radial action for radial orbits) which allows to relate E_i and E_f as

$$E_i^{(4-\gamma)/2(2-\gamma)} \sim E_f^{-1/2}, \tag{6.12}$$

or

$$E_i \sim r^{(2-\gamma)/(4-\gamma)}. \tag{6.13}$$

Using this relation in equation 6.11, one finds that the density of the final cusp is:

$$\rho_f(r) \sim r^{\frac{3}{2}+n\left(\frac{2-\gamma}{4-\gamma}\right)}. \tag{6.14}$$

Gondolo and Silk adopted the formalism applied for baryons by previous studies, and derived the distribution of dark matter particles around the central black hole for different assumptions on the inner slope of the dark matter halo and its phase-space distribution [271]. Indeed, the assumption of adiabatic growth is well motivated for dark matter particles due to its collisionless nature, given that the timescale for black hole growth due to accretion of both baryonic and dark matter is longer than the dynamical timescale of dark matter and baryons in the radius of black hole dominance, $r_h = GM_{\rm BH}/\sigma^2$. It has been argued that the black hole growth timescale will be generically larger than the dynamical timescale of particles within r_h [385]. The shortest black hole growth timescale is given by the Salpeter timescale, $t_S \sim M_{\rm BH}/\dot{M}_{\rm Edd} \sim 5 \times 10^7$ yr, where $\dot{M}_{\rm Edd}$ is the Eddington accretion timescale. This timescale reflects the Eddington limit. At some level of accretion, the black hole heats the accreting material such that

of the system, which leads to a configuration of $\rho(r) \sim r^{-7/4}$ [389]. However, this assumption is not justified for Active Galactic Nuclei, and different solutions are expected.

the resulting luminosity's radiation pressure would counteract the accretion process. The dynamical timescale is on the other hand $t_{\rm dyn} = r_h/\sigma$, where σ is the velocity dispersion of the particles. Our current knowledge on the relation between black hole masses and velocity dispersion indeed points towards the adiabatic growth regime [390] for $M_{\rm BH} \lesssim 10^{10} M_\odot$.

Gondolo and Silk considered models of initial profiles with an inner core and an inner cusp. In both cases the system of equations to solve is given by the conservation of the integrals of motion:

$$\rho_f(r) = \int_{E_f^m}^{0} dE_f \int_{L_m^c}^{L_f^m} dL_f \frac{4\pi L_f}{r^2 v_r} f_f\left(E_f, L_f\right) \tag{6.15}$$

$$v_r = \left[2\left(E_f + \frac{GM}{r} - \frac{L_f}{2r^2}\right)\right]^{1/2}, \tag{6.16}$$

and

$$E_f^m = -\frac{GM}{r}\left(1 - \frac{4R_{\rm S}}{r}\right), \tag{6.17}$$

$$L_f^c = 2cR_{\rm S}, \tag{6.18}$$

$$L_f^m = \left[2r^2\left(E_f + \frac{GM}{r}\right)\right]^{1/2}. \tag{6.19}$$

which is derived from the adiabatic conditions

$$f\left(E_f, L_f\right) = f(E, L), L_f = L, I\left(E_f, L_f\right) = I(E, L) \tag{6.20}$$

corresponding to conservation of the phase-space distribution, angular momentum and radial action of the dark matter particles. As can be appreciated in the equations above, Gondolo and Silk introduced an approximated capture condition of $L = 4Gm$, corresponding to $E_f = 0$. In reality, when characterizing the dark matter particles with a relativistic phase-space distribution function, Sadeghian et al found that the final dark matter profile vanishes at $R = 2R_S$, instead of $R = 4R_S$ as derived by Gondolo and Silk [391].

For models with an inner cusp [373, 374], $\rho(r) = \rho_0 \left(r/r_0\right)^{-\gamma}$, with r_0 the scale radius of the galaxy, and the phase-space distribution reads

$$f(E, L) = \frac{\rho_0}{\left(2\pi\phi_0\right)^{3/2}} \frac{\Gamma(\beta)}{\Gamma\left(\beta - \frac{3}{2}\right)} \frac{\phi_0^\beta}{E^\beta}, \tag{6.21}$$

with $\beta = (6-\gamma)/[2(2-\gamma)]$ and $\phi_0 = 4\pi G r_0^2 \rho_0/[(3-\gamma)(2-\gamma)]$. Assuming a potential proportional to $r^{2-\gamma}$ at small radii, the action integral cannot be performed exactly. Gondolo and Silk found an approximation good to better than 8% over all of phase space for $0 < \gamma < 2$:

$$I(E, L) = \frac{2\pi}{b}\left[-\frac{L}{\lambda} + \sqrt{2r_0^2\phi_0}\left(\frac{E}{\phi_0}\right)^{\frac{4-\gamma}{2(2-\gamma)}}\right], \tag{6.22}$$

where $\lambda = [2/(4-\gamma)]^{1/(2-\gamma)}[(2-\gamma)/(4-\gamma)]^{1/2}$ and $b = \pi(2-\gamma)/\mathrm{B}\left(\frac{1}{2-\gamma}, \frac{3}{2}\right)$. Expressing E as a function of E_f and integrating 6.15, they obtain

$$\rho_f(r) = \rho_R g_\gamma(r) \left(\frac{R_{\rm sp}}{r}\right)^{\gamma_{\rm sp}} \tag{6.23}$$

with $\rho_R = \rho_0 \left(R_{\rm sp}/r_0\right)^{-\gamma}, \gamma_{\rm sp} = (9-2\gamma)/(4-\gamma)$ is the cuspiness of the spike, and the size of the spike is

$$R_{\rm sp} = \alpha_\gamma r_0 \left(M/\rho_0 r_0^3\right)^{1/(3-\gamma)}. \tag{6.24}$$

where α_γ is a normalization factor and $g_\gamma(r)$ accounts for the particles captured by the black hole, and can be approximated for $0 < \gamma < 2$ by $g_\gamma(r) \simeq (1 - \frac{4R_{\rm S}}{r})$, with $R_{\rm S}$ the Schwarzschild radius. In particular, $\alpha_\gamma \simeq 0.293\gamma^{4/9}$ for $\gamma \ll 1$, and is $\alpha_\gamma = 0.00733$, $0.120, 0.140, 0.142, 0.135, 0.122, 0.103, 0.0818, 0.0177$ at $\gamma = 0.05, 0.2, 0.4, \ldots, 1.4, 2$. The density falls abruptly to zero at $r \lesssim 10R_{\rm S}$, and vanishes for $r < 4R_{\rm S}$, which is however a conservative assumption that neglects relativistic and rotating effects in black holes into account [391, 392].

We notice that for $0 < \gamma < 2$, the density slope in the spike, $\gamma_{\rm sp}$, varies only between 2.25 and 2.5 [3]. The slope of the spike profile from equation 6.23 is consistent with the result from Quinlan et al, where models with $0 < \gamma < 2$ obey

$$n = \frac{6-\gamma}{2(2-\gamma)}. \tag{6.25}$$

The profile of equation 6.23 only holds when the dark matter particles do not effectively annihilate (*e.g* as in scenarios of asymmetric dark matter or axions), or do so very slowly. Otherwise, the number density of dark matter particles follows the following differential equation

$$\frac{dn_{\rm DM}(t,r)}{dt} = \langle\sigma v\rangle n_{\rm DM}^2(t,r) \tag{6.26}$$

with approximate solution

$$n_{\rm DM}(t,r) \simeq \frac{n_{\rm DM}(t_f,r)}{1 + n_{\rm DM}(t_f,r)\langle\sigma v\rangle(t-t_f)} \tag{6.27}$$

Therefore, maximal dark matter density in the inner regions of the spike is saturated to

$$\rho_{\rm sat} = m_{\rm DM}/(\langle\sigma v\rangle t_{\rm BH}) \tag{6.28}$$

where $\langle\sigma v\rangle$ is the velocity averaged dark matter annihilation cross section, and $t_{\rm BH}$ is the time elapsed since the black hole formation. Further, the dark matter spike extends

[3] The result from Gondolo and Silk is not valid for $\gamma = 0$. In this case, $n = 1$ and the spike scales as $\rho(r) \sim r^{-2}$ [388]

to a maximal radius $R_{\rm sp}$, beyond which the dark matter distribution follows the pre-existing NFW-like profile. In full generality, the dark matter profile in the spike reads [271, 393, 394])

$$\rho(r) = \begin{cases} 0 & r \leq 4R_{\rm S}, \\ \frac{\rho_{\rm sp}(r)\rho_{\rm sat}}{\rho_{\rm sp}(r)+\rho_{\rm sat}} & 4R_{\rm S} \leq r \leq R_{\rm sp}, \\ \rho_0 \left(\frac{r}{r_0}\right)^{-\gamma} \left(1+\frac{r}{r_0}\right)^{-(3-\gamma)} & r \geq R_{\rm sp}. \end{cases} \tag{6.29}$$

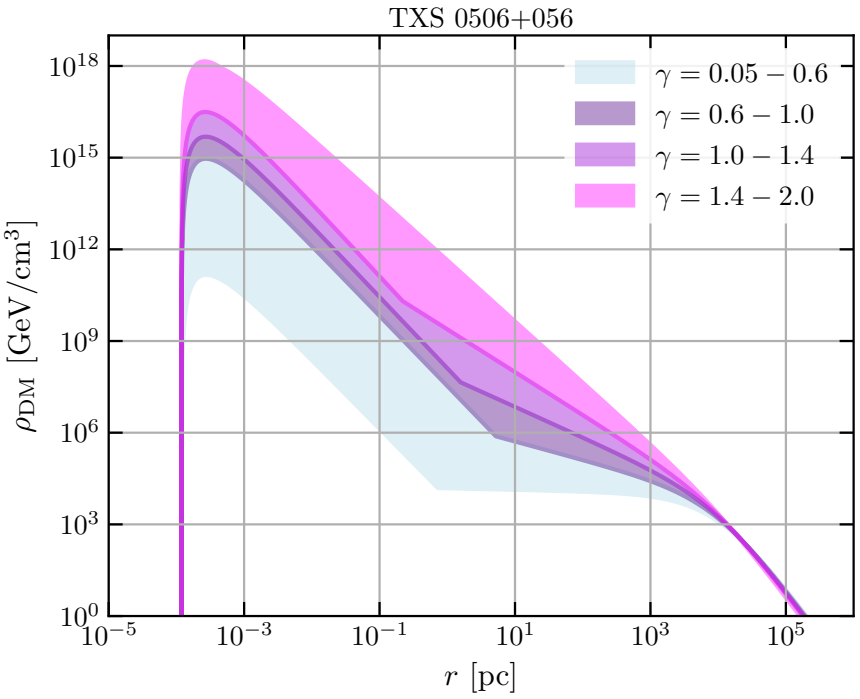

Figure 6.2: Dark matter distribution in the host galaxy of TXS 0506+056, for different values of the initial slope index γ. A black hole mass of (3-10)$\times 10^8 M_\odot$, a scale radius of $r_0 = 10$ kpc, and a mass of the dark matter halo of the galaxy of $M_{\rm DM} = 10^{13} M_\odot$ is assumed [316].

The normalization factor can be obtained from the uncertainty in the black hole mass, in such a way that the profile is compatible with both the total mass of the galaxy and the mass enclosed within the radius of influence of the BH, of order $10^5 R_{\rm S}$. For NFW-like profiles with γ=1, we follow in this thesis the criteria from Gorchtein, Profumo and Ubaldi [395]. The DM mass within the region that is relevant for the determination of the BH mass, typically within $R_0 = 10^5 R_{\rm S}$, must be smaller than the uncertainty on the BH mass $\Delta M_{\rm BH}$. The normalization constant ρ_0 is thus obtained by solving the following equation

$$\int_{4R_{\rm S}}^{10^5 R_{\rm S}} 4\pi r^2 \rho(r) {\rm d}r = \Delta M_{\rm BH} \tag{6.30}$$

Then, we use the fact that the mass is dominated by the contribution from $r \gg R_{\rm S}$, i.e., typically $r > R_{\rm min} = O\left(100 R_{\rm S}\right)$ [393]. One can then obtain

$$\rho_0 = \left(\frac{\left(3-\gamma_{\rm sp}\right) \Delta M_{\rm BH}}{4\pi R_{\rm sp}'^{\gamma_{\rm sp}-\gamma} r_0^{\gamma} \left(R_0^{3-\gamma_{\rm sp}} - R_{\rm min}^{3-\gamma_{\rm sp}} \right)} \right)^{4-\gamma} . \tag{6.31}$$

where $R'_{\rm sp} = \alpha_\gamma r_0 \left(M_{\rm BH}/r_0^3\right)^{\frac{1}{3-\gamma}}$. This criteria yields masses of the dark matter halo below as expected from universal relations between supermassive black hole-galaxy masses [396, 397]. However, for NFW-like profiles with $\gamma \neq 1$, this criteria can underestimate or overestimate the total dark matter mass of the galaxy. For different values of γ, we find in this thesis the normalization value from solving numerically the following equation

$$\int_{4R_S}^{R_{\rm halo}} 4\pi r^2 \rho(r) dr \lesssim M_{\rm DM} \tag{6.32}$$

where $M_{\rm DM}$ is the mass of the dark matter halo and $R_{\rm halo}$ its extension. I this thesis we use $R_{\rm halo} = 5 \times r_0$. In Figure 6.2 we show the dark matter profile of TXS 0506+056, for different values of the the pre-existing NFW profile, and in Figure 6.4, we show a variety of profiles derived under different assumptions on the dark matter self-annihilation cross section and spike indices from TXS 0506+056 and Tidal Disruption Events.

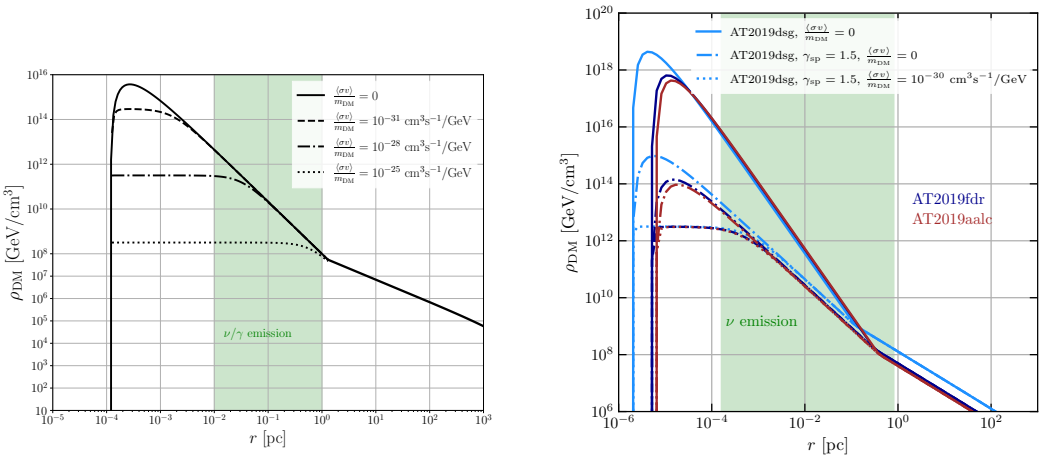

Figure 6.3: *Left panel*: Dark matter profile at TXS 0506+056, for different values of the dark matter self-annihilation cross section and γ=1. *Right panel*: Dark matter profile at the host galaxies of the tidal disruption events AT2019fdr and AT2019aalc, assuming an NFW with $\gamma = 1$, and assuming a spike relaxed by the gravitational scattering with stars and $\gamma_{\rm sp} = 1.5$, see section 7.2 for more details.

Shallower profiles might arise e.g., due to gravitational scattering of dark matter with stars [398, 399], with $\gamma_{\rm sp} = 1.5$, due to mergers of galaxies [400], or due to the black hole formation happening displaced from the center of the galaxy [401], among other possibilities. Dynamical constraints on the existence of spikes have been derived for some sources, with inconclusive results so far, but certainly disfavouring spikes formed from NFW profiles with $\gamma > 1$ *'a la Gondolo and Silk* [402–405], see Figure 6.4. Future gravitational wave observations may help to understand the dark matter distribution around black holes [406–408].

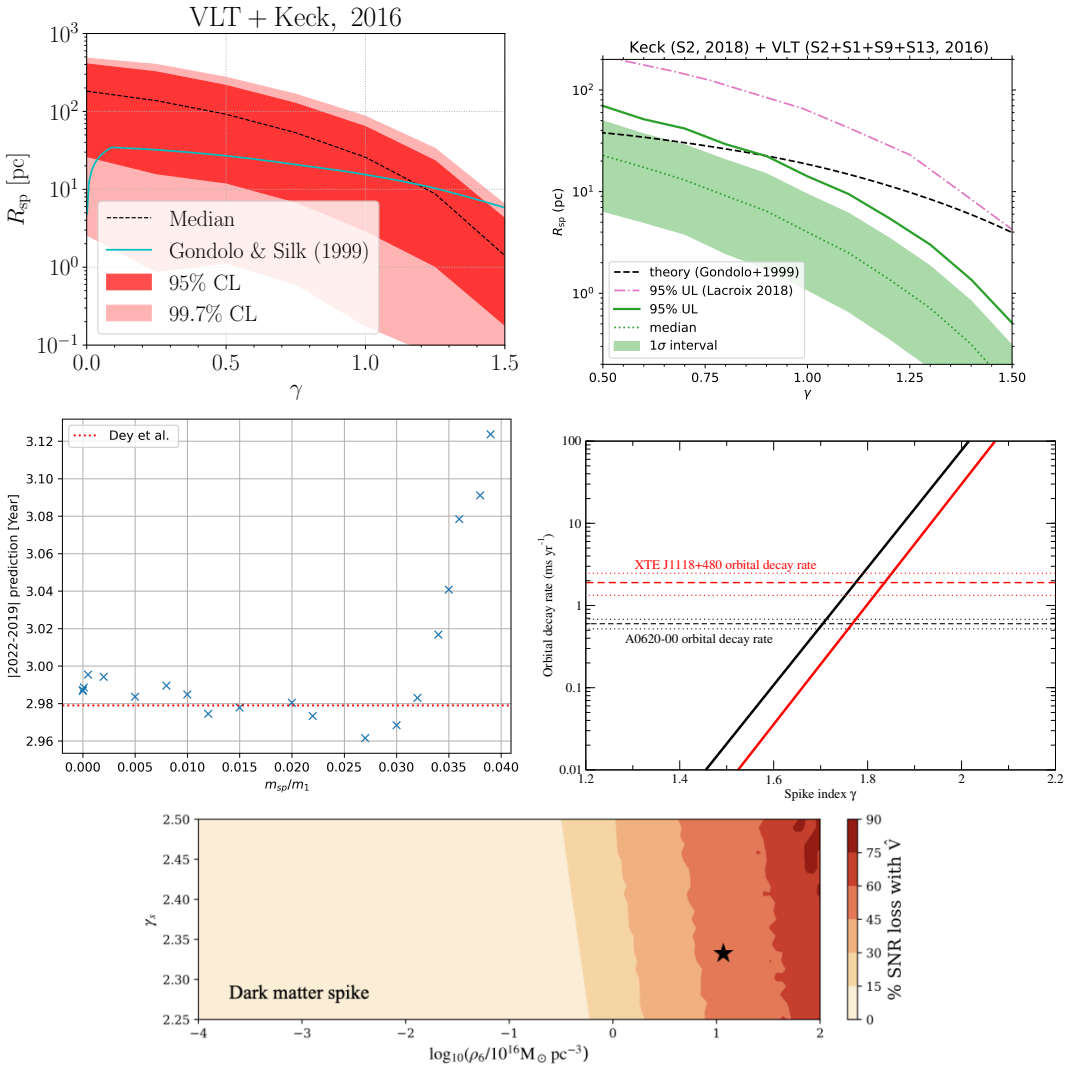

Figure 6.4: *Upper left panel*: Constraints on the spike radius of the milky way vs NFW index γ, from the astrometric and spectroscopic data on the S2 star at the Galactic Centre [402]. The prediction from gondolo and Silk is shown for comparison in blue. *Upper right panel*: More recent constraints on the dark matter spike in the Milky Way, including the motions of stars S2, S1, S9 and S1 [403]. *Middle left panel*: Predictions for the interval between the 2022 and 2019 flares of OJ 287 (vertical axis) for the best fits with the indicated values of the relative spike mass vs model predictions. The spike mass is constrained to be less than 3% of the primary mass [405]. *Middle right panel*: Indirect evidence for dark matter spikes around stellar mass black holes. The black and red lines indicate the relation between the spike index and the orbital period for A0620-00 and XTE J1118+480 respectively [404]. *Lower panel*: Projected signal to noise ratio from a binary black hole gravitational waveform, where the signal is the presence of a dark matter spike formed from an NFW with index $\gamma = 0.05 - 2$[407]

If the dark matter is an axion or an ultralight particle, it may form solitonic cores [409–412]. In this case, the spike formation can be different than for particle dark matter. It has been discussed that wave dark matter halos compressed adiabatically differ from that of the particle halo near the center where the semiclassical approximation breaks down [413].

Chapter 7

Dark matter scatterings with standard model particles in AGN

In previous sections, we have discussed some particle physics models able to account for the dark matter of the Universe, different techniques than can be used to search for these particles, the acceleration and production of high energy particles around black holes, and the distribution of dark matter particles around them. In this section, we put all this information together, studying the impact of dark matter particles on the emitted fluxes of photons and neutrinos in the vicinity of central black holes in AGN

7.1 New constraints on the dark matter-neutrino and dark matter-photon scatterings from TXS 0506+056

The flux of high energy neutrinos and photons produced in a blazar could get attenuated when they propagate through the dark matter spike around the central black hole and the halo of the host galaxy. In this section, using the observation by IceCube of a few high-energy neutrino events from TXS 0506+056, and their coincident gamma ray events in Fermi-LAT and MAGIC, we obtain new constraints on the dark matter-neutrino and dark matter-photon scattering cross sections. We will see that our constraints are orders of magnitude more stringent than those derived from considering the attenuation through the intergalactic medium and the Milky Way dark matter halo. When the cross-section increases with energy, our constraints are also stronger than those derived from the CMB and large-scale structure.

High-energy particles are produced in astrophysical sources and can reach the Earth, providing valuable information about the environment where these particles have been produced and the medium through which they have propagated. While high-energy photons have been detected and their sources had been identified long ago, it is only very recently that sources of high energy neutrinos have been discovered. On 22 September 2017, the IceCube neutrino observatory detected a neutrino event with an energy of 290 TeV, consistent with the direction of the gamma-ray blazar TXS 0506+056, located at a distance of 1421 Mpc [345, 346]. The neutrino alert from IceCube triggered an observation campaign ranging from radio to gamma-ray telescopes [347]. In particular, Fermi-LAT observed an excess of gamma rays from the direction of TXS 0506+056 following the IceCube alert, with more than 5σ significance and reaching energies up to 300 GeV. On the other hand, the initial observations of TXS 0506+056 by ground

based gamma-ray telescopes after the IceCube alert only lead to an upper bound on the gamma-ray flux. Nevertheless, a few days later MAGIC detected high-energy gamma-rays up to 400 GeV with a significance that reached 5σ after a few hours of observation, and these observations are compatible with the upper limits from HESS and VERITAS. Several works have shown that the observed neutrino and gamma-ray fluxes from TXS 0506+056 can be explained with leptohadronic models, where the high energy neutrinos are produced mainly via pp and $p\gamma$ processes, and the bulk of gamma-rays is produced via leptonic processes, with a non-negligible contribution from hadronic processes [349, 414–420].

The gamma ray flux from distant sources is subject to attenuation due to electromagnetic processes in the blazar jet, as well as during their propagation to the Earth due to its interactions with the extragalactic background light, *e.g.* via the process $\gamma\gamma \to e^+e^-$. Neutrinos on the other hand interact very weakly with matter, and therefore they are generically expected to suffer less attenuation during their propagation. Nonetheless, in extensions of the Standard Model, there could be new gamma-ray or neutrino interactions which could affect their propagation to the Earth [421–431]. A notable example arises in scenarios where the dark matter of the Universe is constituted by new elementary particles which interact with the photon or the neutrino. Therefore, the observation of neutrinos from TXS 0506+056 by IceCube can be used to set constraints on the dark matter-neutrino scattering cross-section, from the requirement that the neutrino flux is not significantly attenuated due to interactions with the dark matter during their propagation to the Earth (for previous works considering attenuation in the intergalactic medium and the Milky Way, see [432–435]). Likewise, the observation of photons by MAGIC and Fermi-LAT can be used to set constraints on the dark matter-photon scattering cross-section.

In [315], we consider the attenuation of the gamma-ray and the neutrino flux *within* the host galaxy of TXS-0506+056. Importantly, the supermassive black hole at the center of the blazar is expected to seed the formation of a dark matter spike that extends from $\sim 10^{-4}$ pc to ~ 1 pc, where the density of dark matter particles is substantially larger than the one expected from a naive extrapolation of the galactic density profile. Moreover, it was estimated in [436] that the bulk of the high-energy neutrinos and gamma-rays from TXS 0506+056 are emitted from a region that is close to the Broad Line Region of the blazar $R_{\rm BLR} \sim 0.021$ pc, which lies within the TXS 0506+056 dark matter spike. Therefore, these particles must traverse the spike and the dark matter halo of the host galaxy (and possibly get scattered) before leaving to the intergalactic medium. In this paper we will argue that the absorption of the gamma-ray or neutrino fluxes in the spike can be significant, despite its small size, due to the high density of dark matter particles, and we will derive new limits on the scattering cross-section of dark matter particles with photons or neutrinos.

In the following, we will assume that far away from the black hole, the dark matter distribution follows the standard NFW profile [373, 374], which scales as γ=1 in the central region, resulting in a spike with $\gamma_{\rm sp} = 7/3$ and $\alpha_\gamma \simeq 0.1$. The mass of the supermassive black hole at the center of the blazar TXS 0506+056 was estimated in [436] to be $M_{\rm BH} \approx 3 \times 10^8 M_\odot$, so that $R_S \approx 3.0 \times 10^{-5}$ pc. We have taken r_0=10

kpc, typical of galaxies hosting BL Lac objects, with a similar size as the Milky Way, for example, for which $r_0 \sim 20$ kpc. Finally, the normalization ρ_0 is determined by the uncertainty on the black hole mass [394, 395]. We find the value $\rho_0 \simeq 7 \times 10^3$ GeV/cm^3.

Strictly speaking, this profile only holds when dark matter particles do not annihilate (*e.g* as in scenarios of asymmetric dark matter), or do so very slowly. Otherwise, the maximal dark matter density in the inner regions of the spike is saturated to $\rho_{\rm sat} = m_{\rm DM}/(\langle\sigma v\rangle t_{\rm BH})$, where $\langle\sigma v\rangle$ is the velocity averaged dark matter annihilation cross section, and $t_{\rm BH}$ is the time elapsed since the black hole formation, for which we take the value $t_{\rm BH} = 10^9$ yr [243]. Further, the dark matter profile of the spike extends to a certain maximal radius $R_{\rm sp}$, beyond which the dark matter distribution follows the pre-existing NFW profile. In full generality, the dark matter profile in the spike reads [271] (see also [393, 394])

$$\rho(r) = \begin{cases} 0 & r \leq 4R_S \\ \frac{\rho_{\rm sp}(r)\rho_{\rm sat}}{\rho_{\rm sp}(r)+\rho_{\rm sat}} & 4R_S \leq r \leq R_{sp} \\ \rho_0 \left(\frac{r}{r_0}\right)^{-\gamma} \left(1+\frac{r}{r_0}\right)^{-3+\gamma} & r \geq R_{sp}. \end{cases} \tag{7.1}$$

The dark matter profile of TXS 0506+056 is shown in the left panel of Figure 7.9 for various values of $\langle\sigma v\rangle/m_{\rm DM}$. As apparent from the plot, the dark matter density is extremely high at the position of the broad line region $R_{\rm BLR} \sim 0.023$ pc, where neutrinos and photons are likely to be produced [436], and interactions with dark matter particles may occur with sufficient frequency to produce a sizable attenuation of the flux. In order to be conservative, in our work we will also allow for neutrino/photon emission at larger distances from the black hole, where the density is lower. Concretely, we will consider the range $R_{\rm em} = 10^{-2} - 1$ pc for the region of the blazar jet where neutrinos and gamma-rays are produced, indicated in the Figure as a green region.

Let us note that a more accurate treatment of the adiabatic growth of the dark matter spike including relativistic effects, shows that in fact the spike vanishes at $r = 2R_S$ instead of $4R_S$, and that the density of dark matter particles is significantly boosted near the core [391]. This enhancement is even more pronounced for a rotating black hole [392]. On the other hand, the difference with respect to Eq. (7.23) is only significant close to the Schwarzschild radius, at $r \lesssim 10^{-3}$ pc, whereas the photons and neutrinos are produced further out. We will then disregard these relativistic effects in our analysis, and we will use the profile Eq. (7.23).

The flux of neutrinos and photons produced at the distance $R_{\rm em}$ from the black hole gets attenuated due to interactions with the medium on their way to the Earth[1]

$$\frac{\Phi_i^{\rm obs}}{\Phi_i^{\rm em}} = e^{-\mu_i} \tag{7.2}$$

where $\Phi_i^{\rm obs}$ and $\Phi_i^{\rm em}$ are respectively the observed and emitted fluxes of the particle i ($i = \nu$ or γ), and μ_i is an attenuation coefficient that receives contributions from

[1]Here we are assuming that the emitted flux is much larger that the observed flux, and therefore neglecting the second term in the cascade equation, which accounts for the redistribution of neutrino energies. In the appendix A.1, we discuss the cascade equation in some detail.

scatterings with Standard Model particles (photons, protons, etc.) as well as from dark matter particles. The attenuation due to dark matter reads:

$$\mu_i\big|_{\rm DM} = \frac{\sigma_{\rm DM-i}}{m_{\rm DM}}\Sigma_{\rm DM} \tag{7.3}$$

where $\sigma_{\rm DM-i}$ is the scattering cross section of dark matter with the particle i, and $\Sigma_{\rm DM}$ is the column density of dark matter particles along the path of the particle i:

$$\Sigma_{\rm DM} = \int_{\rm path} dr\rho(r) \tag{7.4}$$

In this paper we focus on the impact on the attenuation of the passage through the dark matter in TXS 0506+056, with density profile given in Eq. (7.23), and that as we will see later it is orders of magnitude stronger than the contribution to $\Sigma_{\rm DM}$ from the dark matter in the intergalactic medium and in the Milky Way. We will then approximate:

$$\Sigma_{\rm DM} \simeq \Sigma_{\rm DM}\Big|_{\rm spike} + \Sigma_{\rm DM}\Big|_{\rm host} \simeq \int_{R_{\rm em}}^{R_{\rm sp}} dr\rho(r) + \int_{R_{\rm sp}}^{\infty} dr\rho(r)\ . \tag{7.5}$$

To calculate $\Sigma_{\rm DM}|_{\rm spike}$ we note that in the region where neutrinos and gamma rays are produced $R_{\rm em} \gg 4R_{\rm S}$, therefore $g_\gamma(r) \simeq 1$. When the annihilation cross-section is very small, the dark matter density in the emission region is much smaller than the saturation density (see the left panel of Fig. 7.9). Then, the density profile in this region reads $\rho_{\rm sp}(r) \simeq \rho_{\rm sp}(R_{\rm em})(\frac{r}{R_{\rm em}})^{-\gamma_{\rm sp}}$ and we can write:

$$\Sigma_{\rm DM}\Big|_{\rm spike} \simeq \int_{R_{\rm em}}^{R_{\rm sp}} dr\rho_{\rm sp}(R_{\rm em})\left(\frac{r}{R_{\rm em}}\right)^{-\gamma_{\rm sp}} \simeq \frac{\rho_{\rm sp}(R_{\rm em})R_{\rm em}}{(\gamma_{\rm sp}-1)}\left[1-\left(\frac{R_{\rm sp}}{R_{\rm em}}\right)^{1-\gamma_{\rm sp}}\right]\ . \tag{7.6}$$

As expected, in this regime $\Sigma_{\rm DM}|_{\rm spike}$ is fairly insensitive to the annihilation cross-section, since annihilations occur at a small rate within the emission region, and the profile in this region is practically indistinguishable from the case with $\langle\sigma v\rangle = 0$. On the other hand, when the cross-section is very large, the dark matter density is approximately equal to the saturation density. Then,

$$\Sigma_{\rm DM}\Big|_{\rm spike} \simeq \int_{R_{\rm em}}^{R_{\rm sp}} dr\rho_{\rm sat} \simeq \rho_{\rm sat}R_{\rm sp}\left[1-\frac{R_{\rm em}}{R_{\rm sp}}\right]\ , \tag{7.7}$$

which is inversely proportional to $\langle\sigma v\rangle/m_{\rm DM}$. In general,

$$\Sigma_{\rm DM}\Big|_{\rm spike} = \int_{R_{\rm em}}^{R_{\rm sp}} dr\frac{\rho_{\rm sp}(r)\rho_{\rm sat}}{\rho_{\rm sp}(r)+\rho_{\rm sat}} \simeq \frac{\rho_{\rm sp}(R_{\rm em})R_{\rm em}}{(\gamma_{\rm sp}-1)}\left[f(1)-f\left(\frac{R_{\rm sp}}{R_{\rm em}}\right)\right]\ , \tag{7.8}$$

where

$$f(x) = x^{1-\gamma_{\rm sp}}\,{}_2F_1\left(1, 1-\frac{1}{\gamma_{\rm sp}}, 2-\frac{1}{\gamma_{\rm sp}}; -\frac{\rho_{\rm sp}(R_{\rm em})}{\rho_{\rm sat}}x^{-\gamma_{\rm sp}}\right)\ , \tag{7.9}$$

with ${}_2F_1(a,b;c;z)$ the hypergeometric function .

Further, the contribution to $\Sigma_{\rm DM}$ from the passage through the halo of the host galaxy is:

$$\Sigma_{\rm DM}\Big|_{\rm host} = \int_{R_{\rm sp}}^{\infty} dr\ \rho_0 \Big(\frac{r}{r_0}\Big)^{-1} \Big(1+\frac{r}{r_0}\Big)^{-2} \simeq \rho_0 r_0 \Big[\log\left(\frac{r_0}{R_{\rm sp}}\right) - 1\Big]\,, \tag{7.10}$$

where we have used $r_0 \gg R_{\rm sp}$. This contribution cannot be neglected. First, the dark matter density is still very large in the proximity of the spike (this is in contrast to the path of the neutrinos or photons from TXS 0506+056 through the Milky Way halo on its way to the Earth, which never gets that close to the Galactic center). Second, the dark matter halo extends for several tens of kpc, which can compensate for the smaller dark matter density.

We show in the right panel of Fig. 7.9 the value of $\Sigma_{\rm DM}$ as a function of the distance from the black hole for three different values of the distance of the emitting region of neutrinos or gamma-rays ($R_{\rm em} = 0.1, 1, 10\, R_{\rm BLR}$) and for the halo profiles considered in the left panel of the figure, sampling different values of the dark matter annihilation cross-section over its mass.

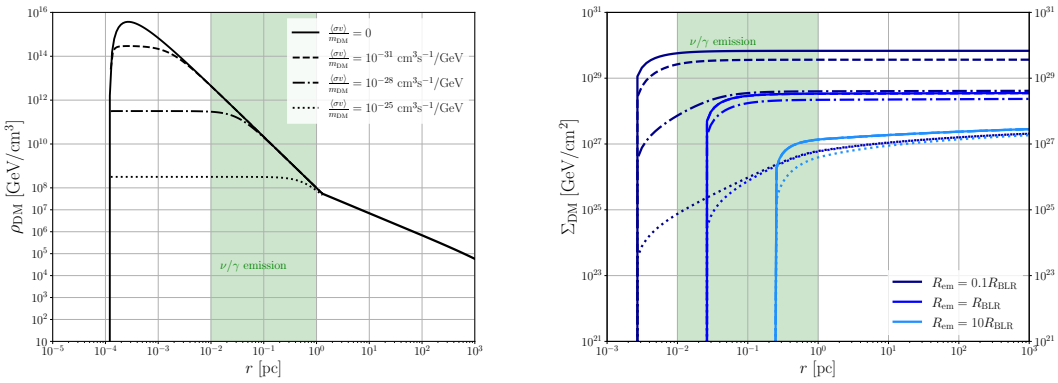

Figure 7.1: *Left panel*: dark matter distribution around the black hole of TXS 0506+056, for different values of the dark matter annihilation cross section over its mass. The green shaded region indicates the range of values considered in this work for the emission region of high-energy neutrinos and gamma rays. *Right panel*: Total dark matter mass along the line of sight to the emission region of high-energy neutrinos and gamma-rays in TXS 0506+056, in terms of the radius of the broad line region of the blazar ($R_{\rm BLR} \simeq 0.023$ pc), for the halo profiles shown in the left panel.

To derive upper bounds on the interaction cross section of neutrinos with dark matter, we follow the same procedure as in [432–434]. Namely, we impose that the attenuation due to dark matter-neutrino interactions is less than 90%, which translates into $\mu_\nu|_{\rm DM} \lesssim 2.3$. The attenuation of the photon flux is more uncertain, since photons interact more strongly than neutrinos with Standard Model particles in the medium. Therefore, we will impose a more aggressive criterion and we will require that the attenuation of the

photon flux due to dark matter interactions is less than 99%, *i.e.* $\mu_\gamma|_{\rm DM} \lesssim 4.6$. These requirements on the attenuation then allow to set upper limits on the scattering cross section over the mass:

$$\frac{\sigma_{\rm DM-\nu}}{m_{\rm DM}} \lesssim \frac{2.3}{\Sigma_{\rm DM}}\,, \frac{\sigma_{\rm DM-\gamma}}{m_{\rm DM}} \lesssim \frac{4.6}{\Sigma_{\rm DM}}\,,$$

with $\Sigma_{\rm DM}$ given in Eq. (7.13) (see also Fig. 7.9).

Our main results are shown in Figures 7.10 and 7.3. The top panels of Figure 7.10 show upper limits on the dark matter-neutrino (left) and dark matter-photon (right) cross-section as a function of the dark matter mass, assuming $\gamma = 1$, when the cross-section is energy independent. The blue lines are the limits derived in this work from imposing Eq. (7.28) in different scenarios: the solid lines assume $\langle\sigma v\rangle = 0$ while the dashed lines are for $\langle\sigma v\rangle = 10^{-28}\,{\rm cm^2 s^{-1}}$, which amount to two different dark matter spike profiles. The different shades of blue correspond to different locations of the emitting region of neutrinos and photons. When $\langle\sigma v\rangle = 0$, we find the upper limits $\frac{\sigma_{\rm DM-\nu}}{m_{\rm DM}} \leq 2.0 \times 10^{-29}$ cm^2/GeV and $\frac{\sigma_{\rm DM-\gamma}}{m_{\rm DM}} \leq 4.1 \times 10^{-29}$ cm^2/GeV. The limits for other halo profiles can be calculated from Eqs. (7.13-7.9). Assuming $R_{\rm em} = R_{\rm BLR}$, our upper limits change by a factor of at most ~ 2 for halo profiles in the range $\gamma = 0.7 - 1.4$.

As the dark matter self-annihilation cross-section increases, the effect of the flux attenuation becomes smaller, and the limits on the dark matter neutrino and photon scattering cross-sections become weaker. This is illustrated in the bottom panels in Figure 7.10, which show the dependence on the upper limits on $\sigma_{\rm DM-i}/m_{\rm DM}$ as a function of $\langle\sigma v\rangle/m_{\rm DM}$ for different values of the location of the emission region $R_{\rm em}$. The lines reflect the dependence of the column density on the cross-section. For small dark matter self-annihilation cross-sections, $\Sigma_{\rm DM}$ is roughly constant, since the halo profiles are practically indistinguishable, and thereby the limit on the scattering cross-section; for larger annihilation cross-sections, $\Sigma_{\rm DM}$ is inversely proportional to $\langle\sigma v\rangle/m_{\rm DM}$, and therefore the limit on the scattering cross-section increases linearly with $\langle\sigma v\rangle/m_{\rm DM}$; for very large annihilation cross-sections, $\Sigma_{\rm DM}$ is dominated by the passage through the dark matter halo of the host galaxy, and again the limit on the scattering cross-section becomes independent of $\langle\sigma v\rangle/m_{\rm DM}$.

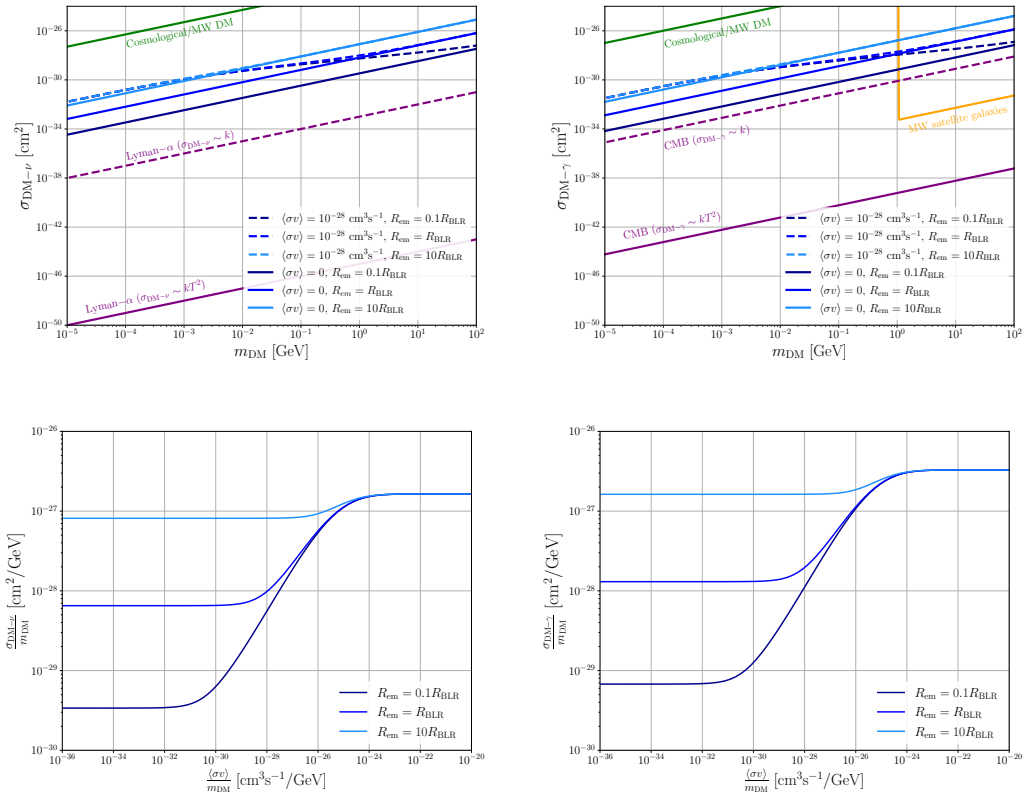

Figure 7.2: *Top panels:* Upper limits on the dark matter-neutrino (left panel) and dark matter-photon (right panel) scattering cross-sections as a function of the dark matter mass, derived from the requirement that the neutrino (photon) flux is attenuated by less than 90% (99%) when traversing the dark matter spike and the galactic halo of TXS 0506+056. The different blue shadings correspond to different locations of the neutrino or photon emission, while the different dashing denote different spike profiles. The green line shows the limits derived from the passage of the neutrinos or photons through the intergalactic medium and the Milky Way halo, the purple lines from Lyman-α observations, and the orange line from Milky Way satellite galaxy counts. *Bottom panels:* Dependence on the limits on $\sigma_{\mathrm{DM}-\nu}/m_{\mathrm{DM}}$ (left panel) and $\sigma_{\mathrm{DM}-\gamma}/m_{\mathrm{DM}}$ (right panel) with the dark matter self-annihilation cross-section, for different locations of the emission region.

For comparison, we also show in the upper panels of the Figure 7.10 (as solid green lines) the upper limits on the dark matter-neutrino and dark matter-photon scattering cross-sections from the attenuation of neutrinos or photons due to interactions with dark matter particles in the intergalactic medium and in the Milky Way halo. As is apparent from the plot, the attenuation of the flux during the passage through the dark

matter spike and the galaxy hosting the blazar is very significant. Specifically, when the neutrinos or photons are emitted at $R_{\rm em} = R_{\rm BLR}$ and the dark matter does not self-annihilate, the limits on the cross-section become about six orders of magnitude stronger than those obtained when neglecting the spike and considering just the propagation through the intergalactic medium and the Milky Way halo; when the annihilation cross-section is $\langle\sigma v\rangle = 10^{-28}\,{\rm cm}^2\,{\rm s}^{-1}$, the limits are four to six orders of magnitude stronger, depending on the dark matter mass.

We also show (as purple lines) the constraints on the cross-section obtained from the suppression of primordial density fluctuations in the early universe, which would affect the cosmic microwave background power spectrum and the Lyman-α forest [437–441][2], for the case when the cross section is constant (dotted line), and when the cross section scales as the square of the temperature of the Universe (solid line). For photons, we additionally show (as a solid orange line) the limit derived in [444] for $m_{\rm DM} \gtrsim 1$ GeV from Milky Way satellite galaxy counts [445] [3].

The cosmological limits on the dark matter-neutrino cross section are a few orders of magnitude stronger than the ones derived in this work from TXS 0506+056. However, in any realistic model, the dark matter-neutrino cross section will have a power-law dependence with the neutrino energy, $\sigma_{{\rm DM}-\nu} = \sigma_0(\frac{E_\nu}{1{\rm GeV}})^n$. Since the neutrinos observed from TXS 0506+056 are significantly more energetic ($E_\nu \sim 290$ TeV) than the neutrinos relevant for the Lyman-α bounds ($E_\nu \sim 100$ eV), the cross-sections involved in these two observations could be largely different. In order to compare the impact of the dark matter-neutrino (or photon) interactions, it is necessary to extrapolate the limits obtained from the TXS 0506+056 to the energy scales relevant for the Lyman-α forest. The same rationale holds for DM-γ interactions.

This is done in Figure 7.3, which shows the upper limit on the dark matter neutrino (left) and dark matter-photon (right) cross-section as a function on the energy, when the cross-section scales with the energy as $\sigma_{{\rm DM}-\nu} = \sigma_0(E_\nu/1\,{\rm GeV})^n$, for $n = 1, 2, 4$ (dotted, dashed and solid lines, respectively). For the plot we took for concreteness $m_{\rm DM} = 1$ GeV, and two spike profiles corresponding to a scenario of asymmetric dark matter ($\langle\sigma v\rangle$=0, dark blue) and of self-annihilating dark matter ($\langle\sigma v\rangle = 10^{-28}\,{\rm cm}^2\,{\rm s}^{-1}$), light blue. For comparison, we also show complementary constraints at different neutrino energies from SN1987A [451], and from Lyman-α observations. As can be seen from the figure, our limits from the attenuation of the flux at the spike of TXS 0506+056 are substantially stronger than previous limits. For instance, for $n = 1$ our limits on the dark matter-neutrino cross-section are ~ 8 orders of magnitude stronger than those from

[2] Recently, stronger constraints on dark matter-neutrino scattering were derived from Milky Way satellites and subhalo modelling for dark acoustic oscillations, adressing on different particle physics scenarios and energy regimes whether astrophysical os comological probes are dominant [442]. The IceCube collaboration has also recently perfomed a dedicated analysis to search for attenuation signatures from AGN in concrete models, see [443]

[3] Stronger constraints can be derived for concrete models. For instance, when the dark matter couples with similar strength to electrons and to neutrinos, the limits on the dark matter-electron cross-section from [246, 255, 446–449] can be translated into limits on the dark matter-neutrino cross-section. Also, when the interaction dark matter-photon is due to a dark matter millicharge, the stringent limits derived in [450] would apply.

Lyman-α observations, and can be even ~ 20 orders of magnitude stronger for $n = 2$. Similar conclusions hold for the dark matter-photon cross-section.

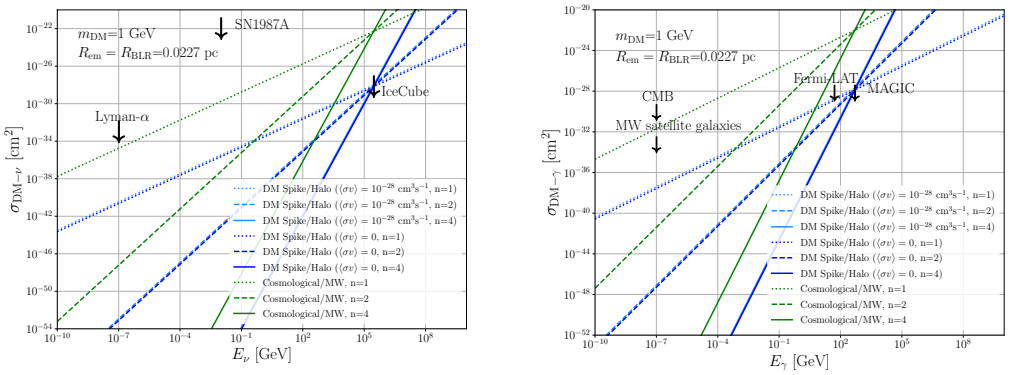

Figure 7.3: Same as the top panels of Fig.7.10, but as a function of the energy for the case $m_{\rm DM} = 1$ GeV and $R_{\rm em} = 0.023$ pc, assuming that the cross-section scales with the energy as $\sigma_{\rm DM-i} = \sigma_0 (E_i/1\,{\rm GeV})^n$, for $n = 1, 2, 4$.

High-energy neutrinos and photons have been detected from the blazar TXS 0506+056, with fluxes which are well compatible with astrophysical models. This indicates that the fluxes are not significantly attenuated by putative interactions of neutrinos or photons with the dark matter particles existing between their production point and the Earth. In this work we have investigated the possible attenuation of the fluxes due to the dark matter spike around the black hole of TXS 0506+056.

For scenarios where dark matter particles do not self-annihilate, we find the upper limits $\frac{\sigma_{\rm DM-\nu}}{m_{\rm DM}} \leq 2.0 \times 10^{-29}$ cm^2/GeV and $\frac{\sigma_{\rm DM-\gamma}}{m_{\rm DM}} \leq 4.1 \times 10^{-29}$ cm^2/GeV, which are ~ 7 orders of magnitude stronger than constraints derived in previous works from the attenuation of the fluxes in the intergalactic medium and the Milky Way halo. Assuming that the cross-section is independent of the energy, the limits on the dark-matter neutrino (dark matter-photon) cross-section are ~ 5 (~ 2) orders of magnitude weaker than those stemming from the cosmic microwave background and from large scale structure. Similar conclusions hold when the dark matter particles can self-annihilate, although in this case the constraints become weaker, due to the flattening of the spike at small distances from the black hole.

We have also considered scenarios where the scattering cross-section depends with the energy as a power-law $\sigma_{\rm DM-i} = \sigma_0 (\frac{E_\nu}{1{\rm GeV}})^n$, with $n = 1, 2$ or 4. In this case the constraints on the dark matter-neutrino and dark matter-photon cross section from the attenuation in the spike of TXS 0506+056 are several orders of magnitude more stringent than those from Cosmology.

Blazar observations in neutrinos and gamma-rays therefore constitute a powerful probe of dark matter interactions, especially for scenarios where the cross-section is energy dependent. The likely discovery of more and more neutrino sources in current and future

neutrino telescopes, and their identification with gamma-ray sources, will provide very valuable information about the dark matter microphysics, and perhaps provide hints for neutrino or photon interactions with dark matter particles.

7.2 Constraints on dark matter-neutrino scatterings in Tidal Disruption Events

We discuss the implications of dark matter neutrino interactions in Tidal Disruption Events (TDEs). In TDEs, neutrinos and photons are likely to be emitted very close to the supermassive black hole, at $R \sim 10^3 R_S$. We have discussed that the neutrino and gamma-ray emission from blazars such as TXS 0506+056 happens further from the center of the galaxy, a the Broad Line Region or beyond $R_{\rm em} \sim 10^4 R_S$, and in non-jetted galaxies as NGC 1068, current observations suggest acceleration and neutrino emission in the coronal region of the central black hole $R_{\rm em} \sim 10^2 R_S$, however, uncertainties are large. In this sense, TDEs may constitute in the future a more robust probe of the dark matter distribution of the vicinity of black holes, since stars are expected to be tidally disrupted mainly in the region of gravitational influence of the black hole. Further, since TDEs are associated with quiet galaxies, the astrophysical background of photon and neutrino emission is lower, and the dark matter spike may have been less depleted due to interactions with stars, in contrast to AGNs [91, 398, 400]. Therefore, it becomes important to derive constraints on dark matter-neutrino scatterings from these sources, and confront them with the constraints obtained from TXS 0506+056 and NGC 1068. In the following table, we show the benchmark parameters considered for some TDEs

	$R_{\rm em}$	$M_{\rm BH}$	$\Delta M_{\rm BH}$	$\gamma_{\rm sp}$	$\langle\sigma v\rangle/m_{\rm DM}$	$\rho_{\rm DM}(R_{\rm em})$
AT2019dsg (1)	5×10^{14} cm	$5\times10^6 M_\odot$	$0.5\times10^6 M_\odot$	2.25	0	5.2×10^{15} GeV/cm^3
AT2019dsg (2)	5×10^{14} cm	$5\times10^6 M_\odot$	$0.5\times10^6 M_\odot$	1.5	0	2.1×10^{13} GeV/cm^3
AT2019dsg (3)	5×10^{16} cm	$5\times10^6 M_\odot$	$0.5\times10^6 M_\odot$	1.5	10^{-30}cm^{3}s^{-1}/GeV	2.2×10^{10} GeV/cm^3
AT2019fdr (1)	4.9×10^{15} cm	$1.3\times10^7 M_\odot$	$1.3\times10^6 M_\odot$	2.25	0	3.6×10^{13} GeV/cm^3
AT2019fdr (2)	4.9×10^{15} cm	$1.3\times10^7 M_\odot$	$1.3\times10^6 M_\odot$	1.5	0	4.3×10^{11} GeV/cm^3
AT2019fdr (3)	2.5×10^{17} cm	$1.3\times10^7 M_\odot$	$1.3\times10^6 M_\odot$	1.5	10^{-30}cm^{3}s^{-1}/GeV	6.1×10^7 GeV/cm^3
AT2019aalc (1)	5×10^{15} cm	$1.6\times10^7 M_\odot$	$1.6\times10^7 M_\odot$	2.25	0	3.8×10^{13} GeV/cm^3
AT2019aalc (2)	2×10^{17} cm	$1.6\times10^7 M_\odot$	$1.3\times10^6 M_\odot$	1.5	0	1.5×10^9 GeV/cm^3
AT2019aalc (3)	2×10^{17} cm	$1.6\times10^7 M_\odot$	$1.3\times10^6 M_\odot$	1.5	10^{-30}cm^{3}s^{-1}/GeV	1.5×10^9 GeV/cm^3

Table 7.1: Relevant parameters considered in this work for the Tidal disruption events considered in this work, for two different sets of assumptions dubbed (1) and (2). $R_{\rm acc}$ is the region where protons and electrons are accelerated, $M_{\rm BH}$ is the mass of the central black hole, $\Delta M_{\rm BH}$ the uncertainty on the measurement of the mass of the central black hole, $\langle\sigma v\rangle/m_{\rm DM}$ denotes the assumed values of the effective dark matter self-annihilation cross section, and $\langle\rho_{\rm DM}\rangle$ is the average density of dark matter particles in the region of the AGN where protons and electrons are accelerated before the bulk of neutrinos and gamma-rays are emitted.

We will derive upper limits assuming that the dark matter-neutrino scattering cross section is constant. Imposing that the attenuation of the neutrino fluxes shall not be larger than 90% of the initial emitted neutrino flux, the upper limit is given by [315]:

$$\frac{\sigma_{\mathrm{DM}-\nu}}{m_{\mathrm{DM}}} \lesssim \frac{2.3}{\Sigma_{\mathrm{DM}}} \tag{7.11}$$

where Σ_{DM} is the column density of dark matter particles along the line of sight between the TDE an the Earth, and is largely dominated by the contribution from the spike and halo of the host galaxy. In the right panel of Figure 7.4, we show constraints on the dark matter-neutrino scattering cross section, for the different TDEs considered in this work, and the different set of assumptions discussed in 7.1.

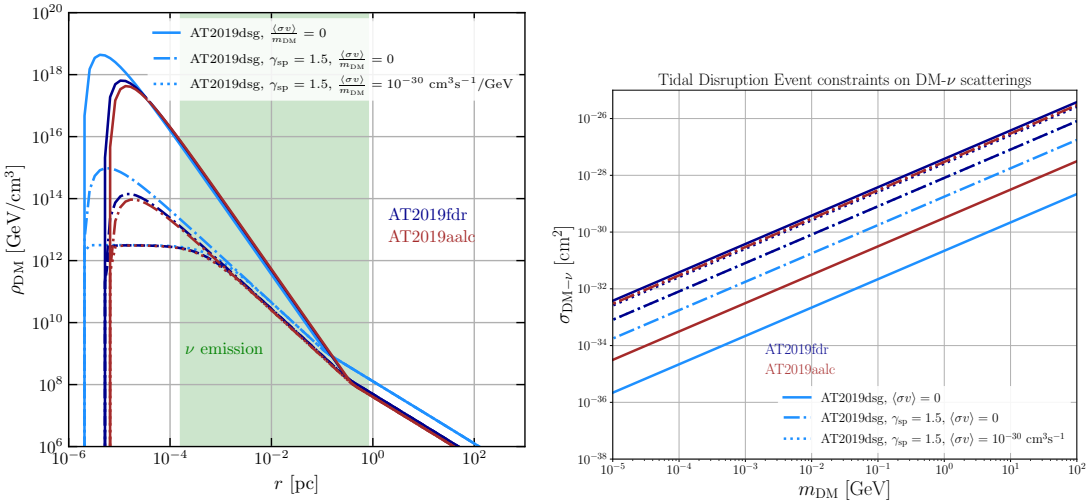

Figure 7.4: *Left panel*: Dark matter distribution around the black holes of AT2019dsg and AT2019fdr, for different values of the dark matter self-annihilation cross section over its mass. The green region shows the likely emitting region of neutrinos from this sources *Right panel*: Upper limits on the constant dark matter-neutrino scattering cross section from AT2019dsg, AT2019fdr and AT2019aalc, for different assumptions on the dark matter distribution and astrophysical emission of neutrinos, see 7.1

The constraints obtained are stronger than those derived from TXS 0506+056 previously by $\sim$ 1 order of magnitude. When considering annihilations with sufficiently large cross section, we also find that the spike is depleted in the same way when taking the intact spike and the relaxed spike due to gravitational scattering with stars. In this sense, for self-annihilating dark matter the relaxation due to stars is less relevant than for asymmetric dark matter. The constraints when including annihilations are still stronger than those obtained from TXS 0506+056, but the enhancement here is lower, due to the larger black hole mass (and age) of TXS 0506+056.

7.3 A hint of dark matter-photon scatterings in NGC 1068

The IceCube collaboration recently reported a 4.2σ measurement of neutrinos with TeV energies from the galaxy NGC 1068 [350]. The neutrino flux is significantly larger than the upper limits on the gamma-ray flux placed by MAGIC at sub-TeV energies [351], and the gamma-ray flux measured by Fermi-LAT in the $0.1 - 100$ GeV energy range [352]. In leptohadronic single-zone models, high-energy neutrinos and gamma-rays are mainly produced in the same region of the Active Galactic Nucleus (AGN), mainly via meson decays in $p\gamma$ and pp interactions [353, 354]. This mechanism yields comparable fluxes in neutrinos and gamma-rays. Additionally, gamma-rays can further be produced by leptonic processes, which poses the question of whether standard leptohadronic models are able to accommodate the deficit of gamma rays from NGC 1068, given the neutrino flux observed by IceCube.

A potential solution to the discrepancy between traditional leptohadronic single-zone models and the telescope data relies on high-energy gamma rays and neutrinos being produced near the central supermassive black hole of NGC 1068, at the coronal region $\sim 10R_S - 1000R_S$ [328, 337, 355]. In these scenarions, NGC 1068 is obscure to gamma-rays due to attenuation with the baryonic matter present in the inner regions. Even then, these models are unable to reproduce the spectrum measured by Fermi-LAT for pp or $p\gamma$ production, overproducing gamma-rays at low energy bins, and underproducing them at the larger ones. Enhanced starbust activity with high supernova rates has been proposed as a potential source of the most energetic gamma rays [356], but these models become increasingly complex and need to invoke a large number of parameters.

We suggest in [452] an alternative mechanism to explain the observations from NGC 1068, which is an enhanced photon absorption due to scatterings with the ambient dark matter particles present in the inner regions of NGC 1068. The supermassive black hole of NGC 1068 is expected to seed the formation of a dark matter spike with very large density within a few parsecs from the SMBH [271], which is expected to be the same region where the bulk of neutrinos and gamma-rays are produced. This enables relatively low scattering cross sections of dark matter particles with photons needed to induce observable attenuation effects. As we will show later, this mechanism yields a gamma-ray flux compatible with Fermi-LAT data in the $0.1-100$ GeV energy range, and allowing for the production of neutrinos and photons at farther regions from the black hole, at the Broad Line Region $\sim 10^4 R_S$, or beyond. In fact, this is the expectation in traditional leptohadronic single-zone models proposed to explain the only other well known extragalactic neutrino source known aside NGC 1068, TXS 0506+056 [436].

NGC1068 is a well studied Seyfert II galaxy, hosting an Active Galactic Nucleus (AGN). The supermassive black hole (SMBH) at the center of NGC1068 is expected to provide the conditions to accelerate protons to very high energies, which then lead to the production of energetic photons and neutrinos via $p\gamma$ and pp interactions. On general grounds, one expects comparable production rates of photons and neutrinos [353, 354]. On the other hand, NGC1068 is known to be fairly opaque to high-energy gamma-rays, due to interactions with photons from the accretion disk and hot corona, line emission from broad-line region (BLR) and infrared emission from the dust torus. As a result,

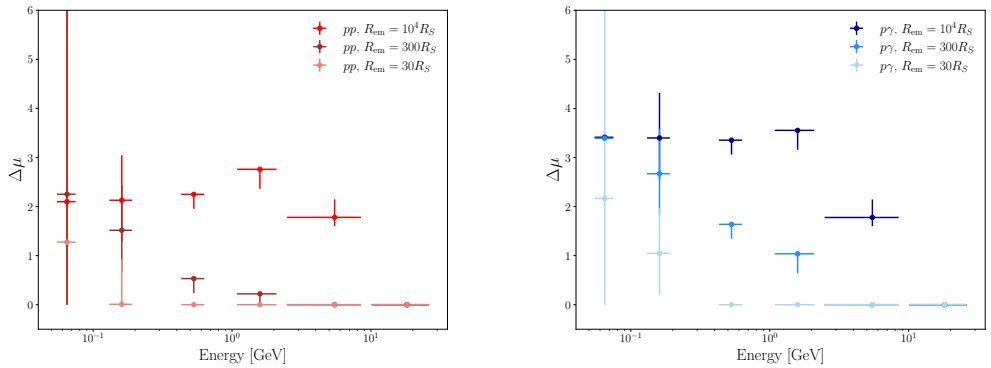

Figure 7.5: Absorption coefficient needed to attenuate the expected gamma-ray flux from NGC 1068 [328, 355] to the observed values by Fermi-LAT (including error bars), for both pp (upper panel) and $p\gamma$ (lower panel) scenarios and different locations of the emitting region of neutrinos and gamma-rays. Absorption coefficients larger than these values would be compatible with Fermi-LAT data as well, if invoking an additional component of gamma-rays arising from the starbust activity with high supernova rates [356].

the photon flux observed at the Earth is attenuated with respect to the emitted flux:

$$\frac{\Phi^{\rm obs}(E_\gamma)}{\Phi^{\rm em}(E_\gamma)} = e^{-\mu_{\gamma\gamma}} \tag{7.12}$$

with $\mu_{\gamma\gamma}$ the attenuation coefficient due to two-photon pair annihilation $\gamma\gamma \to e^+e^-$, which has been calculated in [328], and takes values as large as 2 (4) for values of the emitting region of neutrinos and gamma-rays of $R_{\rm em} = 10^4 R_{\rm S}$ ($30 R_{\rm S}$).

The neutrino flux, on the other hand, is not expected to be significantly attenuated during its propagation. The recent observation by IceCube of a neutrino flux from NGC1068 opens a direct window to the production mechanisms of high energy neutrinos near the SMBH, and thereby to the production of high energy photons [350]. In the simplest single-zone emission models, the predicted gamma-ray flux exceeds the total gamma-ray flux measured by the Fermi-LAT [352], which receives a contribution not only from hadronic processes in the AGN, but also from leptonic processes in the AGN, and from the starburst ring. The gamma-ray deficit could then be due to a more complicated production mechanism [328, 337, 355, 356], or to an additional contribution to the attenuation during the gamma-ray propagation to the Earth, that we denote as $\Delta\mu(E_\gamma)$. We show in Fig 7.5 the lower limit on the absorption coefficient needed in every energy bin measured by Fermi-LAT, in both pp and $p\gamma$ production mechanisms, and for different choices of the emitting region of neutrinos and gamma-rays [328]. We perform the calculation for the central value of Fermi-LAT as well as for the upper and lower error bars reported by the collaboration. As can be seen in the Figure, the absorption coefficient needed to reconcile astrophysical models with Fermi-LAT data increases with

larger values of the emitting region and gamma rays, but it reaches values above one at some energies even when assuming emission in the innermost part of the corona, at $R_{\rm em} = 30R_S$. Further, the attenuation coefficients needed in $p\gamma$ production scenarios is somewhat larger than for the pp channel.

The mass of the SMBH at the center of NGC1068 has been estimated to be $M_{\rm BH} = 1-2\times10^7 M_\odot$ [453, 454], although some works point to masses as large as $M_{\rm BH} = 9\times10^7 M_\odot$ [455]. The Schwarzschild radius is then $R_S \simeq 1.9\times10^{-6}\,{\rm pc}\,(M_{\rm BH}/2\times10^7 M_\odot)$, while the size of the spike is $R_{\rm sp} \simeq 21.57\,{\rm pc}\,(M_{\rm BH}/2\times10^7 M_\odot)^{1/2}$ for $\gamma = 1$ and $R_{\rm sp} \simeq 7.43\,{\rm pc}\,(M_{\rm BH}/2\times10^7 M_\odot)^{3/5}$ for $\gamma = 4/3$.

Emission within the broad line region, $R_{\rm BLR} \sim 10^4 R_S = 0.019\,(M_{\rm BH}/2\times10^7 M_\odot)$ pc [328], which lies well within the dark matter spike.

The column density of dark matter that photons travel through the spike of an AGN can be approximated by:

$$\Sigma_{\rm DM}\big|_{\rm spike} \simeq \int_{R_{\rm em}}^{R_{\rm sp}} dr \rho_{\rm sp}(r) \simeq \frac{\rho_0}{\gamma_{sp}-1}\frac{R_{sp}^{\gamma_{\rm sp}-\gamma}}{r_0^{-\gamma} R_{\rm em}^{\gamma_{sp}-1}} \tag{7.13}$$

where we have used Eq. (**??**) and that $R_{\rm em} \gg R_{\rm S}$. We find numerically that the column density of dark matter particles in the spike is much larger than the column density in the dark matter halos of NGC1068 and the Milky Way, and in the intergalactic medium. Therefore $\Sigma \simeq \Sigma_{\rm DM}\big|_{\rm spike}$. Expressed in terms of the different parameters:

$$\Sigma_{\rm DM} \simeq \left(\frac{4-\gamma}{5-\gamma}\right) M_{\rm BH}^{\frac{3-\gamma}{4-\gamma}} r_0^{\frac{\gamma}{4-\gamma}} R_{\rm em}^{-\frac{5-\gamma}{4-\gamma}} \alpha_\gamma^{-\frac{(-3+\gamma)^2}{-4+\gamma}} \rho_0^{\frac{1}{4-\gamma}} \tag{7.14}$$

The attenuation factor of the emitted photons from the AGN due to dark matter-photon scattering is given by

$$\Delta\mu(E_\gamma) \simeq \frac{\Sigma_{\rm DM}\sigma_{{\rm DM}-\gamma}(E_\gamma)}{m_{\rm DM}} \tag{7.15}$$

where $\sigma_{{\rm DM}-\gamma}$ is the dark matter-photon scattering cross section.

for $\gamma = 1$

$$\Delta\mu(E_\gamma) \simeq 2.15\left(\frac{M_{\rm BH}}{2\times10^7 M_\odot}\right)^{2/3}\left(\frac{r_0}{10\,{\rm kpc}}\right)^{1/3}\left(\frac{\rho_0}{0.043 M_\odot/{\rm pc}^3}\right)^{1/3}\left(\frac{R_{\rm em}}{100R_{\rm S}}\right)^{-4/3}\left(\frac{m_{\rm DM}}{1\,{\rm GeV}}\right)^{-1}\left(\frac{\sigma_{{\rm DM}-\gamma}(E_\gamma)}{10^{-29}\,{\rm cm}^2}\right)$$

For $\gamma = 4/3$

$$\Delta\mu(E_\gamma) \simeq 1.26\left(\frac{M_{\rm BH}}{2\times10^7 M_\odot}\right)^{3/4}\left(\frac{r_0}{10\,{\rm kpc}}\right)^{1/2}\left(\frac{\rho_0}{0.37 M_\odot/{\rm pc}^3}\right)^{3/8}\left(\frac{R_{\rm em}}{100R_{\rm S}}\right)^{-11/8}\left(\frac{m_{\rm DM}}{1\,{\rm GeV}}\right)^{-1}\left(\frac{\sigma_{{\rm DM}-\gamma}(E_\gamma)}{10^{-30}\,{\rm cm}^2}\right)$$

and for $\gamma = 2$

We find that there is a significant absorption if the dark matter-photon interaction cross-section is $\gtrsim 10^{-30}\,{\rm cm}^2$.

Let us consider a scenario where the dark matter particle is a spin 1/2 fermion charged under a hidden $U(1)_D$ gauge symmetry, with coupling strength g_D. We assume that the

$U(1)_D$ gauge symmetry mixes kinetically with the $U(1)_{\rm em}$, with strength χ. The elastic scattering dark matter-photon DM$\gamma \to$ DMγ is suppressed by four powers of the kinetic mixing. We consider instead the inelastic process with a dark photon γ' in the final state, DM$\gamma \to$ DMγ', which is suppressed only by two powers of the kinetic mixing. We estimate the cross-section to be

$$\sigma_{\rm DM\gamma\to DM\gamma'} \sim \sigma_t \epsilon^2 \left(\frac{m_e}{m_{\rm DM}}\right)^2 \tag{7.16}$$

where $\epsilon \equiv \chi g_D/e$, e is the electron charge, m_e the electron mass and $\sigma_{\rm T} = 6.65\times10^{-25}{\rm cm}^2$ the Thomson cross-section. Numerically,

$$\sigma_{\rm DM\gamma\to DM\gamma'} \sim 7.7\times10^{-32}\,{\rm cm}^2 \left(\frac{\epsilon}{0.66}\right)^2 \left(\frac{m_{\rm DM}}{1\,{\rm GeV}}\right)^{-2} \tag{7.17}$$

which is roughly one order of magnitude below the required value to induce significant absorption in NGC 1068.

In more complex hidden sectors there could be additional processes contributing to the total scattering cross section DM$\gamma \to$ DMX, with X any final state, thus enhancing the attenuation of the photon flux. Generically, the cross section for the inelastic process reads [456–459]

$$\sigma = \frac{\alpha g_\chi^2 \epsilon^2}{8s}\frac{p}{k}\left[A(s) + B(s)\frac{\sqrt{s}}{p}\log\frac{2p_0k_0 + 2pk - m_\chi^2}{2p_0k_0 - 2pk - m_\chi^2}\right] \tag{7.18}$$

where g_χ is the dark boson coupling to the dark matter fermion, and ϵ is the kinetic mixing between the dark sector and the standard model via a dark photon mediator. $A(s)$ and $B(s)$ depend on the nature of the final dark state, and $p_0 = \left(s - m_e^2 + m_\chi^2\right)/2\sqrt{s}$, $p = \left(p_0^2 - m_\chi^2\right)^{1/2}$, $k_0 = \left(s + m_e^2\right)/2\sqrt{s}$, and $k = \sqrt{s} - k_0$. We will consider vector and pseudoscalar particles in the final state.

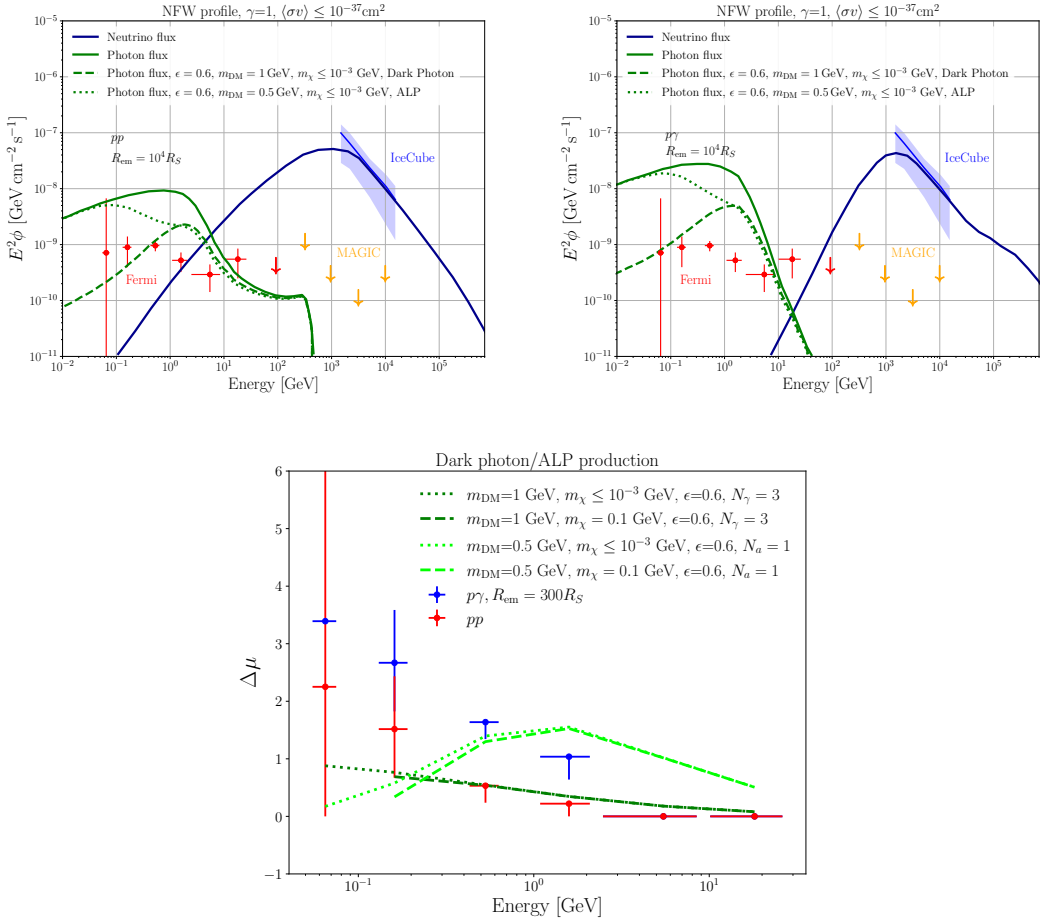

Figure 7.7: *Upper left panel*: Spectral energy distribution from NGC 1068 in photons and neutrinos, confronted with IceCube, MAGIC and Fermi-LAT. We show the original model prediction from [328] for pp emission, and the attenuated fluxes due to inelastic scatterings on fermionic dark matter with a dark photon and and ALP in the final state. *Upper right panel*: Same as in the left plot, but for the $p\gamma$ model *Lower panel*: Absorption coefficient needed to attenuate the expected gamma-ray flux from NGC 1068 to the values observed by Fermi-LAT, assuming emission at $R_{\rm em} = 300 R_S$, and confronted with the expected attenuation in two particle physics models, with 3 dark photons (green) and one ALP (lime).

If a dark photon in the final state is produced, we have

$$A(s) = 2 + \frac{2\left(m_e^2 - m_\chi^2\right)}{s} + \frac{16\left(m_\chi^2 + 2m_e^2\right)s}{\left(s - m^2\right)^2} \tag{7.19}$$

$$B(s) = 2 - \frac{4\left(m_\chi^2 + 2m_e^2\right)}{s - m_e^2} - \frac{4\left(4m_e^4 - m_\chi^4\right)}{\left(s - m_e^2\right)^2} \tag{7.20}$$

In the upper panel of Figure 7.7, we show the absorption coefficient obtained for the inelastic dark matter-photon scattering inducing a dark photon in the final state, for four benchmark values of the dark matter and dark photon parameters. First, we show the absorption coefficient for a dark matter fermion with mass of $m = 1$GeV, a light or massless dark photon mediator, $m_\chi \leq 10^{-3}$GeV, and with kinetic mixing $\epsilon = 0.6$ (dotted line). In this case, the cross section resembles the one for compton scattering in the regime $E_\gamma \sim m_{\rm DM}$, where the cross section decreases roughly linearly with the photon energy. Here, the absorption coefficient obtained works well to suppress the photon flux to the Fermi-LAT observation from $\sim 2 - 20$GeV, while it is slightly large in the lower energy bins. If considering a massive dark photon, we find that the cross section mildly flattens at low energies. One needs $\mathcal{O}(10)$ dark photons to obtained sizable attenuations, for the benchmark parameters used in the estimation of the column density.

The benchmark values of the kinetic mixing for a lighter dark matter fermion with $m_\chi \leq 1$ GeV would yield larger attenuations and only one massless dark photon in the final state would be needed, however, light fermions with large values of kinetic mixing are in tension with collider searches and in mild tension with $N_{\rm eff}$ constraints from the CMB [158, 159, 162, 460].

One may also produce an axion in the final state. In this case, we have

$$A(s) = -3 + \frac{m_e^2 - m_\chi^2}{s} + \frac{8m_\chi^2 s}{\left(s - m_e^2\right)^2} \tag{7.21}$$

$$B(s) = 1 + \frac{2\left(m_\chi^2 - 4m_e^2\right)}{s - m_e^2} + \frac{2\left(m_\chi^4 - 6m_\chi^2 m_e^2 + 8m_e^4\right)}{\left(s - m_e^2\right)^2} \tag{7.22}$$

In the Figure, we also show the absorption coefficient obtained for the inelastic dark matter-photon scattering inducing an Axion Like Particle in the final state, for four benchmark values of the dark matter and axion like particle parameters. First, we show the absorption coefficient for a dark matter fermion with mass of $m = 0.5$GeV, and a light or massless dark photon mediator, $m_\chi \leq 10^{-3}$GeV, and with kinetic mixing $\epsilon = 0.6$ (dotted line). Here, the cross section peaks at $E_\gamma = 2m_{\rm DM}$, roughly linearly decreasing at lower and larger energies. The absorption coefficient obtained in this scenario works well to suppress the photon flux to the Fermi-LAT observation from $\sim 0.2 - 20$GeV, while it is slightly smaller than required in the lower energy bins.

It is worth noting the dark matter column density could also be 1 to 2 orders of magnitude larger in the pre-existing dark matter profile were cuspier than $\gamma = 1$. Another plausible scenario consists in the emitting region of neutrinos and gamma rays being in the corona, e.g $R_{\rm em} \sim 10^2 R_S$, where the absorption coefficients needed to reconcile the emitted photon flux with Fermi-LAT data are smaller, and the column density is larger, requiring lower couplings of the dark matter to the visible sector. Further, we

have neglected contributions to the attenuation from the dark matter in the intergalactic medium and the Milky Way. These contributions are expected to be small compared to the attenuation in NGC 1068, although the distribution of intergalactic dark matter is subject to large uncertainties. Given that the distance that photons need to travel in the intergalactic medium is orders of magnitude larger than at the source and the Milky Way, the column density might be comparable if the average dark matter density were larger than the cosmological value.

Although we have provided some concrete particle physics examples with the correct energy dependence of the cross section, we also notice that a constant dark matter-photon cross section of $\sigma_{\mathrm{DM}-\gamma} \sim 10^{-29}\mathrm{cm}^2$ would also work well, and is subject to less assumptions. This value is however in slight conflict with cosmological constraints [444, 445].

7.4 Probing dark matter-proton and dark matter-electron scatterings through cosmic-ray cooling in AGN

We have discussed in section 5 that recent observations of high-energy neutrinos from active galactic nuclei (AGN), NGC 1068 and TXS 0506+056, suggest that cosmic rays (CRs) are accelerated in the vicinity of the central supermassive black hole and high-energy protons and electrons can cool efficiently via interactions with ambient photons and gas. Further, we have seen in section 6.2 that the dark matter density may be significantly enhanced near the black hole. In this section we discuss that CRs could lose energies predominantly due to scatterings with the ambient dark matter particles. We propose CR cooling in AGN as a new probe of dark matter-proton and dark matter-electron scatterings. Under plausible astrophysical assumptions, our constraints on sub-GeV dark matter can be the strongest derived to date. Some of the parameter space favored by thermal light dark matter models might already be probed with current multimessenger observations of AGN.

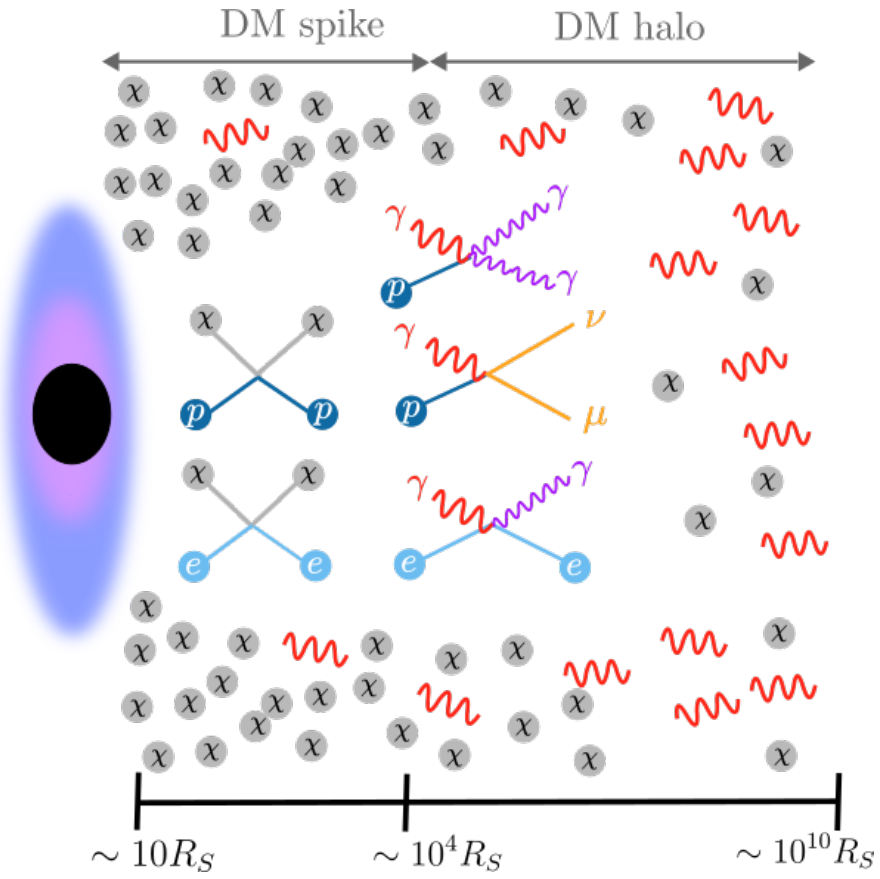

Figure 7.8: Schematic picture of dark cooling of CRs due to elastic scatterings with dark matter particles in AGN. High-energy protons and electrons may traverse a high density of dark matter particles more efficiently than standard cooling processes involving neutrino and photon emission.

	$R_{\rm em}$	$M_{\rm BH}$	$t_{\rm BH}$	r_0	$\langle\sigma v\rangle/m_{\rm DM}$	$\langle\rho_{\rm DM}\rangle$
NGC 1068 (I)	30 R_S	(1-2) $\times 10^7 M_\odot$	10^{10} yr	10 kpc	0	5×10^{18} GeV/cm^3
NGC 1068 (II)	30 R_S	(1-2) $\times 10^7 M_\odot$	10^{10} yr	10 kpc	10^{-31}cm^{3}s^{-1}/GeV	4×10^{13} GeV/cm^3
TXS 0506+056 (I)	$10^4 R_S$	(3-10) $\times 10^8 M_\odot$	10^9 yr	10 kpc	0	8×10^{12} GeV/cm^3
TXS 0506+056 (II)	$10^4 R_S$	(3-10) $\times 10^8 M_\odot$	10^9 yr	10 kpc	10^{-28}cm^{3}s^{-1}/GeV	4×10^{11} GeV/cm^3

Table 7.2: Relevant parameters considered in this work for NGC 1068 and TXS 0506+056, for two different sets of assumptions dubbed (I) and (II). Here $R_{\rm em}$ represents the distance of the emission region from the central SMBH in NGC 1068 (TXS 0506+056), $M_{\rm BH}$ shows the SMBH mass and its uncertainty, $t_{\rm BH}$ is the age elapsed since the black hole was formed, r_0 is the scale radius of the galaxy, $\langle\sigma v\rangle/m_{\rm DM}$ denotes the assumed values of the effective dark matter self-annihilation cross section, and $\langle\rho_{\rm DM}\rangle$ is the average density of dark matter particles within $R_{\rm em}$.

As discussed in section 3.6, light dark matter fermions with sub-GeV masses were historically disfavoured by the cosmological bound [32, 461]. However, large parameter space still remains unexplored in more complicated but well-motivated scenarios [138, 151, 154].

Different approaches have been proposed to extend the sensitivity reach of direct detection experiments for sub-GeV dark matter masses. Some of these consider a boosted component of dark matter particles reaching the Earth, purely via gravitational effects (*e.g.,* Refs. [462–467]), while others rely on a boosted component due to scatterings of dark matter particles with protons, electrons or neutrinos in different astrophysical environments (*e.g.,* Refs. [243–246, 252–256, 258, 259]).

Active galactic nuclei (AGN) are promising sources of high-energy protons and electrons. While the dominant acceleration mechanism of these cosmic rays (CRs) is still under debate, see section 5, modeling of multimessenger data have placed important constraints on not only energetics of CR production but also the emission region of the observed neutrinos that can be produced either via inelastic pp collisions or $p\gamma$ interactions [354, 468, 469]. For example, observations of high-energy neutrinos and gamma rays from NGC 1068 [350, 470] suggest that the neutrino production occurs in the vicinity of the supermassive black hole (SMBH) at $R_{\rm em} \lesssim 30 - 100 R_S$ (where R_S is the Schwarzschild radius), which is consistent with theoretical models [329, 330, 333, 337, 471], and the required proton luminosity is at least $\sim 10\%$ of the intrinsic X-ray luminosity [328, 472]. Another neutrino source candidate, TXS 0506+056 [347, 415, 436, 473, 474], is known to be a jet-loud AGN, and the observed spectral energy distribution in photons is mostly explained by synchrotron and inverse-Compton emission from CR electrons [349, 414–417, 419], and the proton luminosity required by IceCube observations may even exceed the Eddington luminosity [416, 417].

In [316], we propose CRs produced in AGN as a new probe of dark matter-proton and dark matter-electron scatterings through their multimessenger observations. Given that emission regions of neutrinos and gamma rays are constrained to be near the SMBHs,

CRs also need to traverse the dark matter spike around the central SMBH. If such additional cooling beyond the standard model (BSM) was too strong, CR energy losses are modified so that the required CR luminosity would be larger, and the neutrino and photon spectra could even be incompatible with the observations. Our work is different from previous studies on AGN probes of the dark matter scatterings with protons and electrons, which focused either on the boosted flux of dark matter particles from the source at Earth [243, 475, 476], or on the spectral distortions in the gamma-ray flux induced by CR scatterings off dark matter particles [395, 477–481]. Instead we focus on the impact of the dark matter-proton and dark matter-electron scatterings on the neutrino and photon fluxes or the CR power, considering for the first time the cooling of protons and electrons in the inner regions of the AGN, where a dark matter spike is likely to be formed.

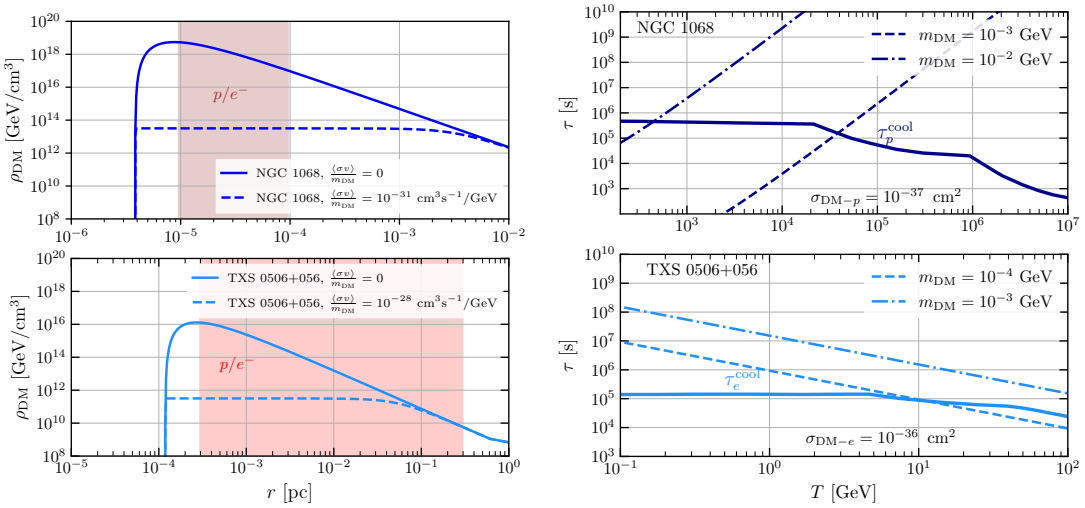

Figure 7.9: *Left panel*: Dark matter distribution around the SMBHs of TXS 0506+056 and NGC 1068, for different values of the dark matter self-annihilation cross section over its mass. The red (brown) shaded region indicates the region where the production of high-energy particles is expected to take place in TXS 0506+056 (NGC 1068) *Right panel*: In solid lines, we show the cooling time scales of protons (electrons) in NGC 1068 (TXS 0506+056) (see main text for details). In dashed and dot-dashed lines we show the time scales due to elastic dark matter proton and dark matter-electron scatterings, for different values of the dark matter mass and scattering cross section.

When the dark matter particles self-annihilate with a sufficiently large cross section, the maximal dark matter density in the inner regions of the spike is saturated to $\rho_{\rm sat} = m_{\rm DM}/(\langle\sigma v\rangle t_{\rm BH})$, where $\langle\sigma v\rangle$ is the velocity averaged dark matter self-annihilation cross section, and $t_{\rm BH}$ is the time passed since the black hole was formed. For TXS 0506+056, we take the value $t_{\rm BH} = 10^9$ yr [475], while for NGC 1068 we use $t_{\rm BH} = 10^{10}$ yr [482]. Furthermore, the dark matter spike extends to a maximal radius $R_{\rm sp}$, beyond which the

dark matter distribution follows the initial NFW profile. The dark matter density profile therefore reads [271, 393, 394])

$$\rho(r) = \begin{cases} 0 & r \leq 4R_{\rm S}, \\ \frac{\rho_{\rm sp}(r)\rho_{\rm sat}}{\rho_{\rm sp}(r)+\rho_{\rm sat}} & 4R_{\rm S} \leq r \leq R_{\rm sp}, \\ \rho_0 \left(\frac{r}{r_0}\right)^{-\gamma} \left(1+\frac{r}{r_0}\right)^{-(3-\gamma)} & r \geq R_{\rm sp}. \end{cases} \tag{7.23}$$

The dark matter profiles in TXS 0506+056 and NGC 1068 are shown in the left panel of Fig. 7.9 for two values of $\langle\sigma v\rangle/m_{\rm DM}$ allowed for sub-GeV dark matter [147, 149, 483]. We find that the dark matter density is extremely high in the region where high-energy particles are produced, and dark interactions with dark matter particles may lead to a sizable depletion of the observed fluxes.

Neutrinos and photons from AGN can be explained by emission from high-energy protons and electrons through purely Standard Model mechanisms. Energy-loss mechanisms include scatterings with other Standard Model particles in the plasma or synchroton radiation as well as adiabatic losses. In addition, there are escape losses due to advection or diffusion via magnetic fields. The presence of dark matter coupling to protons and electrons in the vicinity of SMBHs would naturally introduce additional scattering time scales, leading to the suppression of the observed neutrino and gamma-ray fluxes in certain energy ranges, if the BSM cooling time scales of CRs were shorter than the standard cooling time scales. For example, at $m_{\rm DM} \sim 10^{-3}$ GeV, the currently-allowed maximum dark matter-proton scattering cross section steams from cosmic-ray boosted dark matter at the Super-Kamiokande experiment [484], with a value of $\sigma_{{\rm DM}-p} \sim 10^{-35}$ cm^2. As discussed in the previous section, the average density of (asymmetric) dark matter particles in the coronal region of NGC 1068 is $\langle\rho_{\rm DM}\rangle \sim 5 \times 10^{18}$ GeV/cm^3. Thus, if the corresponding cross section for CR protons is comparable to $\sigma_{{\rm DM}-p}$ (although this is not the case in general), the BSM cooling time scale for the currently allowed values in the literature is $\tau_{{\rm DM}-p} \sim 1/(\langle n_{\rm DM}\rangle \sigma_{{\rm DM}-p} c) \sim 7 \times 10^3$ s, which is well below the proton cooling time inferred by observations of NGC 1068. This simple estimate clearly suggests that CRs in AGN can provide a powerful probe of these interactions.

More quantitatively, the BSM cooling time scale due to elastic dark matter scattering off CRs is given by [481]

$$\tau^{\rm el}_{{\rm DM}-i} = \left[-\frac{1}{E}\left(\frac{dE}{dt}\right)_{{\rm DM}-i} \right]^{-1}, \tag{7.24}$$

with

$$\left(\frac{dE}{dt}\right)_{{\rm DM}-i} = -\frac{\langle\rho_{\rm DM}\rangle}{m_{\rm DM}} \int_0^{T^{\rm max}_{\rm DM}} dT_{\rm DM}\, T_{\rm DM} \frac{d\sigma_{{\rm DM}-{\rm CR}i}}{dT_{\rm DM}}, \tag{7.25}$$

where $\langle\rho_{\rm DM}\rangle$ is the average density of dark matter particles in the region of CR production. See Table 7.2 for the specific values that we use for NGC 1068 and TXS 0506+056. Also, $d\sigma_{{\rm DM}-{\rm CR}i}/dT_{\rm DM}$ is the differential elastic dark matter-proton or dark

matter-electron cross section, $T_{\rm DM}^{\rm max}$ is the maximal allowed value for $T_{\rm DM}$ in a collision with a particle i with kinetic energy $T = E - m_i$, which is

$$T_{\rm DM}^{\rm max} = \frac{2T^2 + 2m_i T}{m_{\rm DM}} \left[\left(1 + \frac{m_i}{m_{\rm DM}} \right)^2 + \frac{2T}{m_{\rm DM}} \right]^{-1} . \tag{7.26}$$

We consider fermionic dark matter which elastically interacts with protons and electrons via a heavy scalar mediator. The differential cross section reads [485]

$$\frac{d\sigma_{{\rm DM}-{\rm CR}i}}{dT_{\rm DM}} = \frac{\sigma_{{\rm DM}-i}}{T_{\rm DM}^{\rm max}} \frac{F_i^2(q^2)}{16\,\mu_{{\rm DM}-i}^2\,s} (q^2 + 4m_i^2)(q^2 + 4m_{\rm DM}^2) , \tag{7.27}$$

where $\sigma_{{\rm DM}-i}$ is the dark matter-proton or dark matter-electron cross section at the zero center-of-mass momentum, $\mu_{{\rm DM}-i}$ is the reduced mass, s is the square of center-of-mass energy, and $q^2 = 2m_{\rm DM}T_{\rm DM}$ is the momentum transfer of the process. The quantity F_i is either the proton form factor [486], or equal to 1 for electrons. This formalism is only valid for elastic scatterings.

In the right panel of Fig. 7.9, the solid lines represent the total standard energy-loss time scales as a function of energy for protons in NGC 1068 [328] and for electrons in TXS 0506+056 [487]. CR protons in NGC 1068 are almost depleted, and the dominant cooling mechanisms at increasing energies are inelastic pp interactions, Bethe-Heitler pair production, and $p\gamma$ interactions [333]. CR protons do not cool efficiently in TXS 0506+056, and the fate is governed by a dynamical time scale of $\sim 10^5$ s in the SMBH frame [487]. For electrons in TXS 0506+056, the dominant cooling mechanisms are inverse Compton scattering and synchroton radiation. The breaks in the solid lines of the plots reflect the energies at which the transition of dominant processes occurs.

For comparison, we also show BSM cooling time scales due to elastic dark matter scatterings with protons and electrons. The dotted-dashed line corresponds to values of the dark matter mass and cross section that would induce a contribution smaller than the proton and electron energy losses due to the Standard Model processes. On the other hand, the dashed line shows values of the parameters that would induce larger energy losses than in the Standard Model at relevant energies (according to our exclusion limit criterion). It is important to point out that inelastic dark matter-proton scatterings are expected to dominate over the elastic channel at energies $E \gtrsim m_p^2/2m_{\rm DM}$, however, the inelastic cross section is sensitive to the details of the dark matter particle model, therefore we decide to restrict our analysis to the elastic scattering channel. Including inelastic channels would probably allow to derive stronger limits, although one should then consider the production of additional neutrinos and photons via pion decay, as done in Refs. [478, 481].

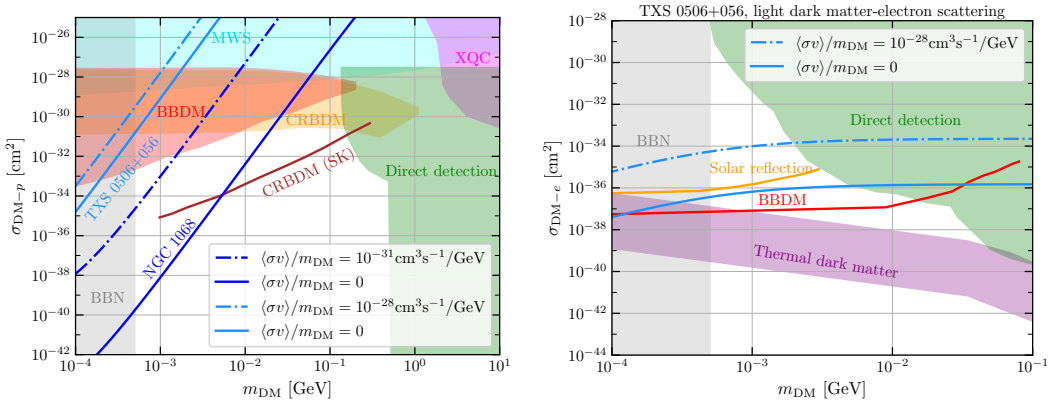

Figure 7.10: *Left panel:* Upper limits on the spin-independent dark matter-proton scattering cross-section as a function of the dark matter mass, derived from the requirement that the required proton luminosity is substantially larger due to scatterings off dark matter particles in NGC 1068 and TXS 0506+056. The different blue shadings correspond to two different assumptions on the dark matter self-annihilation cross section, which affects the average density of dark matter particles in the inner regions of the AGN. Complementary constraints from different searches are shown for comparison (see main text for details). *Right panel:* Analogous upper limits on the dark matter-electron scattering cross section, for TXS 0506+056. We also display values of the dark matter-electron scattering cross section vs dark matter mass compatible with thermal production of light dark matter. Note that we do not have constraints from NGC 1068 because the observed gamma rays may be purely hadronic [470].

For the purpose of constraining the interaction strength, we find for each $m_{\rm DM}$ the largest dark matter-proton (electron) scattering cross section yielding a time scale equal or larger to the cooling time scales determined with models at relevant energies. In particular, we use

$$\tau^{\rm el}_{{\rm DM}-i} \geq C\,\tau^{\rm cool}_i. \tag{7.28}$$

The coefficient C is a model dependent factor, and we use $C = 0.1$ in this work. In other words, we find the maximum dark matter-proton (electron) scattering cross section that would have an $\mathcal{O}(10)$ or less impact on the proton (electron) cooling time scale. This is reasonable and may be even conservative from the energetics requirement of neutrino-emitting AGN. For NGC 1068, the proton luminosity would be 10^{43} erg s^{-1} $\lesssim L_p \lesssim L_X \lesssim 10^{44}$ erg s^{-1} [328, 333], justifying $C \sim 0.1 - 1$. For TXS 0506+056, the proton luminosity in the single-zone model already violates the Eddington luminosity $L_{\rm Edd}$ [416], so our choice is conservative. This is also reasonable for electrons because of $L_e \sim 8 \times 10^{47}$ erg s^{-1} $\sim 20 L_{\rm Edd}$ [487]. In principle, if the CR acceleration mechanism is understood, spectral modification due to BSM cooling may allow us to improve constraints and $C \sim 1$ is possible. For proton energies of interest, we use $10 - 300$ TeV for

NGC 1068 [350], which is required to match the IceCube data [328]. For protons in TXS 0506+056, we use $0.1-20$ PeV [473], and for electrons we use 50 GeV $-$ 2 TeV, following Ref. [487].

Applying the condition of Eq. (7.28) for NGC 1068 and TXS 0506+056, we set constraints on the spin-independent dark matter-proton and dark matter-electron scattering cross sections via a heavy mediator (see Fig. 7.10). The solid lines correspond to scenario (I), and the dashed lines correspond to scenario (II) (see Table 7.2), corresponding to different values of the dark matter self-annihilation cross section consistent with current constraints [483]. When the dark matter self-annihilates, the dark matter spike is saturated near the SMBH, and the average density of dark matter particles in the region where CRs are confined is smaller. We find that our constraints become stronger at lower dark matter masses. This is mainly due to the fact that the number density of dark matter particles increases with decreasing masses, and the cross section needed to induce large energy losses becomes smaller. However, we note that for protons the dependence of the constraint on the dark matter mass is more pronounced than for electrons. This is because we only consider elastic scatterings accounting for energy losses, and the elastic scattering cross section decreases with reference to its maximum value for $E \gtrsim m_p^2/2m_{\rm DM}$

For comparison, we show complementary constraints from other methods. The green region is excluded by dark matter direct detection experiments [224, 488–490], where the maximal cross section unaffected by atmospheric scatterings is considered [491, 492]. The magenta region is constrained by the X-ray Quantum Calorimeter (XQC) experiment [493]. The cyan region is constrained by Milky Way satellite galaxy counts [494], and the grey region is constrained by the Big Bang nucleosynthesis (BBN) [495, 496]. The orange region is constrained by CR boosted dark matter (CRBDM) at XENON1T [252], and the red regions are excluded when considering the blazar-boosted dark matter flux from TXS 0506+056 [243, 475]. Finally, values above the brown line are constrained by CRBDM at the Super-Kamiokande experiment [484]. Further, for dark matter-electron scatterings, we include constraints from the solar reflection [497], and the region of values where light thermal dark matter acquires its relic abundance via various mechanisms [151, 152, 498]. From Fig. 7.10, one sees that our constraints for light dark matter coupling to protons are stronger than complementary bounds for $m_{\rm DM} \lesssim 10^{-3}-10^{-2}$ GeV. For dark matter-electron scatterings, our constraints are stronger than direct detection bounds at masses below $m_{\rm DM} \lesssim 5\times10^{-3}$ GeV. In addition, for dark matter-electron interactions, AGN data allows to probe the parameter space favored for dark matter models with $m_{\rm DM} \lesssim 10^{-4}$ GeV, although this region might be in conflict with BBN.

We have also derived constraints on the dark matter-electron scattering cross section for different values of the pre-existing dark matter profile slope index. For the purpose of concreteness, we consider NFW-like profiles with slope indices in the range $\gamma = 0.05-2$, to assess the conclusions of our work beyond the benchmark case covered in the main text, $\gamma = 1$. We normalize all profiles such that the total mass of the dark matter halo of TXS 0506+056 is bound by $M_{\rm DM} \lesssim 10^{13} M_\odot$. In the left panel of Fig. 7.11, we show the dark matter profiles in the vicinity of TXS 0506+056 for different values of γ. As expected, the dark matter density profile becomes steeper for larger values of

γ, and the size of the spike becomes smaller. Outside the spike, the profiles initially evolve with power $\rho_{\rm DM} \propto r^{-3+\gamma}$, but sufficiently far from the center they converge to a $\rho_{\rm DM} \propto r^{-\gamma}$ behaviour. On the right panel of the figure, we show the upper limits on the dark matter-electron scattering cross section found for those profiles corresponding to asymmetric (or slowly annihilating) dark matter. As can be noticed in the figure, the constraints can vary 5 to 6 orders of magnitude depending on the value of γ, although only vary within 1 order of magnitude in the range $\gamma = 0.6 - 1.4$, which is favoured by some simulations of Milky Way analogues [499, 500].

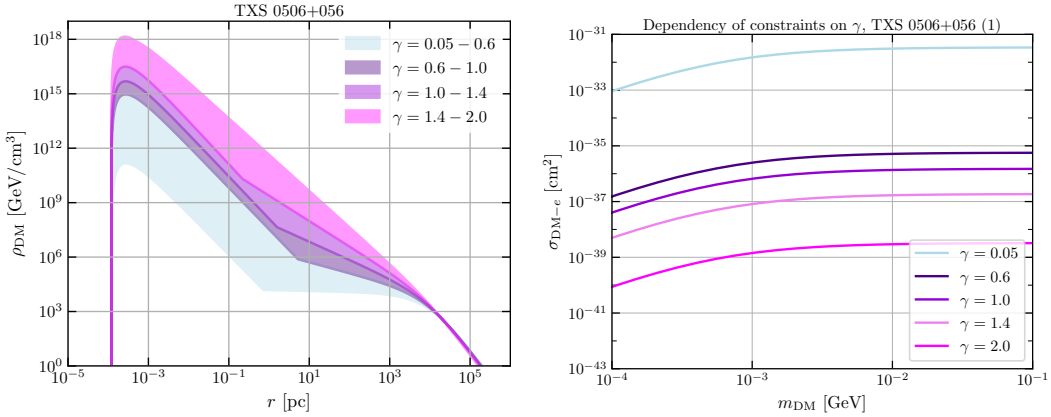

Figure 7.11: *Upper panel*: Dark matter distribution around the black hole of TXS 0506+056, for different values of the pre-existing dark matter profile slope γ. *Lower panel*: Upper limits on the sub-GeV dark matter-electron scattering cross section over the dark matter mass from TXS 0506+056, for different values of the index γ.

To conclude, recent multimessenger measurements of AGN have indicated that high-energy particles, in particular CR protons and secondary neutrinos, are produced in the vicinity of SMBHs. CR cooling could be significantly enhanced by BSM interactions with dark matter, thanks to the formation of a dark matter spike around the central SMBH, with a large density. We demonstrated that neutrino-emitting AGN, NGC 1068 and TXS 0506+056, allow us to set strong constraints on sub-GeV dark matter coupled to protons and/or electrons.

Our constraints on light dark matter coupling to protons are stronger than other complementary bounds for $m_{\rm DM} \lesssim 10^{-3} - 10^{-2}$ GeV. For dark matter-electron scatterings, our constraints are stronger than direct detection bounds at masses below $m_{\rm DM} \lesssim 5 \times 10^{-3}$ GeV, which potentially allows us to probe the parameter space favored for thermal dark matter models with $m_{\rm DM} \lesssim 10^{-4}$ GeV.

The current constraints are subject to uncertainties from the dark matter distribution in the inner regions of AGN as well as on CR cooling time scales. Nevertheless, for the latter, we stress that our constraints are rather conservative especially for NGC 1068. This is because the source has to be nearly calorimetric to explain the neutrino

flux [328], and relaxing assumptions (*e.g.*, with softer CR spectra) will make the limits stronger. Future multimessenger observations and astrophysical modeling will allow us to better understand the sources and reduce uncertainties, and the resulting limits on the dark matter-proton and the dark matter-electron cross section will become more stringent and robust. Understanding acceleration mechanisms will also enable us to compare $\tau^{\rm el}_{{\rm DM}-i}$ to the acceleration time scale for placing constraints. recent multimessenger measurements of AGN have indicated that high-energy particles, in particular CR protons and secondary neutrinos, are produced in the vicinity of SMBHs. CR cooling could be significantly enhanced by BSM interactions with dark matter, thanks to the formation of a dark matter spike around the central SMBH, with a large density. We demonstrated that neutrino-emitting AGN, NGC 1068 and TXS 0506+056, allow us to set strong constraints on sub-GeV dark matter coupled to protons and/or electrons.

Our constraints on light dark matter coupling to protons are stronger than other complementary bounds for $m_{\rm DM} \lesssim 10^{-3} - 10^{-2}$ GeV. For dark matter-electron scatterings, our constraints are stronger than direct detection bounds at masses below $m_{\rm DM} \lesssim 5 \times 10^{-3}$ GeV, which potentially allows us to probe the parameter space favored for thermal dark matter models with $m_{\rm DM} \lesssim 10^{-4}$ GeV.

The current constraints are subject to uncertainties from the dark matter distribution in the inner regions of AGN as well as on CR cooling time scales. Nevertheless, for the latter, we stress that our constraints are rather conservative especially for NGC 1068. This is because the source has to be nearly calorimetric to explain the neutrino flux [328], and relaxing assumptions (*e.g.*, with softer CR spectra) will make the limits stronger. Future multimessenger observations and astrophysical modeling will allow us to better understand the sources and reduce uncertainties, and the resulting limits on the dark matter-proton and the dark matter-electron cross section will become more stringent and robust. Understanding acceleration mechanisms will also enable us to compare $\tau^{\rm el}_{{\rm DM}-i}$ to the acceleration time scale for placing constraints.

Multimessenger observations of neutrino sources have been proposed to study dark matter interactions with photons [315] and neutrinos [315, 432–435, 501–503], as well as historically-investigated annihilating or decaying signatures. Now there is accumulating evidence that AGN can accelerate CRs to TeV–PeV energies. We demonstrated that high-energy particle emission from AGN provides us with a powerful probe of dark matter scatterings with protons and electrons.

Chapter 8

Conclusions

After half a century of worldwide efforts, the particle nature of dark matter remains a mistery. However, we have learned plenty about what the dark matter cannot be like, from the combination of accelerator searches, direct detection experiments at Earth, and indirect astrophysical and cosmological signatures. The flexibility of particle dark matter theories has largely increased, and the perspective from the community has broadened, allowing us to enter an era where novel phenomenological approaches to probe the dark matter particle nature become crucial.

In this thesis we propose the vicinity of supermassive black holes in Active Galactic Nuclei as a promising environment to look for the interactions of dark matter particles with the standard model. Recent multimessenger measurements of AGN have indicated that high-energy particles, in particular cosmic ray protons and secondary neutrinos, are produced in the vicinity of the black hole. The cooling of cosmic rays could be significantly enhanced by scatterings with dark matter, whose density is expected to be largely increased at sub-parsec distances from the black hole, forming a spike. In this thesis, we demonstrated that neutrino-emitting AGN, NGC 1068, TXS 0506+056, allow us to set strong constraints on sub-GeV dark matter coupled to protons and/or electrons, and allow to place strong constraints on dark matter scatterings with neutrinos and photons. Our limits for dark matter scatterings with neutrinos and photons are stronger than cosmological limits in models where the cross section rises with the energy. Further, we have shown that neutrino observations from tidal disruption events may allow to place limits stronger by ~ 1 order of magnitude.

Our constraints on light dark matter coupling to protons are stronger than other complementary bounds for $m_{\rm DM} \lesssim 10^{-3} - 10^{-2}$ GeV. For dark matter-electron scatterings, our constraints are stronger than direct detection bounds at masses below $m_{\rm DM} \lesssim 5 \times 10^{-3}$ GeV, which potentially allows us to probe the parameter space favored for thermal dark matter models with $m_{\rm DM} \lesssim 10^{-4}$ GeV.

The current constraints are subject to uncertainties from the dark matter distribution in the inner regions of AGN as well as on cosmic-ray cooling time scales and emitted neutrino and photon fluxes. Nevertheless, for the two latter, we stress that our constraints are rather conservative, especially for NGC 1068. This is because the source has to be nearly calorimetric to explain the neutrino flux [328], and relaxing assumptions (*e.g.*, with softer cosmic-ray spectra) will make the limits stronger. Future multimessenger observations and astrophysical modeling will allow us to better understand the sources and reduce uncertainties, and the resulting limits on the dark matter-proton,

dark matter-electron, dark matter-photon and dark matter-neutrino scattering cross section will become more stringent and robust. Understanding acceleration mechanisms will also enable us to compare the dark matter elastic scattering timescales with the cosmic-ray acceleration time scales.

In addition, we have proven that $\mathcal{O}(1)$ dark matter-photon absorption coefficients in NGC 1068 can be achieved in some light dark matter models where photons inelastically scatter with dark matter, yielding an invisible particle in the final state. Our calculation suggests that the deficit in gamma-rays observed by Fermi-LAT from NGC 1068 w.r.t to the observed neutrino flux, in principle irreconcilable with single-zone leptohadronic models, can be explained by photon attenuation due to interactios with dark matter particles in the spike.

In summary, in this thesis we demonstrated that multimessenger observations from Active Galactic Nuclei provides us with a powerful probe of dark matter scatterings with protons, electrons, photons and neutrinos.

Chapter 9

Varietés

9.1 Non-galactic dark matter

Astronomical data suggests the existence of diffuse dark matter components homogeneously distributed between clusters and superclusters of galaxies, aside from the localized galactic dark matter halos [504]. Estimations of the mean matter density using all-sky catalogs within the local universe are systematically lower than the cosmological value measured by Planck. More precisely, in the region within 11 Mpc from us, where the Virgo Supercluster and the Local Group are embedded, the matter density is estimated to be Ω_m=0.17 [505, 506], while the cosmological measurement is significantly larger Ω_m=0.315 [507]. This difference could be explained if a substantial fraction of the dark matter in groups and clusters extends beyond their virial radius, [508], but analyses of the Hubble flow yield comparable values for the virial mass and the total mass in the Virgo Supercluster [509]. Another possible explanation is that our galaxy is located within a giant void [510], but some observations of the K-band disfavor this possibility [511]. A third explanation, this one being less constrained by observations, is that a significant fraction of the dark matter is dispersed outside the virial regions of galaxy groups and clusters. These diffuse components, such as cosmic filaments and walls, are predicted in cosmological large scale simulations [512] and can be searched with weak gravitational lensing [513].

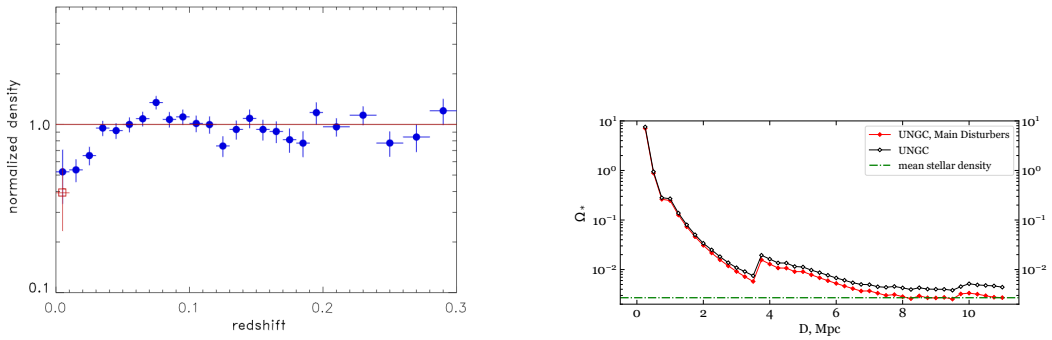

Figure 9.1: *Left panel*: Cluster density distribution as a function of redshift, from [506]. The underdensity at low redshift is clearly visible in the Figure. *Right panel*: Mean density of stellar matter within a distance D in the Local Volume vs the global cosmic value, from [505].

The question that we aim to answer in [465, 466, 514, 515] is whether the diffuse dark matter components of the Local Group and the Virgo Supercluster could have a sizable impact on direct detection experiments searching for light or inelastic dark matter. Similar analyses have been performed focusing on nuclear recoils induced by dark matter particles with masses in the GeV scale, [462, 463, 516, 517]. Here, we concentrate instead on sub-GeV dark matter particles and inelastic dark matter scenarios, for which modifications in the high velocity tail of their distributions are expected to cause a larger impact in direct detection experiments, both for nuclear and electron recoils. In what follows, we briefly describe our modelling of the non-galactic dark matter flux at the Solar System and present upper limits on the dark matter nucleon/electron cross section when considering both the galactic and the non-galactic dark matter components.

9.1.1 The non-galactic dark matter flux on Earth

A crucial ingredient in the calculation of the interaction rate is the dark matter flux at the location of the detector. The flux depends on the number density of dark matter particles at the solar system, which in turn depends on the mass density and the dark matter mass, as well as on the velocity distribution of dark matter particles. None of these quantities are positively known. It is common in the literature to assume a local mass density $\sim 0.3\,\mathrm{GeV/cm^3}$, based on extrapolations of astronomical observations at kpc scales to the small scales of our Solar System, as well as a Maxwell-Boltzmann velocity distribution, based on theoretical considerations that are known to be inaccurate. In fact, numerical simulations and observations of the kinematics of stellar tracers indicate that the true velocity distribution at the Solar System is still qualitatively similar to a Maxwell-Boltzmann distribution, although showing quantitative differences [518–521].

The theoretical modeling of the dark matter phase space distribution in the Solar System normally assumes that the Milky Way is an isolated galaxy. However, the Milky

Way is one among the various members of the Local Group, which include M31, M33 and several dwarf galaxies. Various astronomical observations suggest that the Local Group contains a diffuse component of dark matter, not belonging to the isolated halos of its subsystems, and distributed roughly homogeneously over the cluster [522–524]. This component would permeate the Solar System, and would contain particles moving with speeds larger than the escape velocity from the Milky Way. Further, it has been suggested that the Virgo Supercluster could also contain a diffuse component [525]. The total dark matter flux, which includes the non-galactic components, would therefore be qualitatively different to the one expected from the Standard Halo Model. In the following, we will describe in detail the semi-analytical calculation of the non-galactic dark matter flux at Earth, following [462].

Baushev calculation starts from a stationary and spherically-symmetric system placed at the center in between Andromeda and the Milky Way. The angular momentum $\mu \equiv [\vec{v} \times \vec{r}]$ and maximum radius r_0 the particle moves from the centre of the system are conserved quantities, and the gravitational potential $\phi(r)$ depends only on the radius r . The maximum radius r_0 of the particles in the envelope lie in the range $[r_{in}, r_{\text{out}}]$. The inner radius is roughly $r_{in} = 300\text{kpc}$, corresponding to the size of the Milky Way Roche lobe in system Milky Way - M31. The outer radius is $r_{\text{out}} = 600\text{kpc}$ [524]. Assuming that the particles angular momentum $\mu \equiv [\vec{v} \times \vec{r}]$ follows a Gaussian distribution, which is favoured by N-Body simulations, their distribution in the envelope is [462, 526]:

$$dm = f(r_0) \frac{2\mu}{\alpha(r_0)^2} \exp\left(-\frac{\mu^2}{\alpha(r_0)^2}\right) d\mu dr_0, \quad r_0 \in [r_{\text{in}}, r_{\text{out}}] \tag{9.1}$$

Baushev assumes that the mass of the envelope is $M_{env} = \int_{r_{\text{in}}}^{r_{\text{out}}} f(r_0)\, dr_0 = 10^{12} M_\odot$, which is somewhat smaller than the total mass of the diffuse component [524]. This allows to estimate $\alpha(r_{\text{out}})$ as

$$\alpha(r_{\text{out}}) = \frac{1}{3} r_{\text{out}} \sqrt{\frac{2G(M_{MW} + M_{env})}{r_{\text{out}}}} \tag{9.2}$$

since for larger values, a significant fraction of the particles would exceed the escape velocity at this radius [527]. The exact behavior of $\alpha(r_0)$ is not well known, and it is assumed to follow a power-law

$$\alpha(r_0) = \alpha(r_{\text{out}}) \left(\frac{r_0}{r_{\text{out}}}\right)^i \tag{9.3}$$

The particle distribution within the envelope can be found from the integrals of motion. The radial velocity of the particle is

$$v_r = \sqrt{2(\phi(r_0) - \phi(r)) - \mu^2 \left(\frac{1}{r^2} - \frac{1}{r_0^2}\right)} \tag{9.4}$$

and the maximum angular momentum of a particle that can reach radius r is

$$\mu_{\max}^2 = 2(\phi(r_0) - \phi(r)) \left(\frac{1}{r^2} - \frac{1}{r_0^2}\right)^{-1} \tag{9.5}$$

therefore

$$v_r = \frac{\sqrt{r_0^2 - r^2}}{r r_0}\sqrt{\mu_{\max}^2 - \mu^2} \tag{9.6}$$

The contribution of a single particle of mass m on an interval dr is proportional to the time the particle passes on this interval

$$\frac{dm}{m} = \frac{dtod}{T} = \frac{dr}{v_r T} \tag{9.7}$$

where T is the half-period of the particle, that is, the time it takes for the particle to fall from its maximal radius to the minimal one

$$T(r_0, \mu) = \int_{r_{\min}}^{r_0} \frac{dr}{v_r} \tag{9.8}$$

Now, since $dm = 4\pi r^2 \rho$, the density distribution of dark matter particles at radius r can be found from equation 9.7:

$$\rho = \int_{r_{\text{in}}}^{r_{\text{out}}} \int_0^{\mu_{\max}} \frac{f(r_0)\, r_0 \mu \exp\left(-\mu^2/\alpha^2\right) d\mu dr_0}{2\pi r \alpha^2(r_0)\, T(r_0, \mu)\sqrt{r_0^2 - r^2}\sqrt{\mu_{\max}^2 - \mu^2}} \tag{9.9}$$

We are interested in the non-galactic dark matter distribution at Earth, i.e $r = l_\odot$. Since $l_\odot \ll r_{in} < r_0$, equation 9.9 reduces to

$$\rho = \int_{r_{in}}^{r_{\text{out}}} \int_0^{\mu_{\max}} \frac{f(r_0)\, \mu \exp\left(-\mu^2/\alpha^2\right) d\mu dr_0}{2\pi l_\odot \alpha^2(r_0)\, T(r_0)\sqrt{\mu_{\max}^2 - \mu^2}} \tag{9.10}$$

with $\mu_{\max}(l_\odot) = l_\odot\sqrt{2(\phi(r_0) - \phi(l_\odot))}$. Here we took into account that for $\mu \in [0, \mu_{\max}(l_\odot)]$ period $T(r_0, \mu)$ is almost independent on μ ($T(r_0, \mu) \simeq T(r_0, 0) \equiv T(r_0)$.

Another simplifying assumption can be made, which is that the tangential velocity dispersion in the envelope is higher than $\sim v_{\text{esc}}\frac{l_\odot}{r_{in}}$. This means that $\alpha(r_0) \geqslant \mu_{\max}(l_\odot)$ and 9.10 becomes

$$\rho = \int_{r_{\text{in}}}^{r_{\text{out}}} \int_0^{\mu_{\max}} \frac{f(r_0)\, \mu d\mu dr_0}{2\pi l_\odot \alpha^2(r_0)\, T(r_0)\sqrt{\mu_{\max}^2 - \mu^2}} \tag{9.11}$$

The angular momentum can be further simplified by making some considerations on the particle velocities. The total, radial and tangential velocities of a particle at $r = l_\odot$ will be denoted by u_τ, u_r, and u respectively. We have $\mu = u_\tau l_\odot, u = \sqrt{2(\phi(r_0) - \phi(l_\odot))}, \mu_{\max} = u l_\odot$. Now, considering the particles with the same $u(r_0)$, their angular distribution is

$$d\Omega = \frac{u}{u_r}\frac{2\pi u_\tau du_\tau}{4\pi u^2} = \frac{\mu d\mu}{2l_\odot\sqrt{\mu_{\text{maz}}^2 - \mu^2}\sqrt{2(\phi(r_0) - \phi(l_\odot))}} \tag{9.12}$$

such that

$$\rho = \int_{r_{i=1}}^{r_{\text{out}}} \frac{f(r_0)\sqrt{2(\phi(r_0) - \phi(l_\odot))}dr_0}{\pi\alpha^2(r_0)\, T(r_0)} \int d\Omega \tag{9.13}$$

and one can see that the distribution is isotropic. u and r_0 are related by

$$u = \sqrt{2\left(\phi\left(r_0\right) - \phi\left(l_\odot\right)\right)} \quad du = \frac{\left(\frac{d\phi(r_0)}{dr_0}\right) dr_0}{\sqrt{2\left(\phi\left(r_0\right) - \phi\left(l_\odot\right)\right)}} \tag{9.14}$$

and

$$\rho = \int_{\sqrt{2(\phi(r_{\text{in}})-\phi(l_\odot))}}^{\sqrt{2(\phi(r_{\text{out}})-\phi(l_\odot))}} \frac{8f\left(r_0\right)\left(\phi\left(r_0\right) - \phi\left(l_\odot\right)\right)}{\alpha^2\left(r_0\right) T\left(r_0\right)\left(d\phi\left(r_0\right)/dr_0\right)} du \tag{9.15}$$

So, the density of non-galactic dark matter particles is defined by $\phi\left(r_0\right), T\left(r_0\right)$, and $f\left(r_0\right)$. We will assume $f\left(r_0\right)$ to be a power-law function with some index j. Since $\int f\left(r_0\right) dr_0 = M_{env}$

$$f\left(r_0\right) = \frac{(j+1)M_{env}}{r_{\text{out}} - r_{in}} \left(\frac{r_0}{r_{\text{out}} - r_{\text{in}}}\right)^j \tag{9.16}$$

and

$$M(r) \simeq M_{MW} + M_{env} \left(\frac{r - r_{in}}{r_{out} - r_{in}}\right)^{j+1} \tag{9.17}$$

The assumption of the form of $M(r)$ propagates to $T(r_0)$, such that

$$T\left(r_0\right) = T\left(r_{in}\right) \left(\frac{r_0}{r_{in}}\right)^{1-\frac{j}{2}} \tag{9.18}$$

The gravitational potential is naturally defined by the mass distribution as $\frac{d\phi(r_0)}{dr_0} = \frac{GM(r_0)}{r_0^2}$, then

$$\frac{d\phi\left(r_0\right)}{dr_0} = \frac{G}{r_0^2}\left[M_{MW} + M_{env}\left(\frac{r_0 - r_{in}}{r_{out} - r_{in}}\right)^{j+1}\right] \tag{9.19}$$

We notice that $\sqrt{2\left(\phi\left(r_0\right) - \phi\left(l_\odot\right)\right)}$ remains almost constant for $r_0 \in [r_{\text{in}}\,; r_{\text{out}}\,]$ owing to the smallness of $\mid \phi\left(r_{\text{out}}\right) - \phi\left(r_{in}\right) \mid$ as compared with $\left|\phi\left(r_{in}\right) - \phi\left(r_{l_\odot}\right)\right|$. Therefore one can approximate $\sqrt{2\left(\phi\left(r_0\right) - \phi\left(l_\odot\right)\right)} \simeq \sqrt{2\left(\phi\left(r_{in}\right) - \phi\left(l_\odot\right)\right)} \equiv v_{LG}$. The velocity of the particles is $v_{LG} \sim 600$ km/s, and they have very low velocity dispersion $\sigma_{v_{LG}}$

$$\sigma_{v_{LG}} = \sqrt{v_{LG}^2 + 2\left(\phi\left(r_{\text{out}}\right) - \phi\left(r_{in}\right)\right)} - v_{LG} \sim 16\text{km/s} \tag{9.20}$$

After making some substitutions, and introducing $k \equiv r_{\text{out}}\,/r_{\text{in}} = 2$, one finds the final result

$$\rho = 9\frac{(j+1)}{\left(\frac{3}{2}j - 2i\right)} \frac{k^{2j}\left(k^{\frac{3}{2}j-2i} - 1\right)}{(k-1)^{j+1}} \frac{V}{GT\left(r_{\text{in}}\right) r_{\text{out}}} \tag{9.21}$$

which still depends on the unkowns i and j. For the isothermal sphere ($dM/dr = \text{const}$ and $i = 1, j = 0$. Bushev then arrives to a concrete result for the non-galactic dark matter density at the solar system stemming from the Local Group: $\rho = 3.7 \times 10^{-2}\text{GeV/cm}^3$. The velocity distribution can be very well captured by a delta function at $v_{LG} \sim 600$ km/s, due to the isotropicity of the solution and the small velocity dispersion, which is a

consequence of $|\phi(r_{\text{out}}) - \phi(r_{\text{in}})| \ll -\phi(l_{\odot})$. Therefore, two properties of the velocity distribution are model-independent: the speeds of extragalactic DMPs from the envelope lie in a narrow range, and their angular distribution is isotropic.

The density of the extragalactic dark matter turns out to be fairly high: $3.7 \times 10^{-2}\text{GeV/cm}^3$, around 12% of the total dark matter density at the Earth $\simeq 0.3\text{GeV/cm}^3$.

The main source of the uncertainty in this calculation is given by the mass of the envelope M_{env}. We proceed from the assumption of Cox & Loeb mass M_{env}. The calculation from Baushev relies on the assumption of Cox and Loeb that M_{env} is approximately equal to the masses of the galaxies of the Local Group.

Although the contribution of the non-galactic dark matter particles from the Local Group at Earth with velocities of $v_{\text{LG}} \sim 600\text{km/s}$ is guaranteed, their density may be than the value estimated here. This would be the case if the envelope mass is lower than the masses of the Local Group member galaxies by orders of magnitude, or if the angular momentum distribution of the envelope dark matter particles substantially deviates from the Gaussian. The former case is possible, but requires more observational data and dedicated simulations on the distribution of dark matter particles in between the Milky Way and Andromeda. Some observation of the Hubble flow show that the total mass of the Local Group is similar to the sum of the masses of the Milky Way and M31, enforcing the density of extragalactic dark matter particles to be much smaller [505, 528]. The latter case is disfavoured by N-body simulation results [529]. Further, Andromeda has quite low angular momentum and very oblong orbit [522]. Hence, the presence in the diffuse component of the Local Group of a component of dark matter particles with very oblong orbits that can reach the Earth is plausible.

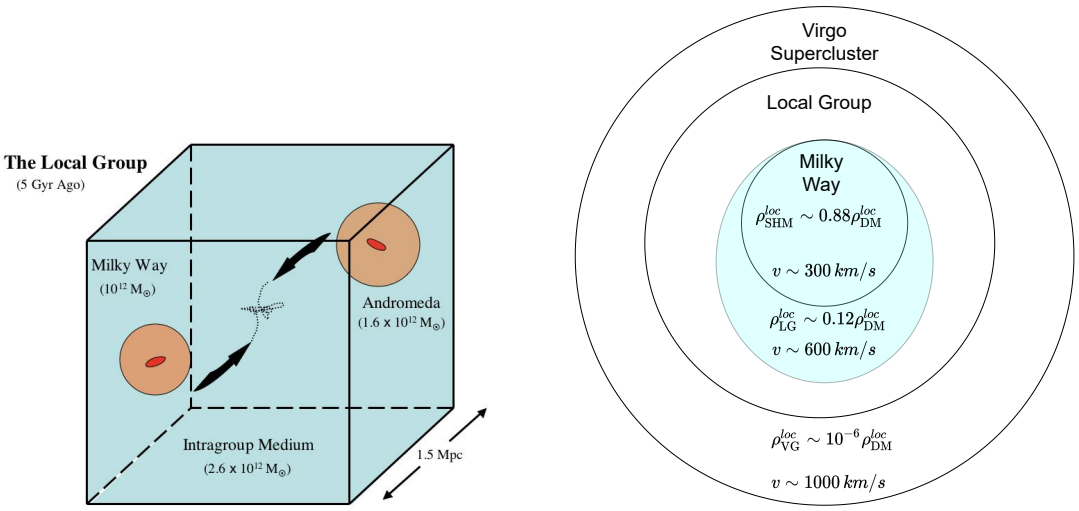

Figure 9.2: *Left panel*: Scheme of the Local Group distances and the likely future collision between the Milky Way and Andromeda [524]. *Right panel*: Scheme of the different components of dark matter particles reaching the Earth, together with their likely densities and velocities.

Therefore, we can approximate the velocity distribution of the non-galactic particles from the Local Group as a delta function (due to isotropy and low velocity dispersion).

The contribution from the Local Group to the dark matter flux at the location of the Solar System can then be written as:

$$\mathscr{F}_{\rm LG}(\vec{v}) = \frac{\rho_{\rm LG}^{\rm loc}}{m_{\rm DM}} v\delta^3(\vec{v} - \vec{v}_{\rm LG}). \tag{9.22}$$

Dark matter in the Virgo Supercluster could also contribute to the dark matter flux in the Solar System. Measurements estimate the average density of the diffuse component to be $\sim 10^{-6}$ GeV/cm^3 [525]. However, the gravitational focusing due to the Local Group leads to a density at the location of the Sun enhanced by a factor $\sim 1 + \frac{v_{esc}^2}{v_{\rm VS}^2}$, which results into a contribution to the total local density of $\rho_{\rm VG}^{\rm loc} \sim 10^{-5}$ GeV/cm^3. Current knowledge on the dark matter velocity distribution in the Virgo Supercluster is much poorer. Following [462], we assume that the dark matter particles have a velocity dispersion comparable to that of the observable members of the Virgo Supercluster, which yields velocities for the Virgo Supercluster dark matter particles at Earth to be (at least) $v_{\rm VS} \sim 1000$ km/s. The contribution from the Virgo Supercluster to the dark matter flux at the location of the Solar System can be written as:

$$\mathscr{F}_{\rm VS}(\vec{v}) = \frac{\rho_{\rm VS}^{\rm loc}}{m_{\rm DM}} v\delta^3(\vec{v} - \vec{v}_{\rm VS}). \tag{9.23}$$

Finally, the dominant contribution stems from dark matter particles of the Milky Way halo. The dark matter density at the location of the Solar System and their velocity distribution is uncertain, however, it is common in the literature to assume the values of the Standard Halo Model, namely a local density $\rho_{\rm SHM}^{\rm loc} = 0.3\,\text{GeV/cm}^3$ and a velocity distribution (expressed in the Solar frame):

$$f_{\rm SHM}(\vec{v}) = \frac{1}{(2\pi\sigma_v^2)^{3/2} N_{\rm esc}} \exp\left[-\frac{v^2}{2\sigma_v^2}\right] \quad \text{for } v \leq v_{\rm esc}\,. \tag{9.24}$$

Here, $v = |\vec{v}|$, $\sigma_v = 156$ km/s is the velocity dispersion [218, 219], $v_\odot \approx 232$ km/s is the local velocity of the Sun with respect to the galactic frame [1], and $v_{\rm esc} = 544$ km/s is the escape velocity from our Galaxy [221, 222]. Further, $N_{\rm esc}$ is a normalization constant, given by:

$$N_{\rm esc} = \text{erf}\left(\frac{v_{\rm esc}}{\sqrt{2}\sigma_v}\right) - \sqrt{\frac{2}{\pi}}\frac{v_{\rm esc}}{\sigma_v}\exp\left(-\frac{v_{\rm esc}^2}{2\sigma_v^2}\right)\,. \tag{9.25}$$

For our chosen parameters, $N_{\rm esc} \simeq 0.993$. The contribution to the local dark matter flux from the Milky Way halo then reads:

$$\mathscr{F}_{\rm SHM}(\vec{v}) = \frac{\rho_{\rm SHM}^{\rm loc}}{m_{\rm DM}} v f_{\rm SHM}(\vec{v}). \tag{9.26}$$

[1] The velocity of the Sun with respect to the galactic rest frame is given by $\vec{v}_\odot = \vec{v}_{\rm LSR} + \vec{v}_{\odot,pec}$, where $\vec{v}_{\rm LSR} = (0, v_c, 0)$ is the motion of the local standard of rest (LSR), $v_c \approx 220$ km/s, and $\vec{v}_{\odot,pec} = (11.1, 12.24, 7.25)$ km/s is the Sun's peculiar motion [220].

with $m_{\rm DM}$ the dark matter mass.

We then model the dark matter flux at the position of the Solar System as the normalized sum of these various contributions:

$$\mathscr{F}(\vec{v}) = \mathscr{F}_{\rm SHM}(\vec{v}) + \mathscr{F}_{\rm LG}(\vec{v}) + \mathscr{F}_{\rm VS}(\vec{v}), \tag{9.27}$$

where we adopt values for the local density of each component derived in [462], such that the total sum yields the canonical value of the local density ($\rho^{\rm loc} = 0.3$ GeV/cm^3) used by direct detection experiments: $\rho^{\rm loc}_{\rm SHM} = 0.26$ GeV/cm^3 ($\sim 88\%$), $\rho^{\rm loc}_{\rm LG} = 0.037$ GeV/cm^3 ($\sim 12\%$), and $\rho^{\rm loc}_{\rm VS} = 10^{-5}$ GeV/cm^3 ($\sim 0.00003\%$).

The parameters of the non-galactic flux components are subject to uncertainties, *e.g.* the determination of the mass of the Local Group envelope [524]. The values we adopt in this work can be regarded as conservative, and are meant to illustrate the potential sensitivity of non-galactic dark matter in light dark matter searches. Recent and future studies of the dynamics of the Virgo Supercluster and Local Group members [530–535], in combination with a more refined modeling of the dark matter distribution in these objects, will be essential to better determine the phase-space distribution of non-galactic dark matter at the Solar System.

It should be noted that the true local density and velocity distribution may differ from these commonly adopted values [217, 536], and a number of refinements to the SHM have been proposed in recent years [521, 537]. The impact of these deviations on direct detection experiments has been discussed in various works [**Fowlie:2018sv**, 210, 538–540]. Moreover, the Milky Way halo could contain substructures, such as streams or subhalos, which may also enhance the dark matter flux at the location at the Solar System [541]. The probability of a sizable enhancement is, on the other hand, modest [542].

9.1.2 Direct detection of non-galactic light dark matter

The differential rate of nuclear recoils induced by scatterings of dark matter particles traversing a detector at the Earth is given by [543, 544] (see section 4.2 for a more detailed discussion):

$$\frac{dR}{dE_R} = \sum_i \frac{\xi_i}{m_{A_i}} \int_{v \geq v^i_{\rm min}(E_R)} {\rm d}^3 v \mathscr{F}(\vec{v} + \vec{v}_\odot) \frac{{\rm d}\sigma_i}{{\rm d}E_R}(v, E_R)\,. \tag{9.28}$$

and he total recoil rate can be calculated from the differential rate using:

$$R = \int_0^\infty {\rm d}E_R\, \epsilon_i(E_R) \frac{dR}{dE_R}, \tag{9.29}$$

with $\epsilon_i(E_R)$ the efficiency, defined as the probability to detect the recoil of the target nucleus i with energy E_R. Finally, the total number of expected recoil events at a direct detection experiment reads $\mathcal{N} = R \cdot \mathcal{E}$, with $\mathcal{E}$ the exposure (i.e. mass multiplied by live-time) of the experiment.

We show in Figure 9.3 the different contributions of the dark matter flux to the differential recoil spectrum with a $CaWO_4$ target (top panels) and a Xe target (bottom panels), assuming a spin-independent interaction only (left panel) or the spin-dependent interaction only (right panel), considering for each case values of the cross section near the current sensitivity of experiments. We take two exemplary choices for the dark matter mass: $m_{\rm DM} = 1$ GeV (red) and 10 GeV (purple) for the $CaWO_4$ target, while $m_{\rm DM} = 10$ GeV (blue) and 100 GeV (brown) for the Xe target. For each mass, we show the differential recoil rate induced just by the SHM component (dotted lines), as well as the differential rate including the contribution from the Local Group (dashed lines) and including also the Virgo Supercluster (solid lines).

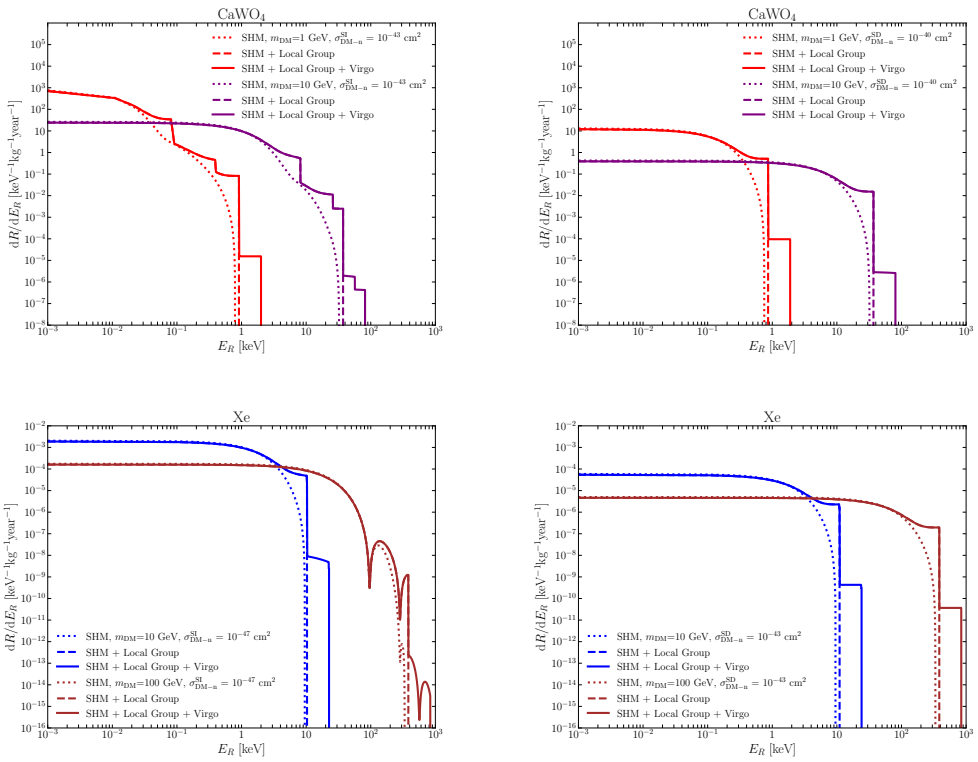

Figure 9.3: Dark matter-nucleon differential recoil rate with a $CaWO_4$ target (top panels) and a Xe target (bottom panels), assuming spin-independent (left panels) or spin-dependent scattering (right panels), for two exemplary choices of the dark matter mass, and for values of the cross-section close to the current upper limit from experiments. The dotted lines indicate the differential rate expected from the Standard Halo Model, the dashed lines include also the contribution from the Local Group, and the solid lines also the contribution from the Virgo Supercluster.

The new contributions modify the differential rate at the highest recoil energies, causing deviations from the differential recoil spectrum expected within the SHM. The non-

galactic contributions could increase the total number of detected recoil events, thus increasing the discovery potential of direct detection experiments. Further, due to the small velocity dispersion of the non-galactic dark matter particles, the differential recoil spectrum presents step-like features which could be crucial to distinguish a dark matter signal from irreducible backgrounds with a smoother spectrum, such as the one arising from the coherent elastic scattering of solar neutrinos off nuclei [206, 545].

Concretely, the ratio between the contributions to the differential recoil rate from the Local Group, and the contribution from the Standard Halo Model can be estimated analytically. Assuming a single target, it reads:

$$\frac{dR/dE\Big|_{\rm LG}}{dR/dE\Big|_{\rm SHM}} \approx \frac{\rho^{\rm loc}_{\rm LG}}{\rho^{\rm loc}_{\rm SHM}}\frac{\sigma_v}{v^*_{\rm LG}}\sqrt{\frac{\pi}{2}}N_{\rm esc}\frac{\theta\Big(v^*_{\rm LG}-v_{\rm min}(E_R)\Big)}{e^{-\frac{v^2_{\rm min}(E_R)}{2\sigma^2_v}}-e^{-\frac{v^{*2}_{\rm esc}}{2\sigma^2_v}}}\,, \tag{9.30}$$

where starred variables refer to the detector frame: $\vec{v}^* = \vec{v} + \vec{v}_\odot$. For most values of E_R the Local Group contributes negligibly, due to the large suppression factor $(\rho^{\rm loc}_{\rm LG}/\rho^{\rm loc}_{\rm SHM})(\sigma_v/v^*_{\rm LG})$. However, for large values of E_R, the Local Group can provide a comparable or even dominant contribution to the rate. Concretely, the Local Group provides a contribution to the differential rate comparable to the one from the Standard Halo Model when

$$E_R \gtrsim E_R^{\rm max,SHM}\Big[1-\frac{2\sigma_v^2}{v^{*2}_{\rm esc}}\ln\Big(\frac{\rho^{\rm loc}_{\rm LG}}{\rho^{\rm loc}_{\rm SHM}}\frac{\sigma_{\rm v}}{\rm v^*_{LG}}\sqrt{\frac{\pi}{2}}{\rm N_{esc}e}^{\frac{\rm v^{*2}_{esc}}{2\sigma^2_{\rm v}}}+1\Big)\Big]\,, \tag{9.31}$$

with $E_R^{\rm max,SHM} = 2\mu_A^2 v^{*2}_{\rm esc}/m_A$ the largest possible recoil energy within the SHM, and dominates the recoil spectrum up to $E_R^{\rm max,LG} = 2\mu_A^2 v^2_{\rm LG}/m_A = v^{*2}_{\rm LG}/v^{*2}_{\rm esc}E_R^{\rm max,SHM}$, which is the largest possible recoil energy from DM particles in the Local Group envelope. For our adopted values, one obtains $E_R \gtrsim 0.29E_R^{\rm max,SHM}$ and extends up to $E_R^{\rm max,LG} \simeq 1.2E_R^{\rm max,SHM}$; these numbers are in qualitative agreement with Fig. 9.3. Analogous expressions hold for the contribution from the Virgo Supercluster: one obtains that this contribution dominates over the SHM one for $E_R \gtrsim 0.94E_R^{\rm max,SHM}$ and extends up to $E_R^{\rm max,VS} \simeq 2.5E_R^{\rm max,SHM}$.

We show in Figure 9.4 the upper limits on the dark matter-nucleon spin independent (left panel) or spin-dependent (right panel) scattering cross section as a function of the dark matter mass from the non-observation of dark matter induced nuclear recoils at the CRESST-III, XENON1T and CDMS experiments. The potential impact of the dark matter envelope of the Local Group for the search of light dark matter is apparent from the Figure. For $m_{\rm DM} \lesssim 1$ GeV, this contribution can enhance the recoil rate at the CRESST experiment by at least a factor ~ 2. As the dark matter mass decreases, the enhancement becomes more and more important, and even allows to probe masses for which the galactic dark matter would not induce detectable recoils. Similarly, for $m_{\rm DM} \lesssim 10$ GeV, the recoil rate at the XENON1T experiment is increased by at least a factor ~ 10, thus increasing the discovery potential of the experiment. [2]

[2]For very large cross-sections, the dark matter flux could be attenuated in its passage through the

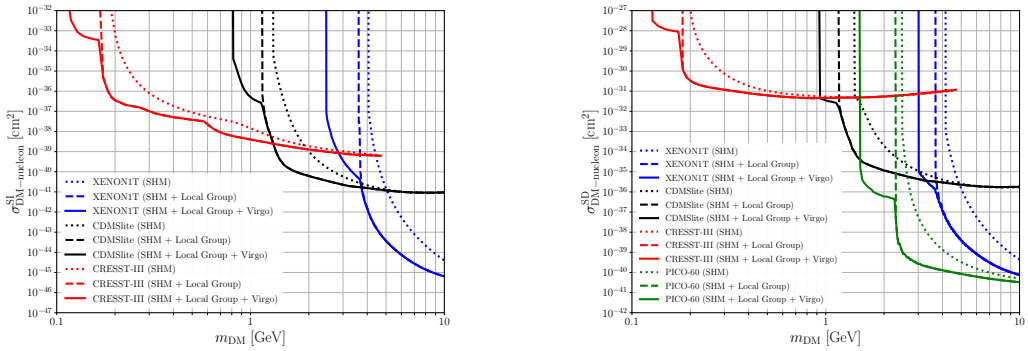

Figure 9.4: Upper limits at the 90% C.L. on the spin-independent (left panel) and spin-dependent (right panel) dark matter-nucleon cross-section from the null search results from the XENON1T (blue), CRESST-III (red), PICO-60 (green) and CDMS (black) experiments, assuming equal coupling to protons and neutrons. The dotted line indicates the upper limit derived under the assumption that only galactic dark matter, described by the Standard Halo Model, contributes to the dark matter flux at the Solar System. The dashed lines show the impact of including in the flux also the non-galactic dark matter component from the Local Group and the solid lines show the impact of including also the diffuse component of the Virgo Supercluster.

The dark matter-electron scattering rate in liquid xenon has been discussed at length in the literature [232, 548–550], see also section 4.2 for a detailed discussion. The differential ionization rate reads:

$$\frac{dR_{ion}}{d\ln E_{er}} = N_T \sum_{n,l} \int_{v \geq v^{nl}_{\rm min}(E_{er})} {\rm d}^3 v \mathscr{F}(\vec{v} + \vec{v}_\odot) \frac{{\rm d}\sigma^{nl}_{\rm ion}}{d\ln E_{er}}(v, E_{er}) \,, \tag{9.32}$$

where N_T is the number of target nuclei and

$$v^{nl}_{\rm min}(E_{er}) = \sqrt{\frac{2}{m_{\rm DM}}(E_{er} + |E^{nl}|)} \tag{9.33}$$

is the minimum dark matter velocity necessary to ionize a bound electron in the (n,l) shell of a xenon atom (with energy E^{nl}), giving a free electron with energy E_{er}. Further, $d\sigma^{nl}_{\rm ion}/d\ln E_{er}$ is the differential ionization cross section, given by:

$$\frac{d\sigma^{nl}_{ion}}{d\ln E_{er}}(v, E_{er}) = \frac{\bar{\sigma}_{\rm DM-e}}{8\mu^2_{\rm DM,e} v^2} \int_{q^{nl}_{\rm min}}^{q^{nl}_{\rm max}} dq q \left| f^{nl}_{ion}(k', q) \right|^2 |F_{\rm DM}(q)|^2 \,. \tag{9.34}$$

Here, $\mu_{\rm DM,e}$ is the reduced mass of the dark matter-electron system, $\bar{\sigma}_{\rm DM-e}$ is the dark matter-free electron scattering cross section at fixed momentum transfer $q = \alpha m_e$, $\left| f^{nl}_{ion}(k', q) \right|^2$ is the ionization form factor of an electron in the (n,l) shell with final

Earth before reaching the detector [546, 547]. We estimate this attenuation to be negligible for the values shown in the Figure.

momentum $k' = \sqrt{2m_e E_{er}}$ and momentum transfer q, and $F_{\rm DM}(q)$ is a form factor that encodes the q-dependence of the squared matrix element for dark matter-electron scattering and depends of the mediator under consideration. Note that the momentum transfer is not univocally determined, due to the fact that the electron momentum in the atomic orbital is not fixed. The maximum and minimum values of the momentum transfer producing an electron recoil with energy E_{er} from the interaction of a dark matter particle with speed v with a bound electron in the (n,l) shell are:

$$q^{nl}_{\rm max\atop min}(E_{er}) = m_{\rm DM} v \left[1 \pm \sqrt{1 - \left(\frac{v^{nl}_{\rm min}(E_{er})}{v}\right)^2}\right], \tag{9.35}$$

with $v^{nl}_{\rm min}(E_{er})$ defined in Eq. (9.46). Finally, the total number of expected ionization events reads $\mathcal{N} = R_{ion} \cdot \mathcal{E}$, with R_{ion} the total ionization rate, calculated from integrating Eq.(9.45) over all possible recoil energies, and $\mathcal{E}$ the exposure (*i.e.* mass multiplied by live-time) of the experiment. [3] In our analysis, we consider the ionization of electrons in the three outermost orbitals (with binding energies in eV shown in parenthesis): $5p^6$ (12.4), $5s^2$ (25.7) and $4d^{10}$ (75.6). The corresponding ionization form factors were calculated using the software `DarkARC` [549]. For the dark matter form factor, we adopt two different parametrizations: the case of a heavy hidden photon A' mediator $m_{A'} \gg q$, with $F_{\rm DM}(q)$=1, and an ultralight hidden photon $m_{A'} \ll q$, with $F_{\rm DM}(q) = \alpha^2 m_e^2/q^2$.

We show in Figure 9.5 the different contributions to the dark matter-electron differential recoil rates at an experiment with a Xe target, for two exemplary choices of the dark matter mass, 10 MeV and 100 MeV, and for the aforementioned two parametrizations. For each case, we assume a value of the cross section near the current sensitivity of experiments. Further, for each mass, we show the differential recoil rate induced just by the SHM component (dotted lines), as well as the enhancement in the differential recoil rate induced by dark matter from the Local Group (dashed lines) and by both the Local Group and the Virgo Supercluster (solid lines).

[3] The efficiency function of XENON10 and XENON100 is taken into account when calculating the upper limit on the number of signal events, as described in Appendix **??**.

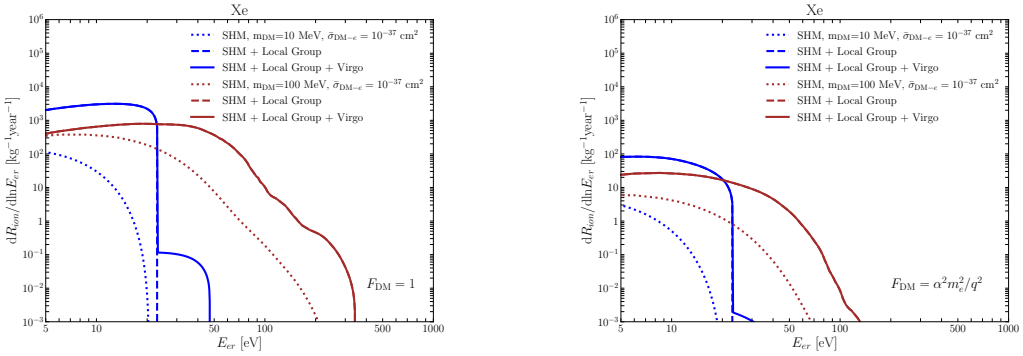

Figure 9.5: Dark matter-electron differential recoil rate with a Xe target, assuming an interaction mediated by a heavy hidden photon (left panel) or an ultralight hidden photon (right panel), for two exemplary choices of the dark matter mass: $m_{\rm DM}$ =100 MeV (brown) and $m_{\rm DM}$ =10 MeV (blue), and values of the cross-section close to the current upper limit from experiments. The dotted lines indicate the differential rate expected from the Standard Halo Model, the dashed lines include also the contribution from the Local Group, and the solid lines also the contribution from the Virgo Supercluster.

As can be seen in the plot, the non-galactic dark matter can have a considerable impact on the electron recoil spectrum. Similarly to the nuclear recoils, the Local Group provides a contribution to the rate $\propto (\rho^{\rm loc}_{\rm LG}/\rho^{\rm loc}_{\rm SHM})(\sigma_v/v^*_{\rm LG})$, but due to the values of the form factors, the enhancement is numerically larger. More importantly, the impact of the Local Group contribution is significant over a wider range of recoil energies, and not just close to the kinematical threshold, which is due to the fact that the momentum transfer is not fixed for scatterings off electrons in an atomic orbital. For very small mass, such as for $m_{\rm DM} = 10$ MeV, the momentum transfer is not fixed, but takes values within a small range, *cf.* Eq. (9.48). Therefore the contribution to the recoil spectrum from the Local Group resembles a step function (as for nuclear recoils). For larger masses, the contribution from the Local Group to the recoil spectrum is the superposition of various step functions (corresponding to different values of the momentum transfer), generating a featureless spectrum that extends to lower recoil energies.

Finally, we show in Figure 9.6 the 90% C.L upper limits on the dark matter-electron scattering cross section at fixed momentum transfer $q = \alpha m_e$ from XENON10 and XENON100 data, including both the galactic and the non-galactic dark matter components, for a heavy mediator (left panel) and for an ultralight mediator (right panel). For $m_{\rm DM} = 50 - 1000$ MeV, dark matter from the Local Group envelope significantly enhances the reach of the XENON100 experiment, by at least one order of magnitude, compared to the expectations of the Standard Halo Model. For $m_{\rm DM} = 30 - 50$ MeV, close to the kinematical threshold of the XENON100 experiment, the enhancement is even more significant. Further, the non-galactic dark matter components allow to probe the mass region $m_{\rm DM} = 13 - 30$ MeV, for which dark matter particles from the host halo do not induce detectable recoils. For the XENON10 experiment the conclusions are

analogous, although in this case the enhancement is somewhat more modest, but still $\mathcal{O}(1)$. We also show in the plot values of parameters expected from theoretical models [232] for a heavy or an ultralight mediator, respectively. For the former, reproducing the correct thermal abundance via freeze-out requires values of $\bar{\sigma}_{\mathrm{DM-e}}$ above the purple line. For the latter, the purple shaded region shows the values favored by the freeze-in mechanism [548]. Clearly, the non-galactic components significantly improve the discovery potential of experiments.

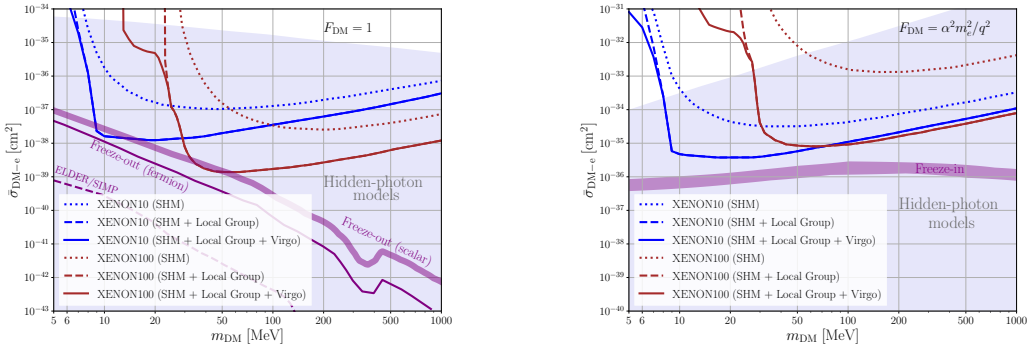

Figure 9.6: Upper limits at the 90% C.L. on the dark matter-electron cross-section from the null search results from the XENON10 (blue) and XENON100 (brown) experiments, assuming an interaction mediated by a heavy hidden photon (left panel) or an ultralight hidden photon (right panel) . The dotted line indicates the upper limit derived under the assumption that only galactic dark matter, described by the Standard Halo Model, contributes to the dark matter flux at the Solar System. The dashed lines show the impact of including in the flux also the non-galactic dark matter component from the Local Group and the solid lines show the impact of including also the diffuse component of the Virgo Supercluster. We also show in the shaded lavender region the values of parameters expected from some selected models (see main text for details).

For nuclear recoils, we have found an enhancement in the energy recoil spectrum compared to the expectations from the Standard Halo Model, most notably close to the kinematical thresholds. Correspondingly, the upper limits on the scattering cross-section become more stringent for light dark matter. More concretely, for the spin-independent interaction, the limits for $m_{\mathrm{DM}} = 1$ GeV (0.2 GeV) from CRESST-III become a factor ~ 2 ($\sim 10^3$) more stringent than in the Standard Halo Model, and the limits for $m_{\mathrm{DM}} = 10$ GeV (4 GeV) from XENON1T, a factor ~ 10 ($\sim 10^4$). Similar conclusions hold for the spin-dependent interaction. Further, the dark matter mass range that experiments are able to probe is extended to lower values. We have also argued that the non-galactic dark matter component would leave a characteristic signature in the recoil spectrum in the form of step-like features, which could be discerned from the smooth spectrum expected from recoils induced by dark matter particles from the host halo or from the irreducible neutrino background. We also expect a non-negligible impact of the non-

galactic contributions to the flux for inelastic dark matter scatterings, or for secondary ionization induced by the Migdal effect. We leave this analysis for future work.

For electron recoils, we find also an enhancement of the differential rate. Furthermore, the enhancement is appreciable over a larger range of recoil energies, and not only close to the kinematical thresholds. In turn, the limits on the dark matter-electron scattering cross-section are significantly strengthened in a wide mass range. For interactions mediated by a heavy hidden photon, the enhancement amounts to a factor of ~ 2 (~ 10) at $m_{\rm DM} = 1000$ MeV for the XENON10 (XENON100) experiment, and increases for lighter dark matter, being the enhancement a factor of $\sim 10^2$ at $m_{\rm DM} = 10$ GeV for the XENON10 experiment and a factor of $\sim 10^2$ as well at $m_{\rm DM} = 40$ GeV for the XENON100 experiment. For an ultralight mediator, the conclusions are analogous, being the strengthening of the limits somewhat larger for the XENON100 experiment.

An obvious caveat of this analysis is the as yet poor understanding of the non-galactic dark matter phase-space distribution. Therefore, the limits on the cross-section derived in this work should be taken with a grain of salt. We hope that future astronomical observations, and a more refined modeling of the dark matter envelope of the Local Group and the Virgo Supercluster, will lead to a more robust assessment of the impact of these two contributions in direct dark matter searches. A proper understanding of the non-galactic components to the dark matter flux may prove to be crucial for the correct interpretation of the experimental data.

9.1.3 Direct detection of non-galactic inelastic dark matter

The kinematics of the inelastic scattering differs from the one in the elastic scenario. In order to allow the production of a heavier neutral particle in the final state, the velocity of the incoming dark matter particle must be larger than a certain threshold. Therefore, as the mass difference between the initial and final neutral particles increases, faster and faster dark matter particles are necessary in order to open kinematically the inelastic process. For dark matter particles bound to our galaxy, and which have speeds smaller than the escape velocity from the Milky Way, $v_{\rm esc} = 544$ km/s [221, 222], the inelastic scattering off a nucleus is kinematically allowed when the mass difference between the two states is $\delta m < 1/2 \mu v_{\rm esc}^2$, with μ the reduced mass of the DM-nucleus system; for the scattering off an electron, the inelastic channel is open when $\delta m < 1/2 \mu_e v_{\rm esc}^2 - |E^{nl}|$, where μ_e is the reduced mass of the DM-electron system, and $|E^{nl}|$ is the binding energy of an electron in the (n, l) shell of the target nucleus. In practice, experiments can only detect recoiling nuclei/ionized electrons within a given energy range, therefore the mass difference that can be probed in direct searches is smaller than this value.

The differential rate of nuclear recoils induced by inelastic up-scatterings of dark matter particles traversing a detector at the Earth is given by:

$$\frac{dR}{dE_R} = \sum_i \frac{\xi_i}{m_{A_i}} \int_{v \geq v^i_{\rm min}(E_R)} {\rm d}^3 v \mathscr{F}(\vec{v} + \vec{v}_\odot) \frac{{\rm d}\sigma_i}{{\rm d}E_R}(v, E_R) \,. \tag{9.36}$$

differing from the elastic case in the minimum velocity necessary to induce a recoil with

energy E_R of the nucleus i with mass m_{A_i} and mass fraction ξ_i in the detector

$$v^i_{\rm min}(E_R) = \frac{1}{\sqrt{2E_R m_{A_i}}}\Big(\frac{E_R m_{A_i}}{\mu_{A_i}} + \delta_{\rm DM}\Big)\,. \tag{9.37}$$

Further, for spin-independent interactions, the differential dark matter-nucleus cross section reads,

$$\frac{d\sigma^{\rm SI}_i}{dE_R}(v, E_R) = \frac{m_{A_i}}{2\mu^2_{A_i} v^2}\sigma^{\rm SI}_{0,i} F^2_i(E_R)\ . \tag{9.38}$$

Here m_{A_i} is mass of the nucleus i, μ_{A_i} is the reduced mass of the dark matter-nucleus i system and $F^2_i(E_R)$ is the nuclear form-factor, for which we adopt the Helm prescription. Besides, $\sigma^{\rm SI}_{0,i}$ is the spin-independent dark matter-nucleus scattering cross section at zero momentum transfer, which depends on the details of the dark matter model and the target nucleus. From the differential rate, one can calculate the total recoil rate using:

$$R = \int_0^\infty {\rm d}E_R\, \epsilon_i(E_R)\frac{dR}{dE_R}\,, \tag{9.39}$$

where $\epsilon_i(E_R)$ is the efficiency of that experiment. Finally, the total number of expected recoil events is $\mathcal{N} = R\cdot\mathcal{E}$, with $\mathcal{E}$ the exposure (*i.e.* mass multiplied by live-time).

In our analysis, we will consider two scenarios for the coupling of dark matter to nucleons. First, we will consider a Majorana dark matter candidate. In this case

$$\sigma^{\rm SI}_{0,i} = \frac{4\mu^2_{A_i}}{\pi}\Big[Z_i f^p_S + (A_i - Z_i) f^n_S\Big]^2\,, \tag{9.40}$$

where f^p_S and f^n_S parametrize the strength of the scalar interactions to the proton and the neutron (see *e.g.* [544, 551]). It is common to write Eq. (9.40) as

$$\sigma^{\rm SI}_{0,i} = \frac{\mu^2_{A_i}}{\mu^2_p}\Big[Z_i + (A_i - Z_i)\frac{f^n_S}{f^p_S}\Big]^2\sigma_{\rm DM,p}\,, \tag{9.41}$$

with μ_p the reduced mass of the DM-proton system and $\sigma_{\rm DM,p}$ an effective DM-proton interaction cross-section. Within the Majorana dark matter scenario, we will consider in particular the widely adopted benchmark case where the interaction is "isoscalar", *i.e.* when the dark matter couples with equal strength to protons and neutrons, for which

$$\sigma^{\rm SI}_{0,i} = \frac{\mu^2_{A_i}}{\mu^2_p}A_i^2\sigma_{\rm DM,p}\,. \tag{9.42}$$

We will also consider a scenario where the dark matter has hypercharge Y, and interacts with the quarks via the exchange of a Z boson. In this case, $\sigma^{\rm SI}_{0,i}$ has the same form as Eq. (9.40), replacing the scalar couplings by the corresponding vector couplings, $f^{p,n}_S \to f^{p,n}_V$. For interactions with the Z boson, f^p_V and f^n_V are explicitly given by:

$$f^p_V = \frac{G_F\zeta Y}{2\sqrt{2}}(1 - 4\sin^2\theta_W)\,, f^n_V = -\frac{G_F\zeta Y}{2\sqrt{2}}\,,$$

with $\zeta = 1$ ($\zeta = 2$) for fermionic (bosonic) dark matter [89, 125, 552]. In this scenario, the dark matter-nucleus cross section can be related to the dark matter-proton cross-section through:

$$\sigma_{0,i}^{\mathrm{SI}} = \frac{\mu_{A_i}^2}{\mu_p^2}\left[Z_i - \frac{(A_i - Z_i)}{(1 - 4\sin^2\theta_W)}\right]^2 \sigma_{\mathrm{DM,p}}\,, \tag{9.43}$$

which is independent of the dark matter hypercharge and spin.

To assess the impact of the non-galactic diffuse components for direct detection experiments, we plot in Figure. 9.7 the differential rate of inelastic scatterings in the LUX-ZEPLIN experiment for the "isoscalar" scenario, assuming $m_{\mathrm{DM}} = 1$ TeV and $\sigma_{\mathrm{DM,p}} = 10^{-38}\,\mathrm{cm}^2$, for $\delta_{\mathrm{DM}} = 100$ keV (light blue) and 200 keV (dark blue), including in the flux only the contribution from dark matter bound to the Milky Way (dotted lines), as commonly assumed in the literature, and including the contribution from the non-galactic diffuse component (solid lines). The impact of the non-galactic component in the differential rate is apparent from the figure, and increases the number of events at all recoil energies, especially in the region with low E_R which is not kinematically accessible to the galactic dark matter. The non-galactic dark matter, therefore, has implications not only for enhancing the sensitivity of the experiment, but also for the interpretation of a putative dark matter signal.

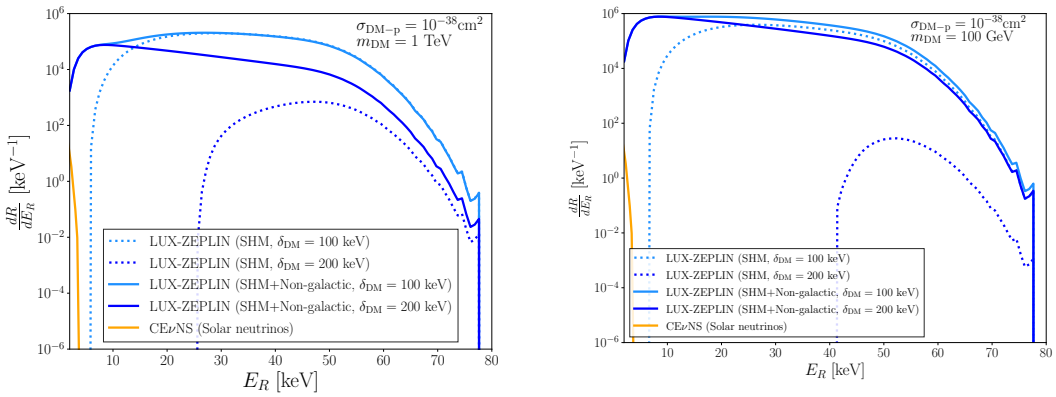

Figure 9.7: Differential rate for the inelastic scattering of a Majorana dark matter candidate in the "isoscalar" scenario with mass $m_{\mathrm{DM}} = 1$ TeV, for $\delta_{\mathrm{DM}} = 100$ keV (light blue) and 200 keV (dark blue), for a dark matter flux at Earth as modelled by the Standard Halo Model (dotted line) or including also the contribution from the non-galactic diffuse dark matter component (solid line). For the plots it was assumed $\sigma_{\mathrm{DM,p}} = 10^{-38}\,\mathrm{cm}^2$.

Current direct search experiments have not observed a significant excess of nuclear recoils, which allows to derive upper limits on the dark matter nucleon cross section for given combinations of the dark matter mass and mass splitting between the dark matter particle and the neutral particle in the final state. In Figure 9.8, we show upper limits on the dark matter-proton spin-independent scattering cross section versus mass splitting

for $m_{\rm DM} = 1$ TeV from LUX-ZEPLIN (blue) [216], PICO60 (green) [488], CRESST-II (red) [553], and from a radiopurity measurement in a $CaWO_4$ crystal (orange) [230, 554]. The dotted lines represent the limits obtained considering the galactic dark matter (described by the SHM) as the only contribution to the dark matter flux, while the solid lines were obtained including also the contributions to the flux from the non-galactic diffuse component in the Solar System. In the upper left plot, we show the limits for a Majorana dark matter candidate in the "isoscalar" scenario, and in the upper right plot, the most conservative limit for the Majorana dark matter, without making assumptions on the coupling strengths, derived following the approach of [105]. Lastly, in the lower plot we show the limits for a scenario where the dark matter interacts with the nucleus via the exchange of a Z-boson. In the latter plot we also show the dark matter-proton scattering cross-section for scenarios of a fermionic dark matter, and $Y = 1/2$ (corresponding to the well motivated scenario of the Higgsino dark matter in the limit of high scale supersymmetry [112, 113]), $Y = 1$ and $Y = 3/2$ (which correspond to different scenarios of minimal dark matter [552]), for a xenon target. For other targets, the expected cross section for $m_{\rm DM} = 1$ TeV scales as $\sim A_i/Z_i$, being indistinguishable in the Figure.

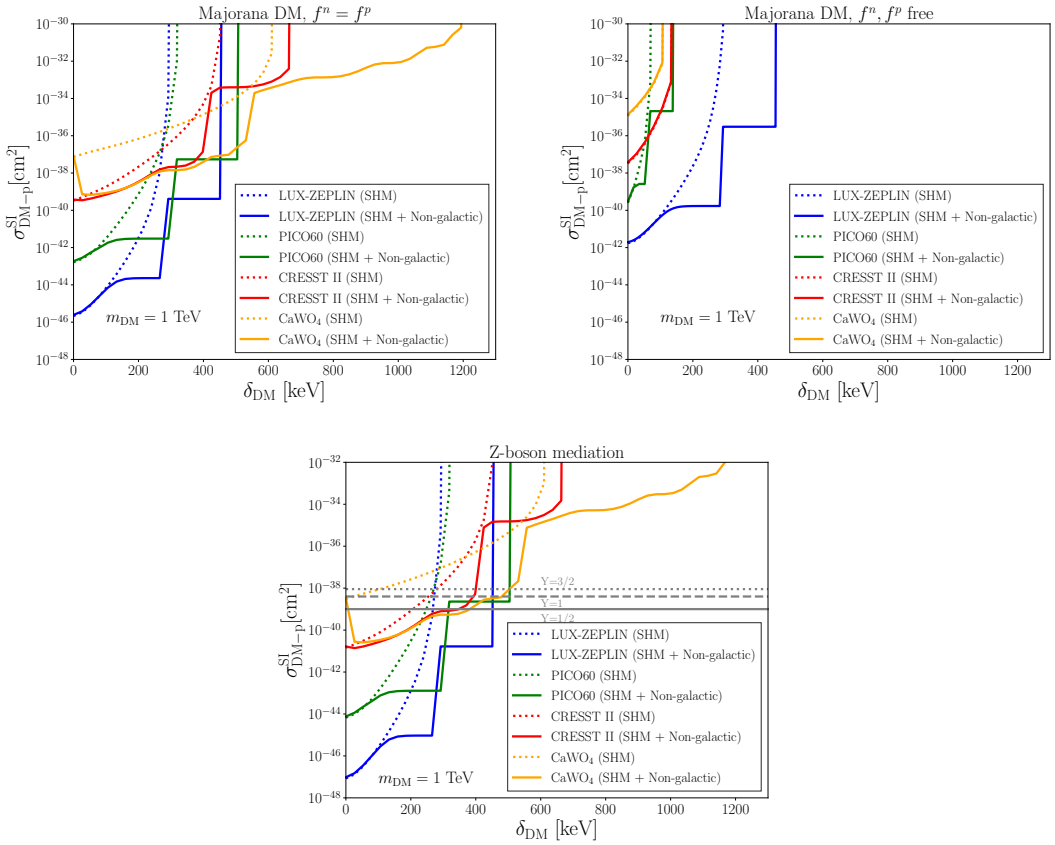

Figure 9.8: 90% C.L upper limits on the spin-independent dark matter-proton inelastic cross section for a dark matter mass of 1 TeV as a function of the mass splitting, from LUX-ZEPLIN (blue), PICO60 (green), CRESST-II (red and orange) and from a $CaWO_4$ detector radiopurity measurement (orange). We show the limits for three different scenarios: Majorana dark matter with isoscalar interactions $f^p = f^n$ (upper left plot), arbitrary f^p and f^n (upper right plot), and dark matter interacting via the Z-boson (lower plot). In the lower plot, we also show for reference the predicted value of the cross-section with a xenon target for scenarios of fermionic dark matter with hypercharge $Y = 1/2, 1, 3/2$.

As seen in the plots, for all the scenarios the non-galactic diffuse component enhances the sensitivity of experiments to inelastic dark matter, allowing to probe larger mass splittings. For instance, for our representative dark matter mass of 1 TeV, the LUX-ZEPLIN experiment is insensitive to dark matter particles of the Milky Way scattering inelastically if the mass difference with the neutral particle in the final state is $\delta_{\rm DM} \gtrsim 300$ keV. However, the presence of dark matter in the Solar System from the envelope of the Local Group extends the reach up to $\delta_{\rm DM} \simeq 330$ keV and allows to probe uncharted parameter space for large mass splittings. Concretely, the LUX-ZEPLIN experiment

sets for the isoscalar scenario the limit $\sigma^{\rm SI}_{\rm DM-p} \lesssim 10^{-44}\,{\rm cm}^2$ for $\delta_{\rm DM} = 250$ keV, which is about three orders of magnitude stronger than the limit obtained assuming that all dark matter is bound to the Milky Way, and only a factor of 100 weaker than the limit on the elastic scattering cross-section *i.e.* for $\delta_{\rm DM} = 0$. For the interaction mediated by the Z-boson the upper limit is $\sigma^{\rm SI}_{\rm DM-p} \lesssim 10^{-44}\,{\rm cm}^2$, and the most conservative limit without making assumptions on the form of the interaction is $\sigma^{\rm SI}_{\rm DM-p} \lesssim 10^{-40}\,{\rm cm}^2$, obviously much weaker than for concrete scenarios. The dark matter particles from the Virgo Supercluster extend the reach to even larger mass differences, up to $\delta_{\rm DM} \simeq 450$ keV and sets for the isoscalar scenario the limit $\sigma^{\rm SI}_{\rm DM-p} \lesssim 5 \times 10^{-40}\,{\rm cm}^2$ for $\delta_{\rm DM} = 450$ keV; for the interaction mediated by the Z-boson the upper limit is $\sigma^{\rm SI}_{\rm DM-p} \lesssim 10^{-41}\,{\rm cm}^2$, while the model independent limit is $\sigma^{\rm SI}_{\rm DM-p} \lesssim 5 \times 10^{-36}\,{\rm cm}^2$. Similar conclusions apply for the PICO and CRESST experiments, and from the radiopurity measurements on a $CaWO_4$ target.

It is interesting to note the complementarity of the different experiments in probing the parameter space of inelastic dark matter scenarios. Both in the scenario of a Majorana dark matter with $f^n = f^p$ and for the scenario with Z-boson mediation, LUX-ZEPLIN is the most sensitive probe for small $\delta_{\rm DM}$, whereas the radiopurity measurements on a $CaWO_4$ is the most sensitive probe for large $\delta_{\rm DM}$. PICO-60 is relevant for intermediate values of $\delta_{\rm DM}$, and is in fact the most sensitive current probe of some well motivated dark matter scenarios, as suggested by the gray lines in the Figure, which correspond to the expected cross-section for different scenarios of electroweakly interacting fermionic dark matter. The complementarity of experiments in probing these scenarios is investigated in Figure 9.9. The dotted lines show the upper limit on the mass splitting as a function of the dark matter mass assuming the Standard Halo Model. Under this common assumption, LUX-ZEPLIN is the most constraining experiment over the whole parameter space considered. However, when including the non-galactic components, different experiments contribute to set the upper limit, as reflected by the breaks in the solid lines in the Figure: LUX-ZEPLIN remains as the most sensitive experiment for small dark matter masses, while PICO-60 is the best experiment for larger masses. Further, the dark matter mass at which PICO-60 becomes the leading experiment becomes larger and larger as the dark matter hypercharge increases. As seen in the Figure, for this class of scenarios the non-galactic components in the dark matter flux enhance the sensitivity of experiments to the mass splitting by a factor ~ 2 for $m_{\rm DM} = 100$ GeV - 1 TeV.

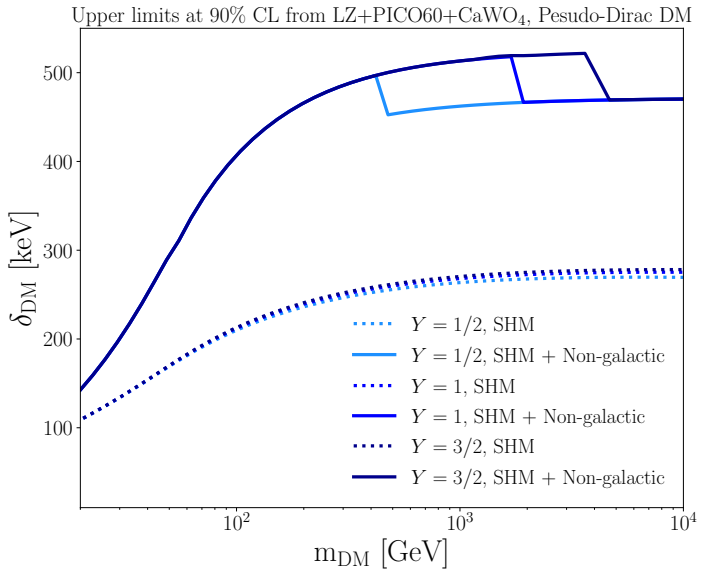

Figure 9.9: Upper limits on the mass splitting for electroweakly charged (pseudo-)dirac dark matter as a function of the dark matter mass, for different choices of the hypercharge, and including in the flux only the Standard Halo Model component (dotted lines) or also the non-galactic diffuse components (solid lines).

It is noteworthy the pivotal role of the radiopurity measurements on a $CaWO_4$ target to probe large mass splittings in inelastic dark matter scenarios. This can be understood from the expression for the minimum DM velocity required to induced a recoil with energy E_R, Eq. (9.37). Let us consider a velocity distribution where the maximum speed is v_*. Then, for an experiment capable of detecting a recoil of a nucleus A_i with energy E_R, the maximum mass splitting that can be probed is:

$$\delta_{\rm DM} \leq \sqrt{2E_R m_{A_i}}v_* - \frac{E_R m_{A_i}}{\mu_{A_i}} \leq \frac{1}{2}\mu_{A_i}v_*^2\,, \tag{9.44}$$

where the absolute maximum is reached when $E_R = \mu_{A_i}^2 v_*^2/(2m_{A_i})$. This is shown in Figure 9.10 for a ^{184}W target, and for $v_* = 764$ km/s, $v_* = 820$ km/s, $v_* = 1220$ km/s (solid lines), corresponding respectively to the maximal velocity at the Earth of dark matter particles bound to the Milky Way (described by the Standard Halo Model), from the Local Group envelope and from the Virgo Supercluster. The plot also shows the range of recoil energies that can be detected by the CRESST-II experiment and by the radiopurity measurements in $CaWO_4$ crystals. As seen in the plot, while CRESST-II can only probe up to $\delta_{\rm DM} \sim 700$ keV, the radiopurity measurements allow to probe up to $\delta_{\rm DM} \sim 1200$ keV, when including the flux component from the dark matter bound to the Virgo Supercluster (however with a lower sensitivity due to the smaller exposure). From this plot it follows that the CRESST experiment would have an enhanced sensitivity

to inelastic dark matter scenarios if the window of recoil energies used in the analysis were extended to larger values. Let us note that for low dark matter masses, extending the search window of a given experiment to higher recoil energies would not always help in probing larger values of the mass splitting. This is illustrated in the Figure for $m_{\rm DM} = 100$ GeV, from where it is apparent that in order to increase the reach in mass splittings it is necessary to extend the search of the radiopurity $CaWO_4$ measurement to lower recoil energies.

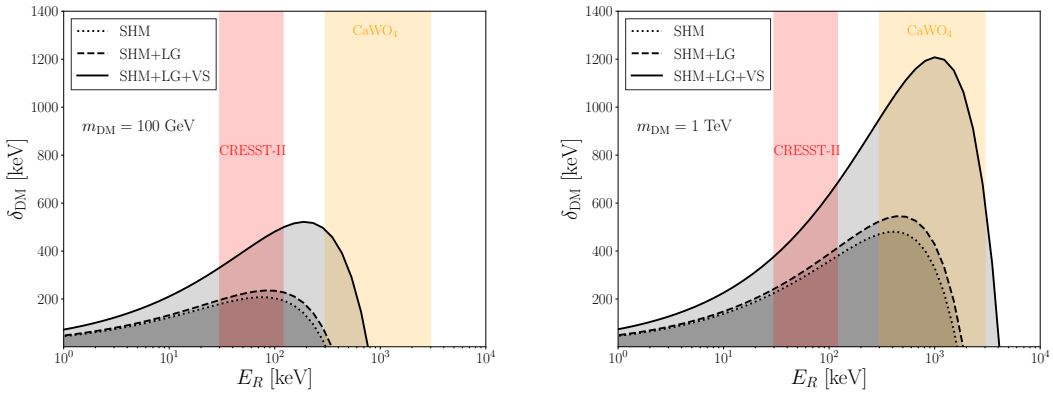

Figure 9.10: Values of the mass splitting $\delta_{\rm DM}$ that can produce a recoil energy in a ^{184}W target for $m_{\rm DM} = 100$ GeV (left plot) and $m_{\rm DM} = 1$ TeV (right plot) when the maximal velocity of the dark matter particles at Earth is $v_* = 764$ km/s (dotted lines), $v_* = 820$ km/s (dashed lines) and $v_* = 1220$ km/s (solid lines), corresponding respectively to dark matter bound to the Milky Way (described by the Standard Halo Model), bound to the Local Group and bound to the Virgo Supercluster. For comparison, we also show the range of recoil energies that can be detected by the CRESST-II experiment (red band) and by the $CaWO_4$ radiopurity measurement (yellow band).

Finally, we show in Figure 9.11 the isocontours with the 90% C.L. upper limits on the cross-section for different dark matter masses and mass splittings, from LUX-ZEPLIN (top panels), PICO60 (middle panels) and from radiopurity measurements on a $CaWO_4$ target (bottom panels), considering that all dark matter in the Solar System is bound to the Milky Way, as commonly assumed (left panels), and including the non-galactic components (right panels). The enhancement in sensitivity is clear from the plots. Further, one can appreciate in the figures a series of "breaks", that correspond to those regions in parameter space where the contribution to the scattering from the Local Group component starts to dominate over the SHM contribution, and to the regions where the contribution from the Virgo Supercluster component starts to dominate over the Local Group contribution. More concretely, if the mass difference is small, the SHM component generates the largest component to the signal rate. However, as the mass difference increases, dark matter particles bound to the Milky Way cannot induce a

visible scattering, whereas dark matter particles bound to the Local Group can, thus allowing to probe larger cross-sections (thus resulting in the "breaks" in the isocontours in the Figure for certain values of the dark matter mass). The same behaviour occurs for larger mass splittings, when dark matter particles from the Local Group cannot induce detectable recoils, while dark matter particles from the Virgo Supercluster can. Since the fraction of dark matter particles bound to the Virgo Supercluster is rather small, only $\sim 0.003\%$, the impact of this component is modest, except around the threshold.

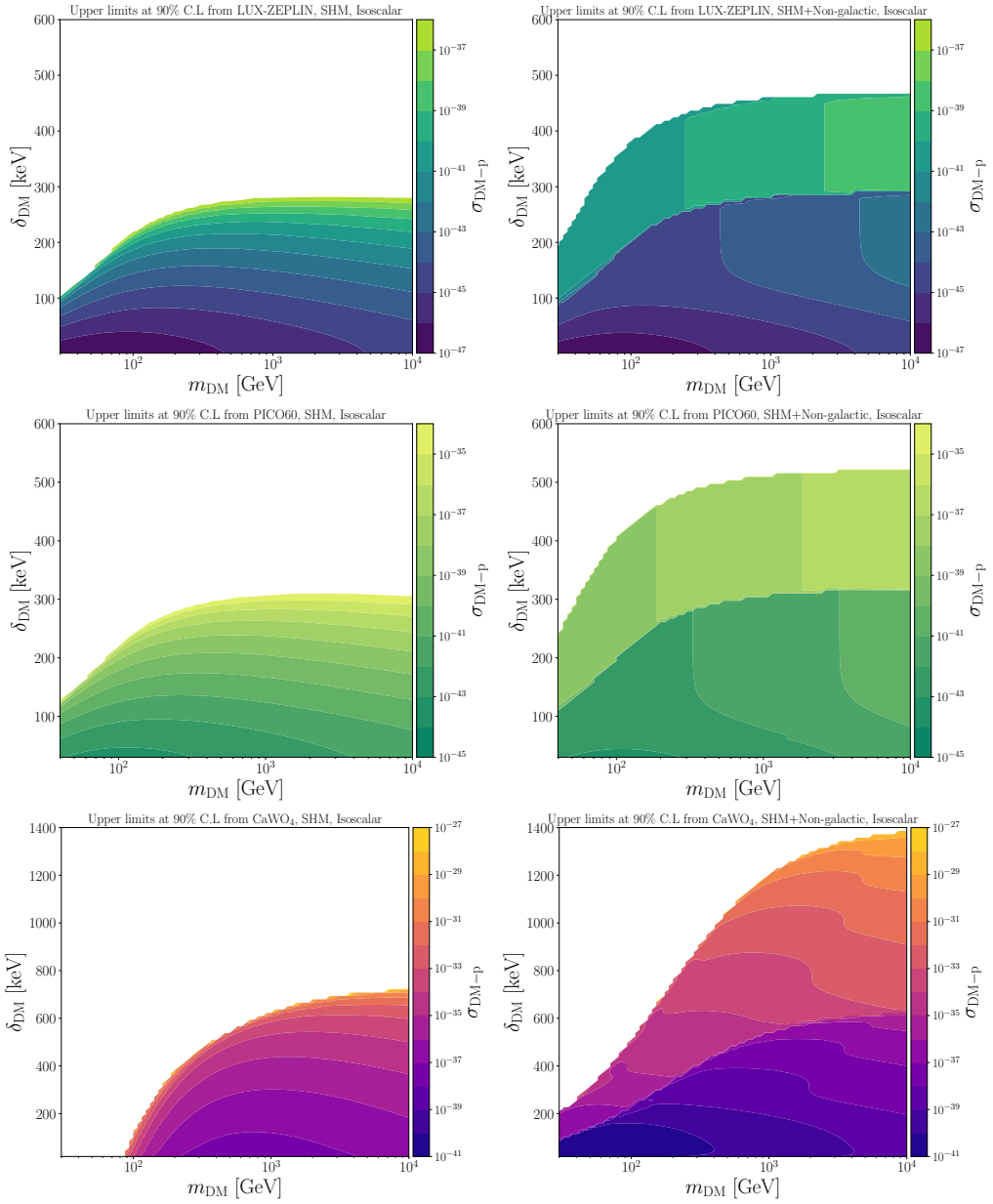

Figure 9.11: Isocontours of the 90% C.L. upper limits on the spin-independent dark matter-proton inelastic cross-section for the isoscalar scenario ($f^p = f^n$) in the parameter space spanned by the dark matter mass and mass splitting, from LUX-ZEPLIN (top panels), PICO60 (middle panels) and radiopurity measurements in a $CaWO_4$ target (lower panels), assuming that all dark matter in the Solar System is bound to the Milky Way (left panels) or including the non-galactic diffuse component (right panels).

The differential ionization rate induced by dark matter-electron inelastic scattering

in liquid xenon, with mass splitting between the two dark matter states given by $\delta_{\rm DM}$, reads:

$$\frac{dR_{\rm ion}}{d\ln E_{er}} = N_T \sum_{n,l} \int_{v \geq v^{nl}_{\rm min}(E_{er})} {\rm d}^3 v \mathscr{F}(\vec{v}+\vec{v}_\odot) \frac{{\rm d}\sigma^{nl}_{\rm ion}}{d\ln E_{er}}(v, E_{er})\,, \tag{9.45}$$

where N_T is the number of target nuclei and

$$v^{nl}_{\rm min}(E_{er}) = \sqrt{\frac{2}{m_{\rm DM}}(E_{er} + |E^{nl}| + \delta_{\rm DM})} \tag{9.46}$$

is the minimum dark matter velocity necessary to ionize a bound electron in the (n,l) shell of a xenon atom (with energy E^{nl}), giving a free electron with energy E_{er}. Further, $d\sigma^{nl}_{\rm ion}/d\ln E_{er}$ is the differential ionization cross section, given by:

$$\frac{d\sigma^{nl}_{\rm ion}}{d\ln E_{er}}(v, E_{er}) = \frac{\bar{\sigma}_{\rm DM-e}}{8\mu^2_{\rm DM,e} v^2} \int_{q^{nl}_{\rm min}}^{q^{nl}_{\rm max}} dq q \left| f^{nl}_{\rm ion}(k', q) \right|^2 |F_{\rm DM}(q)|^2\,. \tag{9.47}$$

Here, $\mu_{\rm DM,e}$ is the reduced mass of the dark matter-electron system, $\bar{\sigma}_{\rm DM-e}$ is the dark matter-free electron scattering cross section at fixed momentum transfer $q = \alpha m_e$, $\left| f^{nl}_{ion}(k', q) \right|^2$ is the ionization form factor of an electron in the (n,l) shell with final momentum $k' = \sqrt{2 m_e E_{er}}$ and momentum transfer q, and $F_{\rm DM}(q)$ is a form factor that encodes the q-dependence of the squared matrix element for dark matter-electron scattering and depends on the mediator under consideration. The maximum and minimum values of the momentum transfer needed to ionize a bound electron in the (n,l) shell recoil with energy E_{er} from the interaction of a dark matter particle with speed v are:

$$q^{nl}_{\rm max\atop min}(E_{er}) = m_{\rm DM} v \left[1 \pm \sqrt{1 - \left(\frac{v^{nl}_{\rm min}(E_{er})}{v} \right)^2} \right], \tag{9.48}$$

with $v^{nl}_{\rm min}(E_{er})$ defined in Eq. (9.46). Finally, the total number of expected ionization events reads $\mathcal{N} = R_{ion} \cdot \mathcal{E}$, with R_{ion} the total ionization rate, calculated from integrating Eq.(9.45) over the experimentally measured recoil energies, and $\mathcal{E}$ the exposure (*i.e.* mass multiplied by live-time) of the experiment.

In semiconductor detectors, the electron excitation rate induced by dark matter-electron inelastic scatterings, with a mass splitting $\delta_{\rm DM}$, reads [233, 234]

$$R = \frac{1}{\rho_T} \frac{\bar{\sigma}_{\rm DM-e}}{\mu^2_{\rm DM,e}} \frac{\pi}{\alpha} \int d^3 v \frac{\mathscr{F}(\vec{v}+\vec{v}_\odot)}{v} \int \frac{d^3 q}{(2\pi)^3} q^2 |F_{\rm DM}(q)|^2 \int \frac{d\omega}{2\pi} \frac{1}{1-e^{-\beta\omega}} {\rm Im}\left[\frac{-1}{\epsilon(\omega, \vec{q})} \right] \delta\left(\omega + \delta_{\rm DM} + \frac{q^2}{2m_\chi} - \vec{q}\cdot\vec{v} \right),$$

where w is the energy deposited in the material, $\vec{q}$ is the momentum transfer of the process, and ρ_T is the target density. The rate involves an integration of the Electronic Loss Function (ELF) of the target material, which we calculate with `DarkELF` [234]. For the dielectric function $\epsilon(\omega, \mathbf{q})$, we use the Lindhard method, which treats the target as a non-interacting Fermi liquid. Finally, the total number of events reads $\mathcal{N} = R \cdot \mathcal{E}$, with $\mathcal{E}$ the exposure (*i.e.* mass multiplied by live-time) of the experiment.

The non-observation of a significant excess of electron recoils in a given experiment allows to set upper limits on the dark matter-electron scattering cross section, for a given dark matter mass and a given mass splitting between the dark matter particle and the heavier neutral state. We show in Figure 9.12, upper limits on the inelastic dark matter-electron cross section versus mass splitting for a fixed dark matter mass of $m_{\rm DM} = 1$ GeV from XENON1T [555](blue lines), and from the semiconductor experiment SENSEI [489](purple lines), both when considering the SHM flux only (solid lines), and when including the non-galactic components to the dark matter flux (dotted lines). In the upper plots, we take the form factor $F_{\rm DM} = \alpha^2 m_e^2/q^2$, corresponding to an ultra-light or massless mediator. In the middle plots, we take the form factor $F_{\rm DM} = \alpha m_e/q$, corresponding to an electric dipole interaction, and in the lower plots we take the form factor $F_{\rm DM} = 1$, corresponding to a heavy mediator [238, 556].

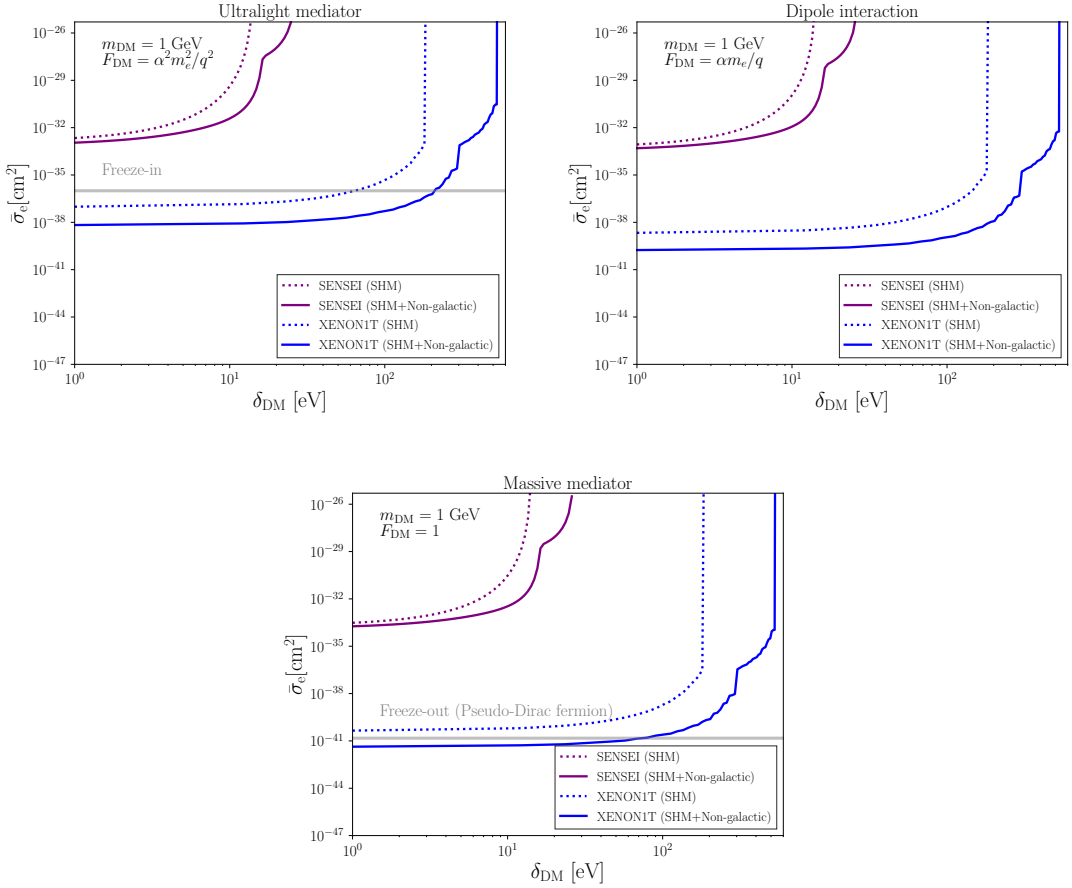

Figure 9.12: 90% C.L upper limits on the spin-independent dark matter-electron inelastic cross section for a dark matter mass of 1 GeV, as a function of the mass splitting, from XENON1T (blue) and SENSEI (purple), when the dark matter-electron interaction is mediated by an ultralight dark photon (upper left plot), by a dipole operator (upper right plot), or by a heavy mediator (lower plot).

As can be seen in the Figure, the non-galactic components enhance the sensitivity to the mass splitting of both XENON1T and SENSEI by a factor of ~ 2, compared to the sensitivity estimated from considering just the galactic component. This conclusion holds independently of the choice of the dark matter form factor. Further, the reach in cross-section is enhanced due to the non-galactic components, especially at low mass splittings, being the effect stronger for XENON1T than for SENSEI. For comparison, we also show as a grey band the cross section for which the observed dark matter abundance is reproduced via freeze-in in the case of an ultralight mediator [548], or via freeze-out in the case of a heavy mediator [127]. Clearly, the non-galactic dark matter components allow to probe larger values of the mass splitting. Finally, we also show in Figure 7 the

isocontours with the 90% C.L. upper limits on the dark matter-electron scattering cross-section for different dark matter masses and mass splittings, from SENSEI (upper panels) and XENON1T (lower panels), considering that all dark matter in the Solar System is bound to the Milky Way (left panels), and including the non-galactic components (right panels). The non-galactic components enhances the reach in mass splittings by a factor or $\sim$ 1.5 for SENSEI and $\sim$ 2.5 for XENON1T, allowing to probe lower dark matter masses and cross sections in both cases.

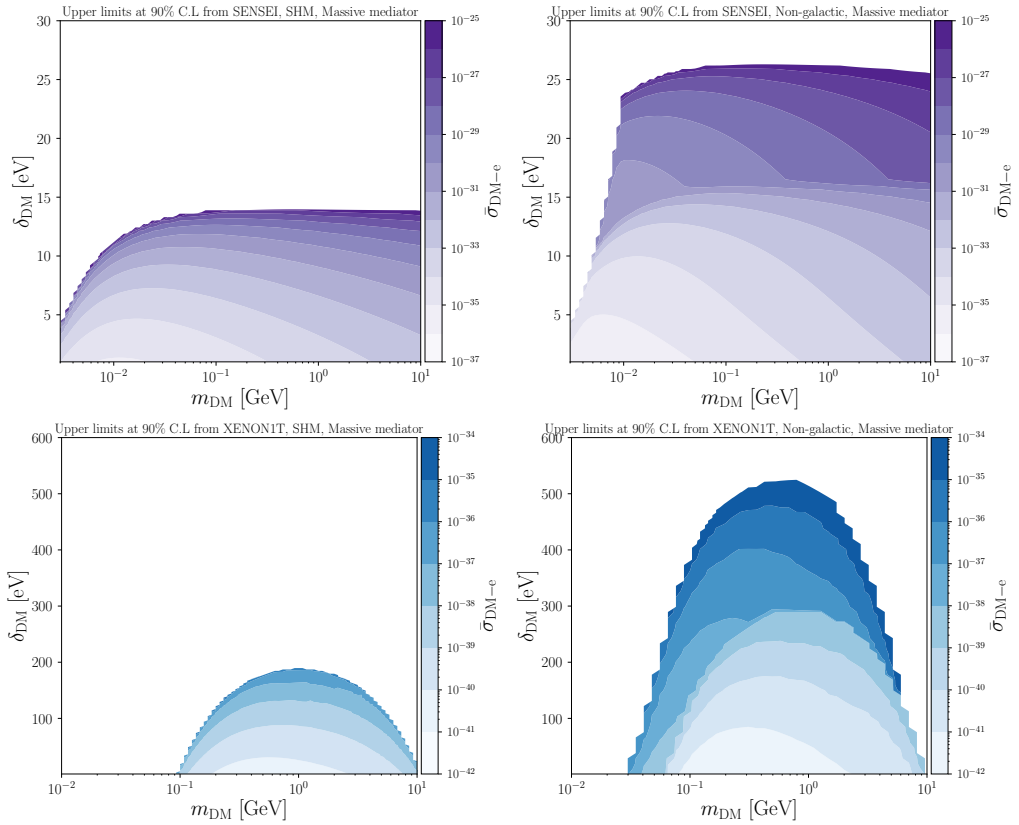

Figure 9.13: Isocontours of the 90% C.L. upper limits on the dark matter-electron inelastic scattering cross-section for the heavy mediator scenario ($F_{\rm DM} = 1$) in the parameter space spanned by the dark matter mass and mass splitting, from SENSEI (top panels), and XENON1T (lower panels), assuming that all dark matter in the Solar System is bound to the Milky Way (left panels) or including the non-galactic component diffuse (right panels).

We have investigated the impact of a non-galactic diffuse dark matter component inside the Solar System for the detection of the inelastic scattering of a dark matter particle in direct search experiments. Concretely, we have considered the contribution to the dark matter flux from dark matter particles in the envelope of the Local Group and from the Virgo Supercluster. Their speeds in the galactic frame are $\sim$ 600 km/s

and ~ 1000 km/s, respectively, which are larger than the maximal speed of dark matter particles bound to the Milky Way, ~ 540 km/s. As a result, the region of parameter space that can be probed with current experiments is larger than reported in previous works, that implicitly assumed that the Milky Way is an isolated galaxy in the Universe.

For nuclear recoils, the non-galactic component expands the reach in mass splitting at the LUX-ZEPLIN, PICO60, and CRESST-II experiments by a factor ~ 2 in the mass range $m_{\rm DM} = 10$ GeV- 10 TeV, and enhances significantly the reach in cross-section, especially close to the kinematic threshold for the galactic dark matter. For instance, for $m_{\rm DM} = 1$ TeV and $\delta_{\rm DM} = 250$ keV, the sensitivity to the cross-section improves by about three orders of magnitude. We have also stressed the relevance of experiments capable of detecting high recoil energies for probing the parameter space of inelastic dark matter scenarios. We have illustrated this capability with the radiopurity measurements in $CaWO_4$ crystals performed by the CRESST collaboration, and which allows to probe up to $\delta_{\rm DM} \sim 1.2$ MeV (1.4 MeV) for $m_{\rm DM} = 1$ TeV (10 TeV). For electron recoils, the conclusions are analogous, allowing to increase reach in mass splitting of the XENON1T and SENSEI experiments also by a factor ~ 2 for dark matter masses in the range $m_{\rm DM} = 0.01$ GeV-10 GeV.

Appendix A

Appendix

A.1 Discussion on the cascade equation

Dark matter-neutrino interactions may attenuate the neutrino flux reaching the Earth, and the attenuation is encoded in the cascade equation

$$\frac{d\Phi(E_\nu)}{d\tau} = -\sigma_{\nu\mathrm{DM}}(E_\nu)\Phi(E_\nu) + \int_{E_\nu}^{\infty} dE'_\nu \frac{d\sigma_{\nu\mathrm{DM}}}{dE_\nu}\left(E'_\nu \to E_\nu\right)\Phi\left(E'_\nu\right) \tag{A.1}$$

where E_ν is the neutrino energy, $\sigma(E_\nu)$ is the neutrino-DM total cross section for a neutrino with energy E_ν, $d\sigma(E'_\nu, E_\nu)/dE_\nu$ is the differential cross-section between energies $\tilde{E}$ and E and τ is the dark matter column density along the line of sight, where b and l are the galactic latitude and longitude respectively, r is the distance from which we calculate the column density along the line of sight and m_{DM} is the DM mass.

The integral part of the equation can be discretized by the Euler method, by choosing equal logarithmic intervals Δx with $x = \log_{10}(E/\mathrm{TeV})$ [502]. We define the dimensionless column density $y = (m_\chi/\Sigma_\chi)\tau$, and then the cascade equation is

$$\frac{d\Phi_i}{dy} = A\left(-\sigma(E_i)\Phi(E_i) \;+\; + \;\Delta x \ln 10 \sum_j^N \tilde{E}_j \frac{d\sigma(\tilde{E}_j, E)}{dE}\Phi(E_j)\right),$$

where $A = (\Sigma_{DM}/m_\chi)(1/E_0)$, $E_i = 10^{x_i}$ is the energy and $y \in [0, 1]$.

A simple benchmark example, that arises naturally in $U(1)$ extensions of the standard model, consists in a fermionic dark matter particle that interacts with neutrinos via a vector boson mediator. The lagrangian in this case reads [557]

$$\mathcal{L}_{\mathrm{int}} \supset -g_{\chi_\mathrm{L}}\overline{\chi_\mathrm{L}}\gamma^\mu Z'_\mu \chi_\mathrm{L} - g_{\chi_\mathrm{R}}\overline{\chi_\mathrm{R}}\gamma^\mu Z'_\mu \chi_\mathrm{R} - g_\nu \overline{\nu_L}\gamma^\mu Z'_\mu \nu_\mathrm{L}$$

where the first term represents the coupling of the of the dark matter fermion to the vector boson and the second term represents its coupling to neutrinos. The (Majorana) fermion dark matter-neutrino elastic scattering cross section reads.

$$\sigma^{\rm el}_{\chi\nu} = \frac{g_\chi^2 g_\nu^2}{16\pi E_\nu^2 m_\chi^2} \times \left[(2E_\nu m_\chi + m_{Z'}^2 + m_\chi^2) \log\left(\frac{m_{Z'}^2(2E_\nu + m_\chi)}{4E_\nu^2 m_\chi + 2E_\nu m_{Z'}^2 + m_\chi m_{Z'}^2} \right) + 4E_\nu^2 \left(1 + \frac{m_\chi^2}{m_{Z'}^2} - \frac{2E_\nu(4E_\nu^2 m_\chi + E_\nu(m_\chi^2 + 2m_{Z'}^2) + m_\chi m_{Z'}^2)}{(2E_\nu + m_\chi)(m_\chi(4E_\nu^2 + m_{Z'}^2) + 2E_\nu m_{Z'}^2)} \right) \right]. \tag{A.2}$$

The cross section dependence on the neutrino energy E_ν presents three distinct regimes. When $E_\nu \gg m_{Z'}^2/m_\chi$, the cross section approaches a constant value. Given that the galactic neutrino energies observed by IceCube are $E_\nu \gtrsim 1$ TeV, this regime applies for GeV-scale dark matter particles with mediator masses below $m_{Z'} \lesssim 1$ TeV, or for light dark matter particles with mediators at the GeV scale or lower. In these cases, since the cross section does not depend on the neutrino energy the neutrino fluxes are attenuated exponentially due to scatterings on dark matter particles in the dark matter halo. However, when $m_{Z'}^2 \gg m_\chi E_\nu$ (e.g. very light dark matter particles and heavy mediators), the cross section rises linearly with the neutrino energy. In this case, the attenuated fluxes are affected by a redistribution of neutrinos energies, depending on the differential scattering cross section of going from an initial neutrino energy E_ν to a final energy E'_ν. This differential cross section reads

$$\frac{d\sigma^{\rm el}_{\chi\nu}}{dE_\nu} = \frac{g_\nu^2 g_\chi^2 m_\chi (5E_\nu^2 + E_\nu(m_\chi - 4E'_\nu) + E'_\nu(E'_\nu - m_\chi))}{8\pi E_\nu^2 (2m_\chi(E'_\nu - E_\nu) + m_{Z'}^2)^2} \tag{A.3}$$

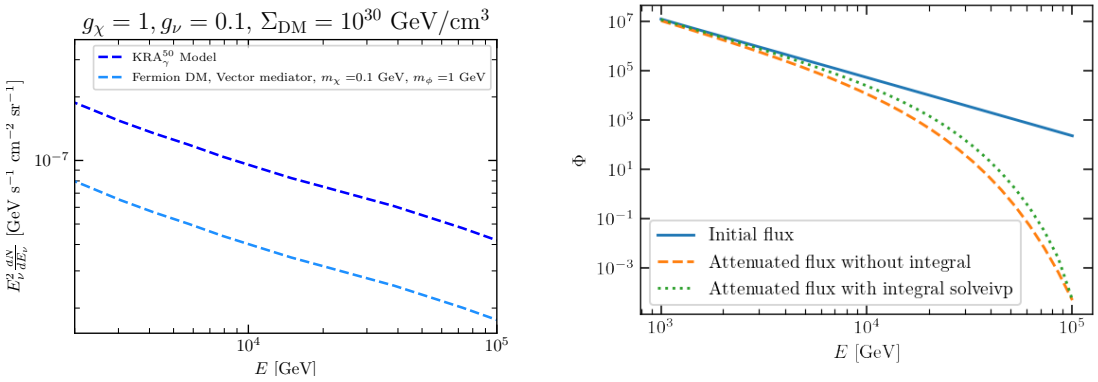

Figure A.1: Attenuated fluxes from solving the full Boltzmann equation.

In the Figure A.1 we calculate the attenuated fluxes using the full Boltzmann equation for the diffuse flux of galactic neutrinos using the KRA$^{50}_\gamma$ model, for fermionic dark matter and a vector mediator in a regime where the second term of the cascade equation play no role. On the right, we construct an idealized example with a lineraly dependent cross

section and choice of parameters where the second integral term is indeed sizable (green line vs orange line).

A.2 Details to calculate upper limits from direct detection experiments on the dark matter-nucleon and dark matter-electron cross section

In this appendix, we include details with our procedure to calculate upper limits on the scattering cross-section from the experimental data.

To derive upper limits on the SI and SD dark matter-nucleon cross section for CRESST-III [224], XENON1T [558] and PICO-60 [559], we follow a poissonian-likelihood approach and use the detector response functions given in the `DDCalc` package [560]. For CRESST-III, we use the published data [561] corresponding to an exposure of 5.594 kg×day, and we account for a finite energy resolution and cut-survival probability in the expected dark matter spectrum as described by the collaboration. All events in the acceptance region are considered signal events, which gives us a conservative 90% C.L upper limit of 873.9 events. For the XENON1T experiment, we use the data from [558] with an exposure of 35.6 tonnes×day. `DDCalc` divides the signal region into two energy bins, which correspond to [3,35] PE and [35,70] PE. The estimated background in both bins are 0.46 and 0.34 events, while the number of observed events are 0 and 2, respectively. The efficiencies were calculated simulating fluctuations of the S1 and S2 signal and using both scintillation and ionization yields. We consider a 90% C.L upper limit on the number of signal events of 3.9. Lastly, for the PICO-60 experiment, we use the results from [559], corresponding to an exposure of 1167 kg×day. Since PICO-60 observed no signal events, we take a 90% C.L. upper limit on the number of signal events of 2.3.

For the calculation of the ionization rate we follow [232] to model the conversion from the electron's recoiling energy E_{er} to the experimental observable at the XENON1T experiment, the number of photoelectrons (PE). The recoiling electron will ionize and excite other atoms, yielding Floor(E_{er}/W) primary quanta in form of observable electrons n_e and unobservable photons. We take the value of the average energy needed to produce a single quanta (photon or electron) to be W=13.8 eV. Further, we choose the probability for the initial electron to recombine with an ion to be zero and the fraction of primary quanta observed as electrons to be 0.83. A more refined modeling of the electron ionization and the associated uncertainties at XENON1T can be found in [548, 562].

We then calculate 90% C.L upper limits on the dark matter-electron scattering cross section at fixed momentum transfer $q = \alpha m_e$ using XENON10 and XENON100 data. The experiments report the number of photoelectrons (PE) produced by an event. To convert the n_e into PE, we assume that an event with n_e electrons produces a gaussian distributed number of PE with mean $n_e\mu$ and width $n_e\sigma$, where $\mu = 27(19.7)$ and $\sigma = 6.7(6.2)$ for XENON10 (XENON100). We consider the energy range in XENON10 going from 14 to 95 PE, corresponding up to $n_e = 3$. For XENON100, we consider the energy range going from 80 to 110 PE, corresponding to n_e=4 and n_e=5. We use

the binned 90% C.L. upper bounds on the event rate calculated in [548], obtained after multiplying the signal with the trigger and acceptance efficiencies. We notice that our limits for the SHM flux are more conservative than those of [548] . This is likely due to the fact that we are considering only the three outermost orbitals of xenon (5p, 5s and 4d), while the referenced work considers the orbitals 4s and 4p as well. Furthermore, the energy thresholds considered in this note for XENON10 and XENON100 are $n_e = 3$ and $n_e = 5$, while [548] considers n_e up to 6 in both cases. We consider the observed event rate for electrons in XENON1T between 150-3000 photoelectrons (PE), which corresponds to the range 0.18 keVee to 3.5 keVee (kiloelectronvolt electron equivalent). We take the efficiency function from [490], an exposure of 22 $\pm$ 3 tonne-days and an upper limit on the number of events of 39.2 For SENSEI, we sum-up the observed events in the energy bins ranging from 4.91 eV to 16.31 eV, resulting in an upper limit of 4.957 events per gram day of exposure. Further, we use the efficiency reported by the collaboration in every energy bin [489].

Bibliography

[1] Gianfranco Bertone and Dan Hooper. "History of dark matter". In: *Rev. Mod. Phys.* 90.4 (2018), p. 045002. DOI: 10.1103/RevModPhys.90.045002. arXiv: 1605.04909 [astro-ph.CO].

[2] Baron Kelvin William Thomson. "Baltimore lectures on molecular dynamics and the wave theory of light". In: (1904).

[3] Jaan Einasto. *Dark Matter*. 2010. arXiv: 0901.0632 [astro-ph.CO].

[4] F. Zwicky. "Die Rotverschiebung von extragalaktischen Nebeln". In: *Helv. Phys. Acta* 6 (1933), pp. 110–127. DOI: 10.1007/s10714-008-0707-4.

[5] F. Zwicky. "On the Masses of Nebulae and of Clusters of Nebulae". In: *Astrophys. J.* 86 (1937), pp. 217–246. DOI: 10.1086/143864.

[6] M. Schwarzschild. "Mass distribution and mass-luminosity ratio in galaxies". In: 59 (Sept. 1954), p. 273. DOI: 10.1086/107013.

[7] Sidney Van den Bergh. "Collapsed Objects in Clusters of Galaxies". In: 224.5222 (Nov. 1969), p. 891. DOI: 10.1038/224891a0.

[8] Vera C. Rubin and Jr. Ford W. Kent. "Rotation of the Andromeda Nebula from a Spectroscopic Survey of Emission Regions". In: 159 (Feb. 1970), p. 379. DOI: 10.1086/150317.

[9] Przemek Mró z et al. "Rotation Curve of the Milky Way from Classical Cepheids". In: *The Astrophysical Journal* 870.1 (Jan. 2019), p. L10. DOI: 10.3847/2041-8213/aaf73f. URL: https://doi.org/10.3847%2F2041-8213%2Faaf73f.

[10] Ramesh Narayan and Matthias Bartelmann. "Lectures on gravitational lensing". In: *13th Jerusalem Winter School in Theoretical Physics: Formation of Structure in the Universe*. June 1996. arXiv: astro-ph/9606001.

[11] Jose M. Diego et al. "Free Form Lensing Implications for the Collision of Dark Matter and Gas in the Frontier Fields Cluster MACSJ0416.1-2403". In: *Mon. Not. Roy. Astron. Soc.* 447 (2015), p. 3130. DOI: 10.1093/mnras/stu2660. arXiv: 1406.1217 [astro-ph.CO].

[12] H. Hildebrandt et al. "KiDS-450: Cosmological parameter constraints from tomographic weak gravitational lensing". In: *Mon. Not. Roy. Astron. Soc.* 465 (2017), p. 1454. DOI: 10.1093/mnras/stw2805. arXiv: 1606.05338 [astro-ph.CO].

[13] Douglas Clowe et al. "A direct empirical proof of the existence of dark matter". In: *Astrophys. J. Lett.* 648 (2006), pp. L109–L113. DOI: 10.1086/508162. arXiv: astro-ph/0608407.

[14] Pieter van Dokkum et al. "A galaxy lacking dark matter". In: *Nature* 555.7698 (Mar. 2018), pp. 629–632. DOI: 10.1038/nature25767. URL: https://doi.org/10.1038%2Fnature25767.

[15] M. Milgrom. "A modification of the Newtonian dynamics - Implications for galaxies." In: 270 (July 1983), pp. 371–383. DOI: 10.1086/161131.

[16] Pieter van Dokkum et al. "A trail of dark-matter-free galaxies from a bullet-dwarf collision". In: *Nature* 605.7910 (2022), pp. 435–439. DOI: 10.1038/s41586-022-04665-6. arXiv: 2205.08552 [astro-ph.GA].

[17] Edwin Hubble. "A Relation between Distance and Radial Velocity among Extra-Galactic Nebulae". In: *Proceedings of the National Academy of Science* 15.3 (Mar. 1929), pp. 168–173. DOI: 10.1073/pnas.15.3.168.

[18] Malcolm A. H. MacCallum. "Milestones of general relativity: Hubble's law (1929) and the expansion of the universe". In: *Class. Quant. Grav.* 32.12 (2015), p. 124002. DOI: 10.1088/0264-9381/32/12/124002. arXiv: 1504.03606 [physics.hist-ph].

[19] Adam G. Riess et al. "Observational evidence from supernovae for an accelerating universe and a cosmological constant". In: *Astron. J.* 116 (1998), pp. 1009–1038. DOI: 10.1086/300499. arXiv: astro-ph/9805201.

[20] S. Perlmutter et al. "Measurements of Ω and Λ from 42 high redshift supernovae". In: *Astrophys. J.* 517 (1999), pp. 565–586. DOI: 10.1086/307221. arXiv: astro-ph/9812133.

[21] Daniel Baumann. *Cosmology*. Cambridge University Press, July 2022. ISBN: 978-1-108-93709-2, 978-1-108-83807-8. DOI: 10.1017/9781108937092.

[22] N. Aghanim et al. "Planck 2018 results. VI. Cosmological parameters". In: *Astron. Astrophys.* 641 (2020). [Erratum: Astron.Astrophys. 652, C4 (2021)], A6. DOI: 10.1051/0004-6361/201833910. arXiv: 1807.06209 [astro-ph.CO].

[23] Daniel J. Eisenstein and Wayne Hu. "Baryonic features in the matter transfer function". In: *Astrophys. J.* 496 (1998), p. 605. DOI: 10.1086/305424. arXiv: astro-ph/9709112.

[24] Alan H. Guth. "Inflationary universe: A possible solution to the horizon and flatness problems". In: *Phys. Rev. D* 23 (2 Jan. 1981), pp. 347–356. DOI: 10.1103/PhysRevD.23.347. URL: https://link.aps.org/doi/10.1103/PhysRevD.23.347.

[25] R. K. Sachs and A. M. Wolfe. "Perturbations of a Cosmological Model and Angular Variations of the Microwave Background". In: 147 (Jan. 1967), p. 73. DOI: 10.1086/148982.

[26] R. A. Alpher, H. Bethe, and G. Gamow. "The Origin of Chemical Elements". In: *Phys. Rev.* 73 (7 Apr. 1948), pp. 803–804. DOI: 10.1103/PhysRev.73.803. URL: https://link.aps.org/doi/10.1103/PhysRev.73.803.

[27] Brian Fields and Subir Sarkar. "Big-Bang nucleosynthesis (2006 Particle Data Group mini-review)". In: (Jan. 2006). arXiv: astro-ph/0601514.

[28] Joshua Frieman, Michael Turner, and Dragan Huterer. "Dark Energy and the Accelerating Universe". In: *Ann. Rev. Astron. Astrophys.* 46 (2008), pp. 385–432. DOI: 10.1146/annurev.astro.46.060407.145243. arXiv: 0803.0982 [astro-ph].

[29] Y. Fukuda et al. "Evidence for oscillation of atmospheric neutrinos". In: *Phys. Rev. Lett.* 81 (1998), pp. 1562–1567. DOI: 10.1103/PhysRevLett.81.1562. arXiv: hep-ex/9807003.

[30] S. Gershtein and Y. a. Zeldovich. In: *JETP Lett* 4.120 (1966).

[31] R. Cowsik and J. McClelland. "An Upper Limit on the Neutrino Rest Mass". In: *Phys. Rev. Lett.* 29 (10 Sept. 1972), pp. 669–670. DOI: 10.1103/PhysRevLett.29.669. URL: https://link.aps.org/doi/10.1103/PhysRevLett.29.669.

[32] P. Hut. "Limits on masses and number of neutral weakly interacting particles". In: *Physics Letters B* 69.1 (1977), pp. 85–88. ISSN: 0370-2693. DOI: https://doi.org/10.1016/0370-2693(77)90139-3. URL: https://www.sciencedirect.com/science/article/pii/0370269377901393.

[33] Benjamin W. Lee and Robert E. Shrock. "Natural Suppression of Symmetry Violation in Gauge Theories: Muon - Lepton and Electron Lepton Number Nonconservation". In: *Phys. Rev. D* 16 (1977), p. 1444. DOI: 10.1103/PhysRevD.16.1444.

[34] J. E. Gunn et al. "Some astrophysical consequences of the existence of a heavy stable neutral lepton." In: 223 (Aug. 1978), pp. 1015–1031. DOI: 10.1086/156335.

[35] V.A. Lubimov et al. "An estimate of the e mass from the -spectrum of tritium in the valine molecule". In: *Physics Letters B* 94.2 (1980), pp. 266–268. ISSN: 0370-2693. DOI: https://doi.org/10.1016/0370-2693(80)90873-4. URL: https://www.sciencedirect.com/science/article/pii/0370269380908734.

[36] M. Aker et al. "Improved Upper Limit on the Neutrino Mass from a Direct Kinematic Method by KATRIN". In: *Phys. Rev. Lett.* 123.22 (2019), p. 221802. DOI: 10.1103/PhysRevLett.123.221802. arXiv: 1909.06048 [hep-ex].

[37] Edward W. Kolb and Michael S. Turner. *The Early Universe*. Vol. 69. 1990. ISBN: 978-0-201-62674-2. DOI: 10.1201/9780429492860.

[38] Julien Lesgourgues and Sergio Pastor. "Massive neutrinos and cosmology". In: *Phys. Rept.* 429 (2006), pp. 307–379. DOI: 10.1016/j.physrep.2006.04.001. arXiv: astro-ph/0603494.

[39] S. D. M. White, C. S. Frenk, and M. Davis. "Clustering in a neutrino-dominated universe". In: 274 (Nov. 1983), pp. L1–L5. DOI: 10.1086/184139.

[40] M. Davis et al. "A survey of galaxy redshifts. II. The large scale space distribution." In: 253 (Feb. 1982), pp. 423–445. DOI: 10.1086/159646.

[41] Scott Tremaine and James E. Gunn. "Dynamical Role of Light Neutral Leptons in Cosmology". In: *Phys. Rev. Lett.* 42 (6 Feb. 1979), pp. 407–410. DOI: 10.1103/PhysRevLett.42.407. URL: https://link.aps.org/doi/10.1103/PhysRevLett.42.407.

[42] Alexey Boyarsky, Oleg Ruchayskiy, and Dmytro Iakubovskyi. "A Lower bound on the mass of Dark Matter particles". In: *JCAP* 03 (2009), p. 005. DOI: 10.1088/1475-7516/2009/03/005. arXiv: 0808.3902 [hep-ph].

[43] Peter Minkowski. "$\mu \to e\gamma$ at a Rate of One Out of 10^9 Muon Decays?" In: *Phys. Lett. B* 67 (1977), pp. 421–428. DOI: 10.1016/0370-2693(77)90435-X.

[44] Rabindra N. Mohapatra and Goran Senjanovic. "Neutrino Mass and Spontaneous Parity Nonconservation". In: *Phys. Rev. Lett.* 44 (1980), p. 912. DOI: 10.1103/PhysRevLett.44.912.

[45] Tsutomu Yanagida. "Horizontal Symmetry and Masses of Neutrinos". In: *Prog. Theor. Phys.* 64 (1980), p. 1103. DOI: 10.1143/PTP.64.1103.

[46] Murray Gell-Mann, Pierre Ramond, and Richard Slansky. "Complex Spinors and Unified Theories". In: *Conf. Proc. C* 790927 (1979), pp. 315–321. arXiv: 1306.4669 [hep-th].

[47] J. Schechter and J. W. F. Valle. "Neutrino Masses in SU(2) x U(1) Theories". In: *Phys. Rev. D* 22 (1980), p. 2227. DOI: 10.1103/PhysRevD.22.2227.

[48] M. Drewes et al. "A White Paper on keV Sterile Neutrino Dark Matter". In: *JCAP* 01 (2017), p. 025. DOI: 10.1088/1475-7516/2017/01/025. arXiv: 1602.04816 [hep-ph].

[49] A. Boyarsky et al. "Sterile neutrino Dark Matter". In: *Prog. Part. Nucl. Phys.* 104 (2019), pp. 1–45. DOI: 10.1016/j.ppnp.2018.07.004. arXiv: 1807.07938 [hep-ph].

[50] Scott Dodelson and Lawrence M. Widrow. "Sterile-neutrinos as dark matter". In: *Phys. Rev. Lett.* 72 (1994), pp. 17–20. DOI: 10.1103/PhysRevLett.72.17. arXiv: hep-ph/9303287.

[51] Torsten Bringmann et al. "A new life for sterile neutrino dark matter after the pandemic". In: (June 2022). arXiv: 2206.10630 [hep-ph].

[52] M. B. Voloshin. "On Compatibility of Small Mass with Large Magnetic Moment of Neutrino". In: *Sov. J. Nucl. Phys.* 48 (1988), p. 512.

[53] K. S. Babu and R. N. Mohapatra. "Model for large transition magnetic moment of the electron neutrino". In: *Phys. Rev. Lett.* 63 (3 July 1989), pp. 228–231. DOI: 10.1103/PhysRevLett.63.228. URL: https://link.aps.org/doi/10.1103/PhysRevLett.63.228.

[54] K. S. Babu, Sudip Jana, and Manfred Lindner. "Large Neutrino Magnetic Moments in the Light of Recent Experiments". In: *JHEP* 10 (2020), p. 040. DOI: 10.1007/JHEP10(2020)040. arXiv: 2007.04291 [hep-ph].

[55] Palash B. Pal and Lincoln Wolfenstein. "Radiative decays of massive neutrinos". In: *Phys. Rev. D* 25 (3 Feb. 1982), pp. 766–773. DOI: 10.1103/PhysRevD.25.766. URL: https://link.aps.org/doi/10.1103/PhysRevD.25.766.

[56] Esra Bulbul et al. "Detection of An Unidentified Emission Line in the Stacked X-ray spectrum of Galaxy Clusters". In: *Astrophys. J.* 789 (2014), p. 13. DOI: 10.1088/0004-637X/789/1/13. arXiv: 1402.2301 [astro-ph.CO].

[57] A. Boyarsky et al. "Unidentified Line in X-Ray Spectra of the Andromeda Galaxy and Perseus Galaxy Cluster". In: *Physical Review Letters* 113.25 (Dec. 2014). ISSN: 1079-7114. DOI: 10.1103/physrevlett.113.251301. URL: http://dx.doi.org/10.1103/PhysRevLett.113.251301.

[58] Hiroyuki Ishida, Kwang Sik Jeong, and Fuminobu Takahashi. "7 keV sterile neutrino dark matter from split flavor mechanism". In: *Phys. Lett. B* 732 (2014), pp. 196–200. DOI: 10.1016/j.physletb.2014.03.044. arXiv: 1402.5837 [hep-ph].

[59] Shunsaku Horiuchi et al. "Sterile neutrino dark matter bounds from galaxies of the Local Group". In: *Phys. Rev. D* 89.2 (2014), p. 025017. DOI: 10.1103/PhysRevD.89.025017. arXiv: 1311.0282 [astro-ph.CO].

[60] Kevork N. Abazajian. "Sterile neutrinos in cosmology". In: *Phys. Rept.* 711-712 (2017), pp. 1–28. DOI: 10.1016/j.physrep.2017.10.003. arXiv: 1705.01837 [hep-ph].

[61] Christopher Dessert, Nicholas L. Rodd, and Benjamin R. Safdi. "The dark matter interpretation of the 3.5-keV line is inconsistent with blank-sky observations". In: *Science* 367.6485 (2020), pp. 1465–1467. DOI: 10.1126/science.aaw3772. arXiv: 1812.06976 [astro-ph.CO].

[62] Mikhail Shaposhnikov and Igor Tkachev. "The nuMSM, inflation, and dark matter". In: *Phys. Lett. B* 639 (2006), pp. 414–417. DOI: 10.1016/j.physletb.2006.06.063. arXiv: hep-ph/0604236.

[63] F. Bezrukov, H. Hettmansperger, and M. Lindner. "keV sterile neutrino Dark Matter in gauge extensions of the Standard Model". In: *Phys. Rev. D* 81 (2010), p. 085032. DOI: 10.1103/PhysRevD.81.085032. arXiv: 0912.4415 [hep-ph].

[64] André De Gouvêa et al. "Dodelson-Widrow Mechanism in the Presence of Self-Interacting Neutrinos". In: *Phys. Rev. Lett.* 124.8 (2020), p. 081802. DOI: 10.1103/PhysRevLett.124.081802. arXiv: 1910.04901 [hep-ph].

[65] Torsten Bringmann and Maxim Pospelov. "Novel Direct Detection Constraints on Light Dark Matter". In: *Physical Review Letters* 122.17 (May 2019). DOI: 10.1103/physrevlett.122.171801. URL: https://doi.org/10.1103%2Fphysrevlett.122.171801.

[66] Carlos Jaramillo. "Reviving keV sterile neutrino dark matter". In: *JCAP* 10 (2022), p. 093. DOI: 10.1088/1475-7516/2022/10/093. arXiv: 2207.11269 [hep-ph].

[67] Ian Holst et al. "Twin Sterile Neutrino Dark Matter". In: (May 2023). arXiv: 2305.06364 [hep-ph].

[68] R. D. Peccei and Helen R. Quinn. "CP Conservation in the Presence of Instantons". In: *Phys. Rev. Lett.* 38 (1977), pp. 1440–1443. DOI: 10.1103/PhysRevLett.38.1440.

[69] Frank Wilczek. "Problem of Strong P and T Invariance in the Presence of Instantons". In: *Phys. Rev. Lett.* 40 (1978), pp. 279–282. DOI: 10.1103/PhysRevLett.40.279.

[70] Steven Weinberg. "A New Light Boson?" In: *Phys. Rev. Lett.* 40 (1978), pp. 223–226. DOI: 10.1103/PhysRevLett.40.223.

[71] Minos Axenides, Robert H. Brandenberger, and Michael S. Turner. "Development of Axion Perturbations in an Axion Dominated Universe". In: *Phys. Lett. B* 126 (1983), pp. 178–182. DOI: 10.1016/0370-2693(83)90586-5.

[72] Ciaran O'Hare. *cajohare/AxionLimits: AxionLimits*. https://cajohare.github.io/AxionLimits/. Version v1.0. July 2020. DOI: 10.5281/zenodo.3932430.

[73] Paola Arias et al. "WISPy Cold Dark Matter". In: *JCAP* 06 (2012), p. 013. DOI: 10.1088/1475-7516/2012/06/013. arXiv: 1201.5902 [hep-ph].

[74] Raymond T. Co, Lawrence J. Hall, and Keisuke Harigaya. "Predictions for Axion Couplings from ALP Cogenesis". In: *JHEP* 01 (2021), p. 172. DOI: 10.1007/JHEP01(2021)172. arXiv: 2006.04809 [hep-ph].

[75] Ciaran A. J. O'Hare et al. "Simulations of axionlike particles in the postinflationary scenario". In: *Phys. Rev. D* 105.5 (2022), p. 055025. DOI: 10.1103/PhysRevD.105.055025. arXiv: 2112.05117 [hep-ph].

[76] Georg G. Raffelt. "Astrophysical axion bounds". In: *Lect. Notes Phys.* 741 (2008). Ed. by Markus Kuster, Georg Raffelt, and Berta Beltran, pp. 51–71. DOI: 10.1007/978-3-540-73518-2_3. arXiv: hep-ph/0611350.

[77] David J. E. Marsh. "Axion Cosmology". In: *Phys. Rept.* 643 (2016), pp. 1–79. DOI: 10.1016/j.physrep.2016.06.005. arXiv: 1510.07633 [astro-ph.CO].

[78] Peter W. Graham et al. "Experimental Searches for the Axion and Axion-Like Particles". In: *Ann. Rev. Nucl. Part. Sci.* 65 (2015), pp. 485–514. DOI: 10.1146/annurev-nucl-102014-022120. arXiv: 1602.00039 [hep-ex].

[79] John Preskill, Mark B. Wise, and Frank Wilczek. "Cosmology of the Invisible Axion". In: *Phys. Lett. B* 120 (1983). Ed. by M. A. Srednicki, pp. 127–132. DOI: 10.1016/0370-2693(83)90637-8.

[80] L. F. Abbott and P. Sikivie. "A Cosmological Bound on the Invisible Axion". In: *Phys. Lett. B* 120 (1983). Ed. by M. A. Srednicki, pp. 133–136. DOI: 10.1016/0370-2693(83)90638-X.

[81] Michael Dine and Willy Fischler. "The Not So Harmless Axion". In: *Phys. Lett. B* 120 (1983). Ed. by M. A. Srednicki, pp. 137–141. DOI: 10.1016/0370-2693(83)90639-1.

[82] T. W. B. Kibble. "Topology of Cosmic Domains and Strings". In: *J. Phys. A* 9 (1976), pp. 1387–1398. DOI: 10.1088/0305-4470/9/8/029.

[83] Heinz Pagels and Joel R. Primack. "Supersymmetry, Cosmology, and New Physics at Teraelectronvolt Energies". In: *Phys. Rev. Lett.* 48 (4 Jan. 1982), pp. 223–226. DOI: 10.1103/PhysRevLett.48.223. URL: https://link.aps.org/doi/10.1103/PhysRevLett.48.223.

[84] Savas Dimopoulos and Howard Georgi. "Softly Broken Supersymmetry and SU(5)". In: *Nucl. Phys. B* 193 (1981), pp. 150–162. DOI: 10.1016/0550-3213(81)90522-8.

[85] N. Cabibbo, G. R. Farrar, and L. Maiani. "Massive Photinos: Unstable and Interesting". In: *Phys. Lett. B* 105 (1981), pp. 155–158. DOI: 10.1016/0370-2693(81)91010-8.

[86] Steven Weinberg. "Upper Bound on Gauge Fermion Masses". In: *Phys. Rev. Lett.* 50 (1983), p. 387. DOI: 10.1103/PhysRevLett.50.387.

[87] H. Goldberg. "Constraint on the Photino Mass from Cosmology". In: *Phys. Rev. Lett.* 50 (19 May 1983), pp. 1419–1422. DOI: 10.1103/PhysRevLett.50.1419. URL: https://link.aps.org/doi/10.1103/PhysRevLett.50.1419.

[88] John R. Ellis et al. "Supersymmetric Relics from the Big Bang". In: *Nucl. Phys. B* 238 (1984). Ed. by M. A. Srednicki, pp. 453–476. DOI: 10.1016/0550-3213(84)90461-9.

[89] Mark W. Goodman and Edward Witten. "Detectability of Certain Dark Matter Candidates". In: *Phys. Rev. D* 31 (1985). Ed. by M. A. Srednicki, p. 3059. DOI: 10.1103/PhysRevD.31.3059.

[90] Joseph Silk and Mark Srednicki. "Cosmic Ray anti-Protons as a Probe of a Photino Dominated Universe". In: *Phys. Rev. Lett.* 53 (1984). Ed. by M. A. Srednicki, p. 624. DOI: 10.1103/PhysRevLett.53.624.

[91] Gianfranco Bertone, Dan Hooper, and Joseph Silk. "Particle dark matter: Evidence, candidates and constraints". In: *Phys. Rept.* 405 (2005), pp. 279–390. DOI: 10.1016/j.physrep.2004.08.031. arXiv: hep-ph/0404175.

[92] Paolo Gondolo and Graciela Gelmini. "Cosmic abundances of stable particles: Improved analysis". In: *Nucl. Phys. B* 360 (1991), pp. 145–179. DOI: 10.1016/0550-3213(91)90438-4.

[93] Leszek Roszkowski, Enrico Maria Sessolo, and Sebastian Trojanowski. "WIMP dark matter candidates and searches—current status and future prospects". In: *Rept. Prog. Phys.* 81.6 (2018), p. 066201. DOI: 10.1088/1361-6633/aab913. arXiv: 1707.06277 [hep-ph].

[94] Giorgio Arcadi et al. "The waning of the WIMP? A review of models, searches, and constraints". In: *Eur. Phys. J. C* 78.3 (2018), p. 203. DOI: 10.1140/epjc/s10052-018-5662-y. arXiv: 1703.07364 [hep-ph].

[95] Maria Eugenia Cabrera-Catalan et al. "Indirect and direct detection prospect for TeV dark matter in the nine parameter MSSM". In: *Phys. Rev. D* 92.3 (2015), p. 035018. DOI: 10.1103/PhysRevD.92.035018. arXiv: 1503.00599 [hep-ph].

[96] Gordon L. Kane et al. "Study of constrained minimal supersymmetry". In: *Phys. Rev. D* 49 (1994), pp. 6173–6210. DOI: 10.1103/PhysRevD.49.6173. arXiv: hep-ph/9312272.

[97] D. Matalliotakis and Hans Peter Nilles. "Implications of nonuniversality of soft terms in supersymmetric grand unified theories". In: *Nucl. Phys. B* 435 (1995), pp. 115–128. DOI: 10.1016/0550-3213(94)00487-Y. arXiv: hep-ph/9407251.

[98] Jonathan L. Feng and Jason Kumar. "The WIMPless Miracle: Dark-Matter Particles without Weak-Scale Masses or Weak Interactions". In: *Phys. Rev. Lett.* 101 (2008), p. 231301. DOI: 10.1103/PhysRevLett.101.231301. arXiv: 0803.4196 [hep-ph].

[99] Howard Baer et al. "Dark matter production in the early Universe: beyond the thermal WIMP paradigm". In: *Phys. Rept.* 555 (2015), pp. 1–60. DOI: 10.1016/j.physrep.2014.10.002. arXiv: 1407.0017 [hep-ph].

[100] Miguel Escudero et al. "Toward (Finally!) Ruling Out Z and Higgs Mediated Dark Matter Models". In: *JCAP* 12 (2016), p. 029. DOI: 10.1088/1475-7516/2016/12/029. arXiv: 1609.09079 [hep-ph].

[101] Rebecca K. Leane et al. "GeV-scale thermal WIMPs: Not even slightly ruled out". In: *Phys. Rev. D* 98.2 (2018), p. 023016. DOI: 10.1103/PhysRevD.98.023016. arXiv: 1805.10305 [hep-ph].

[102] Carlos Blanco et al. "Z' mediated WIMPs: dead, dying, or soon to be detected?" In: *JCAP* 11 (2019), p. 024. DOI: 10.1088/1475-7516/2019/11/024. arXiv: 1907.05893 [hep-ph].

[103] Jason Arakawa and Tim M. P. Tait. "Is a Miracle-less WIMP Ruled out?" In: *SciPost Phys.* 11.2 (2021), p. 019. DOI: 10.21468/SciPostPhys.11.2.019. arXiv: 2101.11031 [hep-ph].

[104] Salvatore Bottaro et al. "Closing the window on WIMP Dark Matter". In: *Eur. Phys. J. C* 82.1 (2022), p. 31. DOI: 10.1140/epjc/s10052-021-09917-9. arXiv: 2107.09688 [hep-ph].

[105] Anja Brenner et al. "Complementarity of experiments in probing the non-relativistic effective theory of dark matter-nucleon interactions". In: *JCAP* 06.06 (2022), p. 026. DOI: 10.1088/1475-7516/2022/06/026. arXiv: 2203.04210 [hep-ph].

[106] Gonzalo Herrera. "Halo-independent limits on the dark matter-nucleon interaction with the CRESST experiment". In: *Master Thesis, Munich, Tech. U.* (2020).

[107] C. P. Burgess, Maxim Pospelov, and Tonnis ter Veldhuis. "The Minimal model of nonbaryonic dark matter: A Singlet scalar". In: *Nucl. Phys. B* 619 (2001), pp. 709–728. DOI: 10.1016/S0550-3213(01)00513-2. arXiv: hep-ph/0011335.

[108] Laura Lopez Honorez et al. "The Inert Doublet Model: An Archetype for Dark Matter". In: *JCAP* 02 (2007), p. 028. DOI: 10.1088/1475-7516/2007/02/028. arXiv: hep-ph/0612275.

[109] Ernest Ma. "Verifiable radiative seesaw mechanism of neutrino mass and dark matter". In: *Phys. Rev. D* 73 (2006), p. 077301. DOI: 10.1103/PhysRevD.73.077301. arXiv: hep-ph/0601225.

[110] Mathias Garny, Alejandro Ibarra, and Stefan Vogl. "Signatures of Majorana dark matter with t-channel mediators". In: *Int. J. Mod. Phys. D* 24.07 (2015), p. 1530019. DOI: 10.1142/S0218271815300190. arXiv: 1503.01500 [hep-ph].

[111] Jose F. Nieves. "Electromagnetic Properties of Majorana Neutrinos". In: *Phys. Rev. D* 26 (1982), p. 3152. DOI: 10.1103/PhysRevD.26.3152.

[112] Natsumi Nagata and Satoshi Shirai. "Higgsino dark matter in high-scale supersymmetry". In: *Journal of High Energy Physics* 2015.1 (Jan. 2015). DOI: 10.1007/jhep01(2015)029. URL: https://doi.org/10.1007%2Fjhep01%282015%29029.

[113] Patrick J. Fox, Graham D. Kribs, and Adam Martin. "Split Dirac Supersymmetry: An Ultraviolet Completion of Higgsino Dark Matter". In: *Phys. Rev. D* 90.7 (2014), p. 075006. DOI: 10.1103/PhysRevD.90.075006. arXiv: 1405.3692 [hep-ph].

[114] Lawrence J. Hall, Takeo Moroi, and Hitoshi Murayama. "Sneutrino cold dark matter with lepton-number violation". In: *Physics Letters B* 424.3-4 (Apr. 1998), pp. 305–312. DOI: 10.1016/s0370-2693(98)00196-8. URL: https://doi.org/10.1016%2Fs0370-2693%2898%2900196-8.

[115] Nicole F. Bell, Giorgio Busoni, and Sandra Robles. "Heating up neutron stars with inelastic dark matter". In: *Journal of Cosmology and Astroparticle Physics* 2018.09 (Sept. 2018), pp. 018–018. DOI: 10.1088/1475-7516/2018/09/018. URL: https://doi.org/10.1088%2F1475-7516%2F2018%2F09%2F018.

[116] Anirban Biswas et al. "Improved White Dwarves Constraints on Inelastic Dark Matter and Left-Right Symmetric Models". In: (June 2022). arXiv: 2206.06667 [hep-ph].

[117] Motoko Fujiwara et al. "Capture of Electroweak Multiplet Dark Matter in Neutron Stars". In: (Apr. 2022). arXiv: 2204.02238 [hep-ph].

[118] Saniya Heeba, Tongyan Lin, and Katelin Schutz. "Inelastic Freeze-in". In: (Apr. 2023). arXiv: 2304.06072 [hep-ph].

[119] Gerardo Alvarez et al. "Heating neutron stars with inelastic dark matter and relativistic targets". In: *Phys. Rev. D* 107.10 (2023), p. 103024. DOI: 10.1103/PhysRevD.107.103024. arXiv: 2301.08767 [hep-ph].

[120] Daniele S.M. Alves et al. "Composite inelastic dark matter". In: *Physics Letters B* 692.5 (Sept. 2010), pp. 323–326. DOI: 10.1016/j.physletb.2010.08.006. URL: https://doi.org/10.1016%2Fj.physletb.2010.08.006.

[121] Thomas Schwetz and Jure Zupan. "Dark matter attempts for CoGeNT and DAMA". In: *Journal of Cosmology and Astroparticle Physics* 2011.08 (Aug. 2011), pp. 008–008. DOI: 10.1088/1475-7516/2011/08/008. URL: https://doi.org/10.1088%2F1475-7516%2F2011%2F08%2F008.

[122] Nima Arkani-Hamed et al. "A theory of dark matter". In: *Physical Review D* 79.1 (Jan. 2009). DOI: 10.1103/physrevd.79.015014. URL: https://doi.org/10.1103%2Fphysrevd.79.015014.

[123] Spencer Chang, Neal Weiner, and Itay Yavin. "Magnetic inelastic dark matter". In: *Physical Review D* 82.12 (Dec. 2010). DOI: 10.1103/physrevd.82.125011. URL: https://doi.org/10.1103%2Fphysrevd.82.125011.

[124] G. Barello, Spencer Chang, and Christopher A. Newby. "A model independent approach to inelastic dark matter scattering". In: *Physical Review D* 90.9 (Nov. 2014). DOI: 10.1103/physrevd.90.094027. URL: https://doi.org/10.1103%2Fphysrevd.90.094027.

[125] Natsumi Nagata and Satoshi Shirai. "Electroweakly interacting Dirac dark matter". In: *Physical Review D* 91.5 (Mar. 2015). DOI: 10.1103/physrevd.91.055035. URL: https://doi.org/10.1103%2Fphysrevd.91.055035.

[126] Timon Emken et al. "Electron recoils from terrestrial upscattering of inelastic dark matter". In: *Physical Review D* 105.5 (Mar. 2022). DOI: 10.1103/physrevd.105.055023. URL: https://doi.org/10.1103%2Fphysrevd.105.055023.

[127] Mariana Carrillo González and Natalia Toro. "Cosmology and signals of light pseudo-Dirac dark matter". In: *JHEP* 04 (2022), p. 060. DOI: 10.1007/JHEP04(2022)060. arXiv: 2108.13422 [hep-ph].

[128] Keisuke Harigaya, Yuichiro Nakai, and Motoo Suzuki. "Inelastic dark matter electron scattering and the XENON1T excess". In: *Physics Letters B* 809 (Oct. 2020), p. 135729. DOI: 10.1016/j.physletb.2020.135729. URL: https://doi.org/10.1016%2Fj.physletb.2020.135729.

[129] Jiwei Li et al. "Spin-dependent sub-GeV Inelastic Dark Matter-electron scattering and Migdal effect: (I). Velocity Independent Operator". In: (Oct. 2022). arXiv: 2210.15474 [hep-ph].

[130] Yuchao Gu, Lei Wu, and Bin Zhu. "Detection of Inelastic Dark Matter via Electron Recoils in SENSEI". In: (Mar. 2022). arXiv: 2203.06664 [hep-ph].

[131] Shiuli Chatterjee and Ranjan Laha. "Explorations of pseudo-Dirac dark matter having keV splittings and interacting via transition electric and magnetic dipole moments". In: *Phys. Rev. D* 107.8 (2023), p. 083036. DOI: 10.1103/PhysRevD.107.083036. arXiv: 2202.13339 [hep-ph].

[132] Anastasiia Filimonova et al. "Inelastic Dirac dark matter". In: *Journal of High Energy Physics* 2022.6 (June 2022). DOI: 10.1007/jhep06(2022)048. URL: https://doi.org/10.1007%2Fjhep06%282022%29048.

[133] David Smith and Neal Weiner. "Inelastic dark matter". In: *Physical Review D* 64.4 (July 2001). DOI: 10.1103/physrevd.64.043502. URL: https://doi.org/10.1103%2Fphysrevd.64.043502.

[134] Katsuhiko Sato and Makoto Kobayashi. "Cosmological Constraints on the Mass and the Number of Heavy Lepton Neutrinos". In: *Prog. Theor. Phys.* 58 (1977), p. 1775. DOI: 10.1143/PTP.58.1775.

[135] M. I. Vysotsky, A. D. Dolgov, and Ya. B. Zeldovich. "Cosmological Restriction on Neutral Lepton Masses". In: *JETP Lett.* 26 (1977). Ed. by M. A. Srednicki, pp. 188–190.

[136] Duane A. Dicus, Edward W. Kolb, and Vigdor L. Teplitz. "Cosmological Upper Bound on Heavy-Neutrino Lifetimes". In: *Phys. Rev. Lett.* 39 (4 July 1977), pp. 168–171. DOI: 10.1103/PhysRevLett.39.168. URL: https://link.aps.org/doi/10.1103/PhysRevLett.39.168.

[137] C. Boehm, T. A. Ensslin, and J. Silk. "Can Annihilating dark matter be lighter than a few GeVs?" In: *J. Phys. G* 30 (2004), pp. 279–286. DOI: 10.1088/0954-3899/30/3/004. arXiv: astro-ph/0208458.

[138] C. Boehm and Pierre Fayet. "Scalar dark matter candidates". In: *Nucl. Phys. B* 683 (2004), pp. 219–263. DOI: 10.1016/j.nuclphysb.2004.01.015. arXiv: hep-ph/0305261.

[139] Celine Boehm et al. "MeV dark matter: Has it been detected?" In: *Phys. Rev. Lett.* 92 (2004), p. 101301. DOI: 10.1103/PhysRevLett.92.101301. arXiv: astro-ph/0309686.

[140] Céline Boehm et al. "Scalar dark matter candidates revisited". In: *Phys. Rev. D* 103.7 (2021), p. 075005. DOI: 10.1103/PhysRevD.103.075005. arXiv: 2010.02954 [hep-ph].

[141] David E. Kaplan, Markus A. Luty, and Kathryn M. Zurek. "Asymmetric Dark Matter". In: *Phys. Rev. D* 79 (2009), p. 115016. DOI: 10.1103/PhysRevD.79.115016. arXiv: 0901.4117 [hep-ph].

[142] S. Nussinov. "TECHNOCOSMOLOGY: COULD A TECHNIBARYON EXCESS PROVIDE A 'NATURAL' MISSING MASS CANDIDATE?" In: *Phys. Lett. B* 165 (1985), pp. 55–58. DOI: 10.1016/0370-2693(85)90689-6.

[143] G. B. Gelmini, Lawrence J. Hall, and M. J. Lin. "What Is the Cosmion?" In: *Nucl. Phys. B* 281 (1987), p. 726. DOI: 10.1016/0550-3213(87)90424-X.

[144] Stephen M. Barr, R. Sekhar Chivukula, and Edward Farhi. "Electroweak Fermion Number Violation and the Production of Stable Particles in the Early Universe". In: *Phys. Lett. B* 241 (1990), pp. 387–391. DOI: 10.1016/0370-2693(90)91661-T.

[145] David B. Kaplan. "A Single explanation for both the baryon and dark matter densities". In: *Phys. Rev. Lett.* 68 (1992), pp. 741–743. DOI: 10.1103/PhysRevLett.68.741.

[146] Michael L. Graesser, Ian M. Shoemaker, and Luca Vecchi. "Asymmetric WIMP dark matter". In: *JHEP* 10 (2011), p. 110. DOI: 10.1007/JHEP10(2011)110. arXiv: 1103.2771 [hep-ph].

[147] Tongyan Lin, Hai-Bo Yu, and Kathryn M. Zurek. "On Symmetric and Asymmetric Light Dark Matter". In: *Phys. Rev. D* 85 (2012), p. 063503. DOI: 10.1103/PhysRevD.85.063503. arXiv: 1111.0293 [hep-ph].

[148] Mathew S. Madhavacheril, Neelima Sehgal, and Tracy R. Slatyer. "Current Dark Matter Annihilation Constraints from CMB and Low-Redshift Data". In: *Phys. Rev. D* 89 (2014), p. 103508. DOI: 10.1103/PhysRevD.89.103508. arXiv: 1310.3815 [astro-ph.CO].

[149] Rouven Essig et al. "Constraining Light Dark Matter with Diffuse X-Ray and Gamma-Ray Observations". In: *JHEP* 11 (2013), p. 193. DOI: 10.1007/JHEP11(2013)193. arXiv: 1309.4091 [hep-ph].

[150] Xiaoyong Chu, Thomas Hambye, and Michel H. G. Tytgat. "The Four Basic Ways of Creating Dark Matter Through a Portal". In: *JCAP* 05 (2012), p. 034. DOI: 10.1088/1475-7516/2012/05/034. arXiv: 1112.0493 [hep-ph].

[151] Yonit Hochberg et al. "Mechanism for Thermal Relic Dark Matter of Strongly Interacting Massive Particles". In: *Phys. Rev. Lett.* 113 (2014), p. 171301. DOI: 10.1103/PhysRevLett.113.171301. arXiv: 1402.5143 [hep-ph].

[152] Eric Kuflik et al. "Elastically Decoupling Dark Matter". In: *Phys. Rev. Lett.* 116.22 (2016), p. 221302. DOI: 10.1103/PhysRevLett.116.221302. arXiv: 1512.04545 [hep-ph].

[153] Yonit Hochberg et al. "Model for Thermal Relic Dark Matter of Strongly Interacting Massive Particles". In: *Phys. Rev. Lett.* 115.2 (2015), p. 021301. DOI: 10.1103/PhysRevLett.115.021301. arXiv: 1411.3727 [hep-ph].

[154] Lawrence J. Hall et al. "Freeze-In Production of FIMP Dark Matter". In: *JHEP* 03 (2010), p. 080. DOI: 10.1007/JHEP03(2010)080. arXiv: 0911.1120 [hep-ph].

[155] Prudhvi N. Bhattiprolu et al. "Freezing-in hadrophilic dark matter at low reheating temperatures". In: *JHEP* 01 (2023), p. 128. DOI: 10.1007/JHEP01(2023)128. arXiv: 2210.15653 [hep-ph].

[156] Gilly Elor, Robert McGehee, and Aaron Pierce. "Maximizing Direct Detection with Highly Interactive Particle Relic Dark Matter". In: *Phys. Rev. Lett.* 130.3 (2023), p. 031803. DOI: 10.1103/PhysRevLett.130.031803. arXiv: 2112.03920 [hep-ph].

[157] Sacha Davidson, Steen Hannestad, and Georg Raffelt. "Updated bounds on millicharged particles". In: *JHEP* 05 (2000), p. 003. DOI: 10.1088/1126-6708/2000/05/003. arXiv: hep-ph/0001179.

[158] Hongwan Liu et al. "Reviving Millicharged Dark Matter for 21-cm Cosmology". In: *Phys. Rev. D* 100.12 (2019), p. 123011. DOI: 10.1103/PhysRevD.100.123011. arXiv: 1908.06986 [hep-ph].

[159] Hendrik Vogel and Javier Redondo. "Dark Radiation constraints on minicharged particles in models with a hidden photon". In: *JCAP* 02 (2014), p. 029. DOI: 10.1088/1475-7516/2014/02/029. arXiv: 1311.2600 [hep-ph].

[160] Bob Holdom. "Two U(1)'s and Epsilon Charge Shifts". In: *Phys. Lett. B* 166 (1986), pp. 196–198. DOI: 10.1016/0370-2693(86)91377-8.

[161] Daniel Feldman, Zuowei Liu, and Pran Nath. "The Stueckelberg Z-prime Extension with Kinetic Mixing and Milli-Charged Dark Matter From the Hidden Sector". In: *Phys. Rev. D* 75 (2007), p. 115001. DOI: 10.1103/PhysRevD.75.115001. arXiv: hep-ph/0702123.

[162] Marco Fabbrichesi, Emidio Gabrielli, and Gaia Lanfranchi. "The Dark Photon". In: (May 2020). DOI: 10.1007/978-3-030-62519-1. arXiv: 2005.01515 [hep-ph].

[163] Martin Bauer and Patrick Foldenauer. "Consistent Theory of Kinetic Mixing and the Higgs Low-Energy Theorem". In: *Phys. Rev. Lett.* 129.17 (2022), p. 171801. DOI: 10.1103/PhysRevLett.129.171801. arXiv: 2207.00023 [hep-ph].

[164] Miguel Escudero et al. "Cosmology with A Very Light $L_\mu - L_\tau$ Gauge Boson". In: *JHEP* 03 (2019), p. 071. DOI: 10.1007/JHEP03(2019)071. arXiv: 1901.02010 [hep-ph].

[165] Admir Greljo et al. "Muonic force behind flavor anomalies". In: *JHEP* 04 (2022), p. 151. DOI: 10.1007/JHEP04(2022)151. arXiv: 2107.07518 [hep-ph].

[166] S. Dimopoulos, S. Raby, and Frank Wilczek. "Supersymmetry and the Scale of Unification". In: *Phys. Rev. D* 24 (1981), pp. 1681–1683. DOI: 10.1103/PhysRevD.24.1681.

[167] Ernest Ma and Jon Okada. "How Many Neutrinos?" In: *Phys. Rev. Lett.* 41 (1978). [Erratum: Phys.Rev.Lett. 41, 1759 (1978)], p. 287. DOI: 10.1103/PhysRevLett.41.287.

[168] Antonio Boveia and Caterina Doglioni. "Dark Matter Searches at Colliders". In: *Ann. Rev. Nucl. Part. Sci.* 68 (2018), pp. 429–459. DOI: 10.1146/annurev-nucl-101917-021008. arXiv: 1810.12238 [hep-ex].

[169] Felix Kahlhoefer. "Review of LHC Dark Matter Searches". In: *Int. J. Mod. Phys. A* 32.13 (2017), p. 1730006. DOI: 10.1142/S0217751X1730006X. arXiv: 1702.02430 [hep-ph].

[170] Jessica Goodman et al. "Constraints on Light Majorana dark Matter from Colliders". In: *Phys. Lett. B* 695 (2011), pp. 185–188. DOI: 10.1016/j.physletb.2010.11.009. arXiv: 1005.1286 [hep-ph].

[171] Yang Bai, Patrick J. Fox, and Roni Harnik. "The Tevatron at the Frontier of Dark Matter Direct Detection". In: *JHEP* 12 (2010), p. 048. DOI: 10.1007/JHEP12(2010)048. arXiv: 1005.3797 [hep-ph].

[172] Ian M. Shoemaker and Luca Vecchi. "Unitarity and Monojet Bounds on Models for DAMA, CoGeNT, and CRESST-II". In: *Phys. Rev. D* 86 (2012), p. 015023. DOI: 10.1103/PhysRevD.86.015023. arXiv: 1112.5457 [hep-ph].

[173] Giorgio Busoni et al. "On the Validity of the Effective Field Theory for Dark Matter Searches at the LHC". In: *Phys. Lett. B* 728 (2014), pp. 412–421. DOI: 10.1016/j.physletb.2013.11.069. arXiv: 1307.2253 [hep-ph].

[174] Fabiola Fortuna and Pablo Roig. "Impact of ATLAS constraints on effective dark matter-standard model interactions with spin-one mediators". In: *Phys. Rev. D* 107.7 (2023), p. 075003. DOI: 10.1103/PhysRevD.107.075003. arXiv: 2208.12330 [hep-ph].

[175] Anibal D. Medina et al. "Elusive muonic WIMP". In: *Phys. Rev. D* 106.7 (2022), p. 075018. DOI: 10.1103/PhysRevD.106.075018. arXiv: 2112.09103 [hep-ph].

[176] Torben Ferber, Alexander Grohsjean, and Felix Kahlhoefer. "Dark Higgs Bosons at Colliders". In: (May 2023). arXiv: 2305.16169 [hep-ph].

[177] Peter Athron et al. "Thermal WIMPs and the scale of new physics: global fits of Dirac dark matter effective field theories". In: *Eur. Phys. J. C* 81.11 (2021), p. 992. DOI: 10.1140/epjc/s10052-021-09712-6. arXiv: 2106.02056 [hep-ph].

[178] *Dark matter summary plots for s-channel, 2HDM+a, Higgs portal and Dark Higgs models*. Tech. rep. All figures including auxiliary figures are available at https://atlas.web.cern.ch/Atlas/GROUPS/PHYSICS/PUBNOTES/ATL-PHYS-PUB-2023-018. Geneva: CERN, 2023. URL: http://cds.cern.ch/record/2865335.

[179] Pierre Fayet. "U-boson production in e+ e- annihilations, psi and Upsilon decays, and Light Dark Matter". In: *Phys. Rev. D* 75 (2007), p. 115017. DOI: 10.1103/PhysRevD.75.115017. arXiv: hep-ph/0702176.

[180] Rouven Essig, Philip Schuster, and Natalia Toro. "Probing Dark Forces and Light Hidden Sectors at Low-Energy e+e- Colliders". In: *Phys. Rev. D* 80 (2009), p. 015003. DOI: 10.1103/PhysRevD.80.015003. arXiv: 0903.3941 [hep-ph].

[181] Michael Duerr et al. "Invisible and displaced dark matter signatures at Belle II". In: *JHEP* 02 (2020), p. 039. DOI: 10.1007/JHEP02(2020)039. arXiv: 1911.03176 [hep-ph].

[182] Michael Duerr et al. "Long-lived Dark Higgs and Inelastic Dark Matter at Belle II". In: *JHEP* 04 (2021), p. 146. DOI: 10.1007/JHEP04(2021)146. arXiv: 2012.08595 [hep-ph].

[183] Asher Berlin et al. "Sub-GeV dark matter production at fixed-target experiments". In: *Phys. Rev. D* 102.9 (2020), p. 095011. DOI: 10.1103/PhysRevD.102.095011. arXiv: 2003.03379 [hep-ph].

[184] Asli M. Abdullahi et al. "Semi-Visible Dark Photons below the Electroweak Scale". In: (Feb. 2023). arXiv: 2302.05410 [hep-ph].

[185] Matt Graham, Christopher Hearty, and Mike Williams. "Searches for Dark Photons at Accelerators". In: *Ann. Rev. Nucl. Part. Sci.* 71 (2021), pp. 37–58. DOI: 10.1146/annurev-nucl-110320-051823. arXiv: 2104.10280 [hep-ph].

[186] Rouven Essig et al. "Discovering New Light States at Neutrino Experiments". In: *Phys. Rev. D* 82 (2010), p. 113008. DOI: 10.1103/PhysRevD.82.113008. arXiv: 1008.0636 [hep-ph].

[187] Patrick deNiverville, Maxim Pospelov, and Adam Ritz. "Observing a light dark matter beam with neutrino experiments". In: *Phys. Rev. D* 84 (2011), p. 075020. DOI: 10.1103/PhysRevD.84.075020. arXiv: 1107.4580 [hep-ph].

[188] Pilar Coloma et al. "Dark matter beams at LBNF". In: *JHEP* 04 (2016), p. 047. DOI: 10.1007/JHEP04(2016)047. arXiv: 1512.03852 [hep-ph].

[189] Valentina De Romeri, Kevin J. Kelly, and Pedro A. N. Machado. "DUNE-PRISM Sensitivity to Light Dark Matter". In: *Phys. Rev. D* 100.9 (2019), p. 095010. DOI: 10.1103/PhysRevD.100.095010. arXiv: 1903.10505 [hep-ph].

[190] Andrea Celentano et al. "New production channels for light dark matter in hadronic showers". In: *Phys. Rev. D* 102.7 (2020), p. 075026. DOI: 10.1103/PhysRevD.102.075026. arXiv: 2006.09419 [hep-ph].

[191] Vedran Brdar et al. "Probing new physics at DUNE operating in a beam-dump mode". In: *Phys. Rev. D* 107.5 (2023), p. 055043. DOI: 10.1103/PhysRevD.107.055043. arXiv: 2206.06380 [hep-ph].

[192] Marco Costa, Rashmish K. Mishra, and Sonali Verma. "Model Agnostic Probes of Dark Sectors at Neutrino Experiments". In: (Nov. 2022). arXiv: 2211.13253 [hep-ph].

[193] A. Drukier and L. Stodolsky. "Principles and applications of a neutral-current detector for neutrino physics and astronomy". In: 30.11 (Dec. 1984), pp. 2295–2309. DOI: 10.1103/PhysRevD.30.2295.

[194] Ira Wasserman. "Possibility of detecting heavy neutral fermions in the Galaxy". In: 33.8 (Apr. 1986), pp. 2071–2078. DOI: 10.1103/PhysRevD.33.2071.

[195] S. P. Ahlen et al. "Limits on cold dark matter candidates from an ultralow background germanium spectrometer". In: *Physics Letters B* 195.4 (Sept. 1987), pp. 603–608. DOI: 10.1016/0370-2693(87)91581-4.

[196] David O. Caldwell et al. "Laboratory Limits on Galactic Cold Dark Matter". In: *Phys. Rev. Lett.* 61 (1988). Ed. by M. A. Srednicki, p. 510. DOI: 10.1103/PhysRevLett.61.510.

[197] E. Aprile et al. "Search for Coherent Elastic Scattering of Solar ^{8}B Neutrinos in the XENON1T Dark Matter Experiment". In: *Phys. Rev. Lett.* 126 (2021), p. 091301. DOI: 10.1103/PhysRevLett.126.091301. arXiv: 2012.02846 [hep-ex].

[198] Katarzyna Frankiewicz and for the Super-Kamiokande collaboration. "Dark matter searches with the Super-Kamiokande detector". In: *Journal of Physics: Conference Series* 888.1 (Sept. 2017), p. 012210. DOI: 10.1088/1742-6596/888/1/012210. URL: https://dx.doi.org/10.1088/1742-6596/888/1/012210.

[199] Andrzej K. Drukier, Katherine Freese, and David N. Spergel. "Detecting cold dark-matter candidates". In: 33.12 (June 1986), pp. 3495–3508. DOI: 10.1103/PhysRevD.33.3495.

[200] R. Bernabei et al. "Recent Results from DAMA/LIBRA and Comparisons". In: *Moscow Univ. Phys. Bull.* 77.2 (2022), pp. 291–300. DOI: 10.3103/S0027134922020138.

[201] E. Armengaud et al. "Searching for low-mass dark matter particles with a massive Ge bolometer operated above-ground". In: *Phys. Rev. D* 99.8 (2019), p. 082003. DOI: 10.1103/PhysRevD.99.082003. arXiv: 1901.03588 [astro-ph.GA].

[202] R. Agnese et al. "Results from the Super Cryogenic Dark Matter Search Experiment at Soudan". In: *Phys. Rev. Lett.* 120.6 (2018), p. 061802. DOI: 10.1103/PhysRevLett.120.061802. arXiv: 1708.08869 [hep-ex].

[203] E. Aprile et al. "First Dark Matter Search with Nuclear Recoils from the XENONnT Experiment". In: (Mar. 2023). arXiv: 2303.14729 [hep-ex].

[204] Yue Meng et al. "Dark Matter Search Results from the PandaX-4T Commissioning Run". In: *Phys. Rev. Lett.* 127.26 (2021), p. 261802. DOI: 10.1103/PhysRevLett.127.261802. arXiv: 2107.13438 [hep-ex].

[205] C. Amole et al. "Dark Matter Search Results from the Complete Exposure of the PICO-60 C_3F_8 Bubble Chamber". In: *Phys. Rev. D* 100.2 (2019), p. 022001. DOI: 10.1103/PhysRevD.100.022001. arXiv: 1902.04031 [astro-ph.CO].

[206] J. Billard, L. Strigari, and E. Figueroa-Feliciano. "Implication of neutrino backgrounds on the reach of next generation dark matter direct detection experiments". In: *Phys. Rev. D* 89.2 (2014), p. 023524. DOI: 10.1103/PhysRevD.89.023524. arXiv: 1307.5458 [hep-ph].

[207] J. Billard, L. E. Strigari, and E. Figueroa-Feliciano. "Solar neutrino physics with low-threshold dark matter detectors". In: *Phys. Rev. D* 91.9 (2015), p. 095023. DOI: 10.1103/PhysRevD.91.095023. arXiv: 1409.0050 [astro-ph.CO].

[208] R. Bernabei et al. "Searching for WIMPs by the annual modulation signature". In: *Physics Letters B* 424.1-2 (Apr. 1998), pp. 195–201. DOI: 10.1016/S0370-2693(98)00172-5.

[209] C. Savage et al. "Compatibility of DAMA/LIBRA dark matter detection with other searches". In: *JCAP* 0904 (2009), p. 010. DOI: 10.1088/1475-7516/2009/04/010. arXiv: 0808.3607 [astro-ph].

[210] Alejandro Ibarra, Bradley J. Kavanagh, and Andreas Rappelt. "Bracketing the impact of astrophysical uncertainties on local dark matter searches". In: *JCAP* 12 (2018), p. 018. DOI: 10.1088/1475-7516/2018/12/018. arXiv: 1806.08714 [hep-ph].

[211] Sunghyun Kang et al. "DAMA/LIBRA-phase2 in WIMP effective models". In: *JCAP* 07 (2018), p. 016. DOI: 10.1088/1475-7516/2018/07/016. arXiv: 1804.07528 [hep-ph].

[212] Sunniva Jacobsen et al. "Inelastic dark matter scattering off Thallium cannot save DAMA". In: *JCAP* 10 (2021), p. 070. DOI: 10.1088/1475-7516/2021/10/070. arXiv: 2102.08367 [hep-ph].

[213] Douglas Q. Adams, Sunniva Jacobsen, and Chris Kelso. "DAMA annual modulation is not due to electron recoils from plasma/mirror dark matter with kinetic mixing". In: *JCAP* 10 (2021), p. 060. DOI: 10.1088/1475-7516/2021/10/060. arXiv: 2011.03079 [hep-ph].

[214] J. Amare et al. "Annual modulation results from three-year exposure of ANAIS-112". In: *Phys. Rev. D* 103.10 (2021), p. 102005. DOI: 10.1103/PhysRevD.103.102005. arXiv: 2103.01175 [astro-ph.IM].

[215] Govinda Adhikari et al. "Strong constraints from COSINE-100 on the DAMA dark matter results using the same sodium iodide target". In: *Sci. Adv.* 7.46 (2021), abk2699. DOI: 10.1126/sciadv.abk2699. arXiv: 2104.03537 [hep-ex].

[216] J. Aalbers et al. "First Dark Matter Search Results from the LUX-ZEPLIN (LZ) Experiment". In: (July 2022). arXiv: 2207.03764 [hep-ex].

[217] J. I. Read. "The Local Dark Matter Density". In: *J. Phys. G* 41 (2014), p. 063101. DOI: 10.1088/0954-3899/41/6/063101. arXiv: 1404.1938 [astro-ph.GA].

[218] F. J. Kerr and Donald Lynden-Bell. "Review of galactic constants". In: *Mon. Not. Roy. Astron. Soc.* 221 (1986), p. 1023.

[219] Anne M. Green. "Astrophysical uncertainties on direct detection experiments". In: *Mod. Phys. Lett. A* 27 (2012), p. 1230004. DOI: 10.1142/S0217732312300042. arXiv: 1112.0524 [astro-ph.CO].

[220] Christopher McCabe. "The Earth's velocity for direct detection experiments". In: *JCAP* 02 (2014), p. 027. DOI: 10.1088/1475-7516/2014/02/027. arXiv: 1312.1355 [astro-ph.CO].

[221] Martin C. Smith et al. "The RAVE Survey: Constraining the Local Galactic Escape Speed". In: *Mon. Not. Roy. Astron. Soc.* 379 (2007), pp. 755–772. DOI: 10.1111/j.1365-2966.2007.11964.x. arXiv: astro-ph/0611671.

[222] Til Piffl et al. "The RAVE survey: the Galactic escape speed and the mass of the Milky Way". In: *Astron. Astrophys.* 562 (2014), A91. DOI: 10.1051/0004-6361/201322531. arXiv: 1309.4293 [astro-ph.GA].

[223] Francesco Iachello, Lawrence M. Krauss, and Giuseppe Maino. "Spin Dependent Scattering of Weakly Interacting Massive Particles in Heavy Nuclei". In: *Phys. Lett. B* 254 (1991), pp. 220–224. DOI: 10.1016/0370-2693(91)90424-O.

[224] A. H. Abdelhameed et al. "First results from the CRESST-III low-mass dark matter program". In: *Phys. Rev. D* 100.10 (2019), p. 102002. DOI: 10.1103/PhysRevD.100.102002. arXiv: 1904.00498 [astro-ph.CO].

[225] Matti Heikinheimo et al. "Identification of the low-energy excess in dark matter searches with crystal defects". In: *Phys. Rev. D* 106.8 (2022), p. 083009. DOI: 10.1103/PhysRevD.106.083009. arXiv: 2112.14495 [hep-ph].

[226] Prakruth Adari et al. "EXCESS workshop: Descriptions of rising low-energy spectra". In: *SciPost Phys. Proc.* 9 (2022). Ed. by A. Fuss et al., p. 001. DOI: 10.21468/SciPostPhysProc.9.001. arXiv: 2202.05097 [astro-ph.IM].

[227] Peter Abbamonte et al. "Revisiting the dark matter interpretation of excess rates in semiconductors". In: *Phys. Rev. D* 105.12 (2022), p. 123002. DOI: 10.1103/PhysRevD.105.123002. arXiv: 2202.03436 [hep-ph].

[228] G. Angloher et al. "Results on sub-GeV dark matter from a 10 eV threshold CRESST-III silicon detector". In: *Phys. Rev. D* 107.12 (2023), p. 122003. DOI: 10.1103/PhysRevD.107.122003. arXiv: 2212.12513 [astro-ph.CO].

[229] J. Aalbers et al. "First Dark Matter Search Results from the LUX-ZEPLIN (LZ) Experiment". In: (July 2022). arXiv: 2207.03764 [hep-ex].

[230] A Münster et al. "Radiopurity of CaWO4 crystals for direct dark matter search with CRESST and EURECA". In: 2014.05 (May 2014), pp. 018–018. DOI: 10.1088/1475-7516/2014/05/018. URL: https://doi.org/10.1088%2F1475-7516%2F2014%2F05%2F018.

[231] M. F. Albakry et al. "Search for low-mass dark matter via bremsstrahlung radiation and the Migdal effect in SuperCDMS". In: *Phys. Rev. D* 107.11 (2023), p. 112013. DOI: 10.1103/PhysRevD.107.112013. arXiv: 2302.09115 [hep-ex].

[232] Rouven Essig et al. "First Direct Detection Limits on sub-GeV Dark Matter from XENON10". In: *Phys. Rev. Lett.* 109 (2012), p. 021301. DOI: 10.1103/PhysRevLett.109.021301. arXiv: 1206.2644 [astro-ph.CO].

[233] Simon Knapen, Tongyan Lin, and Kathryn M. Zurek. "Light dark matter: Models and constraints". In: *Physical Review D* 96.11 (Dec. 2017). DOI: 10.1103/physrevd.96.115021. URL: https://doi.org/10.1103%2Fphysrevd.96.115021.

[234] Simon Knapen, Jonathan Kozaczuk, and Tongyan Lin. "python package for dark matter scattering in dielectric targets". In: *Physical Review D* 105.1 (Jan. 2022). DOI: 10.1103/physrevd.105.015014. URL: https://doi.org/10.1103%2Fphysrevd.105.015014.

[235] Liron Barak et al. "SENSEI: Direct-Detection Results on sub-GeV Dark Matter from a New Skipper-CCD". In: *Phys. Rev. Lett.* 125.17 (2020), p. 171802. DOI: 10.1103/PhysRevLett.125.171802. arXiv: 2004.11378 [astro-ph.CO].

[236] I. Arnquist et al. "First Constraints from DAMIC-M on Sub-GeV Dark-Matter Particles Interacting with Electrons". In: *Phys. Rev. Lett.* 130.17 (2023), p. 171003. DOI: 10.1103/PhysRevLett.130.171003. arXiv: 2302.02372 [hep-ex].

[237] E. Aprile et al. "Light Dark Matter Search with Ionization Signals in XENON1T". In: *Phys. Rev. Lett.* 123.25 (2019), p. 251801. DOI: 10.1103/PhysRevLett.123.251801. arXiv: 1907.11485 [hep-ex].

[238] Rouven Essig et al. "Snowmass2021 Cosmic Frontier: The landscape of low-threshold dark matter direct detection in the next decade". In: *2022 Snowmass Summer Study*. Mar. 2022. arXiv: 2203.08297 [hep-ph].

[239] Raffaele Tito D'Agnolo, Duccio Pappadopulo, and Joshua T. Ruderman. "Fourth Exception in the Calculation of Relic Abundances". In: *Phys. Rev. Lett.* 119.6 (2017), p. 061102. DOI: 10.1103/PhysRevLett.119.061102. arXiv: 1705.08450 [hep-ph].

[240] Jae Hyeok Chang, Rouven Essig, and Annika Reinert. "Light(ly)-coupled Dark Matter in the keV Range: Freeze-In and Constraints". In: *JHEP* 03 (2021), p. 141. DOI: 10.1007/JHEP03(2021)141. arXiv: 1911.03389 [hep-ph].

[241] Chris Kouvaris. "Probing Light Dark Matter via Evaporation from the Sun". In: *Phys. Rev. D* 92.7 (2015), p. 075001. DOI: 10.1103/PhysRevD.92.075001. arXiv: 1506.04316 [hep-ph].

[242] Yongsoo Jho et al. "Leptonic New Force and Cosmic-ray Boosted Dark Matter for the XENON1T Excess". In: *Phys. Lett. B* 811 (2020), p. 135863. DOI: 10.1016/j.physletb.2020.135863. arXiv: 2006.13910 [hep-ph].

[243] Jin-Wei Wang, Alessandro Granelli, and Piero Ullio. "Direct Detection Constraints on Blazar-Boosted Dark Matter". In: (Nov. 2021). arXiv: 2111.13644 [astro-ph.HE].

[244] Kaustubh Agashe et al. "(In)direct Detection of Boosted Dark Matter". In: *JCAP* 10 (2014), p. 062. DOI: 10.1088/1475-7516/2014/10/062. arXiv: 1405.7370 [hep-ph].

[245] Doojin Kim, Jong-Chul Park, and Seodong Shin. "Dark Matter "Collider" from Inelastic Boosted Dark Matter". In: *Phys. Rev. Lett.* 119.16 (2017), p. 161801. DOI: 10.1103/PhysRevLett.119.161801. arXiv: 1612.06867 [hep-ph].

[246] Anirban Das and Manibrata Sen. "Boosted dark matter from diffuse supernova neutrinos". In: *Phys. Rev. D* 104.7 (2021), p. 075029. DOI: 10.1103/PhysRevD.104.075029. arXiv: 2104.00027 [hep-ph].

[247] Wenyu Wang et al. "Spin-dependent scattering of boosted dark matter". In: *Phys. Rev. D* 107.7 (2023), p. 073002. DOI: 10.1103/PhysRevD.107.073002. arXiv: 2111.04000 [hep-ph].

[248] Timon Emken. "Solar reflection of light dark matter with heavy mediators". In: *Phys. Rev. D* 105.6 (2022), p. 063020. DOI: 10.1103/PhysRevD.105.063020. arXiv: 2102.12483 [hep-ph].

[249] Debjyoti Bardhan et al. "Bounds on boosted dark matter from direct detection: The role of energy-dependent cross sections". In: *Phys. Rev. D* 107.1 (2023), p. 015010. DOI: 10.1103/PhysRevD.107.015010. arXiv: 2208.09405 [hep-ph].

[250] Jinmian Li, Junle Pei, and Cong Zhang. "Investigating the collinear splitting effects of boosted dark matter at neutrino detectors". In: *JHEP* 02 (2023), p. 068. DOI: 10.1007/JHEP02(2023)068. arXiv: 2209.10816 [hep-ph].

[251] Michael Geller and Zamir Heller-Algazi. "Boosting asymmetric charged DM via thermalization". In: *JHEP* 03 (2023), p. 184. DOI: 10.1007/JHEP03(2023)184. arXiv: 2210.03126 [hep-ph].

[252] Torsten Bringmann and Maxim Pospelov. "Novel direct detection constraints on light dark matter". In: *Phys. Rev. Lett.* 122.17 (2019), p. 171801. DOI: 10.1103/PhysRevLett.122.171801. arXiv: 1810.10543 [hep-ph].

[253] Christopher V. Cappiello, Neal P. Avis Kozar, and Aaron C. Vincent. "Dark matter from Monogem". In: *Phys. Rev. D* 107.3 (2023), p. 035003. DOI: 10.1103/PhysRevD.107.035003. arXiv: 2210.09448 [hep-ph].

[254] Carlos A. Argüelles et al. "Hadrophilic light dark matter from the atmosphere". In: *Phys. Lett. B* 833 (2022), p. 137363. DOI: 10.1016/j.physletb.2022.137363. arXiv: 2203.12630 [hep-ph].

[255] Yen-Hsun Lin et al. "Searching for Afterglow: Light Dark Matter boosted by Supernova Neutrinos". In: (June 2022). arXiv: 2206.06864 [hep-ph].

[256] Tarak Nath Maity and Ranjan Laha. "Cosmic-ray boosted dark matter in Xe-based direct detection experiments". In: (Oct. 2022). arXiv: 2210.01815 [hep-ph].

[257] Yen-Hsun Lin et al. "Signatures of afterglows from light dark matter boosted by supernova neutrinos in current and future large underground detectors". In: (July 2023). arXiv: 2307.03522 [hep-ph].

[258] Yohei Ema, Filippo Sala, and Ryosuke Sato. "Light Dark Matter at Neutrino Experiments". In: *Phys. Rev. Lett.* 122.18 (2019), p. 181802. DOI: 10.1103/PhysRevLett.122.181802. arXiv: 1811.00520 [hep-ph].

[259] James Alvey et al. "Detecting Light Dark Matter via Inelastic Cosmic Ray Collisions". In: *Phys. Rev. Lett.* 123 (2019), p. 261802. DOI: 10.1103/PhysRevLett.123.261802. arXiv: 1905.05776 [hep-ph].

[260] Christopher V. Cappiello and John F. Beacom. "Strong New Limits on Light Dark Matter from Neutrino Experiments". In: *Phys. Rev. D* 100.10 (2019). [Erratum: Phys.Rev.D 104, 069901 (2021)], p. 103011. DOI: 10.1103/PhysRevD.104.069901. arXiv: 1906.11283 [hep-ph].

[261] James B. Dent et al. "Bounds on Cosmic Ray-Boosted Dark Matter in Simplified Models and its Corresponding Neutrino-Floor". In: *Phys. Rev. D* 101.11 (2020), p. 116007. DOI: 10.1103/PhysRevD.101.116007. arXiv: 1907.03782 [hep-ph].

[262] Wenyu Wang et al. "Cosmic ray boosted sub-GeV gravitationally interacting dark matter in direct detection". In: *JHEP* 12 (2020). [Erratum: JHEP 02, 052 (2021)], p. 072. DOI: 10.1007/JHEP12(2020)072. arXiv: 1912.09904 [hep-ph].

[263] Gang Guo, Yue-Lin Sming Tsai, and Meng-Ru Wu. "Probing cosmic-ray accelerated light dark matter with IceCube". In: *JCAP* 10 (2020), p. 049. DOI: 10.1088/1475-7516/2020/10/049. arXiv: 2004.03161 [astro-ph.HE].

[264] Shao-Feng Ge et al. "Diurnal Effect of Sub-GeV Dark Matter Boosted by Cosmic Rays". In: *Phys. Rev. Lett.* 126.9 (2021), p. 091804. DOI: 10.1103/PhysRevLett.126.091804. arXiv: 2005.09480 [hep-ph].

[265] F. W. Stecker. "The cosmic gamma -ray background from the annihilation of primordial stable neutral heavy leptons." In: 223 (Aug. 1978), pp. 1032–1036. DOI: 10.1086/156336.

[266] J. Silk and M. Srednicki. "Cosmic-Ray Antiprotons as a Probe of a Photino-Dominated Universe". In: 53.6 (Aug. 1984), pp. 624–627. DOI: 10.1103/PhysRevLett.53.624.

[267] L. M. Krauss et al. "Cold dark matter candidates and the solar neutrino problem". In: 299 (Dec. 1985), pp. 1001–1006. DOI: 10.1086/163767.

[268] Mario Mateo. "Dwarf galaxies of the Local Group". In: *Ann. Rev. Astron. Astrophys.* 36 (1998), pp. 435–506. DOI: 10.1146/annurev.astro.36.1.435. arXiv: astro-ph/9810070.

[269] M. Ackermann et al. "Searching for Dark Matter Annihilation from Milky Way Dwarf Spheroidal Galaxies with Six Years of Fermi Large Area Telescope Data". In: *Phys. Rev. Lett.* 115.23 (2015), p. 231301. DOI: 10.1103/PhysRevLett.115.231301. arXiv: 1503.02641 [astro-ph.HE].

[270] Tracy R. Slatyer. "Les Houches Lectures on Indirect Detection of Dark Matter". In: *SciPost Phys. Lect. Notes* 53 (2022), p. 1. DOI: 10.21468/SciPostPhysLectNotes.53. arXiv: 2109.02696 [hep-ph].

[271] Paolo Gondolo and Joseph Silk. "Dark Matter Annihilation at the Galactic Center". In: *Physical Review Letters* 83.9 (Aug. 1999), pp. 1719–1722. DOI: 10.1103/physrevlett.83.1719. URL: https://doi.org/10.1103%2Fphysrevlett.83.1719.

[272] Dan Hooper and Lisa Goodenough. "Dark Matter Annihilation in The Galactic Center As Seen by the Fermi Gamma Ray Space Telescope". In: *Phys. Lett. B* 697 (2011), pp. 412–428. DOI: 10.1016/j.physletb.2011.02.029. arXiv: 1010.2752 [hep-ph].

[273] Oscar Macias et al. "Improved Galactic diffuse emission model strengthens the case for a Millisecond Pulsar explanation of the Fermi GeV excess". In: *SciPost Phys. Proc.* 12 (2023), p. 049. DOI: 10.21468/SciPostPhysProc.12.049.

[274] Alexey Boyarsky, Denys Malyshev, and Oleg Ruchayskiy. "A comment on the emission from the Galactic Center as seen by the Fermi telescope". In: *Phys. Lett. B* 705 (2011), pp. 165–169. DOI: 10.1016/j.physletb.2011.10.014. arXiv: 1012.5839 [hep-ph].

[275] Kevork N. Abazajian. "The Consistency of Fermi-LAT Observations of the Galactic Center with a Millisecond Pulsar Population in the Central Stellar Cluster". In: *JCAP* 03 (2011), p. 010. DOI: 10.1088/1475-7516/2011/03/010. arXiv: 1011.4275 [astro-ph.HE].

[276] Francesca Calore, Ilias Cholis, and Christoph Weniger. "Background Model Systematics for the Fermi GeV Excess". In: *JCAP* 03 (2015), p. 038. DOI: 10.1088/1475-7516/2015/03/038. arXiv: 1409.0042 [astro-ph.CO].

[277] Tansu Daylan et al. "The characterization of the gamma-ray signal from the central Milky Way: A case for annihilating dark matter". In: *Phys. Dark Univ.* 12 (2016), pp. 1–23. DOI: 10.1016/j.dark.2015.12.005. arXiv: 1402.6703 [astro-ph.HE].

[278] Kevork N. Abazajian et al. "Astrophysical and Dark Matter Interpretations of Extended Gamma-Ray Emission from the Galactic Center". In: *Phys. Rev. D* 90.2 (2014), p. 023526. DOI: 10.1103/PhysRevD.90.023526. arXiv: 1402.4090 [astro-ph.HE].

[279] Samuel K. Lee et al. "Evidence for Unresolved γ-Ray Point Sources in the Inner Galaxy". In: *Phys. Rev. Lett.* 116.5 (2016), p. 051103. DOI: 10.1103/PhysRevLett.116.051103. arXiv: 1506.05124 [astro-ph.HE].

[280] Oscar Macias et al. "Galactic bulge preferred over dark matter for the Galactic centre gamma-ray excess". In: *Nature Astron.* 2.5 (2018), pp. 387–392. DOI: 10.1038/s41550-018-0414-3. arXiv: 1611.06644 [astro-ph.HE].

[281] Dan Hooper. "The status of the galactic center gamma-ray excess". In: *SciPost Phys. Proc.* 12 (2023), p. 006. DOI: 10.21468/SciPostPhysProc.12.006. arXiv: 2209.14370 [astro-ph.HE].

[282] Lisa Goodenough and Dan Hooper. "Possible Evidence For Dark Matter Annihilation In The Inner Milky Way From The Fermi Gamma Ray Space Telescope". In: (Oct. 2009). arXiv: 0910.2998 [hep-ph].

[283] Hasan Yuksel et al. "Neutrino Constraints on the Dark Matter Total Annihilation Cross Section". In: *Phys. Rev. D* 76 (2007), p. 123506. DOI: 10.1103/PhysRevD.76.123506. arXiv: 0707.0196 [astro-ph].

[284] Sergio Palomares-Ruiz and Silvia Pascoli. "Testing MeV dark matter with neutrino detectors". In: *Phys. Rev. D* 77 (2008), p. 025025. DOI: 10.1103/PhysRevD.77.025025. arXiv: 0710.5420 [astro-ph].

[285] Á Moliné, Alejandro Ibarra, and Sergio Palomares-Ruiz. "Future sensitivity of neutrino telescopes to dark matter annihilations from the cosmic diffuse neutrino signal". In: *JCAP* 06 (2015), p. 005. DOI: 10.1088/1475-7516/2015/06/005. arXiv: 1412.4308 [astro-ph.CO].

[286] Camilo Garcia-Cely and Julian Heeck. "Neutrino Lines from Majoron Dark Matter". In: *JHEP* 05 (2017), p. 102. DOI: 10.1007/JHEP05(2017)102. arXiv: 1701.07209 [hep-ph].

[287] Carlos A. Argüelles et al. "Dark matter annihilation to neutrinos". In: *Rev. Mod. Phys.* 93.3 (2021), p. 035007. DOI: 10.1103/RevModPhys.93.035007. arXiv: 1912.09486 [hep-ph].

[288] Rupert Coy and Thomas Hambye. "Neutrino lines from DM decay induced by high-scale seesaw interactions". In: *JHEP* 05 (2021), p. 101. DOI: 10.1007/JHEP05(2021)101. arXiv: 2012.05276 [hep-ph].

[289] Thomas Hambye, Marco Hufnagel, and Matteo Lucca. "Cosmological constraints on the decay of heavy relics into neutrinos". In: *JCAP* 05.05 (2022), p. 033. DOI: 10.1088/1475-7516/2022/05/033. arXiv: 2112.09137 [hep-ph].

[290] S. Basegmez Du Pree et al. "Robust Limits from Upcoming Neutrino Telescopes and Implications on Minimal Dark Matter Models". In: *JCAP* 05 (2021), p. 054. DOI: 10.1088/1475-7516/2021/05/054. arXiv: 2103.01237 [hep-ph].

[291] Mathieu Boudaud, Julien Lavalle, and Pierre Salati. "Novel cosmic-ray electron and positron constraints on MeV dark matter particles". In: *Phys. Rev. Lett.* 119.2 (2017), p. 021103. DOI: 10.1103/PhysRevLett.119.021103. arXiv: 1612.07698 [astro-ph.HE].

[292] Laura Lopez-Honorez et al. "Constraints on dark matter annihilation from CMB observationsbefore Planck". In: *JCAP* 07 (2013), p. 046. DOI: 10.1088/1475-7516/2013/07/046. arXiv: 1303.5094 [astro-ph.CO].

[293] Tracy R. Slatyer. "Indirect dark matter signatures in the cosmic dark ages. I. Generalizing the bound on s-wave dark matter annihilation from Planck results". In: *Phys. Rev. D* 93.2 (2016), p. 023527. DOI: 10.1103/PhysRevD.93.023527. arXiv: 1506.03811 [hep-ph].

[294] C. P. Liu et al. "Model-independent determination of the Migdal effect via photoabsorption". In: *Phys. Rev. D* 102.12 (2020), p. 121303. DOI: 10.1103/PhysRevD.102.121303. arXiv: 2007.10965 [hep-ph].

[295] R. Abbasi et al. "Search for GeV-scale dark matter annihilation in the Sun with IceCube DeepCore". In: *Phys. Rev. D* 105.6 (2022), p. 062004. DOI: 10.1103/PhysRevD.105.062004. arXiv: 2111.09970 [astro-ph.HE].

[296] Nicole F. Bell et al. "Improved Treatment of Dark Matter Capture in Neutron Stars II: Leptonic Targets". In: *JCAP* 03 (2021), p. 086. DOI: 10.1088/1475-7516/2021/03/086. arXiv: 2010.13257 [hep-ph].

[297] Gianfranco Bertone and Malcolm Fairbairn. "Compact Stars as Dark Matter Probes". In: *Phys. Rev. D* 77 (2008), p. 043515. DOI: 10.1103/PhysRevD.77.043515. arXiv: 0709.1485 [astro-ph].

[298] Chris Kouvaris. "WIMP Annihilation and Cooling of Neutron Stars". In: *Phys. Rev. D* 77 (2008), p. 023006. DOI: 10.1103/PhysRevD.77.023006. arXiv: 0708.2362 [astro-ph].

[299] Marina Cermeño, M. Ángeles Pérez-Garcıa, and Joseph Silk. "Light dark matter scattering in outer neutron star crusts". In: *Phys. Rev. D* 94.6 (2016), p. 063001. DOI: 10.1103/PhysRevD.94.063001. arXiv: 1607.06815 [astro-ph.HE].

[300] Masha Baryakhtar et al. "Dark Kinetic Heating of Neutron Stars and An Infrared Window On WIMPs, SIMPs, and Pure Higgsinos". In: *Phys. Rev. Lett.* 119.13 (2017), p. 131801. DOI: 10.1103/PhysRevLett.119.131801. arXiv: 1704.01577 [hep-ph].

[301] Nirmal Raj, Philip Tanedo, and Hai-Bo Yu. "Neutron stars at the dark matter direct detection frontier". In: *Phys. Rev. D* 97.4 (2018), p. 043006. DOI: 10.1103/PhysRevD.97.043006. arXiv: 1707.09442 [hep-ph].

[302] Raghuveer Garani, Yoann Genolini, and Thomas Hambye. "New Analysis of Neutron Star Constraints on Asymmetric Dark Matter". In: *JCAP* 05 (2019), p. 035. DOI: 10.1088/1475-7516/2019/05/035. arXiv: 1812.08773 [hep-ph].

[303] Chian-Shu Chen and Yen-Hsun Lin. "Reheating neutron stars with the annihilation of self-interacting dark matter". In: *JHEP* 08 (2018), p. 069. DOI: 10.1007/JHEP08(2018)069. arXiv: 1804.03409 [hep-ph].

[304] Joseph Bramante et al. "Terrestrial and Martian Heat Flow Limits on Dark Matter". In: *Phys. Rev. D* 101.4 (2020), p. 043001. DOI: 10.1103/PhysRevD.101.043001. arXiv: 1909.11683 [hep-ph].

[305] Daniel A. Camargo, Farinaldo S. Queiroz, and Riccardo Sturani. "Detecting Dark Matter with Neutron Star Spectroscopy". In: *JCAP* 09 (2019), p. 051. DOI: 10.1088/1475-7516/2019/09/051. arXiv: 1901.05474 [hep-ph].

[306] Matthew McCullough and Malcolm Fairbairn. "Capture of Inelastic Dark Matter in White Dwarves". In: *Phys. Rev. D* 81 (2010), p. 083520. DOI: 10.1103/PhysRevD.81.083520. arXiv: 1001.2737 [hep-ph].

[307] Rebecca K. Leane and Juri Smirnov. "Exoplanets as Sub-GeV Dark Matter Detectors". In: *Phys. Rev. Lett.* 126.16 (2021), p. 161101. DOI: 10.1103/PhysRevLett.126.161101. arXiv: 2010.00015 [hep-ph].

[308] Nicole F. Bell et al. "Improved treatment of dark matter capture in white dwarfs". In: *JCAP* 10 (2021), p. 083. DOI: 10.1088/1475-7516/2021/10/083. arXiv: 2104.14367 [hep-ph].

[309] Pooja Bhattacharjee, Francesca Calore, and Pasquale Dario Serpico. "Gamma-ray flux limits from brown dwarfs: Implications for dark matter annihilating into long-lived mediators". In: *Phys. Rev. D* 107.4 (2023), p. 043012. DOI: 10.1103/PhysRevD.107.043012. arXiv: 2211.08067 [astro-ph.HE].

[310] Rebecca K. Leane and Tim Linden. "First Analysis of Jupiter in Gamma Rays and a New Search for Dark Matter". In: (Apr. 2021). arXiv: 2104.02068 [astro-ph.HE].

[311] Rebecca K. Leane and Juri Smirnov. "Floating Dark Matter in Celestial Bodies". In: (Sept. 2022). arXiv: 2209.09834 [hep-ph].

[312] Raghuveer Garani, Nirmal Raj, and Javier Reynoso-Cordova. "Could compact stars in globular clusters constrain dark matter?" In: *JCAP* 07 (2023), p. 038. DOI: 10.1088/1475-7516/2023/07/038. arXiv: 2303.18009 [astro-ph.HE].

[313] Jaime Hoefken Zink and Maura E. Ramirez-Quezada. "Exploring the dark sectors via the cooling of white dwarfs". In: (June 2023). arXiv: 2306.00517 [hep-ph].

[314] Raghuveer Garani and Sergio Palomares-Ruiz. "Evaporation of dark matter from celestial bodies". In: *JCAP* 05.05 (2022), p. 042. DOI: 10.1088/1475-7516/2022/05/042. arXiv: 2104.12757 [hep-ph].

[315] Francesc Ferrer, Gonzalo Herrera, and Alejandro Ibarra. "New constraints on the dark matter-neutrino and dark matter-photon scattering cross sections from TXS 0506+056". In: (Sept. 2022). arXiv: 2209.06339 [hep-ph].

[316] Gonzalo Herrera and Kohta Murase. "Probing Light Dark Matter through Cosmic-Ray Cooling in Active Galactic Nuclei". In: (July 2023). arXiv: 2307.09460 [hep-ph].

[317] Edward Arthur Fath. "The spectra of some spiral nebulae and globular star clusters". In: *Lick Observatory Bulletin* 149 (Jan. 1909), pp. 71–77. DOI: 10.5479/ADS/bib/1909LicOB.5.71F.

[318] V. M. Slipher. "The spectrum and velocity of the nebula N.G.C. 1068 (M 77)". In: *Lowell Observatory Bulletin* 3 (Jan. 1917), pp. 59–62.

[319] Gregory A. Shields. "A brief history of agn". In: *Publ. Astron. Soc. Pac.* 111 (1999), p. 661. DOI: 10.1086/316378. arXiv: astro-ph/9903401.

[320] P. Padovani et al. "Active galactic nuclei: what's in a name?" In: *Astron. Astrophys. Rev.* 25.1 (2017), p. 2. DOI: 10.1007/s00159-017-0102-9. arXiv: 1707.07134 [astro-ph.GA].

[321] Carl K. Seyfert. "Nuclear Emission in Spiral Nebulae." In: 97 (Jan. 1943), p. 28. DOI: 10.1086/144488.

[322] M. Schmidt. "3C 273 : A Star-Like Object with Large Red-Shift". In: 197.4872 (Mar. 1963), p. 1040. DOI: 10.1038/1971040a0.

[323] ENRICO Fermi. "On the Origin of the Cosmic Radiation". In: *Phys. Rev.* 75 (8 Apr. 1949), pp. 1169–1174. DOI: 10.1103/PhysRev.75.1169. URL: https://link.aps.org/doi/10.1103/PhysRev.75.1169.

[324] G. F. Krymskii. "A regular mechanism for the acceleration of charged particles on the front of a shock wave". In: *Akademiia Nauk SSSR Doklady* 234 (June 1977), pp. 1306–1308.

[325] A. M. Hillas. "The Origin of Ultra-High-Energy Cosmic Rays". In: 22 (Jan. 1984), pp. 425–444. DOI: 10.1146/annurev.aa.22.090184.002233.

[326] Kseniya V. Ptitsyna and Sergei V. Troitsky. "Physical conditions in potential sources of ultra-high-energy cosmic rays. I. Updated Hillas plot and radiation-loss constraints". In: *Phys. Usp.* 53 (2010), pp. 691–701. DOI: 10.3367/UFNe.0180.201007c.0723. arXiv: 0808.0367 [astro-ph].

[327] M. G. Aartsen et al. "Astrophysical neutrinos and cosmic rays observed by IceCube". In: *Adv. Space Res.* 62 (2018), pp. 2902–2930. DOI: 10.1016/j.asr.2017.05.030. arXiv: 1701.03731 [astro-ph.HE].

[328] Kohta Murase. "Hidden Hearts of Neutrino Active Galaxies". In: (Nov. 2022). arXiv: 2211.04460 [astro-ph.HE].

[329] Yoshiyuki Inoue, Dmitry Khangulyan, and Akihiro Doi. "On the Origin of High-energy Neutrinos from NGC 1068: The Role of Nonthermal Coronal Activity". In: *Astrophys. J. Lett.* 891.2 (2020), p. L33. DOI: 10.3847/2041-8213/ab7661. arXiv: 1909.02239 [astro-ph.HE].

[330] Ali Kheirandish, Kohta Murase, and Shigeo S. Kimura. "High-energy Neutrinos from Magnetized Coronae of Active Galactic Nuclei and Prospects for Identification of Seyfert Galaxies and Quasars in Neutrino Telescopes". In: *Astrophys. J.* 922.1 (2021), p. 45. DOI: 10.3847/1538-4357/ac1c77. arXiv: 2102.04475 [astro-ph.HE].

[331] Shigeo S. Kimura et al. "Stochastic Particle Acceleration in Turbulence Generated by Magnetorotational Instability". In: *Astrophys. J.* 822.2 (2016), p. 88. DOI: 10.3847/0004-637X/822/2/88. arXiv: 1602.07773 [astro-ph.HE].

[332] Charles D. Dermer, James A. Miller, and Hui Li. "Stochastic particle acceleration near accreting black holes". In: *Astrophys. J.* 456 (1996), p. 106. DOI: 10.1086/176631. arXiv: astro-ph/9508069.

[333] Kohta Murase, Shigeo S. Kimura, and Peter Meszaros. "Hidden Cores of Active Galactic Nuclei as the Origin of Medium-Energy Neutrinos: Critical Tests with the MeV Gamma-Ray Connection". In: *Phys. Rev. Lett.* 125.1 (2020), p. 011101. DOI: 10.1103/PhysRevLett.125.011101. arXiv: 1904.04226 [astro-ph.HE].

[334] Bin Chen et al. "Particle Acceleration by a Solar Flare Termination Shock". In: *Science* 350 (2015), p. 1238. DOI: 10.1126/science.aac8467. arXiv: 1512.02237 [astro-ph.SR].

[335] Zuowei Liu et al. "A combined analysis of PandaX, LUX, and XENON1T experiments within the framework of dark matter effective theory". In: *JHEP* 11 (2017), p. 024. DOI: 10.1007/JHEP11(2017)024. arXiv: 1708.04630 [hep-ph].

[336] F. W. Stecker et al. "High-energy neutrinos from active galactic nuclei". In: *Phys. Rev. Lett.* 66 (1991). [Erratum: Phys.Rev.Lett. 69, 2738 (1992)], pp. 2697–2700. DOI: 10.1103/PhysRevLett.66.2697.

[337] Susumu Inoue et al. "High-energy neutrinos and gamma rays from winds and tori in active galactic nuclei". In: (July 2022). arXiv: 2207.02097 [astro-ph.HE].

[338] A. Lamastra et al. "Galactic outflow driven by the active nucleus and the origin of the gamma-ray emission in NGC 1068". In: *Astron. Astrophys.* 596 (2016), A68. DOI: 10.1051/0004-6361/201628667. arXiv: 1609.09664 [astro-ph.HE].

[339] V. S. Berezinskii et al. *Astrophysics of cosmic rays*. 1990.

[340] Thomas K. Gaisser, Ralph Engel, and Elisa Resconi. *Cosmic Rays and Particle Physics*. 2nd ed. Cambridge University Press, 2016. DOI: 10.1017/CBO9781139192194.

[341] Talvikki Hovatta and Elina Lindfors. "Relativistic Jets of Blazars". In: *New Astron. Rev.* 87 (2019), p. 101541. DOI: 10.1016/j.newar.2020.101541. arXiv: 2003.06322 [astro-ph.HE].

[342] Foteini Oikonomou et al. "High energy neutrino flux from individual blazar flares". In: *Mon. Not. Roy. Astron. Soc.* 489.3 (2019), pp. 4347–4366. DOI: 10.1093/mnras/stz2246. arXiv: 1906.05302 [astro-ph.HE].

[343] Foteini Oikonomou et al. "Multi-messenger emission from the parsec-scale jet of the flat-spectrum radio quasar coincident with high-energy neutrino IceCube-190730A". In: *JCAP* 10 (2021), p. 082. DOI: 10.1088/1475-7516/2021/10/082. arXiv: 2107.11437 [astro-ph.HE].

[344] Maria Petropoulou et al. "Comprehensive Multimessenger Modeling of the Extreme Blazar 3HSP J095507.9+355101 and Predictions for IceCube". In: *Astrophys. J.* 899.2 (2020), p. 113. DOI: 10.3847/1538-4357/aba8a0. arXiv: 2005.07218 [astro-ph.HE].

[345] Mark Aartsen et al. "Neutrino emission from the direction of the blazar TXS 0506056 prior to the IceCube-170922A alert". In: *Science* 361.6398 (July 2018), pp. 147–151. DOI: 10.1126/science.aat2890. URL: https://doi.org/10.1126%2Fscience.aat2890.

[346] Yasuyuki T. Tanaka, Sara Buson, and Daniel Kocevski. "Fermi-LAT detection of increased gamma-ray activity of TXS 0506+056, located inside the IceCube-170922A error region." In: *The Astronomer's Telegram* 10791 (Sept. 2017), p. 1.

[347] M. G. Aartsen et al. "Multimessenger observations of a flaring blazar coincident with high-energy neutrino IceCube-170922A". In: *Science* 361.6398 (2018), eaat1378. DOI: 10.1126/science.aat1378. arXiv: 1807.08816 [astro-ph.HE].

[348] Foteini Oikonomou. "High-energy neutrino emission from blazars". In: *PoS* ICRC2021 (2022), p. 030. DOI: 10.22323/1.395.0030. arXiv: 2201.05623 [astro-ph.HE].

[349] B. Theodore Zhang et al. "A Neutral Beam Model for High-Energy Neutrino Emission from the Blazar TXS 0506+056". In: *Astrophys. J.* 889 (2020), p. 118. DOI: 10.3847/1538-4357/ab659a. arXiv: 1910.11464 [astro-ph.HE].

[350] R. Abbasi et al. "Evidence for neutrino emission from the nearby active galaxy NGC 1068". In: *Science* 378.6619 (2022), pp. 538–543. DOI: 10.1126/science.abg3395. arXiv: 2211.09972 [astro-ph.HE].

[351] V. A. Acciari et al. "Constraints on gamma-ray and neutrino emission from NGC 1068 with the MAGIC telescopes". In: *Astrophys. J.* 883 (2019), p. 135. DOI: 10.3847/1538-4357/ab3a51. arXiv: 1906.10954 [astro-ph.HE].

[352] S. Abdollahi and and. "iFermi/i Large Area Telescope Fourth Source Catalog". In: *The Astrophysical Journal Supplement Series* 247.1 (Mar. 2020), p. 33. DOI: 10.3847/1538-4365/ab6bcb. URL: https://doi.org/10.3847%2F1538-4365%2Fab6bcb.

[353] V. S. Berezinsky and A. Yu. Smirnov. "Cosmic neutrinos of ultra-high energies and detection possibility". In: *Astrophys. Space Sci.* 32 (1975), pp. 461–482. DOI: 10.1007/BF00643157.

[354] Kohta Murase, Dafne Guetta, and Markus Ahlers. "Hidden Cosmic-Ray Accelerators as an Origin of TeV-PeV Cosmic Neutrinos". In: *Physical Review Letters* 116.7 (Feb. 2016). DOI: 10.1103/physrevlett.116.071101. URL: https://doi.org/10.1103%2Fphysrevlett.116.071101.

[355] Yoshiyuki Inoue, Dmitry Khangulyan, and Akihiro Doi. "On the Origin of High-energy Neutrinos from NGC 1068: The Role of Nonthermal Coronal Activity". In: *The Astrophysical Journal* 891.2 (Mar. 2020), p. L33. DOI: 10.3847/2041-8213/ab7661. URL: https://doi.org/10.3847%2F2041-8213%2Fab7661.

[356] Björn Eichmann et al. "Solving the Multimessenger Puzzle of the AGN-starburst Composite Galaxy NGC 1068". In: *The Astrophysical Journal* 939.1 (Nov. 2022), p. 43. DOI: 10.3847/1538-4357/ac9588. URL: https://doi.org/10.3847%2F1538-4357%2Fac9588.

[357] J. G. Hills. "Possible power source of Seyfert galaxies and QSOs". In: 254.5498 (Mar. 1975), pp. 295–298. DOI: 10.1038/254295a0.

[358] Martin J. Rees. "Tidal disruption of stars by black holes of 10 to the 6th-10 to the 8th solar masses in nearby galaxies". In: *Nature* 333 (1988), pp. 523–528. DOI: 10.1038/333523a0.

[359] S. Komossa. "Tidal disruption of stars by supermassive black holes: Status of observations". In: *JHEAp* 7 (2015), pp. 148–157. DOI: 10.1016/j.jheap.2015.04.006. arXiv: 1505.01093 [astro-ph.HE].

[360] Glennys R. Farrar and Tsvi Piran. "Tidal disruption jets as the source of Ultra-High Energy Cosmic Rays". In: (Nov. 2014). arXiv: 1411.0704 [astro-ph.HE].

[361] Daniel N. Pfeffer, Ely D. Kovetz, and Marc Kamionkowski. "Ultrahigh-energy cosmic ray hotspots from tidal disruption events". In: *Mon. Not. Roy. Astron. Soc.* 466.3 (2017), pp. 2922–2926. DOI: 10.1093/mnras/stw3337. arXiv: 1512.04959 [astro-ph.HE].

[362] Xiang-Yu Wang et al. "Probing the tidal disruption flares of massive black holes with high-energy neutrinos". In: *Physical Review D* 84.8 (Oct. 2011). DOI: 10.1103/physrevd.84.081301. URL: https://doi.org/10.1103%2Fphysrevd.84.081301.

[363] Cecilia Lunardini and Walter Winter. "High Energy Neutrinos from the Tidal Disruption of Stars". In: *Phys. Rev. D* 95.12 (2017), p. 123001. DOI: 10.1103/PhysRevD.95.123001. arXiv: 1612.03160 [astro-ph.HE].

[364] Robert Stein et al. "A tidal disruption event coincident with a high-energy neutrino". In: *Nature Astron.* 5.5 (2021), pp. 510–518. DOI: 10.1038/s41550-020-01295-8. arXiv: 2005.05340 [astro-ph.HE].

[365] Simeon Reusch et al. "Candidate Tidal Disruption Event AT2019fdr Coincident with a High-Energy Neutrino". In: *Phys. Rev. Lett.* 128.22 (2022), p. 221101. DOI: 10.1103/PhysRevLett.128.221101. arXiv: 2111.09390 [astro-ph.HE].

[366] S. van Velzen et al. "Establishing accretion flares from massive black holes as a major source of high-energy neutrinos". In: (Nov. 2021). arXiv: 2111.09391 [astro-ph.HE].

[367] Walter Winter and Cecilia Lunardini. "Interpretation of the Observed Neutrino Emission from Three Tidal Disruption Events". In: *Astrophys. J.* 948.1 (2023), p. 42. DOI: 10.3847/1538-4357/acbe9e. arXiv: 2205.11538 [astro-ph.HE].

[368] J. A. Peacock. *Cosmological Physics*. Cambridge University Press, 1998. DOI: 10.1017/CBO9780511804533.

[369] P. Meszaros. "The behaviour of point masses in an expanding cosmological substratum." In: 37.2 (Dec. 1974), pp. 225–228.

[370] Max Tegmark et al. "The 3-D power spectrum of galaxies from the SDSS". In: *Astrophys. J.* 606 (2004), pp. 702–740. DOI: 10.1086/382125. arXiv: astro-ph/0310725.

[371] Ivo Labbé et al. "A population of red candidate massive galaxies ~600 Myr after the Big Bang". In: *Nature* 616.7956 (Feb. 2023), pp. 266–269. DOI: 10.1038/s41586-023-05786-2. URL: https://doi.org/10.1038%2Fs41586-023-05786-2.

[372] Michael Boylan-Kolchin. "Stress testing ΛCDM with high-redshift galaxy candidates". In: *Nature Astron.* 7.6 (2023), pp. 731–735. DOI: 10.1038/s41550-023-01937-7. arXiv: 2208.01611 [astro-ph.CO].

[373] Julio F. Navarro, Carlos S. Frenk, and Simon D. M. White. "The Structure of cold dark matter halos". In: *Astrophys. J.* 462 (1996), pp. 563–575. DOI: 10.1086/177173. arXiv: astro-ph/9508025.

[374] Julio F. Navarro, Carlos S. Frenk, and Simon D. M. White. "A Universal density profile from hierarchical clustering". In: *Astrophys. J.* 490 (1997), pp. 493–508. DOI: 10.1086/304888. arXiv: astro-ph/9611107.

[375] J. Einasto. "On the Construction of a Composite Model for the Galaxy and on the Determination of the System of Galactic Parameters". In: *Trudy Astrofizicheskogo Instituta Alma-Ata* 5 (Jan. 1965), pp. 87–100.

[376] Alister W. Graham et al. "Empirical models for Dark Matter Halos. I. Nonparametric Construction of Density Profiles and Comparison with Parametric Models". In: *Astron. J.* 132 (2006), pp. 2685–2700. DOI: 10.1086/508988. arXiv: astro-ph/0509417.

[377] Ben Moore. "Evidence against dissipation-less dark matter from observations of galaxy haloes". In: 370.6491 (Aug. 1994), pp. 629–631. DOI: 10.1038/370629a0.

[378] W. J. G. de Blok. "The Core-Cusp Problem". In: *Advances in Astronomy* 2010 (2010), pp. 1–14. DOI: 10.1155/2010/789293. URL: https://doi.org/10.1155%2F2010%2F789293.

[379] Antonino Del Popolo and Morgan Le Delliou. "Review of Solutions to the Cusp-Core Problem of the ΛCDM Model". In: *Galaxies* 9.4 (2021), p. 123. DOI: 10.3390/galaxies9040123. arXiv: 2209.14151 [astro-ph.CO].

[380] A. Eckart and R. Genzel. "Observations of stellar proper motions near the Galactic Centre". In: *Nature* 383 (1996), pp. 415–417. DOI: 10.1038/383415a0.

[381] A. M. Ghez et al. "High proper motion stars in the vicinity of Sgr A*: Evidence for a supermassive black hole at the center of our galaxy". In: *Astrophys. J.* 509 (1998), pp. 678–686. DOI: 10.1086/306528. arXiv: astro-ph/9807210.

[382] D. Richstone et al. "Supermassive black holes and the evolution of galaxies". In: *Nature* 395 (1998), A14–A19. arXiv: astro-ph/9810378.

[383] J. M. Huntley and W. C. Saslaw. "The distribution of stars in galactic nuclei: loaded polytropes." In: 199 (July 1975), pp. 328–335. DOI: 10.1086/153695.

[384] Scott Tremaine et al. "A Family of models for spherical stellar systems". In: *Astron. J.* 107 (1994), p. 634. DOI: 10.1086/116883. arXiv: astro-ph/9309044.

[385] Kris Sigurdson et al. "Dark-matter electric and magnetic dipole moments". In: *Phys. Rev. D* 70 (2004). [Erratum: Phys.Rev.D 73, 089903 (2006)], p. 083501. DOI: 10.1103/PhysRevD.70.083501. arXiv: astro-ph/0406355.

[386] P. Young. "Numerical models of star clusters with a central black hole. I - Adiabatic models." In: 242 (Dec. 1980), pp. 1232–1237. DOI: 10.1086/158553.

[387] J. Goodman and J. Binney. "Adding a point mass to a spherical stellar system". In: 207 (Apr. 1984), pp. 511–515. DOI: 10.1093/mnras/207.3.511.

[388] Gerald D. Quinlan, Lars Hernquist, and Steinn Sigurdsson. "Models of Galaxies with Central Black Holes: Adiabatic Growth in Spherical Galaxies". In: *Astrophys. J.* 440 (1995), pp. 554–564. DOI: 10.1086/175295. arXiv: astro-ph/9407005.

[389] J. N. Bahcall and R. A. Wolf. "Star distribution around a massive black hole in a globular cluster." In: 209 (Oct. 1976), pp. 214–232. DOI: 10.1086/154711.

[390] Laura Ferrarese and David Merritt. "A Fundamental relation between supermassive black holes and their host galaxies". In: *Astrophys. J. Lett.* 539 (2000), p. L9. DOI: 10.1086/312838. arXiv: astro-ph/0006053.

[391] Laleh Sadeghian, Francesc Ferrer, and Clifford M. Will. "Dark-matter distributions around massive black holes: A general relativistic analysis". In: *Physical Review D* 88.6 (Sept. 2013). DOI: 10.1103/physrevd.88.063522. URL: https://doi.org/10.1103%2Fphysrevd.88.063522.

[392] Francesc Ferrer, Augusto Medeiros da Rosa, and Clifford M. Will. "Dark matter spikes in the vicinity of Kerr black holes". In: *Phys. Rev. D* 96.8 (2017), p. 083014. DOI: 10.1103/PhysRevD.96.083014. arXiv: 1707.06302 [astro-ph.CO].

[393] Thomas Lacroix, Céline Bœhm, and Joseph Silk. "Ruling out thermal dark matter with a black hole induced spiky profile in the M87 galaxy". In: *Physical Review D* 92.4 (Aug. 2015). DOI: 10.1103/physrevd.92.043510. URL: https://doi.org/10.1103%2Fphysrevd.92.043510.

[394] Thomas Lacroix et al. "Unique probe of dark matter in the core of M87 with the Event Horizon Telescope". In: *Physical Review D* 96.6 (Sept. 2017). DOI: 10.1103/physrevd.96.063008. URL: https://doi.org/10.1103%2Fphysrevd.96.063008.

[395] Mikhail Gorchtein, Stefano Profumo, and Lorenzo Ubaldi. "Probing dark matter with active galactic nuclei jets". In: *Physical Review D* 82.8 (Oct. 2010). DOI: 10.1103/physrevd.82.083514. URL: https://doi.org/10.1103%2Fphysrevd.82.083514.

[396] Tiziana Di Matteo et al. "Black hole growth and activity in a lambda CDM universe". In: *Astrophys. J.* 593 (2003), pp. 56–68. DOI: 10.1086/376501. arXiv: astro-ph/0301586.

[397] Laura Ferrarese. "Beyond the bulge: a fundamental relation between supermassive black holes and dark matter halos". In: *Astrophys. J.* 578 (2002), pp. 90–97. DOI: 10.1086/342308. arXiv: astro-ph/0203469.

[398] David Merritt. "Evolution of the dark matter distribution at the galactic center". In: *Phys. Rev. Lett.* 92 (2004), p. 201304. DOI: 10.1103/PhysRevLett.92.201304. arXiv: astro-ph/0311594.

[399] Oleg Y. Gnedin and Joel R. Primack. "Dark Matter Profile in the Galactic Center". In: *Phys. Rev. Lett.* 93 (2004), p. 061302. DOI: 10.1103/PhysRevLett.93.061302. arXiv: astro-ph/0308385.

[400] David Merritt, Stefan Harfst, and Gianfranco Bertone. "Collisionally Regenerated Dark Matter Structures in Galactic Nuclei". In: *Phys. Rev. D* 75 (2007), p. 043517. DOI: 10.1103/PhysRevD.75.043517. arXiv: astro-ph/0610425.

[401] Piero Ullio, HongSheng Zhao, and Marc Kamionkowski. "A Dark matter spike at the galactic center?" In: *Phys. Rev. D* 64 (2001), p. 043504. DOI: 10.1103/PhysRevD.64.043504. arXiv: astro-ph/0101481.

[402] Thomas Lacroix. "Dynamical constraints on a dark matter spike at the Galactic Centre from stellar orbits". In: *Astron. Astrophys.* 619 (2018), A46. DOI: 10.1051/0004-6361/201832652. arXiv: 1801.01308 [astro-ph.GA].

[403] Zhao-Qiang Shen et al. "Exploring dark matter spike distribution around the Galactic centre with stellar orbits". In: (Mar. 2023). arXiv: 2303.09284 [astro-ph.GA].

[404] Man Ho Chan and Chak Man Lee. "Indirect Evidence for Dark Matter Density Spikes around Stellar-mass Black Holes". In: *Astrophys. J. Lett.* 943.2 (2023), p. L11. DOI: 10.3847/2041-8213/acaafa. arXiv: 2212.05664 [astro-ph.HE].

[405] Ahmad Alachkar, John Ellis, and Malcolm Fairbairn. "Dark matter constraints from the eccentric supermassive black hole binary OJ 287". In: *Phys. Rev. D* 107.10 (2023), p. 103033. DOI: 10.1103/PhysRevD.107.103033. arXiv: 2207.10021 [hep-ph].

[406] Adam Coogan et al. "Measuring the dark matter environments of black hole binaries with gravitational waves". In: *Phys. Rev. D* 105.4 (2022), p. 043009. DOI: 10.1103/PhysRevD.105.043009. arXiv: 2108.04154 [gr-qc].

[407] Philippa S. Cole et al. "Disks, spikes, and clouds: distinguishing environmental effects on BBH gravitational waveforms". In: (Nov. 2022). arXiv: 2211.01362 [gr-qc].

[408] Niklas Becker and Laura Sagunski. "Comparing accretion disks and dark matter spikes in intermediate mass ratio inspirals". In: *Phys. Rev. D* 107.8 (2023), p. 083003. DOI: 10.1103/PhysRevD.107.083003. arXiv: 2211.05145 [gr-qc].

[409] Sang-Jin Sin. "Late time cosmological phase transition and galactic halo as Bose liquid". In: *Phys. Rev. D* 50 (1994), pp. 3650–3654. DOI: 10.1103/PhysRevD.50.3650. arXiv: hep-ph/9205208.

[410] Luca Amendola and Riccardo Barbieri. "Dark matter from an ultra-light pseudo-Goldsone-boson". In: *Phys. Lett. B* 642 (2006), pp. 192–196. DOI: 10.1016/j.physletb.2006.08.069. arXiv: hep-ph/0509257.

[411] David J. E. Marsh and Ana-Roxana Pop. "Axion dark matter, solitons and the cusp–core problem". In: *Mon. Not. Roy. Astron. Soc.* 451.3 (2015), pp. 2479–2492. DOI: 10.1093/mnras/stv1050. arXiv: 1502.03456 [astro-ph.CO].

[412] Lam Hui et al. "Ultralight scalars as cosmological dark matter". In: *Phys. Rev. D* 95.4 (2017), p. 043541. DOI: 10.1103/PhysRevD.95.043541. arXiv: 1610.08297 [astro-ph.CO].

[413] Hyungjin Kim et al. "Adiabatically compressed wave dark matter halo and intermediate-mass-ratio inspirals". In: *Phys. Rev. D* 107.8 (2023), p. 083005. DOI: 10.1103/PhysRevD.107.083005. arXiv: 2212.07528 [astro-ph.GA].

[414] M Cerruti et al. "Leptohadronic single-zone models for the electromagnetic and neutrino emission of TXS 0506056". In: *Monthly Notices of the Royal Astronomical Society: Letters* 483.1 (Nov. 2018), pp. L12–L16. DOI: 10.1093/mnrasl/sly210. URL: https://doi.org/10.1093%2Fmnrasl%2Fsly210.

[415] A. Keivani et al. "A Multimessenger Picture of the Flaring Blazar TXS 0506+056: implications for High-Energy Neutrino Emission and Cosmic Ray Acceleration". In: *Astrophys. J.* 864.1 (2018), p. 84. DOI: 10.3847/1538-4357/aad59a. arXiv: 1807.04537 [astro-ph.HE].

[416] Kohta Murase, Foteini Oikonomou, and Maria Petropoulou. "Blazar Flares as an Origin of High-Energy Cosmic Neutrinos?" In: *Astrophys. J.* 865.2 (2018), p. 124. DOI: 10.3847/1538-4357/aada00. arXiv: 1807.04748 [astro-ph.HE].

[417] Shan Gao et al. "Modelling the coincident observation of a high-energy neutrino and a bright blazar flare". In: *Nature Astron.* 3.1 (2019), pp. 88–92. DOI: 10.1038/s41550-018-0610-1. arXiv: 1807.04275 [astro-ph.HE].

[418] Rui Xue et al. "A Two-zone Model for Blazar Emission: Implications for TXS 0506056 and the Neutrino Event IceCube-170922A". In: *The Astrophysical Journal* 886.1 (Nov. 2019), p. 23. DOI: 10.3847/1538-4357/ab4b44. URL: https://doi.org/10.3847%2F1538-4357%2Fab4b44.

[419] Maria Petropoulou et al. "Multi-epoch Modeling of TXS 0506056 and Implications for Long-term High-energy Neutrino Emission". In: *The Astrophysical Journal* 891.2 (Mar. 2020), p. 115. DOI: 10.3847/1538-4357/ab76d0. URL: https://doi.org/10.3847%2F1538-4357%2Fab76d0.

[420] F. Capel et al. "Assessing coincident neutrino detections using population models". In: (Jan. 2022). arXiv: 2201.05633 [astro-ph.HE].

[421] S. P. Mikheyev and A. Yu. Smirnov. "Resonance Amplification of Oscillations in Matter and Spectroscopy of Solar Neutrinos". In: *Sov. J. Nucl. Phys.* 42 (1985), pp. 913–917.

[422] Manibrata Sen and Alexei Y. Smirnov. "Refractive neutrino masses, ultralight dark matter and cosmology". In: (June 2023). arXiv: 2306.15718 [hep-ph].

[423] C. Döring and S. Vogl. "Astrophysical neutrino point sources as a probe of new physics". In: (Apr. 2023). arXiv: 2304.08533 [hep-ph].

[424] H. Athar, M. Jezabek, and O. Yasuda. "Effects of neutrino mixing on high-energy cosmic neutrino flux". In: *Phys. Rev. D* 62 (2000), p. 103007. DOI: 10.1103/PhysRevD.62.103007. arXiv: hep-ph/0005104.

[425] Olga Mena, Sergio Palomares-Ruiz, and Aaron C. Vincent. "Flavor Composition of the High-Energy Neutrino Events in IceCube". In: *Phys. Rev. Lett.* 113 (2014), p. 091103. DOI: 10.1103/PhysRevLett.113.091103. arXiv: 1404.0017 [astro-ph.HE].

[426] Ian M. Shoemaker and Kohta Murase. "Probing BSM Neutrino Physics with Flavor and Spectral Distortions: Prospects for Future High-Energy Neutrino Telescopes". In: *Phys. Rev. D* 93.8 (2016), p. 085004. DOI: 10.1103/PhysRevD.93.085004. arXiv: 1512.07228 [astro-ph.HE].

[427] Mauricio Bustamante, John F. Beacom, and Walter Winter. "Theoretically Palatable Flavor Combinations of Astrophysical Neutrinos". In: *Physical Review Letters* 115.16 (Oct. 2015). DOI: 10.1103/physrevlett.115.161302. URL: https://doi.org/10.1103%2Fphysrevlett.115.161302.

[428] Peter B. Denton and Irene Tamborra. "Invisible Neutrino Decay Could Resolve IceCube's Track and Cascade Tension". In: *Phys. Rev. Lett.* 121.12 (2018), p. 121802. DOI: 10.1103/PhysRevLett.121.121802. arXiv: 1805.05950 [hep-ph].

[429] Kohta Murase and Ian M. Shoemaker. "Neutrino Echoes from Multimessenger Transient Sources". In: *Phys. Rev. Lett.* 123.24 (2019), p. 241102. DOI: 10.1103/PhysRevLett.123.241102. arXiv: 1903.08607 [hep-ph].

[430] Ivan Esteban et al. "Probing secret interactions of astrophysical neutrinos in the high-statistics era". In: *Phys. Rev. D* 104.12 (2021), p. 123014. DOI: 10.1103/PhysRevD.104.123014. arXiv: 2107.13568 [hep-ph].

[431] Jeffrey M. Hyde. "Constraints on Neutrino Self-Interactions from IceCube Observation of NGC 1068". In: (July 2023). arXiv: 2307.02361 [hep-ph].

[432] Ki-Young Choi, Jongkuk Kim, and Carsten Rott. "Constraining dark matter-neutrino interactions with IceCube-170922A". In: *Phys. Rev. D* 99.8 (2019), p. 083018. DOI: 10.1103/PhysRevD.99.083018. arXiv: 1903.03302 [astro-ph.CO].

[433] Kevin J. Kelly and Pedro A. N. Machado. "Multimessenger Astronomy and New Neutrino Physics". In: *JCAP* 10 (2018), p. 048. DOI: 10.1088/1475-7516/2018/10/048. arXiv: 1808.02889 [hep-ph].

[434] J.B.G. Alvey and M. Fairbairn. "Linking scalar dark matter and neutrino masses with IceCube 170922A". In: *Journal of Cosmology and Astroparticle Physics* 2019.07 (July 2019), pp. 041–041. DOI: 10.1088/1475-7516/2019/07/041. URL: https://doi.org/10.1088%2F1475-7516%2F2019%2F07%2F041.

[435] Carlos A. Argüelles, Ali Kheirandish, and Aaron C. Vincent. "Imaging Galactic Dark Matter with High-Energy Cosmic Neutrinos". In: *Physical Review Letters* 119.20 (Nov. 2017). DOI: 10.1103/physrevlett.119.201801. URL: https://doi.org/10.1103%2Fphysrevlett.119.201801.

[436] P Padovani et al. "TXS 0506056, the first cosmic neutrino source, is not a BL Lac". In: *Monthly Notices of the Royal Astronomical Society: Letters* 484.1 (Jan. 2019), pp. L104–L108. DOI: 10.1093/mnrasl/slz011. URL: https://doi.org/10.1093%2Fmnrasl%2Fslz011.

[437] Gianpiero Mangano et al. "Cosmological bounds on dark-matter-neutrino interactions". In: *Physical Review D* 74.4 (Aug. 2006). DOI: 10.1103/physrevd.74.043517. URL: https://doi.org/10.1103%2Fphysrevd.74.043517.

[438] Ryan J. Wilkinson, Julien Lesgourgues, and Céline Boehm. "Using the CMB angular power spectrum to study Dark Matter-photon interactions". In: *JCAP* 04 (2014), p. 026. DOI: 10.1088/1475-7516/2014/04/026. arXiv: 1309.7588 [astro-ph.CO].

[439] Ryan J. Wilkinson, Celine Boehm, and Julien Lesgourgues. "Constraining Dark Matter-Neutrino Interactions using the CMB and Large-Scale Structure". In: *JCAP* 05 (2014), p. 011. DOI: 10.1088/1475-7516/2014/05/011. arXiv: 1401.7597 [astro-ph.CO].

[440] Miguel Escudero et al. "Exploring dark matter microphysics with galaxy surveys". In: *JCAP* 09 (2015), p. 034. DOI: 10.1088/1475-7516/2015/9/034. arXiv: 1505.06735 [astro-ph.CO].

[441] Philippe Brax et al. "Extended Analysis of Neutrino-Dark Matter Interactions with Small-Scale CMB Experiments". In: (May 2023). arXiv: 2305.01383 [astro-ph.CO].

[442] Kensuke Akita and Shin'ichiro Ando. "Constraints on dark matter-neutrino scattering from the Milky-Way satellites and subhalo modeling for dark acoustic oscillations". In: (May 2023). arXiv: 2305.01913 [astro-ph.CO].

[443] Woosik Kang et al. "Search for the rare interactions of neutrinos from distant point sources with the IceCube Neutrino Telescope". In: *PoS* ICRC2023 (2023), p. 1380. DOI: 10.22323/1.444.1380.

[444] Miguel Escudero et al. "A fresh look into the interacting dark matter scenario". In: *Journal of Cosmology and Astroparticle Physics* 2018.06 (June 2018), pp. 007–007. DOI: 10.1088/1475-7516/2018/06/007. URL: https://doi.org/10.1088%2F1475-7516%2F2018%2F06%2F007.

[445] C. Bœhm et al. "Using the Milky Way satellites to study interactions between cold dark matter and radiation". In: *Monthly Notices of the Royal Astronomical Society: Letters* 445.1 (Sept. 2014), pp. L31–L35. DOI: 10.1093/mnrasl/slu115. URL: https://doi.org/10.1093%2Fmnrasl%2Fslu115.

[446] Yongsoo Jho et al. "Cosmic-Neutrino-Boosted Dark Matter (νBDM)". In: (Jan. 2021). arXiv: 2101.11262 [hep-ph].

[447] Yue Zhang. "Speeding up dark matter with solar neutrinos". In: *PTEP* 2022.1 (2022), 013B05. DOI: 10.1093/ptep/ptab156. arXiv: 2001.00948 [hep-ph].

[448] Diptimoy Ghosh, Atanu Guha, and Divya Sachdeva. "Exclusion limits on dark matter-neutrino scattering cross section". In: *Phys. Rev. D* 105.10 (2022), p. 103029. DOI: 10.1103/PhysRevD.105.103029. arXiv: 2110.00025 [hep-ph].

[449] Yasaman Farzan and Sergio Palomares-Ruiz. "Dips in the Diffuse Supernova Neutrino Background". In: *JCAP* 06 (2014), p. 014. DOI: 10.1088/1475-7516/2014/06/014. arXiv: 1401.7019 [hep-ph].

[450] Cora Dvorkin, Kfir Blum, and Marc Kamionkowski. "Constraining dark matter-baryon scattering with linear cosmology". In: *Physical Review D* 89.2 (Jan. 2014). DOI: 10.1103/physrevd.89.023519. URL: https://doi.org/10.1103%2Fphysrevd.89.023519.

[451] Georg G. Raffelt. *Stars as laboratories for fundamental physics : the astrophysics of neutrinos, axions, and other weakly interacting particles*. 1996.

[452] Gonzalo Herrera, Alejandro Ibarra, and Elisa Resconi. "A hint of dark matter-photon scatterings from NGC 1068". In: *In progress* (XXXX).

[453] Jong-Hak Woo and C. Megan Urry. "AGN black hole masses and bolometric luminosities". In: *Astrophys. J.* 579 (2002), pp. 530–544. DOI: 10.1086/342878. arXiv: astro-ph/0207249.

[454] Francesca Panessa et al. "On the X-ray, optical emission line and black hole mass properties of local Seyfert galaxies". In: *Astron. Astrophys.* 455 (2006), p. 173. DOI: 10.1051/0004-6361:20064894. arXiv: astro-ph/0605236.

[455] Takeo Minezaki and Kyoko Matsushita. "A NEW BLACK HOLE MASS ESTIMATE FOR OBSCURED ACTIVE GALACTIC NUCLEI". In: *The Astrophysical Journal* 802.2 (Mar. 2015), p. 98. DOI: 10.1088/0004-637x/802/2/98. URL: https://doi.org/10.1088%2F0004-637x%2F802%2F2%2F98.

[456] Karnig O. Mikaelian. "Astrophysical implications of new light Higgs bosons". In: *Phys. Rev. D* 18 (10 Nov. 1978), pp. 3605–3609. DOI: 10.1103/PhysRevD.18.3605. URL: https://link.aps.org/doi/10.1103/PhysRevD.18.3605.

[457] Stanley J. Brodsky et al. "LASER INDUCED AXION PHOTOPRODUCTION". In: *Phys. Rev. Lett.* 56 (1986). [Erratum: Phys.Rev.Lett. 57, 502 (1986)], p. 1763. DOI: 10.1103/PhysRevLett.56.1763.

[458] Paolo Gondolo and Georg G. Raffelt. "Solar neutrino limit on axions and keV-mass bosons". In: *Phys. Rev. D* 79 (2009), p. 107301. DOI: 10.1103/PhysRevD.79.107301. arXiv: 0807.2926 [astro-ph].

[459] James B. Dent et al. "New Directions for Axion Searches via Scattering at Reactor Neutrino Experiments". In: *Phys. Rev. Lett.* 124.21 (2020), p. 211804. DOI: 10.1103/PhysRevLett.124.211804. arXiv: 1912.05733 [hep-ph].

[460] Sacha Davidson, Steen Hannestad, and Georg Raffelt. "Updated bounds on millicharged particles". In: *Journal of High Energy Physics* 2000.05 (May 2000), pp. 003–003. DOI: 10.1088/1126-6708/2000/05/003. URL: https://doi.org/10.1088%2F1126-6708%2F2000%2F05%2F003.

[461] Benjamin W. Lee and Steven Weinberg. "Cosmological Lower Bound on Heavy Neutrino Masses". In: *Phys. Rev. Lett.* 39 (1977). Ed. by M. A. Srednicki, pp. 165–168. DOI: 10.1103/PhysRevLett.39.165.

[462] A.N. Baushev. "Extragalactic dark matter and direct detection experiments". In: *Astrophys. J.* 771 (2013), p. 117. DOI: 10.1088/0004-637X/771/2/117. arXiv: 1208.0392 [astro-ph.CO].

[463] Peter S Behroozi, Abraham Loeb, and Risa H Wechsler. "Unbound particles in dark matter halos". In: *Journal of Cosmology and Astroparticle Physics* 2013.06 (June 2013), pp. 019–019. ISSN: 1475-7516. DOI: 10.1088/1475-7516/2013/06/019. URL: http://dx.doi.org/10.1088/1475-7516/2013/06/019.

[464] Gurtina Besla, Annika Peter, and Nicolas Garavito-Camargo. "The highest-speed local dark matter particles come from the Large Magellanic Cloud". In: *JCAP* 11 (2019), p. 013. DOI: 10.1088/1475-7516/2019/11/013. arXiv: 1909.04140 [astro-ph.GA].

[465] Gonzalo Herrera and Alejandro Ibarra. "Direct detection of non-galactic light dark matter". In: *Phys. Lett. B* 820 (2021), p. 136551. DOI: 10.1016/j.physletb.2021.136551. arXiv: 2104.04445 [hep-ph].

[466] Gonzalo Herrera, Alejandro Ibarra, and Satoshi Shirai. "Enhanced prospects for direct detection of inelastic dark matter from a non-galactic diffuse component". In: *JCAP* 04 (2023), p. 026. DOI: 10.1088/1475-7516/2023/04/026. arXiv: 2301.00870 [hep-ph].

[467] Adam Smith-Orlik et al. "The impact of the Large Magellanic Cloud on dark matter direct detection signals". In: (Feb. 2023). arXiv: 2302.04281 [astro-ph.GA].

[468] Kohta Murase, Markus Ahlers, and Brian C. Lacki. "Testing the Hadronuclear Origin of PeV Neutrinos Observed with IceCube". In: *Phys. Rev. D* 88.12 (2013), p. 121301. DOI: 10.1103/PhysRevD.88.121301. arXiv: 1306.3417 [astro-ph.HE].

[469] Walter Winter. "Photohadronic Origin of the TeV-PeV Neutrinos Observed in IceCube". In: *Phys. Rev. D* 88 (2013), p. 083007. DOI: 10.1103/PhysRevD.88.083007. arXiv: 1307.2793 [astro-ph.HE].

[470] Marco Ajello, Kohta Murase, and Alex McDaniel. "Disentangling the Hadronic Components in NGC 1068". In: (July 2023). arXiv: 2307.02333 [astro-ph.HE].

[471] Björn Eichmann et al. "Solving the Multimessenger Puzzle of the AGN-starburst Composite Galaxy NGC 1068". In: *Astrophys. J.* 939.1 (2022), p. 43. DOI: 10.3847/1538-4357/ac9588. arXiv: 2207.00102 [astro-ph.HE].

[472] Carlos Blanco et al. "On the Neutrino and Gamma-Ray Emission from NGC 1068". In: (July 2023). arXiv: 2307.03259 [astro-ph.HE].

[473] M. G. Aartsen et al. "Neutrino emission from the direction of the blazar TXS 0506+056 prior to the IceCube-170922A alert". In: *Science* 361.6398 (2018), pp. 147–151. DOI: 10.1126/science.aat2890. arXiv: 1807.08794 [astro-ph.HE].

[474] S. Ansoldi et al. "The blazar TXS 0506+056 associated with a high-energy neutrino: insights into extragalactic jets and cosmic ray acceleration". In: *Astrophys. J. Lett.* 863 (2018), p. L10. DOI: 10.3847/2041-8213/aad083. arXiv: 1807.04300 [astro-ph.HE].

[475] Alessandro Granelli, Piero Ullio, and Jin-Wei Wang. "Blazar-boosted dark matter at Super-Kamiokande". In: *Journal of Cosmology and Astroparticle Physics* 2022.07 (July 2022), p. 013. DOI: 10.1088/1475-7516/2022/07/013. URL: https://doi.org/10.1088%2F1475-7516%2F2022%2F07%2F013.

[476] Supritha Bhowmick, Diptimoy Ghosh, and Divya Sachdeva. "Blazar boosted Dark Matter – direct detection constraints on $\sigma_{e\chi}$: Role of energy dependent cross sections". In: (Dec. 2022). arXiv: 2301.00209 [hep-ph].

[477] Elliott D. Bloom and James D. Wells. "Multi-GeV photons from electron–dark-matter scattering near active galactic nuclei". In: *Physical Review D* 57.2 (Jan. 1998), pp. 1299–1302. DOI: 10.1103/physrevd.57.1299. URL: https://doi.org/10.1103%2Fphysrevd.57.1299.

[478] Dan Hooper and Samuel D. McDermott. "Robust Constraints and Novel Gamma-Ray Signatures of Dark Matter That Interacts Strongly With Nucleons". In: *Phys. Rev. D* 97.11 (2018), p. 115006. DOI: 10.1103/PhysRevD.97.115006. arXiv: 1802.03025 [hep-ph].

[479] Christopher V. Cappiello, Kenny C. Y. Ng, and John F. Beacom. "Reverse Direct Detection: Cosmic Ray Scattering With Light Dark Matter". In: *Phys. Rev. D* 99.6 (2019), p. 063004. DOI: 10.1103/PhysRevD.99.063004. arXiv: 1810.07705 [hep-ph].

[480] Marina Cermeño, Céline Degrande, and Luca Mantani. "Signatures of leptophilic t-channel dark matter from active galactic nuclei". In: *Phys. Rev. D* 105.8 (2022), p. 083019. DOI: 10.1103/PhysRevD.105.083019. arXiv: 2201.07247 [hep-ph].

[481] Antonio Ambrosone et al. "Starburst Nuclei as Light Dark Matter Laboratories". In: (Oct. 2022). arXiv: 2210.05685 [astro-ph.HE].

[482] Olmo Piana et al. "The mass assembly of high-redshift black holes". In: *Monthly Notices of the Royal Astronomical Society* 500.2 (Oct. 2020), pp. 2146–2158. DOI: 10.1093/mnras/staa3363. URL: https://doi.org/10.1093%2Fmnras%2Fstaa3363.

[483] Marco Cirelli et al. "Integral X-ray constraints on sub-GeV Dark Matter". In: *Phys. Rev. D* 103.6 (2021), p. 063022. DOI: 10.1103/PhysRevD.103.063022. arXiv: 2007.11493 [hep-ph].

[484] K. Abe et al. "Search for Cosmic-Ray Boosted Sub-GeV Dark Matter Using Recoil Protons at Super-Kamiokande". In: *Phys. Rev. Lett.* 130.3 (2023), p. 031802. DOI: 10.1103/PhysRevLett.130.031802. arXiv: 2209.14968 [hep-ex].

[485] Kyrylo Bondarenko et al. "Direct detection and complementary constraints for sub-GeV dark matter". In: *JHEP* 03 (2020), p. 118. DOI: 10.1007/JHEP03(2020)118. arXiv: 1909.08632 [hep-ph].

[486] I. Angeli. "A consistent set of nuclear rms charge radii: properties of the radius surface R(N,Z)". In: *Atom. Data Nucl. Data Tabl.* 87.2 (2004), pp. 185–206. DOI: 10.1016/j.adt.2004.04.002.

[487] A. Keivani et al. "A Multimessenger Picture of the Flaring Blazar TXS 0506056: Implications for High-energy Neutrino Emission and Cosmic-Ray Acceleration". In: *The Astrophysical Journal* 864.1 (Aug. 2018), p. 84. DOI: 10.3847/1538-4357/aad59a. URL: https://doi.org/10.3847%2F1538-4357%2Faad59a.

[488] C. Amole et al. "Dark matter search results from the PICO-60 CF_3I bubble chamber". In: *Phys. Rev. D* 93.5 (2016), p. 052014. DOI: 10.1103/PhysRevD.93.052014. arXiv: 1510.07754 [hep-ex]. URL: https://doi.org/10.1103%2Fphysrevd.93.052014.

[489] Liron Barak et al. "SENSEI: Direct-Detection Results on sub-GeV Dark Matter from a New Skipper CCD". In: *Physical Review Letters* 125.17 (Oct. 2020). DOI: 10.1103/physrevlett.125.171802. URL: https://doi.org/10.1103%2Fphysrevlett.125.171802.

[490] E. Aprile et al. "Light Dark Matter Search with Ionization Signals in XENON1T". In: *Physical Review Letters* 123.25 (Dec. 2019). DOI: 10.1103/physrevlett.123.251801. URL: https://doi.org/10.1103%2Fphysrevlett.123.251801.

[491] Timon Emken, Chris Kouvaris, and Ian M. Shoemaker. "Terrestrial Effects on Dark Matter-Electron Scattering Experiments". In: *Phys. Rev. D* 96.1 (2017), p. 015018. DOI: 10.1103/PhysRevD.96.015018. arXiv: 1702.07750 [hep-ph].

[492] Timon Emken et al. "Direct Detection of Strongly Interacting Sub-GeV Dark Matter via Electron Recoils". In: *JCAP* 09 (2019), p. 070. DOI: 10.1088/1475-7516/2019/09/070. arXiv: 1905.06348 [hep-ph].

[493] M. Shafi Mahdawi and Glennys R. Farrar. "Constraints on Dark Matter with a moderately large and velocity-dependent DM-nucleon cross-section". In: *Journal of Cosmology and Astroparticle Physics* 2018.10 (Oct. 2018), pp. 007–007. DOI: 10.1088/1475-7516/2018/10/007. URL: https://doi.org/10.1088%2F1475-7516%2F2018%2F10%2F007.

[494] Manuel A. Buen-Abad et al. "Cosmological constraints on dark matter interactions with ordinary matter". In: *Phys. Rept.* 961 (2022), pp. 1–35. DOI: 10.1016/j.physrep.2022.02.006. arXiv: 2107.12377 [astro-ph.CO].

[495] Paul Frederik Depta et al. "BBN constraints on the annihilation of MeV-scale dark matter". In: *Journal of Cosmology and Astroparticle Physics* 2019.04 (Apr. 2019), pp. 029–029. DOI: 10.1088/1475-7516/2019/04/029. URL: https://doi.org/10.1088%2F1475-7516%2F2019%2F04%2F029.

[496] Cara Giovanetti et al. "Joint Cosmic Microwave Background and Big Bang Nucleosynthesis Constraints on Light Dark Sectors with Dark Radiation". In: *Phys. Rev. Lett.* 129.2 (2022), p. 021302. DOI: 10.1103/PhysRevLett.129.021302. arXiv: 2109.03246 [hep-ph].

[497] Haipeng An et al. "Directly Detecting MeV-Scale Dark Matter Via Solar Reflection". In: *Physical Review Letters* 120.14 (Apr. 2018). DOI: 10.1103/physrevlett.120.141801. URL: https://doi.org/10.1103%2Fphysrevlett.120.141801.

[498] Rouven Essig, Tomer Volansky, and Tien-Tien Yu. "New constraints and prospects for sub-GeV dark matter scattering off electrons in xenon". In: *Physical Review D* 96.4 (Aug. 2017). DOI: 10.1103/physrevd.96.043017. URL: https://doi.org/10.1103%2Fphysrevd.96.043017.

[499] Y. P. Jing and Yasushi Suto. "Density profiles of dark matter halo are not universal". In: *Astrophys. J. Lett.* 529 (2000), pp. L69–72. DOI: 10.1086/312463. arXiv: astro-ph/9909478.

[500] Darren Reed et al. "Evolution of the density profiles of dark matter halos". In: *Mon. Not. Roy. Astron. Soc.* 357 (2005), pp. 82–96. DOI: 10.1111/j.1365-2966.2005.08612.x. arXiv: astro-ph/0312544.

[501] Kohta Murase and Ian M. Shoemaker. "Neutrino Echoes from Multimessenger Transient Sources". In: *Physical Review Letters* 123.24 (Dec. 2019). DOI: 10.1103/physrevlett.123.241102. URL: https://doi.org/10.1103%2Fphysrevlett.123.241102.

[502] James M. Cline et al. "Blazar constraints on neutrino-dark matter scattering". In: (Sept. 2022). arXiv: 2209.02713 [hep-ph].

[503] James M. Cline and Matteo Puel. "NGC 1068 constraints on neutrino-dark matter scattering". In: (Jan. 2023). arXiv: 2301.08756 [hep-ph].

[504] I. D. Karachentsev. "Missing dark matter in the local universe". In: *Astrophysical Bulletin* 67.2 (Apr. 2012), pp. 123–134. ISSN: 1990-3421. DOI: 10.1134/s1990341312020010. URL: http://dx.doi.org/10.1134/S1990341312020010.

[505] I. D. Karachentsev and K. N. Telikova. "Stellar and dark matter density in the Local Universe". In: *Astronomische Nachrichten* 339.7-8 (Aug. 2018), pp. 615–622. ISSN: 0004-6337. DOI: 10.1002/asna.201813520. URL: http://dx.doi.org/10.1002/asna.201813520.

[506] Hans Böhringer, Gayoung Chon, and Chris A. Collins. "Observational evidence for a local underdensity in the Universe and its effect on the measurement of the Hubble Constant". In: *Astron. Astrophys.* 633 (2020), A19. DOI: 10.1051/0004-6361/201936400. arXiv: 1907.12402 [astro-ph.CO].

[507] N. Aghanim et al. "Planck 2018 results". In: *Astronomy Astrophysics* 641 (Sept. 2020), A6. ISSN: 1432-0746. DOI: 10.1051/0004-6361/201833910. URL: http://dx.doi.org/10.1051/0004-6361/201833910.

[508] Shogo Masaki, Masataka Fukugita, and Naoki Yoshida. "MATTER DISTRIBUTION AROUND GALAXIES". In: *The Astrophysical Journal* 746.1 (Jan. 2012), p. 38. ISSN: 1538-4357. DOI: 10.1088/0004-637x/746/1/38. URL: http://dx.doi.org/10.1088/0004-637X/746/1/38.

[509] Igor. D. Karachentsev et al. "Infall of nearby galaxies into the Virgo cluster as traced with HST". In: *Astrophys. J.* 782 (2014), p. 4. DOI: 10.1088/0004-637X/782/1/4. arXiv: 1312.6769 [astro-ph.GA].

[510] Antonio Enea Romano, Alexei A. Starobinsky, and Misao Sasaki. "Effects of inhomogeneities on apparent cosmological observables: "fake" evolving dark energy". In: *The European Physical Journal C* 72.12 (Dec. 2012). ISSN: 1434-6052. DOI: 10.1140/epjc/s10052-012-2242-4. URL: http://dx.doi.org/10.1140/epjc/s10052-012-2242-4.

[511] Tomonori Totani et al. "Near-Infrared Faint Galaxies in the Subaru Deep Field: Comparing the Theory with Observations for Galaxy Counts, Colors, and Size Distributions toK 24.5". In: *The Astrophysical Journal* 559.2 (Oct. 2001), pp. 592–605. ISSN: 1538-4357. DOI: 10.1086/322338. URL: http://dx.doi.org/10.1086/322338.

[512] Marius Cautun et al. "Evolution of the cosmic web". In: *Monthly Notices of the Royal Astronomical Society* 441.4 (May 2014), pp. 2923–2973. ISSN: 0035-8711. DOI: 10.1093/mnras/stu768. URL: http://dx.doi.org/10.1093/mnras/stu768.

[513] Satoshi Miyazaki et al. "A large sample of shear-selected clusters from the Hyper Suprime-Cam Subaru Strategic Program S16A Wide field mass maps". In: *Publications of the Astronomical Society of Japan* 70.SP1 (Dec. 2017). ISSN: 2053-051X. DOI: 10.1093/pasj/psx120. URL: http://dx.doi.org/10.1093/pasj/psx120.

[514] Gonzalo Herrera and Alejandro Ibarra. "Direct detection of non-galactic light dark matter". In: *Physics Letters B* 820 (Sept. 2021), p. 136551. ISSN: 0370-2693. DOI: 10.1016/j.physletb.2021.136551. URL: http://dx.doi.org/10.1016/j.physletb.2021.136551.

[515] Gonzalo Herrera and Alejandro Ibarra. "Implications of non-galactic dark matter for sub-GeV direct detection searches". In: *J. Phys. Conf. Ser.* 2156 (2021), p. 012040. DOI: 10.1088/1742-6596/2156/1/012040.

[516] Katherine Freese, Paolo Gondolo, and Leo Stodolsky. "On the direct detection of extragalactic WIMPs". In: *Phys. Rev. D* 64 (2001), p. 123502. DOI: 10.1103/PhysRevD.64.123502. arXiv: astro-ph/0106480.

[517] G. Besla, A.H.G. Peter, and N. Garavito-Camargo. "The highest-speed local dark matter particles come from the Large Magellanic Cloud". In: *Journal of Cosmology and Astroparticle Physics* 2019.11 (Nov. 2019), pp. 013–013. ISSN: 1475-7516. DOI: 10.1088/1475-7516/2019/11/013. URL: http://dx.doi.org/10.1088/1475-7516/2019/11/013.

[518] Mark Vogelsberger et al. "Phase-space structure in the local dark matter distribution and its signature in direct detection experiments". In: *Mon. Not. Roy. Astron. Soc.* 395 (2009), pp. 797–811. DOI: 10.1111/j.1365-2966.2009.14630.x. arXiv: 0812.0362 [astro-ph].

[519] Jonathan D. Sloane et al. "Assessing Astrophysical Uncertainties in Direct Detection with Galaxy Simulations". In: *Astrophys. J.* 831 (2016), p. 93. DOI: 10.3847/0004-637X/831/1/93. arXiv: 1601.05402 [astro-ph.GA].

[520] N. W. Evans, C. M. Carollo, and P. T. de Zeeuw. "Triaxial haloes and particle dark matter detection". In: *Mon. Not. Roy. Astron. Soc.* 318 (2000), p. 1131. DOI: 10.1046/j.1365-8711.2000.03787.x. arXiv: astro-ph/0008156.

[521] N. Wyn Evans, Ciaran A. J. O'Hare, and Christopher McCabe. "Refinement of the standard halo model for dark matter searches in light of the Gaia Sausage". In: *Phys. Rev. D* 99.2 (2019), p. 023012. DOI: 10.1103/PhysRevD.99.023012. arXiv: 1810.11468 [astro-ph.GA].

[522] F. D. Kahn and L. Woltjer. "Intergalactic Matter and the Galaxy." In: *Astrophys. J.* 130 (1959), p. 705. DOI: 10.1086/146762.

[523] James Binney and Scott Tremaine. *Galactic Dynamics: Second Edition*. 2008.

[524] T. J. Cox and Abraham Loeb. "The Collision Between The Milky Way And Andromeda". In: *Mon. Not. Roy. Astron. Soc.* 386 (2008), p. 461. DOI: 10.1111/j.1365-2966.2008.13048.x. arXiv: 0705.1170 [astro-ph].

[525] Dmitry Makarov and Igor Karachentsev. "Galaxy groups and clouds in the Local (z $\sim$ 0.01) universe". In: *Mon. Not. Roy. Astron. Soc.* 412 (2011), p. 2498. DOI: 10.1111/j.1365-2966.2010.18071.x. arXiv: 1011.6277 [astro-ph.CO].

[526] A. N. Baushev. "GALAXY HALO FORMATION IN THE ABSENCE OF VIOLENT RELAXATION AND A UNIVERSAL DENSITY PROFILE OF THE HALO CENTER". In: *The Astrophysical Journal* 786.1 (Apr. 2014), p. 65. DOI: 10.1088/0004-637x/786/1/65. URL: https://doi.org/10.1088%2F0004-637x%2F786%2F1%2F65.

[527] Anton N Baushev. "Principal properties of the velocity distribution of dark matter particles near the Solar System". In: *Journal of Physics: Conference Series* 375.1 (July 2012), p. 012048. DOI: 10.1088/1742-6596/375/1/012048. URL: https://doi.org/10.1088%2F1742-6596%2F375%2F1%2F012048.

[528] Anton N. Baushev. "The radius, at which a galaxy group stops the Hubble stream, and the group mass: an exact analytical solution". In: *Mon. Not. Roy. Astron. Soc.* 490.1 (2019), pp. L38–L41. DOI: 10.1093/mnrasl/slz143. arXiv: 1907.08716 [astro-ph.CO].

[529] Joachim Stadel et al. "Quantifying the heart of darkness with GHALO - a multi-billion particle simulation of our galactic halo". In: *Mon. Not. Roy. Astron. Soc.* 398 (2009), pp. L21–L25. DOI: 10.1111/j.1745-3933.2009.00699.x. arXiv: 0808.2981 [astro-ph].

[530] Roeland P. van der Marel et al. "First Gaia Dynamics of the Andromeda System: DR2 Proper Motions, Orbits, and Rotation of M31 and M33". In: *The Astrophysical Journal* 872.1 (Feb. 2019), p. 24. ISSN: 1538-4357. DOI: 10.3847/1538-4357/ab001b. URL: http://dx.doi.org/10.3847/1538-4357/ab001b.

[531] Ehsan Kourkchi and R. Brent Tully. "Galaxy Groups Within 3500 km s^{-1}". In: *The Astrophysical Journal* 843.1 (June 2017), p. 16. ISSN: 1538-4357. DOI: 10.3847/1538-4357/aa76db. URL: http://dx.doi.org/10.3847/1538-4357/aa76db.

[532] Noam I Libeskind et al. "The scphestia/scp project: simulations of the Local Group". In: *Monthly Notices of the Royal Astronomical Society* 498.2 (Aug. 2020), pp. 2968–2983. DOI: 10.1093/mnras/staa2541. URL: https://doi.org/10.1093%2Fmnras%2Fstaa2541.

[533] Maria K Neuzil, Philip Mansfield, and Andrey V Kravtsov. "The Sheet of Giants: Unusual properties of the Milky Way's immediate neighbourhood". In: *Monthly Notices of the Royal Astronomical Society* 494.2 (Apr. 2020), pp. 2600–2617. DOI: 10.1093/mnras/staa898. URL: https://doi.org/10.1093%2Fmnras%2Fstaa898.

[534] Stuart McAlpine et al. "SIBELIUS-DARK: a galaxy catalogue of the local volume from a constrained realization simulation". In: *Monthly Notices of the Royal Astronomical Society* 512.4 (Feb. 2022), pp. 5823–5847. DOI: 10.1093/mnras/stac295. URL: https://doi.org/10.1093%2Fmnras%2Fstac295.

[535] Till Sawala et al. "The SIBELIUS Project: E Pluribus Unum". In: *Monthly Notices of the Royal Astronomical Society* 509.1 (Nov. 2021), pp. 1432–1446. DOI: 10.1093/mnras/stab2684. URL: https://doi.org/10.1093%2Fmnras%2Fstab2684.

[536] Anne M Green. "Astrophysical uncertainties on the local dark matter distribution and direct detection experiments". In: *J. Phys. G* 44.8 (2017), p. 084001. DOI: 10.1088/1361-6471/aa7819. arXiv: 1703.10102 [astro-ph.CO].

[537] Nassim Bozorgnia and Gianfranco Bertone. "Implications of hydrodynamical simulations for the interpretation of direct dark matter searches". In: *Int. J. Mod. Phys. A* 32.21 (2017), p. 1730016. DOI: 10.1142/S0217751X17300162. arXiv: 1705.05853 [astro-ph.CO].

[538] Brian Feldstein and Felix Kahlhoefer. "Quantifying (dis)agreement between direct detection experiments in a halo-independent way". In: *JCAP* 12 (2014), p. 052. DOI: 10.1088/1475-7516/2014/12/052. arXiv: 1409.5446 [hep-ph].

[539] Muping Chen, Graciela B. Gelmini, and Volodymyr Takhistov. "Halo-independent analysis of direct dark matter detection through electron scattering". In: *Journal of Cosmology and Astroparticle Physics* 2021.12 (Dec. 2021), p. 048. DOI: 10.1088/1475-7516/2021/12/048. URL: https://doi.org/10.1088%2F1475-7516%2F2021%2F12%2F048.

[540] Muping Chen, Graciela B. Gelmini, and Volodymyr Takhistov. "Halo-Independent Dark Matter Electron Scattering Analysis with In-Medium Effects". In: (Sept. 2022). arXiv: 2209.10902 [hep-ph].

[541] Ciaran A. J. O'Hare et al. "Dark matter hurricane: Measuring the S1 stream with dark matter detectors". In: *Phys. Rev. D* 98.10 (2018), p. 103006. DOI: 10.1103/PhysRevD.98.103006. arXiv: 1807.09004 [astro-ph.CO].

[542] Alejandro Ibarra, Bradley J. Kavanagh, and Andreas Rappelt. "Impact of substructure on local dark matter searches". In: *JCAP* 12 (2019), p. 013. DOI: 10.1088/1475-7516/2019/12/013. arXiv: 1908.00747 [hep-ph].

[543] J. D. Lewin and P. F. Smith. "Review of mathematics, numerical factors, and corrections for dark matter experiments based on elastic nuclear recoil". In: *Astropart. Phys.* 6 (1996), pp. 87–112. DOI: 10.1016/S0927-6505(96)00047-3.

[544] David G. Cerdeno and Anne M. Green. "Direct detection of WIMPs". In: (Feb. 2010), pp. 347–369. DOI: 10.1017/CBO9780511770739.018. arXiv: 1002.1912 [astro-ph.CO].

[545] A. Drukier and Leo Stodolsky. "Principles and Applications of a Neutral Current Detector for Neutrino Physics and Astronomy". In: *Phys. Rev. D* 30 (1984). Ed. by J. Tran Thanh Van, p. 2295. DOI: 10.1103/PhysRevD.30.2295.

[546] E. Armengaud et al. "Searching for low-mass dark matter particles with a massive Ge bolometer operated above-ground". In: *Phys. Rev. D* 99.8 (2019), p. 082003. DOI: 10.1103/PhysRevD.99.082003. arXiv: 1901.03588 [astro-ph.GA].

[547] Chris Kouvaris. "Earth's stopping effect in directional dark matter detectors". In: *Phys. Rev. D* 93.3 (2016), p. 035023. DOI: 10.1103/PhysRevD.93.035023. arXiv: 1509.08720 [hep-ph].

[548] Rouven Essig, Tomer Volansky, and Tien-Tien Yu. "New Constraints and Prospects for sub-GeV Dark Matter Scattering off Electrons in Xenon". In: *Phys. Rev. D* 96.4 (2017), p. 043017. DOI: 10.1103/PhysRevD.96.043017. arXiv: 1703.00910 [hep-ph].

[549] Riccardo Catena et al. "Atomic responses to general dark matter-electron interactions". In: *Phys. Rev. Res.* 2.3 (2020), p. 033195. DOI: 10.1103/PhysRevResearch.2.033195. arXiv: 1912.08204 [hep-ph].

[550] Louis Hamaide and Christopher McCabe. "Fueling the search for light dark matter-electron scattering with spherical proportional counters". In: *Phys. Rev. D* 107.6 (2023), p. 063002. DOI: 10.1103/PhysRevD.107.063002. arXiv: 2110.02985 [hep-ph].

[551] G. Belanger et al. "Dark matter direct detection rate in a generic model with micrOMEGAs 2.2". In: *Comput. Phys. Commun.* 180 (2009), pp. 747–767. DOI: 10.1016/j.cpc.2008.11.019. arXiv: 0803.2360 [hep-ph].

[552] Marco Cirelli, Nicolao Fornengo, and Alessandro Strumia. "Minimal dark matter". In: *Nucl. Phys. B* 753 (2006), pp. 178–194. DOI: 10.1016/j.nuclphysb.2006.07.012. arXiv: hep-ph/0512090.

[553] G. Angloher et al. "Results on light dark matter particles with a low-threshold CRESST-II detector". In: *The European Physical Journal C* 76.1 (Jan. 2016). DOI: 10.1140/epjc/s10052-016-3877-3. URL: https://doi.org/10.1140%2Fepjc%2Fs10052-016-3877-3.

[554] Ningqiang Song, Serge Nagorny, and Aaron C. Vincent. "Pushing the frontier of WIMPy inelastic dark matter: Journey to the end of the periodic table". In: *Phys. Rev. D* 104.10 (2021), p. 103032. DOI: 10.1103/PhysRevD.104.103032. arXiv: 2104.09517 [hep-ph].

[555] E. Aprile et al. "Dark Matter Search Results from a One Ton-Year Exposure of XENON1T". In: *Physical Review Letters* 121.11 (Sept. 2018). DOI: 10.1103/physrevlett.121.111302. URL: https://doi.org/10.1103%2Fphysrevlett.121.111302.

[556] Riccardo Catena et al. "Atomic responses to general dark matter-electron interactions". In: *Physical Review Research* 2.3 (Aug. 2020). DOI: 10.1103/physrevresearch.2.033195. URL: https://doi.org/10.1103%2Fphysrevresearch.2.033195.

[557] Andrés Olivares-Del Campo et al. "Dark matter-neutrino interactions through the lens of their cosmological implications". In: *Phys. Rev. D* 97.7 (2018), p. 075039. DOI: 10.1103/PhysRevD.97.075039. arXiv: 1711.05283 [hep-ph].

[558] E. Aprile et al. "Dark Matter Search Results from a One Ton-Year Exposure of XENON1T". In: *Phys. Rev. Lett.* 121.11 (2018), p. 111302. DOI: 10.1103/PhysRevLett.121.111302. arXiv: 1805.12562 [astro-ph.CO].

[559] C. Amole et al. "Dark Matter Search Results from the PICO-60 C_3F_8 Bubble Chamber". In: *Phys. Rev. Lett.* 118.25 (2017), p. 251301. DOI: 10.1103/PhysRevLett.118.251301. arXiv: 1702.07666 [astro-ph.CO].

[560] Peter Athron et al. "Global analyses of Higgs portal singlet dark matter models using GAMBIT". In: *Eur. Phys. J.* C79.1 (2019), p. 38. DOI: 10.1140/epjc/s10052-018-6513-6. arXiv: 1808.10465 [hep-ph].

[561] A. H. Abdelhameed et al. "Description of CRESST-III Data". In: (May 2019). arXiv: 1905.07335 [astro-ph.CO].

[562] Daniel Baxter, Yonatan Kahn, and Gordan Krnjaic. "Electron Ionization via Dark Matter-Electron Scattering and the Migdal Effect". In: *Phys. Rev. D* 101.7 (2020), p. 076014. DOI: 10.1103/PhysRevD.101.076014. arXiv: 1908.00012 [hep-ph].